Attitude Control/Momentum Management and Payload Pointing in Advanced Space Vehicles

Alexander G. Parlos
Principal Investigator/Project Director
Decision & Information Systems Laboratory
Mail Stop 3133
Texas A&M University
College Station, Texas, 77843-3133
(409) 845-7092

Suhada Jayasuriya
Co-Principal Investigator
Mail Stop 3123
Texas A&M University
College Station, Texas, 77843

Prepared for
The National Aeronautics and Space Administration
Lyndon B. Johnson Space Center
Houston, Texas 77058
Grant No. NAG 9-275

August 1990

Attitude Control/Momentum Management and Payload Pointing in Advanced Space Vehicles

Final Report for the Period June 1, 1988 to May 31, 1990

Alexander G. Parlos, Principal Investigator/Project Director
Decision & Information Systems Laboratory
Mail Stop 3133
Texas A&M University
College Station, Texas, 77843-3133
(409) 845-7092

Suhada Jayasuriya, Co-Principal Investigator
Mail Stop 3123
Texas A&M University
College Station, Texas, 77843

Prepared for
The National Aeronautics and Space Administration
Lyndon B. Johnson Space Center
Houston, Texas 77058
Grant No. NAG 9-275

August 1990

Acknowledgments

The support and contributions of several graduate research assistants and other staff at Texas A&M University is greatly appreciated. Throughout the project the support provided by the grant technical monitor Dr. John W. Sunkel of NASA Johnson Space Center, Navigation, Control, and Aeronautics Division is gratefully acknowledged.

Executive Summary

This report describes the research performed in the two year period between June 1988 and May 1990, under the NASA Johnson Space Center Grant NAG 9-275 to Texas A&M University. The research results and findings of the two major tasks of the project are included. Namely, the report details the design and evaluation of an Attitude Control/Momentum Management System for highly asymmetric spacecraft configurations, and the preliminary development and application of a nonlinear control system design methodology for tracking control of uncertain systems, such as spacecraft payload pointing systems. Control issues relevant to both linear and nonlinear rigid-body spacecraft dynamics are addressed, whereas any structural flexibilities are not taken into consideration.

Results from the first task indicate that certain commonly used simplifications in the equations of motions result in unstable attitude control systems, when used for highly asymmetric spacecraft configurations. An approach is suggested circumventing this problem. Additionally, even though preliminary results from the second task are encouraging, the proposed nonlinear control system design method requires further investigation prior to its application and use as an effective payload pointing system design technique.

Contents

List of Figures

Part I

Project Description

Chapter 1

Overview of the Project

In Part II of this report an attitude control/momentum management (ACMM) system is proposed for large angle torque-equilibrium-attitude (TEA) configurations of the Space Station Freedom (SSF). The fully coupled equations of motion for the SSF are linearized around an arbitrary TEA and the linear-quadratic-regulator (LQR) method with pole placement is used to synthesize the full–state feedback gains. The actuators used are control moment gyros (CMGs) and both the gyroscopic and the gravity gradient torques are utilized in stabilizing the spacecraft, in the presence of external cyclic and secular disturbances. As it is anticipated during the earlier flights of the SSF and during some of the Mobile Remote Manipulator System (MRMS) operations, the contributions of the cross–products of inertia on the overall spacecraft attitude determination will be significant, resulting in large pitch angle TEAs. Therefore, a fully coupled control system will be required for these earlier flights and for certain modes of operation. The proposed gain-scheduled controller can be utilized for attitude control

and momentum management of any flight during the assembly sequence once the CMGs are available and/or during the MRMS operations. As shown in this paper, for certain SSF configurations characterized by large pitch angle TEAs, failure to include the contributions of the cross–products of the inertia terms in the linearization of the SSF dynamics results in the design of unstable controllers. These instabilities can only be observed on the nonlinear simulator, with the linearized closed-loop system appearing stable. The proposed gain-scheduled controller has been tested with inertia matrix element variations from Flight #3 (MB3) to Assembly Complete (AC) configurations, corresponding to up to 1600% changes in some cross-inertia terms. Computer simulation results indicate that because of the slowly changing dynamics of the SSF, a gain-scheduled controller provides satisfactory form of adaptation, as compared to other adaptive schemes, requiring more complex control architectures.

Part III of this report is focused on servo-tracking in the context of the ability to follow a desired output, within a prespecified error bound, over its entire duration; that is, to obtain a closed-loop system which has the ability to track a reference input vector while rejecting a class of external disturbances, to the extent required by the error bound. This type of tracking is referred to as tracking in the sense of spheres. It has been shown in the literature that a solution to this tracking problem may be obtained by a quantitative pole placement (QPP) approach. In particular, a nonlinear observer-based state feedback controller will guarantee the desired tracking performance, provided state feedback gains can be found such that a specific induced norm of a linear closed-loop operator can be made sufficiently small.

In this report a systematic procedure is given for solving the QPP problem when the induced norm is the L_∞ - norm. In particular, a Lurе type system is considered with the input and output spheres measured with respect to the L_∞ - norm, and an algorithm is developed on the basis of minimizing the H_∞ - norm of a linear closed-loop operator for solving the QPP problem. Relevant design criteria are derived by first embedding the problem in the L_2 function space, leading to an H_∞ - minimization problem which is followed by an exponential weighting technique for estimating the tracking error bounds in terms of L_∞ - norms. The approach to this problem is based on fixed-point techniques, the multivariable circle criterion, and H_∞-optimal control. The controller gains satisfying the design criteria and the QPP are obtained by solving a Riccati equation and a Lyapunov equation.

The controller synthesis methodology for servo-tracking in uncertain, nonlinear systems of the Lure type presented in the report is applied to a simple single input-single output, nonlinear, uncertain system and a two degree of freedom robotic manipulator. The manipulator tip is required to carry an unknown payload, lying between a given upper and a lower bound, along a semi-circular trajectory to a prespecified accuracy. The resulting controller resembles a robust computed torque arrangement with the feedback gains chosen specifically to provide the necessary reduction in sensitivity due to possible variations in the payload. Simulations results confirm the effectiveness of the synthesis technique.

Part II

Attitude Control/Momentum Management of Advanced Space Vehicles

Chapter 2

Introduction

The Space Station Freedom (SSF) will be the first permanently manned spacecraft to be assembled and operated by NASA. Currently, the schedule calls for the First Element Launch (FEL) in March of 1995 and the Assembly Complete (AC) configuration towards the last quarter of 1999. Two of the planned uses of the SSF are as a transportation node for future space missions, such as the Lunar and Mars Initiative, and as an experimental facility for zero-gravity materials processing and life sciences research. As a result of these program objectives, there is a need for the SSF environment to be effectively controlled. That is attitude control during assembly, normal flight and other operating conditions, such as operation of the Mobile Remote Manipulator System (MRMS).

Even though during the first few flights of the SSF reaction jets will be used as actuators, Control-Moment-Gyros (CMGs) will be utilized as the primary actuating devices for most of the assembly sequence and subsequent man-tended operations. Additionally, the gravity gradient torque

will be used to unload the spacecraft momentum from the CMGs and bring it to its nominal level. Previous studies have presented the trade-offs in selecting the various momentum management techniques [1]. In the current study, the momentum management approach proposed in reference [1] is used, however, only the attitude hold mode of the SSF operation is examined. The designed control law uses proportional-derivative (PD) for attitude control and proportional-integral (PI) for momentum management.

In addressing the attitude hold of the SSF, no explicit design specifications are placed upon the control system, other than the desired closed-loop system stability. The ultimate objective of this work is the application of direct nonlinear control system design techniques to the SSF Attitude Control/Momentum Management (ACMM) system. In order, however, to determine the benefits, if any, of using a more complex nonlinear controller, a gain-scheduled ACMM system is designed for comparison purposes. The gain-scheduled control system, a simplified and open-loop form of adaptive control, will allow attitude control and momentum management throughout the entire operating regime of the SSF dynamics. In order to design a gain-scheduled controller, however, it is necessary to have the linearized system dynamics at various operating points. These will then be used along with linear control synthesis techniques to arrive at the various gain sets which will in turn be fitted to obtain an analytic form for the gain matrix elements as a function of a system variable, called the scheduling variable.

This paper addresses the linearization of the equations of motion around an arbitrary operating point, which in this case is the torque-equilibrium-attitude (TEA). It is shown that for some SSF configurations, resulting

in large pitch angle TEAs, it is necessary to consider the full coupling of the roll/yaw with the pitch equations, through the contributions of the cross-products of inertia terms. Computer simulations show that use of linearized models without the roll/yaw and pitch coupling in the design of the ACMM system, result in closed-loop systems that exhibit instabilities for large pitch angle TEA configurations of the SSF. Such configurations will be encountered during the assembly sequence and during some of the MRMS operations [2].

Part II of this report is organized in the following manner. Chapter 3 presents the complete governing equations of motion for the SSF under the assumption of a single rigid body. Following, in chapter 4 is the derivation of the linearized equations of motion for an arbitrary TEA resulting from possible asymmetric configurations where the control axes are misaligned with the body axes. Chapter 5 presents the relevant issues in the design of an ACMM control law, as well as the Linear Quadratic Regulator (LQR) used in this study for the various SSF configurations. The section concludes with the gain-scheduling approach used in this study. Chapter 6 includes some of the simulation results necessary to substantiate the major points of this study. Chapter 7 summarizes the findings of this study with some concluding remarks.

Chapter 3

Nonlinear Dynamics of the Space-Station Rigid-Body Motion

The SSF is expected to operate in a circular orbit at an altitude of approximately 200 nm, with a period of approximately 5700 seconds. In reality SSF represents a flexible multi-body system, subject to various external disturbances which may not be accurately known. During the assembly sequence the spacecraft will undergo increasingly complex modifications as a results of the attached solar panels, thermal radiators, payloads, pressurized modules, etc. As a result, there will be an increased interaction among the various structural components and the spacecraft guidance, navigation and control system. In order to guarantee safe and reliable operation, the ACMM system should be able to keep the attitude excursions within some, yet unspecified, bounds while using only the available control torque and

without saturating the CMGs. Therefore, there is a need to systematically design ACMM systems which will have predictable and reliable operation.

Assuming single rigid-body motion, the nonlinear equations of motion for the gravity gradient stabilized SSF, with body-fixed control axes, can be expressed as follows [1,3]:

$$\mathbf{I}\,\dot{\boldsymbol{\omega}}(t) \;=\; \boldsymbol{\tau}_{gyro}(t) \;+\; \boldsymbol{\tau}_{gg}(t) \;+\; (\mathbf{w}(t) \;-\; \mathbf{u}(t)) \tag{3.1}$$

where $\boldsymbol{\omega}(t) = [\omega_1(t),\ \omega_2(t),\ \omega_3(t)]^T$ are the body-axis components of the absolute angular velocity of the spacecraft, with the subscripts (1,2,3) representing the (roll, pitch, yaw) axes, respectively. The matrix $\mathbf{I}$ contains the principal moments of inertia, $I_{ii},\ i = 1,2,3$, as well as the products of inertia $I_{ij},\ i = 1,2,3$ and $j = 1,2,3$ with $i \neq j$. It is also assumed that $I_{ij} \;=\; I_{ji},\ i,j = 1,2,3$. The first two terms on the right-hand-side of equation (3.1) represent the gyroscopic and gravity gradient torques. The vectors $\mathbf{w}(t) \;=\; [w_1(t),\ w_2(t),\ w_3(t)]^T$ and $\mathbf{u}(t) \;=\; [u_1(t),\ u_2(t),\ u_3(t)]^T$ represent the body-axis components of the external disturbance torque and the CMG control torque, respectively.

The gyroscopic torque term is expressed in terms of the absolute angular velocities as follows:

$$\boldsymbol{\tau}_{gyro}(t) \;=\; -\begin{bmatrix} 0 & -\omega_3(t) & \omega_2(t) \\ \omega_3(t) & 0 & -\omega_1(t) \\ -\omega_2(t) & \omega_1(t) & 0 \end{bmatrix} \begin{bmatrix} I_{11} & I_{12} & I_{13} \\ I_{21} & I_{22} & I_{23} \\ I_{31} & I_{32} & I_{33} \end{bmatrix} \begin{bmatrix} \omega_1(t) \\ \omega_2(t) \\ \omega_3(t) \end{bmatrix} \tag{3.2}$$

The gravity gradient torque term is expressed in terms of the body-axis

angles with respect to LVLH as:

$$\boldsymbol{\tau}_{gg}(t) = 3n^2 \begin{bmatrix} 0 & -c_3(t) & c_2(t) \\ c_3(t) & 0 & -c_1(t) \\ -c_2(t) & c_1(t) & 0 \end{bmatrix} \begin{bmatrix} I_{11} & I_{12} & I_{13} \\ I_{21} & I_{22} & I_{23} \\ I_{31} & I_{32} & I_{33} \end{bmatrix} \begin{bmatrix} c_1(t) \\ c_2(t) \\ c_3(t) \end{bmatrix} \quad (3.3)$$

where n is the SSF orbital rate of 0.0011 rad/sec and the components of the nadir vector $\mathbf{c}(t)$ are given by the following expressions:

$$\begin{aligned} c_1(t) &\equiv -sin(\theta_2(t))cos(\theta_3(t)) \\ c_2(t) &\equiv cos(\theta_1(t))sin(\theta_2(t))sin(\theta_3(t)) + sin(\theta_1(t))cos(\theta_2(t)) \\ c_3(t) &\equiv -sin(\theta_1(t))sin(\theta_2(t))sin(\theta_3(t)) + cos(\theta_1(t))cos(\theta_2(t)) \end{aligned} \quad (3.4)$$

The attitude kinematics express the relation between the absolute angular velocities and the body-axis angular rates with respect to LVLH, as follows:

$$\dot{\boldsymbol{\theta}}(t) = \mathbf{f}(\boldsymbol{\theta}(t))\boldsymbol{\omega}(t) + \mathbf{q} \quad (3.5)$$

where

$$\mathbf{f}(\boldsymbol{\theta}(t)) = \frac{1}{cos(\theta_3(t))} \begin{bmatrix} 1 & -cos(\theta_1(t))sin(\theta_3(t)) & sin(\theta_1(t))sin(\theta_3(t)) \\ 0 & cos(\theta_1(t)) & -sin(\theta_1(t)) \\ 0 & sin(\theta_1(t))cos(\theta_3(t)) & cos(\theta_1(t))cos(\theta_3(t)) \end{bmatrix} \quad (3.6)$$

and

$$\mathbf{q} = \begin{bmatrix} 0 \\ n \\ 0 \end{bmatrix}, \quad \boldsymbol{\theta}(t) = \begin{bmatrix} \theta_1(t) \\ \theta_2(t) \\ \theta_3(t) \end{bmatrix} \quad (3.7)$$

The CMG dynamics are expressed in terms of the body-axis components of the CMG momentum and the external control torque $\mathbf{u}(t)$ applied by the

ACMM system as follows:

$$\dot{\mathbf{h}}(t) = \mathbf{u}(t) - \begin{bmatrix} 0 & -\omega_3(t) & \omega_2(t) \\ \omega_3(t) & 0 & -\omega_1(t) \\ -\omega_2(t) & \omega_1(t) & 0 \end{bmatrix} \mathbf{h}(t) \tag{3.8}$$

The general form of the external disturbance torque used in this study is as proposed in references [1,3]. That is:

$$w_i(t) = (Bias)_i + A_i sin(nt) + B_i sin(2nt) \tag{3.9}$$

where $i = 1, 2, 3$ for roll, pitch and yaw, respectively.

Chapter 4

Derivation of the Linearized Equations of Motion

The equations of motion presented in the previous section are highly non-linear and therefore not suitable for control system design. In order to allow use of linear control system design techniques some form of linearization must be performed. There have been successful applications of the small angle linearized and the roll/yaw and pitch decoupled equations of motion for the attitude control and momentum management of the SSF [1,4]. However, for configurations resulting to large angle TEAs the applicability of this approximation will be extremely limited [3]. An alternate approach in resolving this problem would be the linearization of the equations of motion around an arbitrary TEA, without decoupling the pitch from the roll/yaw equations of motion. This is justified on the basis that the large angle TEA configurations of the SSF result from the misalignment of the control axes with principal body axes. Therefore, neglecting the cross-inertia terms for

large angle TEA configurations would result in highly erroneous linearized models.

4.1 Determination of the Torque Equilibrium Attitude

In order to perform linearization of equations (3.1), (3.5) and (3.8) around an arbitrary TEA, it is necessary to estimate the average TEA of a given configuration over an orbit, after equilibrium conditions have been reached. Assuming that (θ_1^*, θ_2^*, θ_3^*) represent the TEA (or the average value of TEA) at steady-state for a given configuration, these angles can be calculated using the following set of nonlinear equations:

$$\tau_{gyro}(\omega^*) + \tau_{gg}(\theta^*) + \mathbf{Bias} = 0 \tag{4.1}$$

where ω^* is the absolute angular velocity of the spacecraft evaluated at θ^*, and

$$\mathbf{f}(\theta^*)\,\omega^* + \mathbf{q} = \mathbf{0} \tag{4.2}$$

where the function $\mathbf{f}(\theta)$ and $\mathbf{q}$ are defined in the previous section. The latter of these two system of equations can be used to solve for ω^* in terms of θ^* obtaining the following relations:

$$\omega^* = \begin{bmatrix} -nsin(\theta_3^*) \\ -ncos(\theta_1^*)cos(\theta_3^*) \\ nsin(\theta_1^*)cos(\theta_3^*) \end{bmatrix} \tag{4.3}$$

Substitution of these expressions into equation (4.1), reveals a system

of three nonlinear equations which, for a given inertia matrix **I**, could be solved to estimate the average value of the TEA.

4.2 Linearization of the Attitude Kinematics

The attitude kinematics, expressed by equation (3.5), can be linearized around $(\boldsymbol{\theta}^*, \boldsymbol{\omega}^*)$ obtaining the following linearized attitude kinematics:

$$\dot{\boldsymbol{\theta}}(t) = \frac{1}{cos(\theta_3^*)} \left\{ \begin{bmatrix} 0 \\ 0 \\ -n(cos(\theta_3^*))^2 \end{bmatrix} \delta\theta_1(t) + \begin{bmatrix} n \\ -nsin(\theta_3^*) \\ 0 \end{bmatrix} \delta\theta_3(t) + \right.$$
$$\begin{bmatrix} cos(\theta_3^*) \\ 0 \\ 0 \end{bmatrix} \delta\omega_1(t) + \begin{bmatrix} -cos(\theta_1^*)sin(\theta_3^*) \\ cos(\theta_1^*) \\ sin(\theta_1^*)cos(\theta_3^*) \end{bmatrix} \delta\omega_2(t) + \quad (4.4)$$
$$\left. \begin{bmatrix} sin(\theta_1^*)sin(\theta_3^*) \\ -sin(\theta_1^*) \\ cos(\theta_1^*)cos(\theta_3^*) \end{bmatrix} \delta\omega_3(t) \right\}$$

where, for $i = 1, 2, 3$,

$$\delta\theta_i(t) = \theta_i(t) - \theta_i^* \quad (4.5)$$

$$\delta\omega_i(t) = \omega_i(t) - \omega_i^* \quad (4.6)$$

represent the perturbations of the attitude and of the absolute angular velocities from the TEA and from the angular velocities corresponding to the TEA, respectively.

4.3 Linearization of the Gyroscopic Torque

The gyroscopic torque term, given by equation (3.2), can be linearized as follows:

$$\Delta\tau_{gyr}(t) = \left\{ \frac{\partial\tau_{gyr}}{\partial\omega_1}\delta\omega_1(t) + \frac{\partial\tau_{gyr}}{\partial\omega_2}\delta\omega_2(t) + \frac{\partial\tau_{gyr}}{\partial\omega_3}\delta\omega_3(t) \right\} \tag{4.7}$$

where each of the partial derivatives in the above equation, evaluated at $\theta(t) = \theta^*$, depends upon the elements of the inertia matrix, $\mathbf{I}$, and the TEA vector, θ^*.

The partial derivatives of the gyroscopic torque term, with respect to the absolute angular velocity of the spacecraft, are given by the following expressions:

$$\frac{\partial\tau_{gyr}}{\partial\omega_1} = -n \begin{bmatrix} -I_{12}sin(\theta_1^*)cos(\theta_3^*) - I_{13}cos(\theta_1^*)cos(\theta_3^*) \\ 2I_{13}sin(\theta_3^*) + I_{23}cos(\theta_1^*)cos(\theta_3^*) + (I_{11} - I_{33})sin(\theta_1^*)cos(\theta_3^*) \\ I_{23}sin(\theta_1^*)cos(\theta_3^*) - 2I_{12}sin(\theta_3^*) + (I_{11} - I_{22})cos(\theta_1^*)cos(\theta_3^*) \end{bmatrix} \tag{4.8}$$

$$\frac{\partial\tau_{gyr}}{\partial\omega_2} = -n \begin{bmatrix} -2I_{23}cos(\theta_1^*)cos(\theta_3^*) - I_{13}sin(\theta_3^*) + (I_{33} - I_{22})sin(\theta_1^*)cos(\theta_3^*) \\ I_{12}sin(\theta_1^*)cos(\theta_3^*) + I_{23}sin(\theta_3^*) \\ 2I_{12}cos(\theta_1^*)cos(\theta_3^*) - I_{13}sin(\theta_1^*)cos(\theta_3^*) + (I_{11} - I_{22})sin(\theta_3^*) \end{bmatrix} \tag{4.9}$$

$$\frac{\partial\tau_{gyr}}{\partial\omega_3} = -n \begin{bmatrix} I_{12}sin(\theta_3^*) - 2I_{23}sin(\theta_1^*)cos(\theta_3^*) + (I_{22} - I_{33})cos(\theta_1^*)cos(\theta_3^*) \\ -I_{12}cos(\theta_1^*)cos(\theta_3^*) + 2I_{13}sin(\theta_1^*)cos(\theta_3^*) + (I_{33} - I_{11})sin(\theta_3^*) \\ I_{13}cos(\theta_1^*)cos(\theta_3^*) - I_{23}sin(\theta_3^*) \end{bmatrix} \tag{4.10}$$

4.4 Linearization of the Gravity Gradient Torque

The gravity gradient torque term, given by equation (3.3), can be linearized as follows:

$$\Delta\tau_{gg}(t) = \left\{ \frac{\partial\tau_{gg}}{\partial\theta_1}\delta\theta_1(t) + \frac{\partial\tau_{gg}}{\partial\theta_2}\delta\theta_2(t) + \frac{\partial\tau_{gg}}{\partial\theta_3}\delta\theta_3(t) \right\} \tag{4.11}$$

where each of the partial derivatives in the above equation, evaluated at $\boldsymbol{\theta}(t) = \boldsymbol{\theta}^*$, depends upon the elements of the inertia matrix, $\mathbf{I}$, and the TEA vector, $\boldsymbol{\theta}^*$. The elements of the vectors containing the partial derivatives of the gravity gradient torque with respect to the spacecraft attitude angles are given by the following expressions:

$$\frac{\partial\tau_{gg}}{\partial\theta_1} = -3n^2 \begin{bmatrix} (-I_{12}A_1 + I_{13}B_1)C_1 + (I_{22} - I_{33})(A_1^2 - B_1^2) - 4I_{23}A_1B_1 \\ (I_{11} - I_{33})A_1C_1 + I_{12}(B_1^2 - A_1^2) + 2I_{13}A_1B_1 \\ \{(I_{22} - I_{11})B_1 + I_{23}A_1\}C_1 + I_{13}(A_1^2 - B_1^2) + 2I_{12}A_1B_1 \end{bmatrix} \tag{4.12}$$

$$\begin{aligned} \frac{\partial\tau_{gg}}{\partial\theta_2} = -3n^2 \Bigg[& -I_{12}(A_2C_1 + C_2B_1) + I_{13}(B_2C_1 - C_2A_1) \\ & I_{11}(B_1C_2 - C_1A_2) - I_{33}(A_2C_1 - B_1C_2) \\ & I_{11}(A_1C_2 + B_2C_1) - I_{22}(A_1C_2 + C_1B_2) \\ & +I_{22}(A_1A_2 - B_1B_2) \\ & +I_{12}(B_1B_2 - A_1A_2) \\ & +I_{23}(B_1C_2 - C_1A_2) \end{aligned}$$

$$\left.\begin{array}{l} -I_{33}(B_1B_2 + A_1A_2) - 2I_{23}(A_2B_1 + A_1B_2) \\ +2I_{13}(C_1C_2 + A_2B_1) + I_{23}(A_1C_2 + C_1B_2) \\ +I_{13}(A_1A_2 - B_1B_2) + 2I_{12}(A_1B_2 - C_1C_2) \end{array}\right] \quad (4.13)$$

$$\frac{\partial \tau_{gg}}{\partial \theta_3} = -3n^2 \left[\begin{array}{l} (I_{22} - I_{33})(A_1A_3 - B_1B_3) - I_{12}(A_3C_1 - B_1C_3) \\ (I_{33} - I_{11})(A_3C_1 - B_1C_3) - I_{12}(A_1A_3 - B_1B_3) \\ (I_{11} - I_{22})(A_1C_3 + B_3C_1) + I_{23}(B_1C_3 - A_3C_1) \\ \left.\begin{array}{l} -2I_{23}(A_3B_1 + A_1B_3) - I_{13}(B_3C_1 + A_1C_3) \\ +2I_{13}(A_3B_1 + C_1C_3) + I_{23}(A_1C_3 + B_3C_1) \\ +I_{13}(B_1B_3 + A_1A_3) + 2I_{12}(A_1B_3 - C_1C_3) \end{array}\right] \end{array}\right] \quad (4.14)$$

where

$$A_1 = cos(\theta_1^*)sin(\theta_2^*)sin(\theta_3^*) + sin(\theta_1^*)cos(\theta_2^*) \quad (4.15)$$

$$B_1 = sin(\theta_1^*)sin(\theta_2^*)sin(\theta_3^*) - cos(\theta_1^*)cos(\theta_2^*) \quad (4.16)$$

$$C_1 = sin(\theta_2^*)cos(\theta_3^*) \quad (4.17)$$

$$A_2 = sin(\theta_1^*)cos(\theta_2^*)sin(\theta_3^*) + cos(\theta_1^*)sin(\theta_2^*) \quad (4.18)$$

$$B_2 = -cos(\theta_1^*)cos(\theta_2^*)sin(\theta_3^*) + sin(\theta_1^*)sin(\theta_2^*) \quad (4.19)$$

$$C_2 = cos(\theta_2^*)cos(\theta_3^*) \quad (4.20)$$

$$A_3 = sin(\theta_1^*)sin(\theta_2^*)cos(\theta_3^*) \quad (4.21)$$

$$B_3 = -cos(\theta_1^*)sin(\theta_2^*)cos(\theta_3^*) \quad (4.22)$$

$$C_3 = -sin(\theta_2^*)sin(\theta_3^*) \quad (4.23)$$

4.5 Linearized System Equations

The above equations can now be assembled to form the overall linearized dynamics for the rigid-body motion of the SSF in the vicinity of an arbitrary TEA.

4.5.1 Orbital Dynamics/Kinematics Equations

The following three dimensional vector definitions are introduced for the partial derivative terms of the external torques to simplify the mathematical form of the final equations:

$$\tau^i_{gyr} = \frac{\partial \tau_{gyr}}{\partial \omega_i} \tag{4.24}$$

$$\tau^i_{gg} = \frac{\partial \tau_{gg}}{\partial \theta_i} \tag{4.25}$$

Each of the components of the above vectors correspond to the roll, pitch and yaw components of the external torques. Following the standard formulation [1,3,4,6], the following state vector is defined for the orbital dynamics and the kinematics, to be used for control system design purposes:

$$\mathbf{x}_1(t) = [\delta\omega_1(t),\ \dot{\theta}_2(t),\ \delta\omega_3(t),\ \delta\theta_1(t),\ \delta\theta_2(t),\ \delta\theta_3(t)]^T \tag{4.26}$$

In order to eliminate $\delta\omega_2(t)$ and substitute $\dot{\theta}_2(t)$ in the system equations, the kinematic relation for $\dot{\theta}_2(t)$ is substituted in the orbital dynamics. The overall linearized orbital dynamics/kinematics then take the following form:

$$\mathbf{E}_1\ \dot{\mathbf{x}}_1(t) = \mathbf{A}_1\ \mathbf{x}_1(t) + \mathbf{B}_1\ \mathbf{u}(t) + \mathbf{B}_2\ \mathbf{w}(t) \tag{4.27}$$

where $\mathbf{x}_1(t)$ is given by equation (4.26) and the matrices $\mathbf{E}_1$, $\mathbf{A}_1$, $\mathbf{B}_1$ and $\mathbf{B}_2$ are as follows:

$$\mathbf{E}_1 = \frac{1}{cos(\theta_1^*)} \begin{bmatrix} I_{11}cos(\theta_1^*) & I_{12}cos(\theta_3^*) & I_{13}cos(\theta_1^*) + I_{12}sin(\theta_1^*) \\ I_{21}cos(\theta_1^*) & I_{22}cos(\theta_3^*) & I_{23}cos(\theta_1^*) + I_{22}sin(\theta_1^*) \\ I_{31}cos(\theta_1^*) & I_{32}cos(\theta_3^*) & I_{33}cos(\theta_1^*) + I_{32}sin(\theta_1^*) \\ 0 & 0 & 0 \\ 0 & 0 & 0 \\ 0 & 0 & 0 \end{bmatrix} \begin{bmatrix} 1 & 0 & 0 \\ 0 & 1 & 0 \\ 0 & 0 & 1 \\ 0 & 0 & I_{12}nsin(\theta_3^*) \\ 0 & 0 & I_{22}nsin(\theta_3^*) \\ 0 & 0 & I_{32}nsin(\theta_3^*) \end{bmatrix} \tag{4.28}$$

$$\mathbf{A}_1 = \frac{1}{cos(\theta_1^*)} \begin{bmatrix} \tau_{gyr}^1(1)cos(\theta_1^*) & \tau_{gyr}^2(1)cos(\theta_3^*) \\ \tau_{gyr}^1(2)cos(\theta_1^*) & \tau_{gyr}^2(2)cos(\theta_3^*) \\ \tau_{gyr}^1(3)cos(\theta_1^*) & \tau_{gyr}^2(3)cos(\theta_3^*) \\ cos(\theta_1^*) & -sin(\theta_3^*)cos(\theta_1^*) \\ 0 & cos(\theta_1^*) \\ 0 & sin(\theta_1^*)cos(\theta_3^*) \end{bmatrix}$$

$$
\begin{bmatrix}
\tau^3_{gyr}(1)cos(\theta^*_1) + \tau^2_{gyr}(1)sin(\theta^*_1) \\
\tau^3_{gyr}(2)cos(\theta^*_1) + \tau^2_{gyr}(2)sin(\theta^*_1) \\
\tau^3_{gyr}(3)cos(\theta^*_1) + \tau^2_{gyr}(3)sin(\theta^*_1) \\
0 \\
0 \\
1
\end{bmatrix}
$$

$$
\begin{bmatrix}
\tau^1_{gg}(1)cos(\theta^*_1) \\
\tau^1_{gg}(2)cos(\theta^*_1) \\
\tau^1_{gg}(3)cos(\theta^*_1) \\
0 \\
0 \\
-ncos(\theta^*_1)cos(\theta^*_3)
\end{bmatrix}
$$

$$
\begin{bmatrix}
\tau^2_{gg}(1)cos(\theta^*_1) & \tau^3_{gg}(1)cos(\theta^*_1) + \tau^2_{gg}(1)nsin(\theta^*_3) \\
\tau^2_{gg}(2)cos(\theta^*_1) & \tau^3_{gg}(2)cos(\theta^*_1) + \tau^2_{gg}(2)nsin(\theta^*_3) \\
\tau^2_{gg}(3)cos(\theta^*_1) & \tau^3_{gg}(3)cos(\theta^*_1) + \tau^2_{gg}(3)nsin(\theta^*_3) \\
0 & ncos(\theta^*_1)\frac{1-(sin(\theta^*_3))^2}{cos(\theta^*_3)} \\
0 & 0 \\
0 & nsin(\theta^*_1)sin(\theta^*_3)
\end{bmatrix}
\tag{4.29}
$$

$$
\mathbf{B}_1 = \begin{bmatrix}
1 & 0 & 0 & 0 & 0 & 0 \\
0 & 1 & 0 & 0 & 0 & 0 \\
0 & 0 & 1 & 0 & 0 & 0 \\
0 & 0 & 0 & 0 & 0 & 0 \\
0 & 0 & 0 & 0 & 0 & 0 \\
0 & 0 & 0 & 0 & 0 & 0
\end{bmatrix}, \quad \mathbf{B}_2 = -\mathbf{B}_1 \tag{4.30}
$$

4.5.2 CMG Dynamic Equations

In addition to the above linearizations, the CMG dynamics can also be linearized as follows:

$$\dot{\mathbf{h}}(t) \;=\; \mathbf{u}(t) \;-\; \begin{bmatrix} 0 & -\omega_3^* & \omega_2^* \\ \omega_3^* & 0 & -\omega_1^* \\ -\omega_2^* & \omega_1^* & 0 \end{bmatrix} \mathbf{h}(t) \tag{4.31}$$

where the vector $\mathbf{h}(t)$ represents deviations of the CMG momentum from equilibrium conditions and where the vector $\boldsymbol{\omega}^*$ is given by equation (4.3) in terms of the TEA. As both the CMG momentum and its integral will be used in the feedback controller, the following state vector is defined for the CMGs:

$$\mathbf{x}_2(t) \;=\; [h_1(t), h_2(t), h_3(t), \int h_1(t), \int h_2(t), \int h_3(t)]^T \tag{4.32}$$

Then the standard state-space form for the CMG dynamics becomes:

$$\dot{\mathbf{x}}_2(t) \;=\; \mathbf{A}_2\, \mathbf{x}_2(t) \;+\; \mathbf{B}_2\mathbf{u}(t) \tag{4.33}$$

where $\mathbf{x}_2(t)$ is given by equation (4.32) and the matrix $\mathbf{A}_2$ is as follows:

$$\mathbf{A}_2 \;=\; \begin{bmatrix} 0 & nsin(\theta_1^*)cos(\theta_3^*) & ncos(\theta_1^*)cos(\theta_3^*) \\ -nsin(\theta_1^*)cos(\theta_3^*) & 0 & -nsin(\theta_3^*) \\ ncos(\theta_1^*)cos(\theta_3^*) & nsin(\theta_3^*) & 0 \\ 1 & 0 & 0 \\ 0 & 1 & 0 \\ 0 & 0 & 1 \end{bmatrix}$$

$$\begin{bmatrix} 0 & 0 & 0 \\ 0 & 0 & 0 \\ 0 & 0 & 0 \\ 0 & 0 & 0 \\ 0 & 0 & 0 \\ 0 & 0 & 0 \end{bmatrix} \tag{4.34}$$

4.5.3 Disturbance Rejection Filter Equations

As the frequencies of the external disturbances are known, the following disturbance rejection filters (DRFs) can be used for asymptotic rejection [1]:

$$\ddot{\alpha}_1(t) + n^2\alpha_1(t) = h_1(t) \tag{4.35}$$

$$\ddot{\alpha}_2(t) + n^2\alpha_2(t) = \theta_2(t) \tag{4.36}$$

$$\ddot{\alpha}_3(t) + n^2\alpha_3(t) = \theta_3(t) \tag{4.37}$$

$$\ddot{\beta}_1(t) + (2n)^2\beta_1(t) = h_1(t) \tag{4.38}$$

$$\ddot{\beta}_2(t) + (2n)^2\beta_2(t) = \theta_2(t) \tag{4.39}$$

$$\ddot{\beta}_3(t) + (2n)^2\beta_3(t) = \theta_3(t) \tag{4.40}$$

where, $\alpha_i(t)$, $\beta_i(t)$ are the filter states with arbitrary initial conditions. It is worth mentioning that the above filters are for attitude hold, only. If momentum hold is desired then a separate set of DRFs should be designed with inputs $h_1(t)$, $h_2(t)$, $\theta_3(t)$. The reasons for not using $\theta_1(t)$ or $h_3(t)$ in the DRFs are given in reference [1]. The above equations can be expressed in the following state-space form:

$$\dot{\mathbf{x}}_3(t) \;=\; \mathbf{A}_3\,\mathbf{x}_3(t) + \mathbf{A}_4\,\mathbf{x}_1(t) + \mathbf{A}_5\,\mathbf{x}_2(t) \tag{4.41}$$

where $\mathbf{x}_3(t)$ is given by:

$$\begin{aligned}\mathbf{x}_3(t) &= [\dot{\alpha}_1(t), \alpha_1(t), \dot{\alpha}_2(t), \alpha_2(t), \dot{\alpha}_3(t), \alpha_3(t), \\ &\quad \dot{\beta}_1(t), \beta_1(t), \dot{\beta}_2(t), \beta_2(t), \dot{\beta}_3(t), \beta_3(t),]^T \end{aligned} \tag{4.42}$$

and the matrices $\mathbf{A}_3$, $\mathbf{A}_4$ and $\mathbf{A}_5$ are as follows:

$$\mathbf{A}_3 = \begin{bmatrix} 0 & -n^2 & 0 & 0 & 0 & 0 \\ 1 & 0 & 0 & 0 & 0 & 0 \\ 0 & 0 & 0 & -n^2 & 0 & 0 \\ 0 & 0 & 1 & 0 & 0 & 0 \\ 0 & 0 & 0 & 0 & 0 & -n^2 \\ 0 & 0 & 0 & 0 & 1 & 0 \\ 0 & 0 & 0 & 0 & 0 & 0 \\ 0 & 0 & 0 & 0 & 0 & 0 \\ 0 & 0 & 0 & 0 & 0 & 0 \\ 0 & 0 & 0 & 0 & 0 & 0 \\ 0 & 0 & 0 & 0 & 0 & 0 \end{bmatrix}$$

$$\begin{bmatrix} 0 & 0 & 0 & 0 & 0 & 0 \\ 0 & 0 & 0 & 0 & 0 & 0 \\ 0 & 0 & 0 & 0 & 0 & 0 \\ 0 & 0 & 0 & 0 & 0 & 0 \\ 0 & 0 & 0 & 0 & 0 & 0 \\ 0 & 0 & 0 & 0 & 0 & 0 \\ 0 & -4n^2 & 0 & 0 & 0 & 0 \\ 1 & 0 & 0 & 0 & 0 & 0 \\ 0 & 0 & 0 & -4n^2 & 0 & 0 \\ 0 & 0 & 1 & 0 & 0 & 0 \\ 0 & 0 & 0 & 0 & 0 & -4n^2 \\ 0 & 0 & 0 & 0 & 1 & 0 \end{bmatrix} \tag{4.43}$$

$$\mathbf{A}_4 = \begin{bmatrix} 0 & 0 & 0 & 0 & 0 & 0 & 0 & 0 & 0 & 0 & 0 & 0 \\ 0 & 0 & 0 & 0 & 0 & 0 & 0 & 0 & 0 & 0 & 0 & 0 \\ 0 & 0 & 0 & 0 & 0 & 0 & 0 & 0 & 0 & 0 & 0 & 0 \\ 0 & 0 & 0 & 0 & 0 & 0 & 0 & 0 & 0 & 0 & 0 & 0 \\ 0 & 0 & 1 & 0 & 0 & 0 & 0 & 0 & 0 & 1 & 0 & 0 \\ 0 & 0 & 0 & 0 & 1 & 0 & 0 & 0 & 0 & 0 & 0 & 1 \end{bmatrix}^T \tag{4.44}$$

$$\mathbf{A}_5 = \begin{bmatrix} 1 & 0 & 0 & 0 & 0 & 0 & 1 & 0 & 0 & 0 & 0 & 0 \\ 0 & 0 & 0 & 0 & 0 & 0 & 0 & 0 & 0 & 0 & 0 & 0 \\ 0 & 0 & 0 & 0 & 0 & 0 & 0 & 0 & 0 & 0 & 0 & 0 \\ 0 & 0 & 0 & 0 & 0 & 0 & 0 & 0 & 0 & 0 & 0 & 0 \\ 0 & 0 & 0 & 0 & 0 & 0 & 0 & 0 & 0 & 0 & 0 & 0 \\ 0 & 0 & 0 & 0 & 0 & 0 & 0 & 0 & 0 & 0 & 0 & 0 \end{bmatrix}^T \tag{4.45}$$

The system of equations (4.27), (4.33) and (4.41) can now be transformed into the following state-space form:

$$\dot{\mathbf{x}}(t) = \mathbf{A}\mathbf{x}(t) + \mathbf{B}\mathbf{u}(t) + \mathbf{G}\mathbf{w}(t) \tag{4.46}$$

where the 24th order state vector is:

$$\mathbf{x}(t) = \begin{bmatrix} \mathbf{x}_1(t) \\ \mathbf{x}_2(t) \\ \mathbf{x}_3(t) \end{bmatrix} \tag{4.47}$$

and the system matrices $\mathbf{A}$ (24 $\times$ 24), $\mathbf{B}$ (24 $\times$ 3), and $\mathbf{G}$ (24 $\times$ 3) are:

$$\mathbf{A} = \begin{bmatrix} \mathbf{E}_1^{-1}\mathbf{A}_1 & \mathbf{0} & \mathbf{0} \\ \mathbf{0} & \mathbf{A}_2 & \mathbf{0} \\ \mathbf{A}_4 & \mathbf{A}_5 & \mathbf{A}_3 \end{bmatrix} \tag{4.48}$$

$$\mathbf{B} = \begin{bmatrix} \mathbf{E}_1^{-1}\mathbf{B}_1 \\ \mathbf{B}_2 \\ \mathbf{0} \end{bmatrix} \tag{4.49}$$

$$\mathbf{G} = \begin{bmatrix} \mathbf{E}_1^{-1}\mathbf{B}_2 \\ \mathbf{0} \\ \mathbf{0} \end{bmatrix} \tag{4.50}$$

with the rest of the submatrices previously defined and dependent upon the specific value of the estimated TEA vector. By setting $\theta_i^* = 0$ for $i = 1,2,3$ and $I_{ij} = 0$ for $i \neq j$, in equation (4.46), the small-angle linearized and the roll/yaw and pitch decoupled SSF models are obtained, respectively.

Chapter 5

Design of the Attitude Control/Momentum Management System

The dynamic system described by equation (4.46) is used to design an ACMM system. The disturbance rejection filters proposed in reference [1] are used to accomplish either attitude or momentum hold, depending upon the desired mode of operation. As mentioned earlier, however, only attitude hold is examined in this study. The results presented in this paper are equally applicable to the momentum hold mode, as the only change occurs in the input variables to the DRFs.

5.1 Control System Architecture

The overall architecture of the investigated ACMM system is shown in Figure 5.1. The controller is composed of two gain-scheduled control laws. One for attitude control and momentum management, and the other for rejection of the environmental disturbances. Both control laws are scheduled using the estimated average TEA as the scheduling variable. The input signals to the ACMM controller are the angles and the angular rates, the CMG momentum and the momentum build-up, i.e. the momentum integral, and an estimate of the average SSF TEA based upon estimates of the available mass properties. The input to the DRFs are the angle and momentum vectors. However, as at most three independent variables can be simulaneously controlled, either the vector $(h_1(t), \theta_2(t), \theta_3(t))$ or the vector $(h_1(t), h_2(t), \theta_3(t))$ is used as input to the DRFs, depending upon the desired operating mode of the ACMM system.

The use of the TEA estimate in the control law is necessary because of the inadequacy of the linear control system design tools to account for the controller gain variations with changing inertia matrix elements. The static calculation involved in obtaining the TEA estimate could be performed off-line, with table look-ups used during actual operation. It is assumed that a separate module provides on-line or tabulated estimates of the SSF mass properties. A saturation element is included as part of the simulated closed-loop system, because of the possible differences in the commanded and actual control signal that could be caused by high demanded control torques (the control torque saturation is set at 150 lb_f, whereas CMG saturation is set at $20,000\ ft - lb_f - sec$).

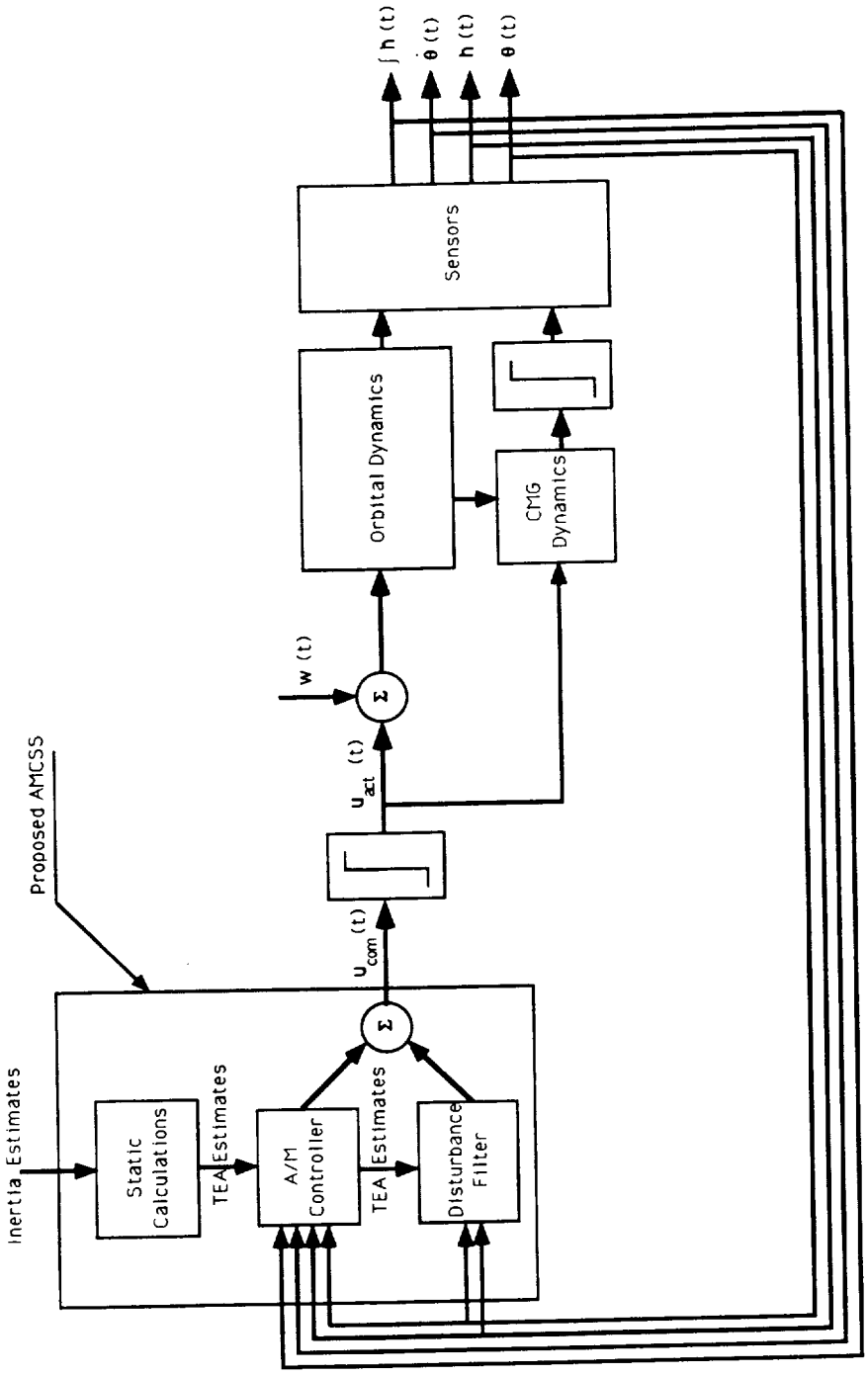

Figure 5.1: Attitude/Momentum Control and Stabilization System Architecture.

The attitude/momentum control law used in this study is as follows:

$$\mathbf{u}(t) = -\mathbf{K}(\boldsymbol{\theta}^*)\mathbf{x}(t) \tag{5.1}$$

where the state vector $\mathbf{x}(t)$ is given by equation (4.47) and the 3×24 gain matrices, $\mathbf{K}$, are determined for various TEAs, using the LQR algorithm described in the following section.

5.2 LQR Design with Pole Placement

Because the full state considered in equation (4.47) is available for measurement and because a time-optimal control law of minimal complexity is desired, the LQR is appropriate for use in obtaining the constant gains of the ACMM control system. The various linear designs are performed using the dynamic system described by equation (4.46), with the elements of the system matrices evaluated at specific values of the TEA, corresponding to various assumed configurations of the SSF during the assembly sequence.

Assuming the state-space form of equation (4.46) with an n-dimensional state vector, an m-dimensional input vector and without the external disturbance term, the LQR problem can be stated as the minimization of the following functional:

$$J = \int_0^\infty (\mathbf{x}^T(t)\mathbf{Q}\mathbf{x}(t) + \mathbf{u}^T(t)\mathbf{R}\mathbf{u}(t))dt \tag{5.2}$$

where the weight matrices $\mathbf{Q}$ and $\mathbf{R}$ are $(n \times n)$-dimensional non-negative definite and $(m \times m)$-dimensional positive definite symmetric matrices, respectively. The full-state feedback control law that minimizes the above

functional is given by:

$$\mathbf{u}(t) = -\mathbf{K}\mathbf{x}(t) = -\mathbf{R}^{-1}\mathbf{B}^T\mathbf{P}\mathbf{x}(t) \tag{5.3}$$

where $\mathbf{K}$ is the feedback gain matrix and $\mathbf{P}$, a $(n \times n)$-dimensional non-negative definite symmetric matrix, is the solution of the following Riccati equation:

$$\mathbf{P}\mathbf{B}\mathbf{R}^{-1}\mathbf{B}^T\mathbf{P} - \mathbf{P}\mathbf{A} - \mathbf{A}^T\mathbf{P} - \mathbf{Q} = \mathbf{0} \tag{5.4}$$

where the pair $(\mathbf{Q}, \mathbf{A})$ is assumed detectable.

It is usual practice to arbitrarily choose the matrices $\mathbf{Q}$ and $\mathbf{R}$, resulting in a certain gain matrix $\mathbf{K}$ and the associated stable closed-loop poles. However, these closed-loop pole locations, though in the left-half plane, may or may not be desirable. The problem of selecting the matrices $\mathbf{Q}$ and $\mathbf{R}$ such that the resulting closed-loop pole locations fall in a desired sector, has been widely investigated. This is the so-called LQR problem with pole placement and it has most recently been addressed by Sunkel et al.[6]. Throughout this study the LQR with pole placement suggested in the above reference has been used with some modifications in the solution approach of the Riccati equation. The algorithm proposed by Sunkel and Shieh [6], allows the choice of the weight matrix $\mathbf{R}$ and the desired sector within which the closed-loop poles are to be located. The feedback gain matrix $\mathbf{K}$ and the weight matrix $\mathbf{Q}$ which place the closed-loop poles in the chosen sector are then determined.

One of the numerical issues encountered in using the LQR problem for the SSF with large TEAs is the solution of the associated Riccati equation. As the order of the Riccati equation to be solved in this study is fairly high

- the closed-loop system is 24th order, however, the Hamiltonian formed is 48th order - use of the algorithms existing in the various control system design packages resulted in very inaccurate solutions. Therefore, the Riccati equation involved in the LQR/Pole placement algorithm was solved using the matrix sign function [6], with the following expression used for the evaluation of the matrix sign function:

$$sign(\mathbf{A}) = \lim_{k \to \infty} \mathbf{S}(k) \tag{5.5}$$

where $\mathbf{S}(k)$ is evaluated using the following recursive expression:

$$\mathbf{S}(k+1) = \mathbf{S}(k)[5\mathbf{I} + 10\mathbf{S}^2(k) + \mathbf{S}^4(k)][\mathbf{I} + 10\mathbf{S}(k) + 5\mathbf{S}^4(k)]^{-1} \tag{5.6}$$

with $\mathbf{S}(0) = \mathbf{A}$.

The LQR based control gains have been obtained for various assumed SSF configurations. The inertias for two of the configurations analyzed are given in Table 1, along with the corresponding estimated values of the TEA. The Assembly Flight #3 (MB3) corresponds to a highly non-symmetric SSF configuration, resulting in a large value of pitch TEA. In contrast the AC configuration corresponds to a highly symmetric configuration with small TEA. The numerical values of the gains for these two configurations can be obtained from the figures presented in the following pages. For all of the linear designs the closed-loop pole locations are chosen to be within the sector shown in Figure 5.2, as it has been the experience of the authors that containing the closed-loop poles in this region reveals relatively "good" system performance.

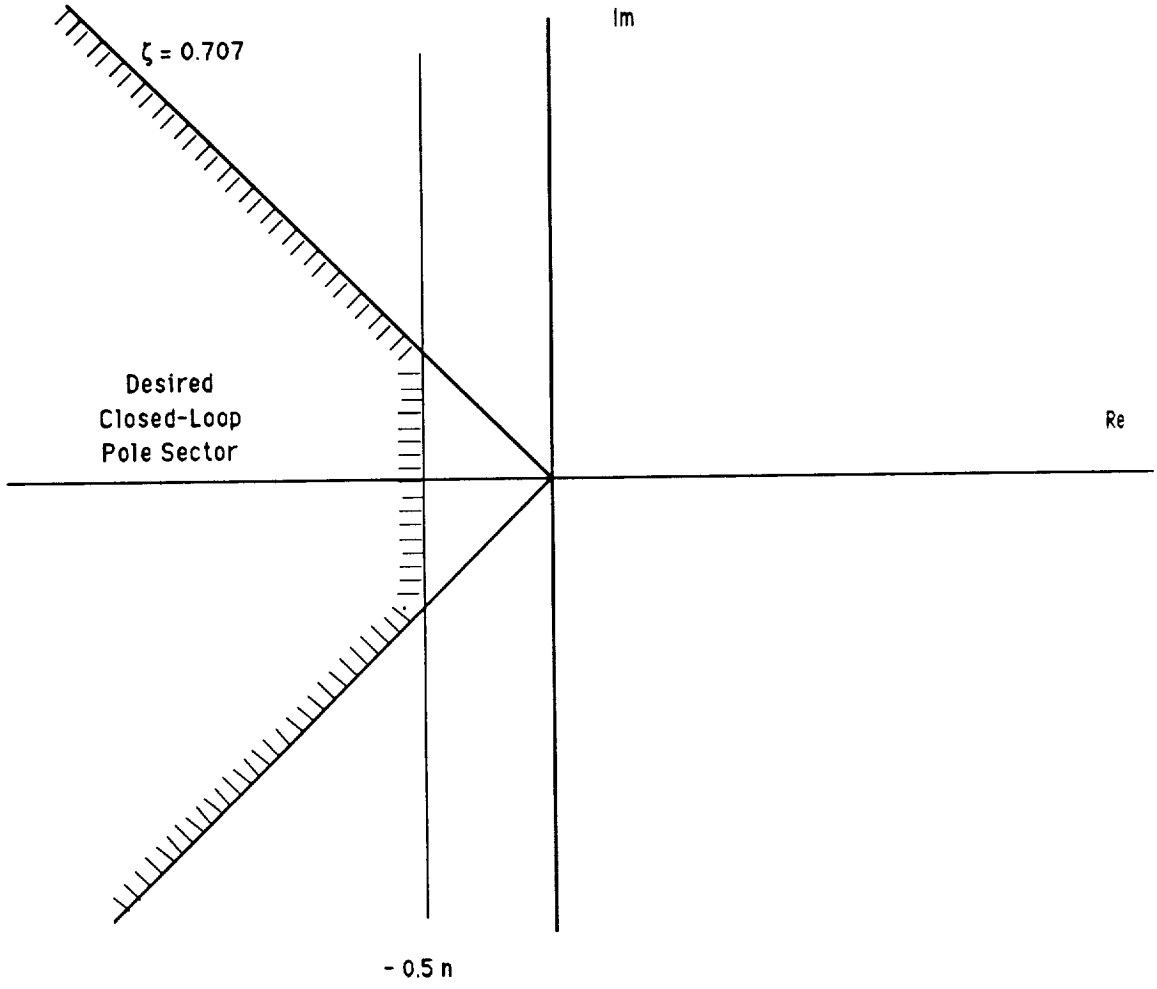

Figure 5.2: Pole Assignment Sector for the LQ Pole Placement Algorithm.

Table 1. Space Station Freedom Configuration Parameters

Parameters	MB3	AC
Inertia $(slug - ft^2)$		
I_{11}	23.22×10^6	50.28×10^6
I_{22}	1.30×10^6	10.80×10^6
I_{33}	23.23×10^6	58.57×10^6
I_{12}	-0.023×10^6	-0.39×10^6
I_{13}	0.477×10^6	0.16×10^6
I_{23}	-0.011×10^6	0.16×10^6
TEA $(degrees)$		
θ_1^*	1.3	0.19
θ_2^*	-44.7	-5.0
θ_3^*	2.1	0.56

5.3 Gain-Scheduling of the Linear Gains

Gain-scheduling allows nonlinear control system implementation of linear control laws, which have been designed using any linear design method. A gain-scheduled control law is an open-loop adaptive control system [7]. Even though feedback control is used, the adaptation is open-loop and the system performance may suffer. A continuous gain-scheduled control system is designed by simply fitting the various LQR gain matrices to a certain nonlinear function.

In view of the linearized system model of equation (4.46), the linear

control law obtained by repeated application of the LQR algorithm is:

$$\mathbf{u}(t) = \mathbf{K}_i \mathbf{x}(t) \tag{5.7}$$

where $i = 1, 2, ..$ is the number of SSF configurations for which the LQR algorithm has been applied. Second order polynomials were used to schedule the elements of the gain matrices $\mathbf{K}_i$. The behavior of the fitted gains as a function of the TEA are depicted in Figures 5.3 through 5.25.

As a result of the nonlinear nature of the gain-scheduled controller and of the open-loop system, there is no systematic procedure to determine the performance and the stability characteristics of the nominal SSF configuration, other than to exhaustively simulate the system for a variety of scenarios and for sufficiently large number of orbits. Additionally, the robustness properties of the controller can only be investigated via numerical simulations. The results of these studies are presented in the following section.

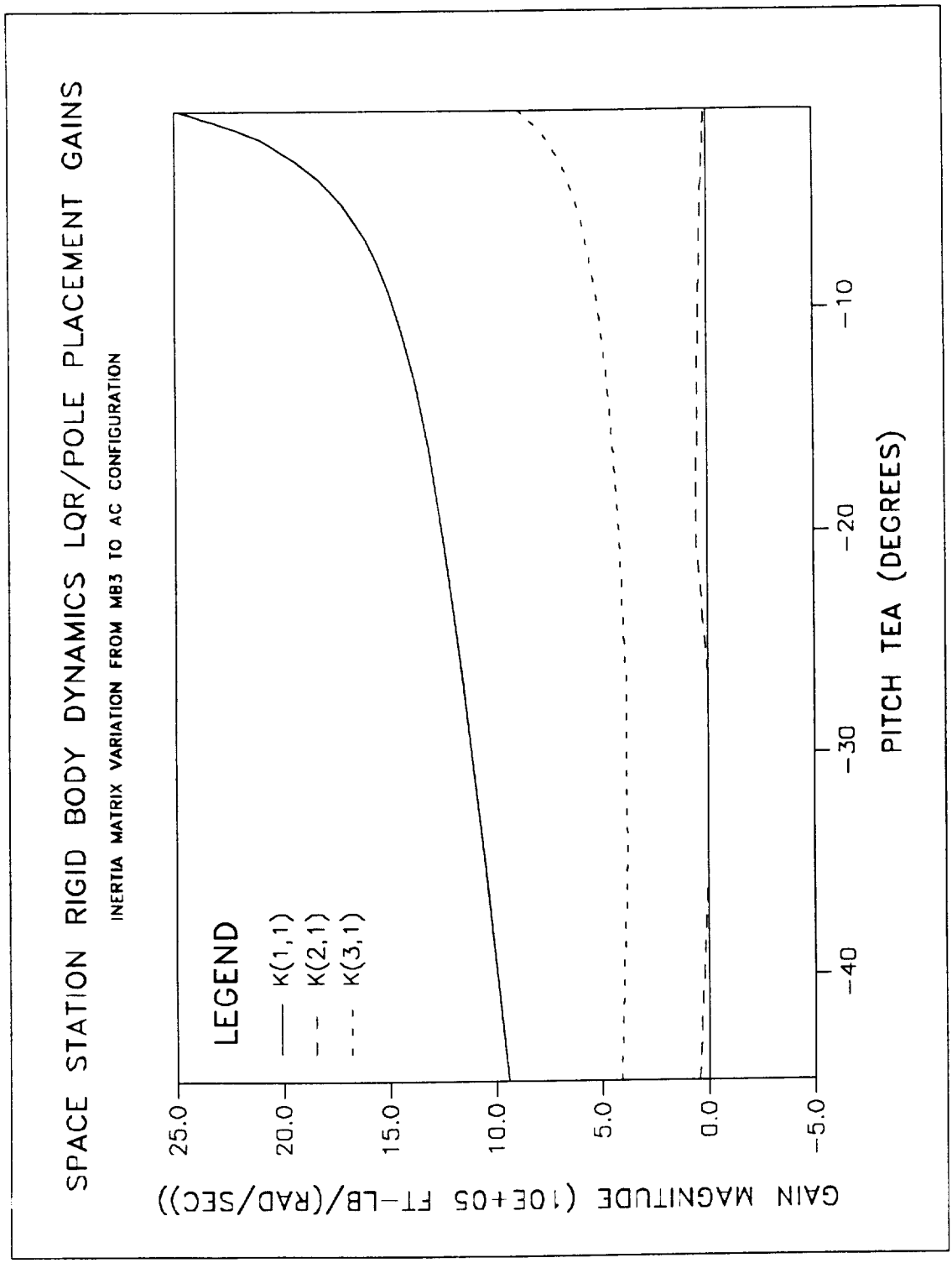

Figure 5.3: K(i,1) Gain Variation with the TEA.

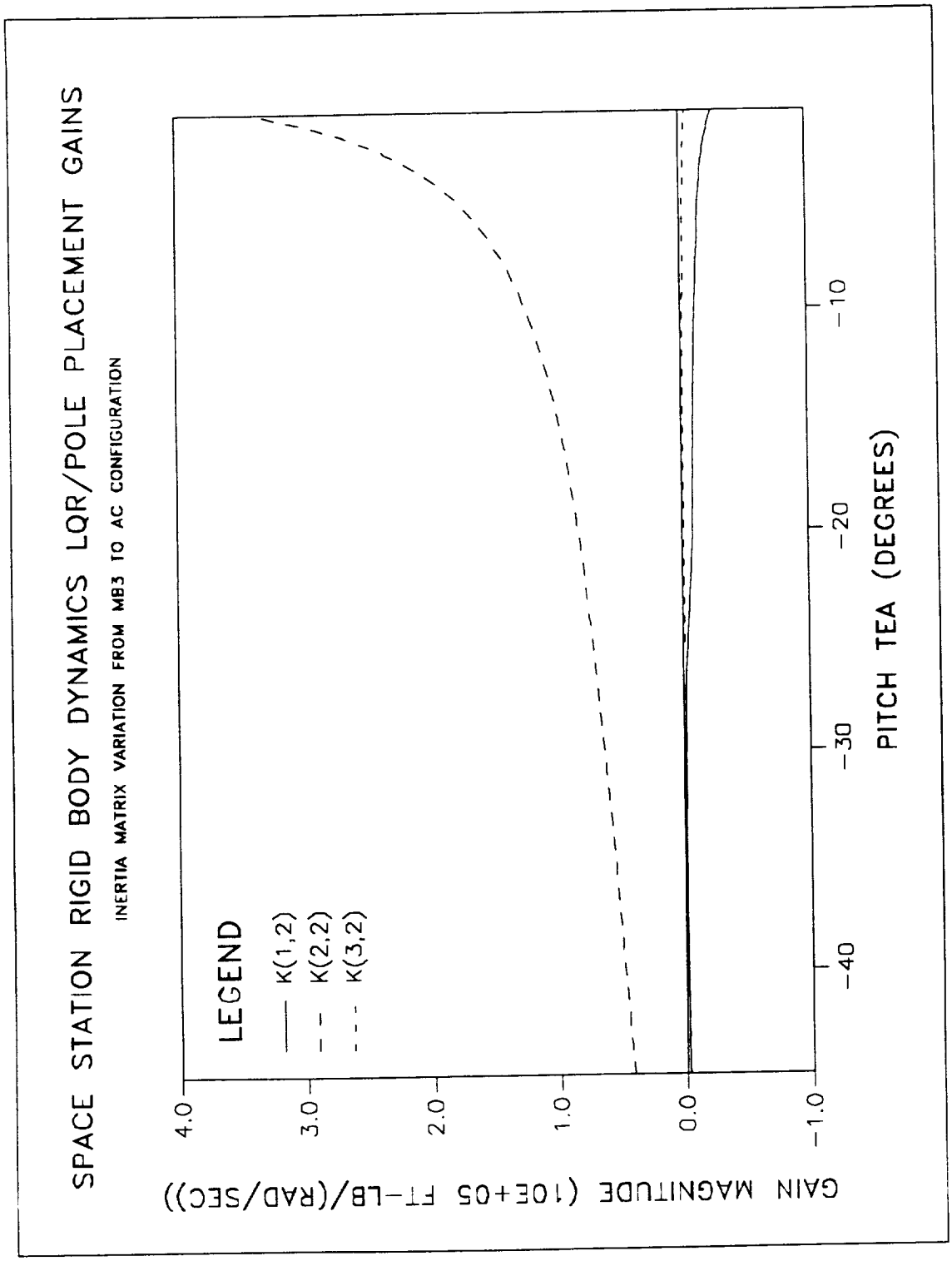

Figure 5.4: K(i,2) Gain Variation with the TEA.

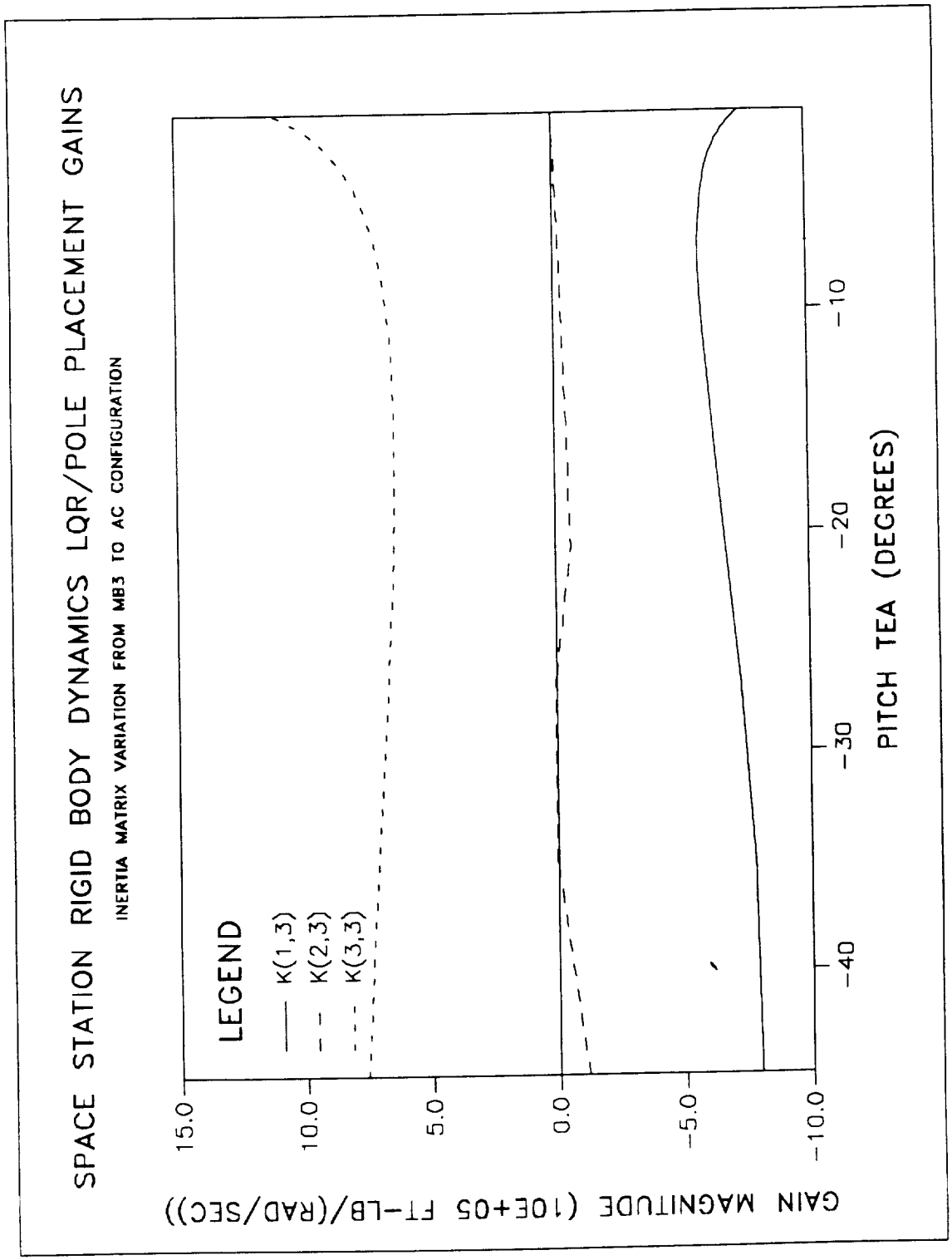

Figure 5.5: K(i,3) Gain Variation with the TEA.

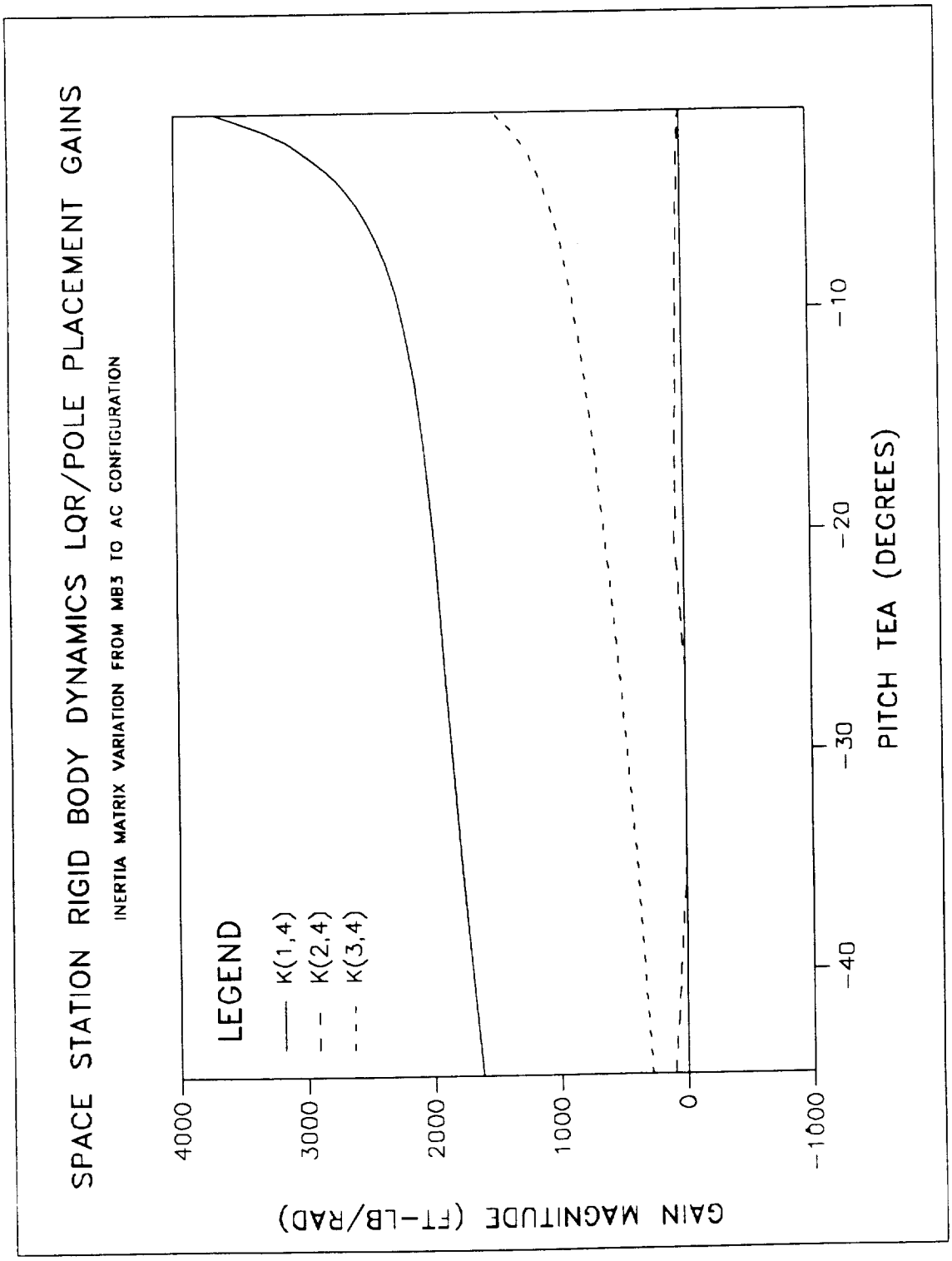

Figure 5.6: K(i,4) Gain Variation with the TEA.

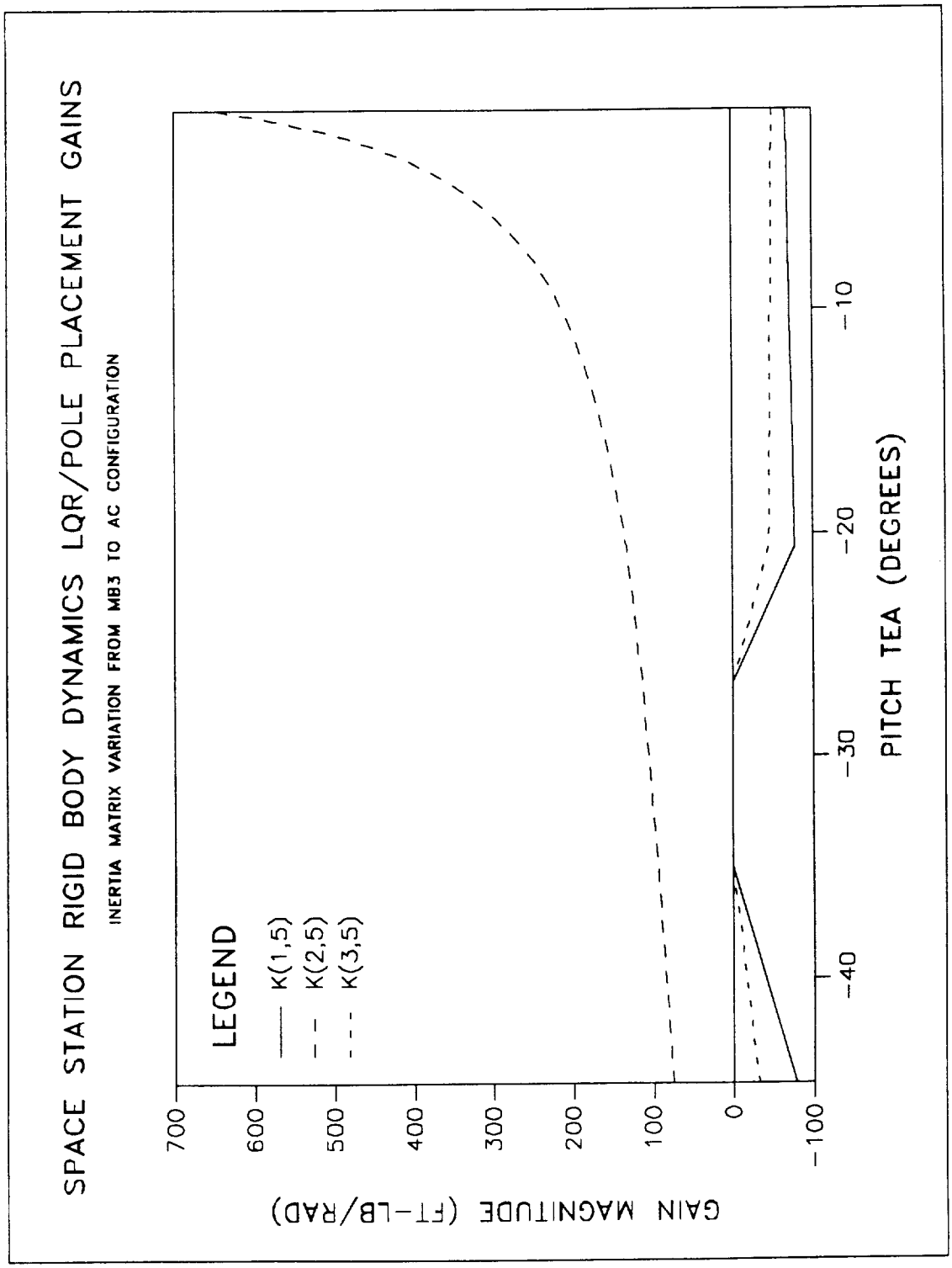

Figure 5.7: K(i,5) Gain Variation with the TEA.

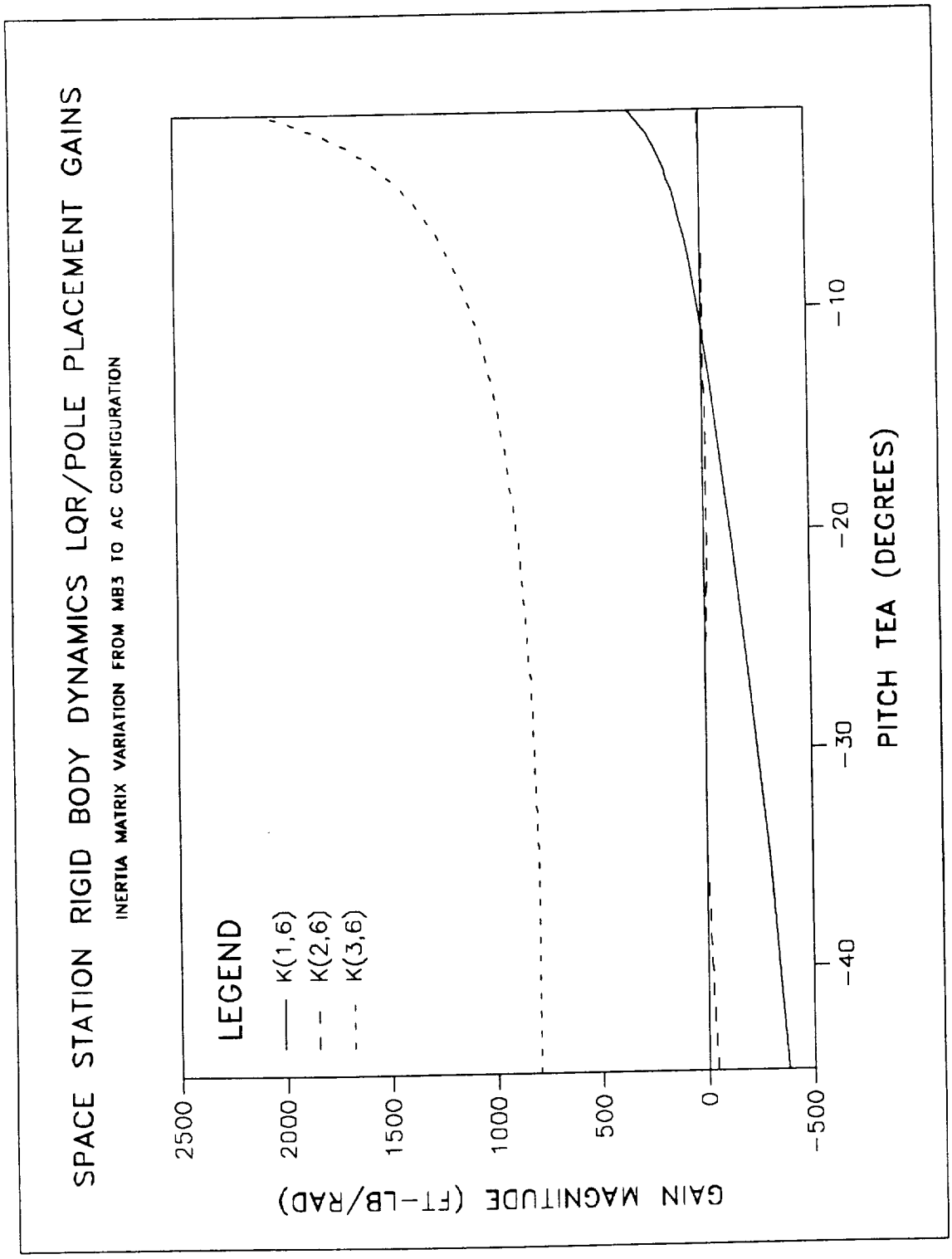

Figure 5.8: K(i,6) Gain Variation with the TEA.

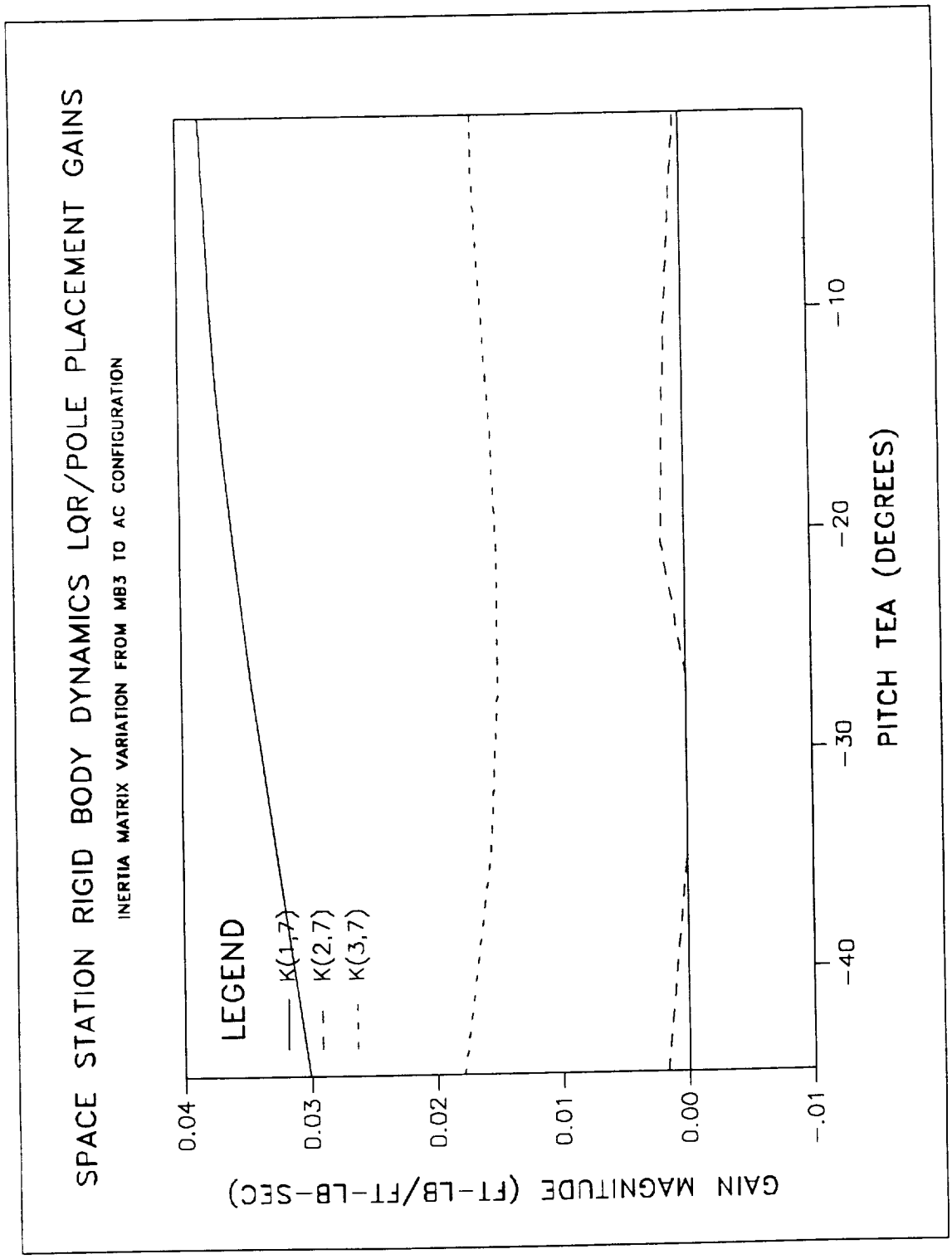

Figure 5.9: K(i,7) Gain Variation with the TEA.

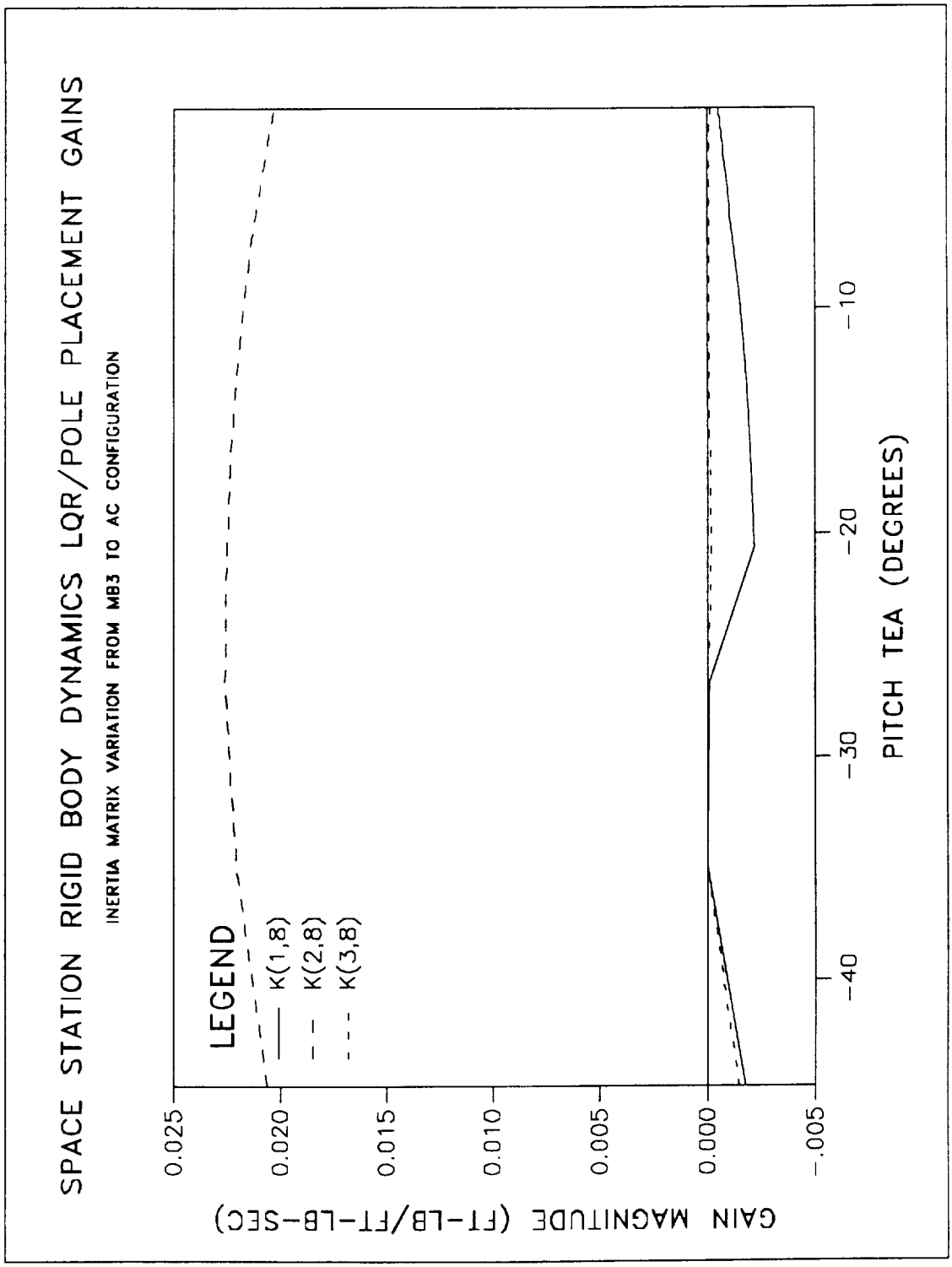

Figure 5.10: K(i,8) Gain Variation with the TEA.

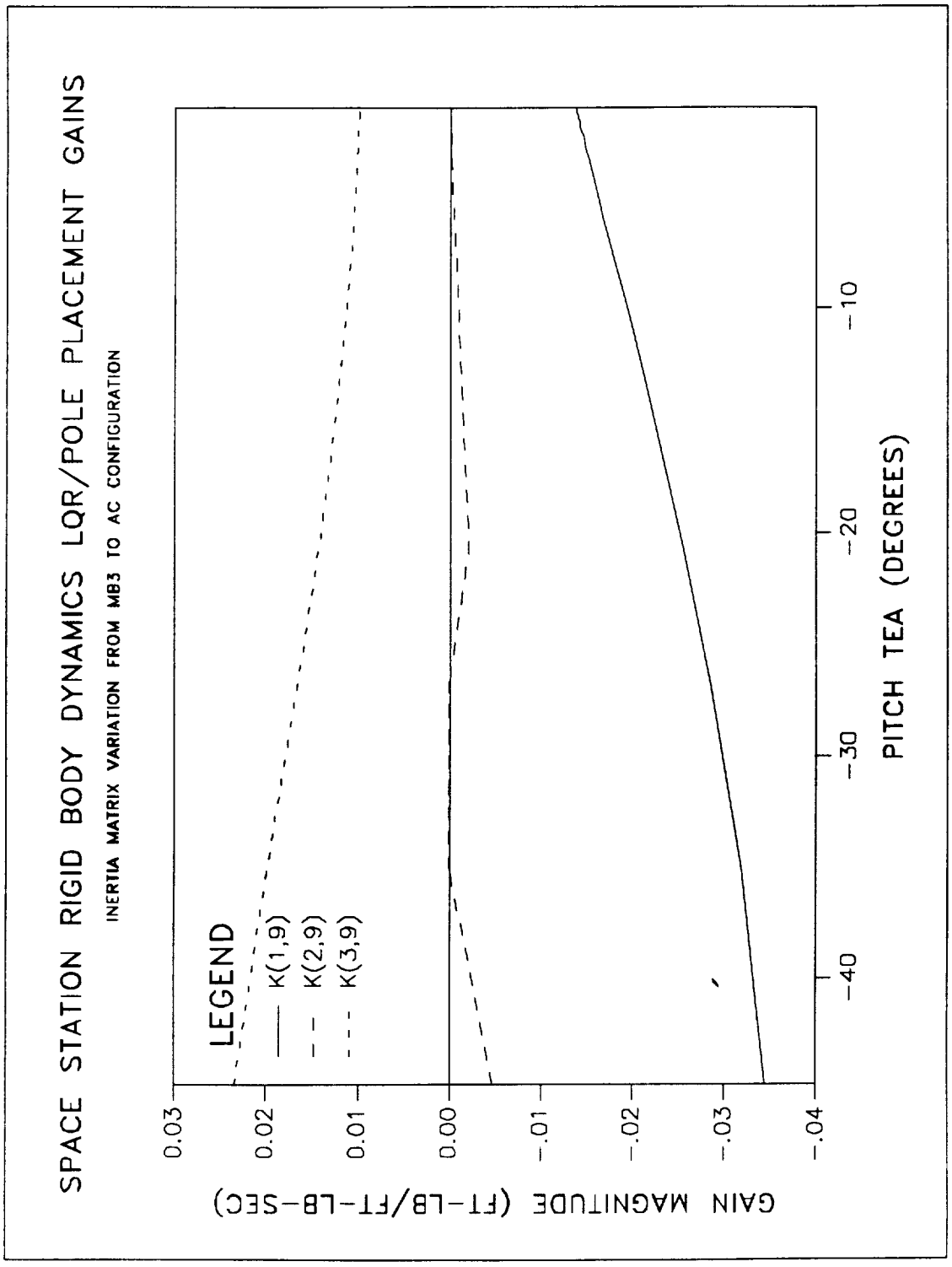

Figure 5.11: K(i,9) Gain Variation with the TEA.

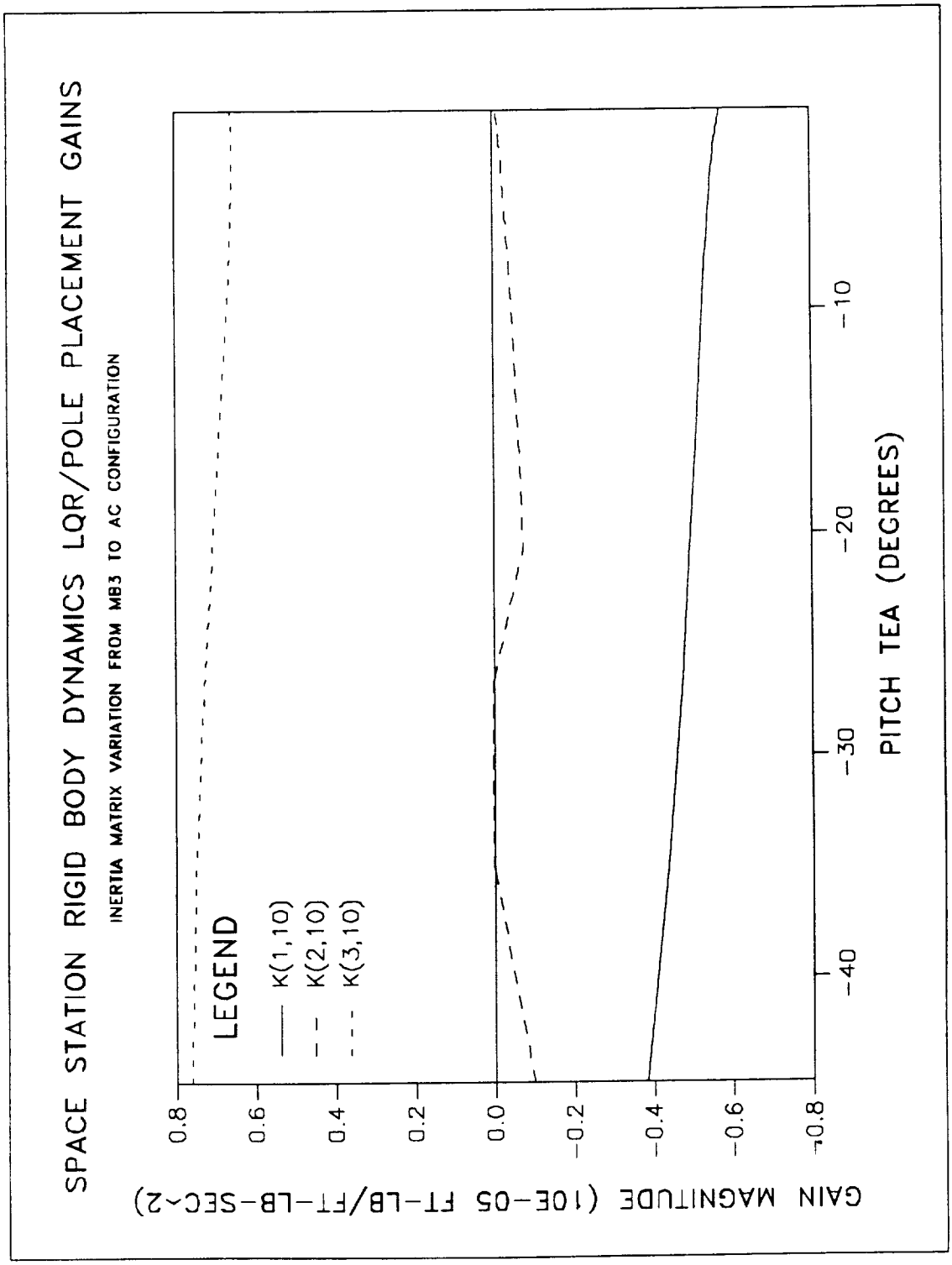

Figure 5.12: K(i,10) Gain Variation with the TEA.

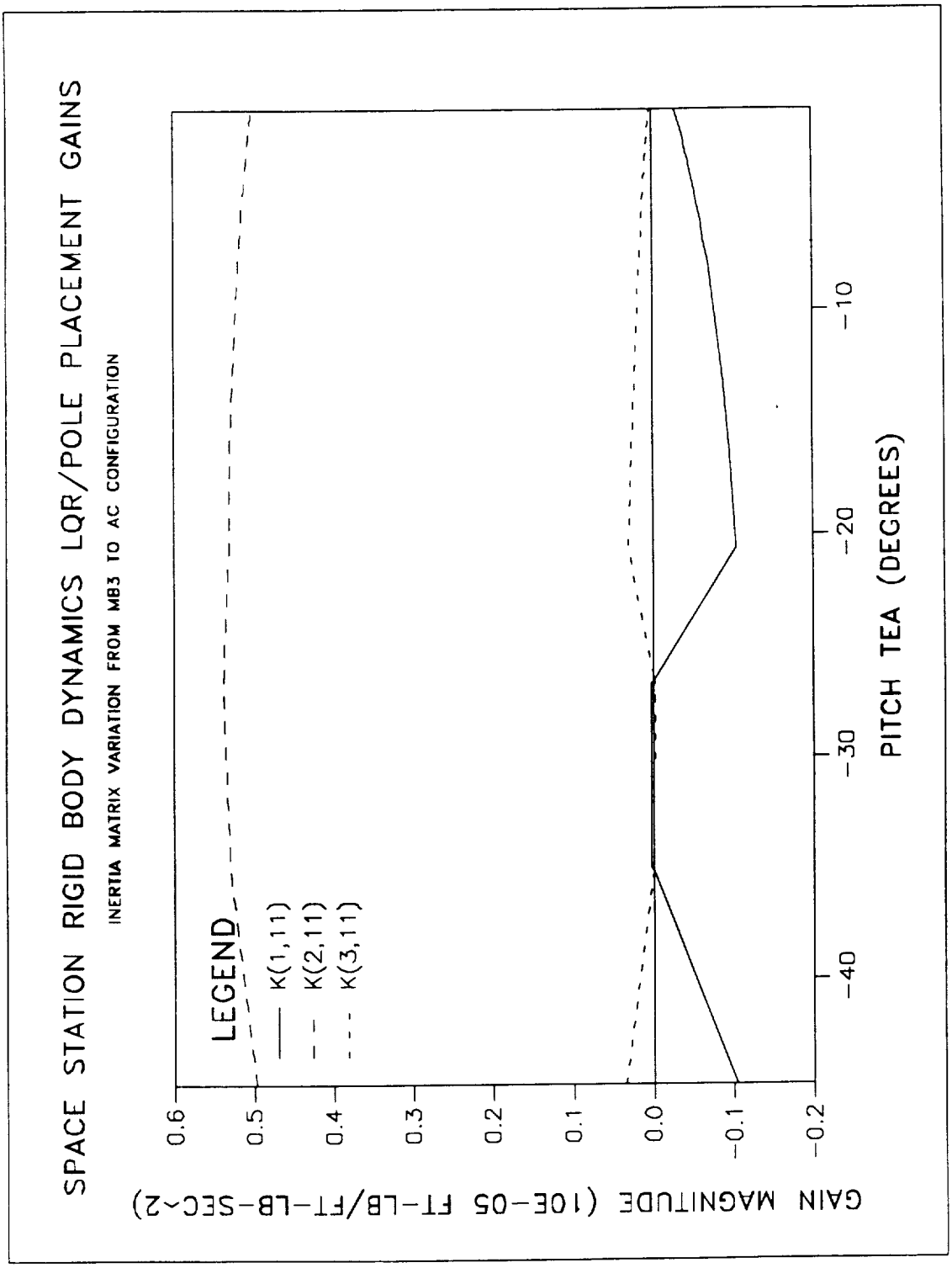

Figure 5.13: K(i,11) Gain Variation with the TEA.

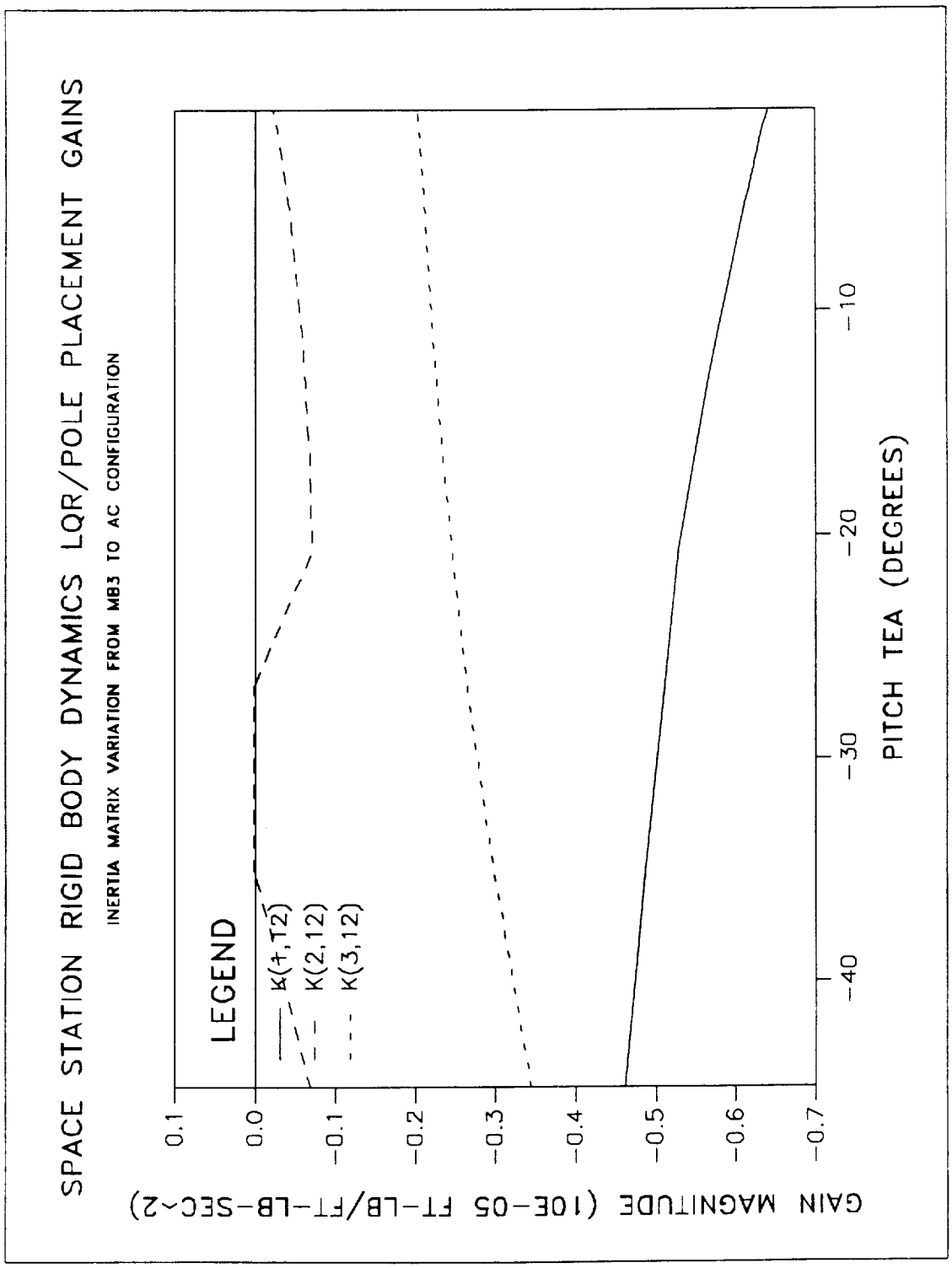

Figure 5.14: K(i,12) Gain Variation with the TEA.

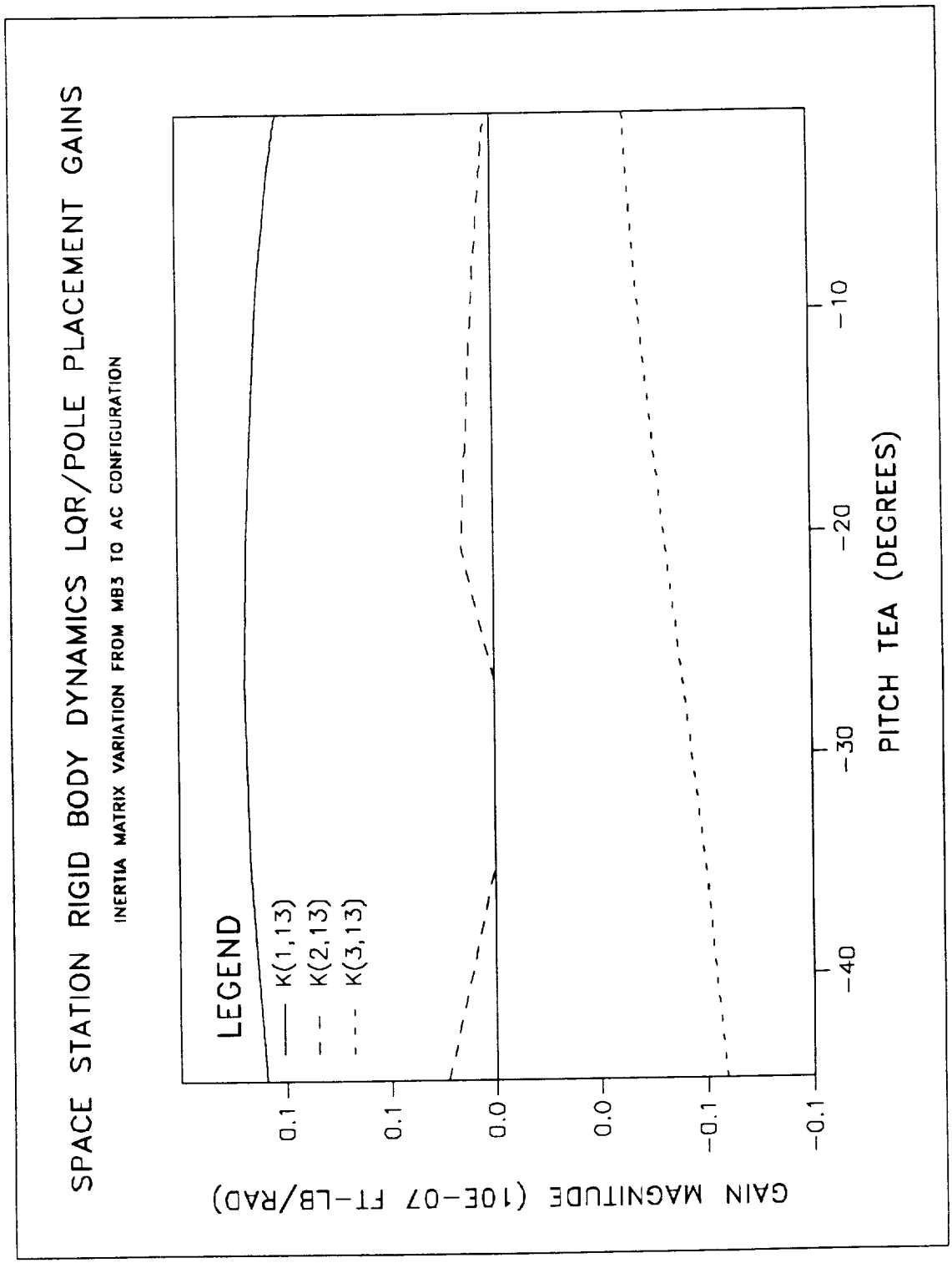

Figure 5.15: K(i,13) Gain Variation with the TEA.

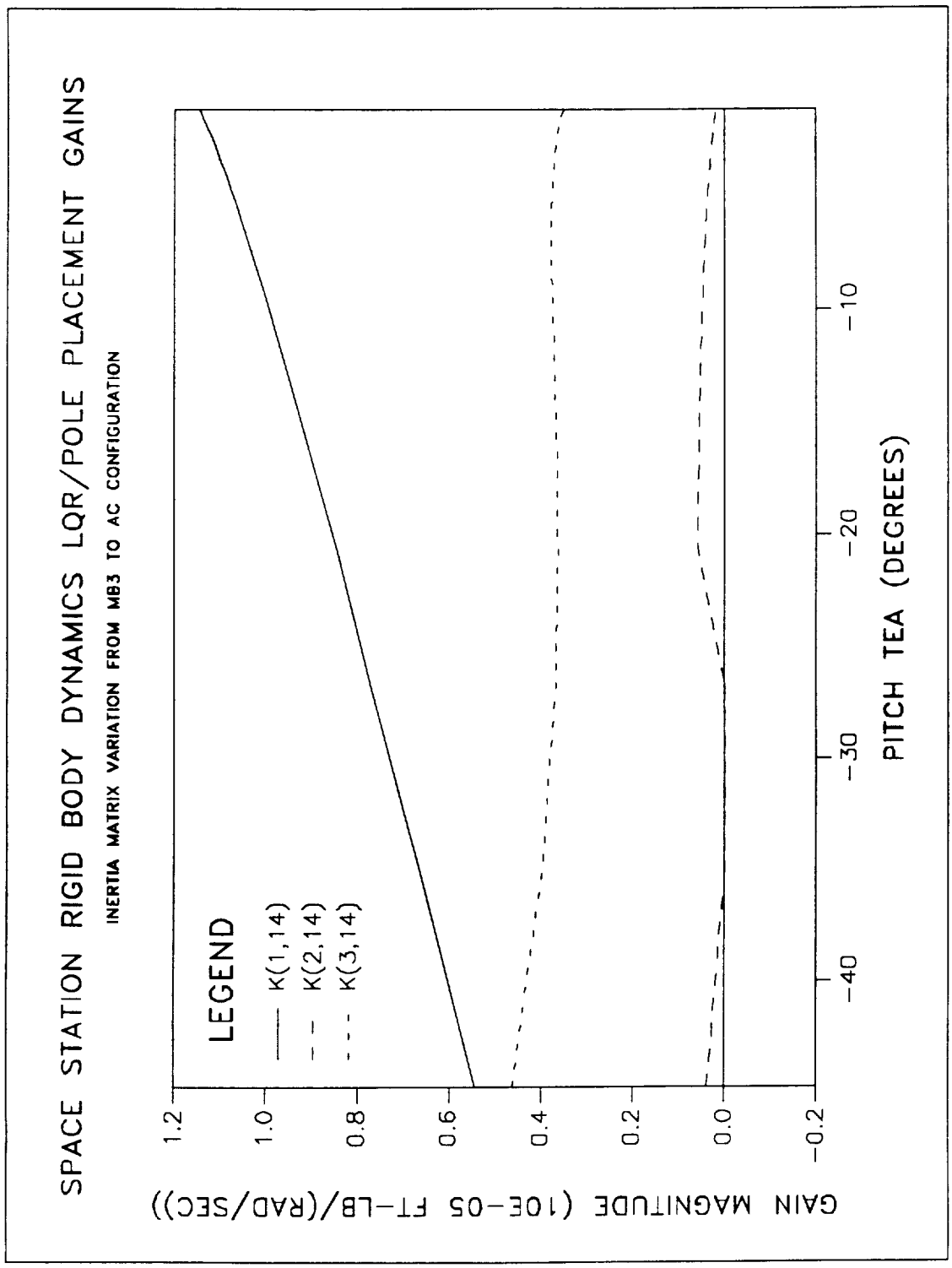

Figure 5.16: K(i,14) Gain Variation with the TEA.

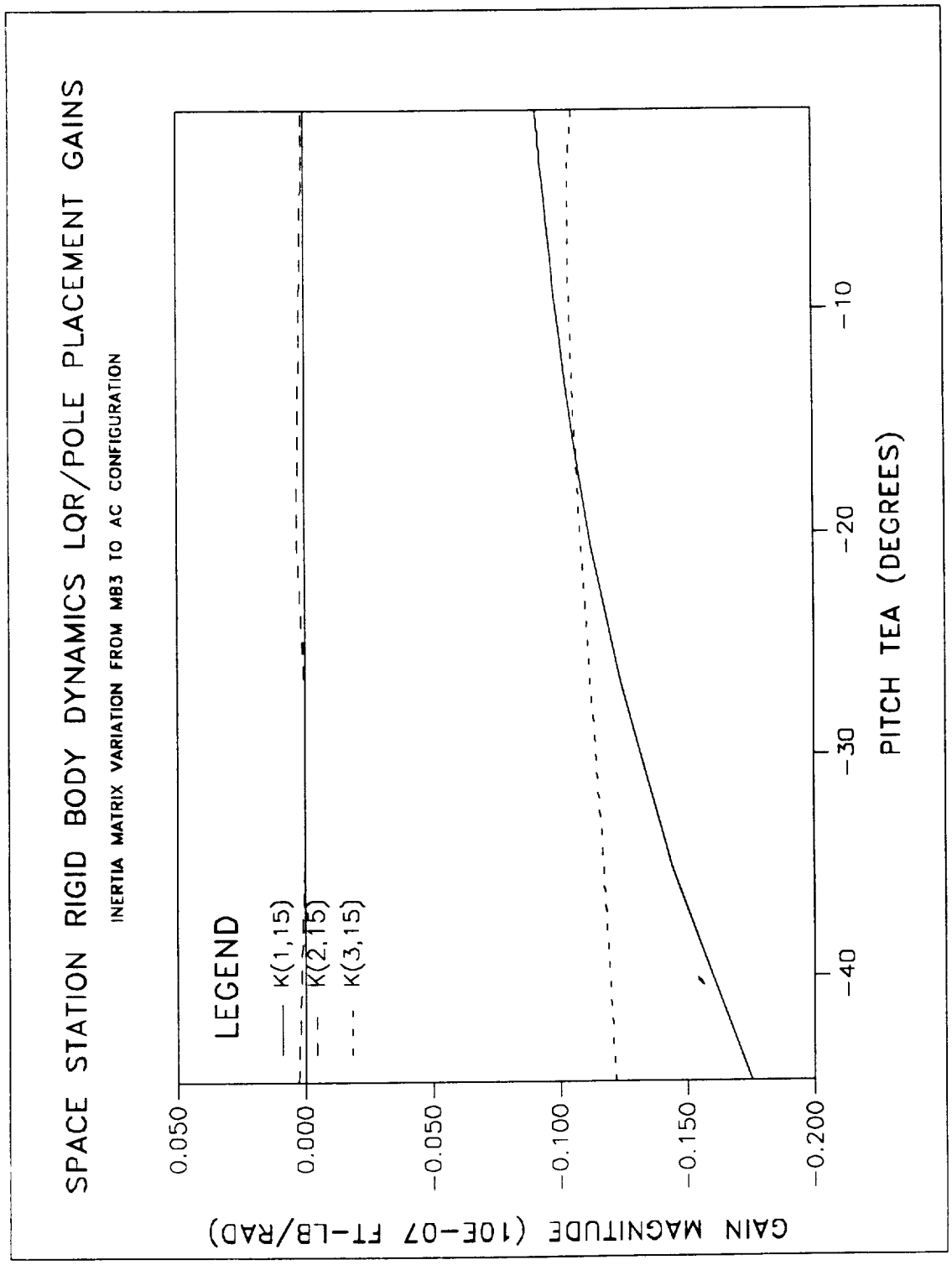

Figure 5.17: K(i,15) Gain Variation with the TEA.

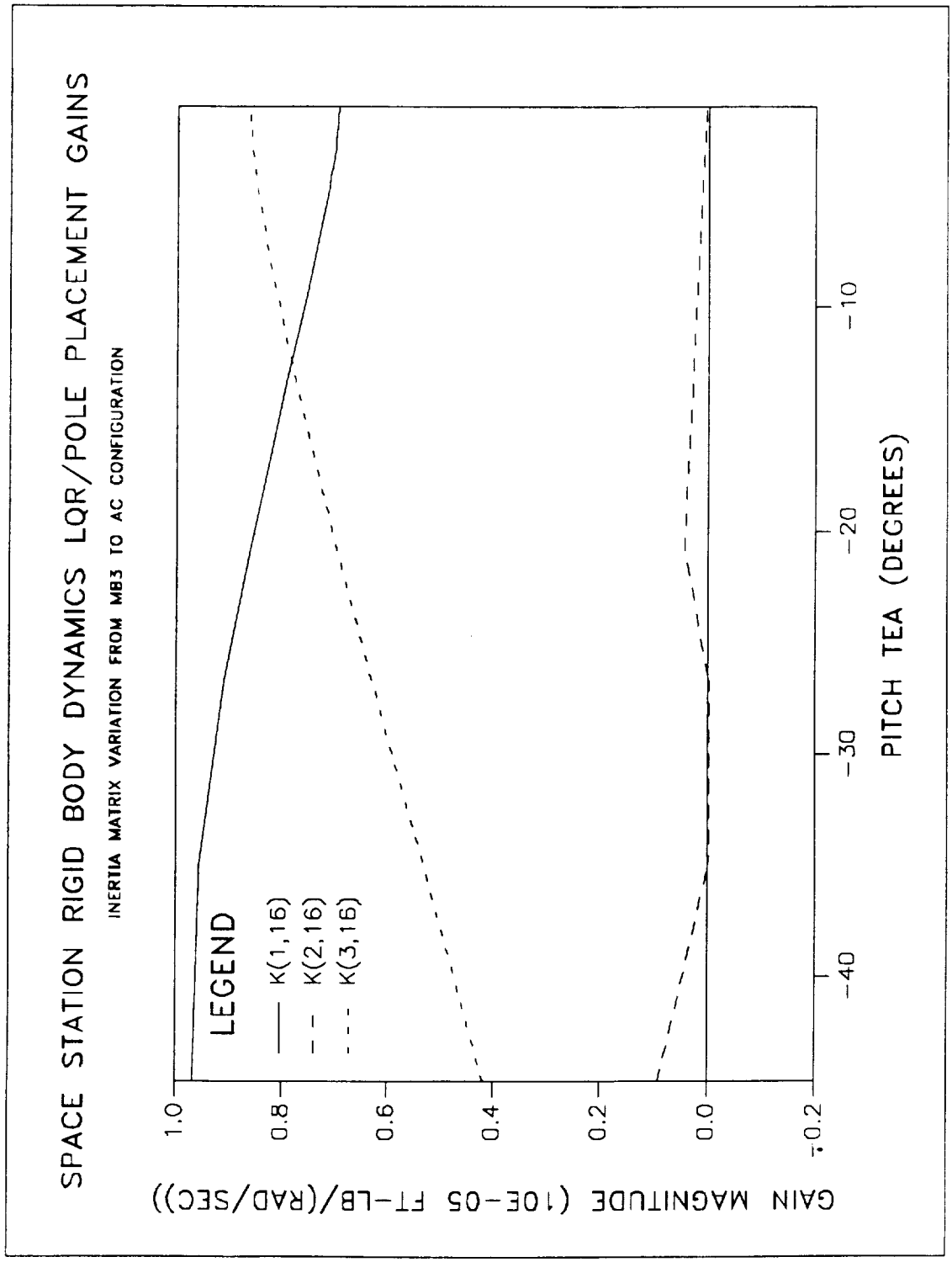

Figure 5.18: K(i,16) Gain Variation with the TEA.

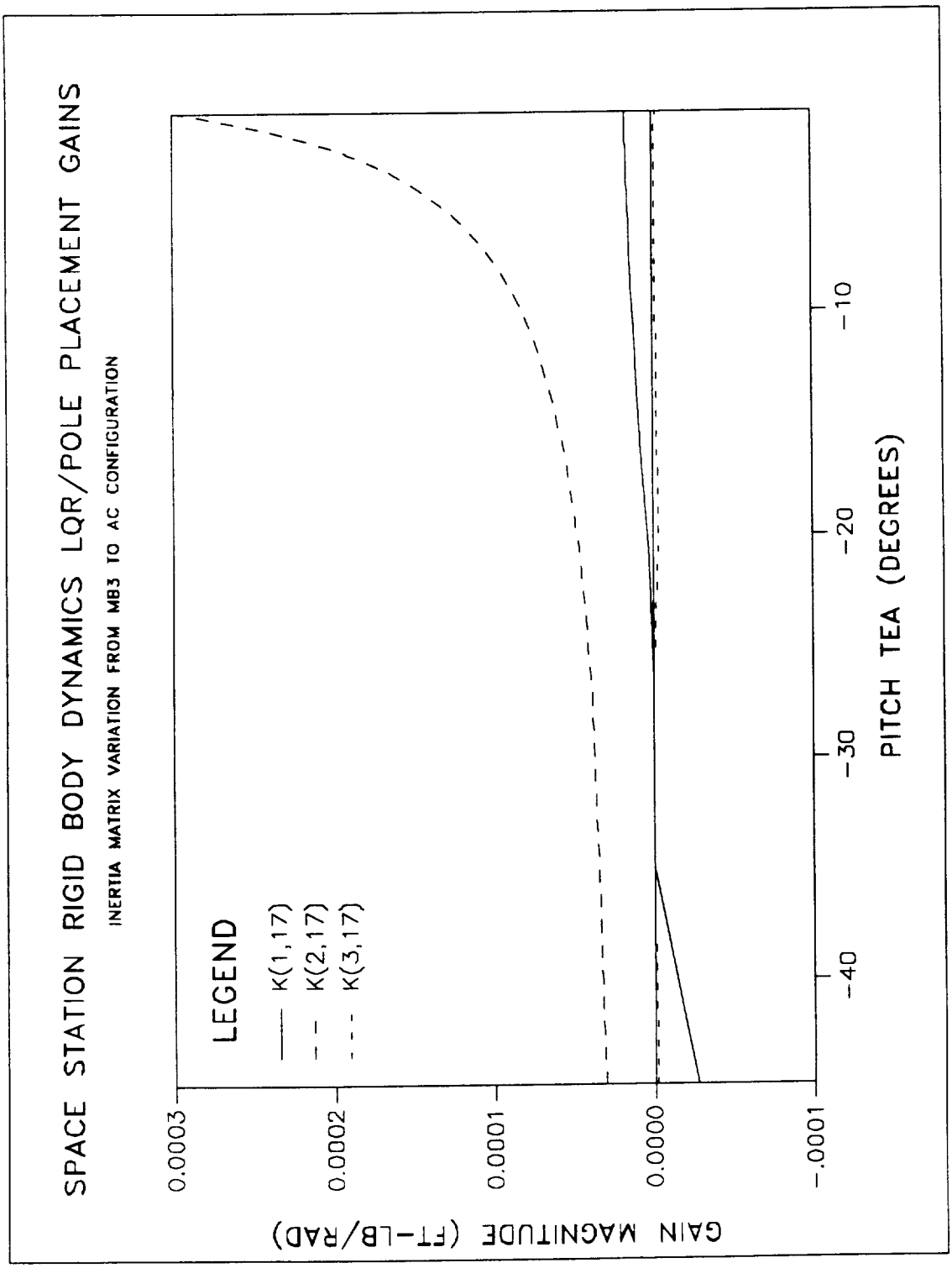

Figure 5.19: K(i,17) Gain Variation with the TEA.

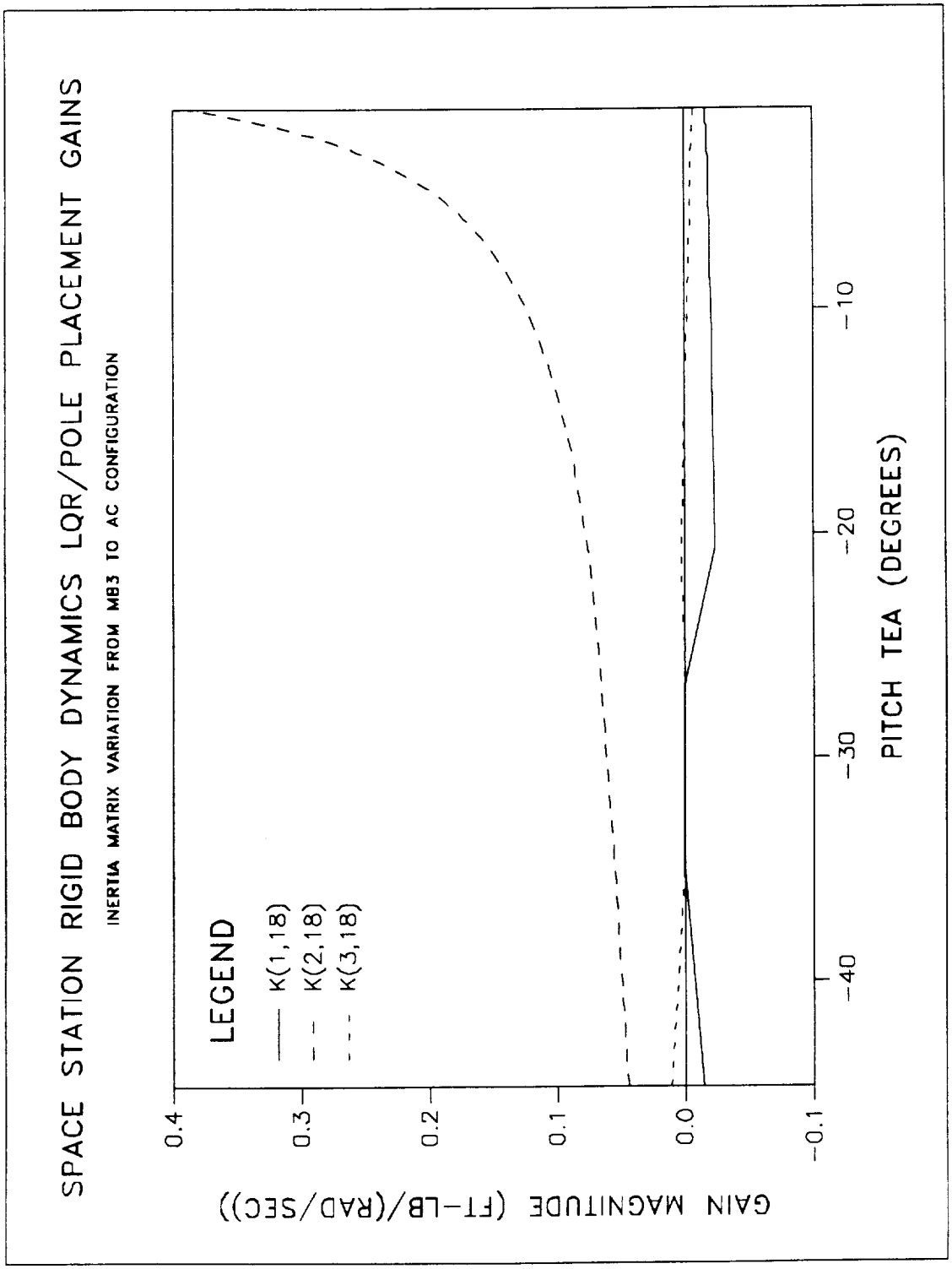

Figure 5.20: K(i,18) Gain Variation with the TEA.

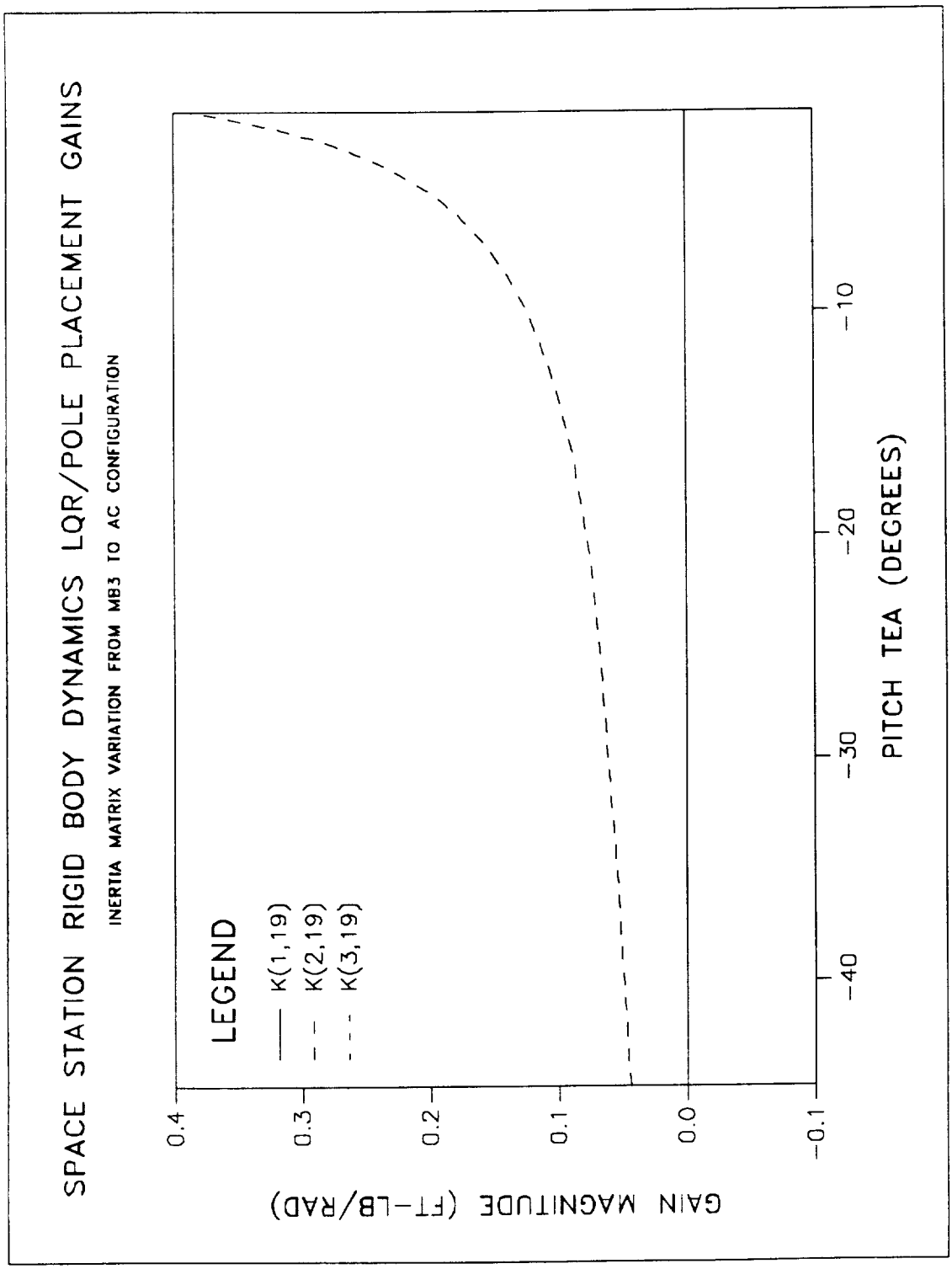

Figure 5.21: K(i,19) Gain Variation with the TEA.

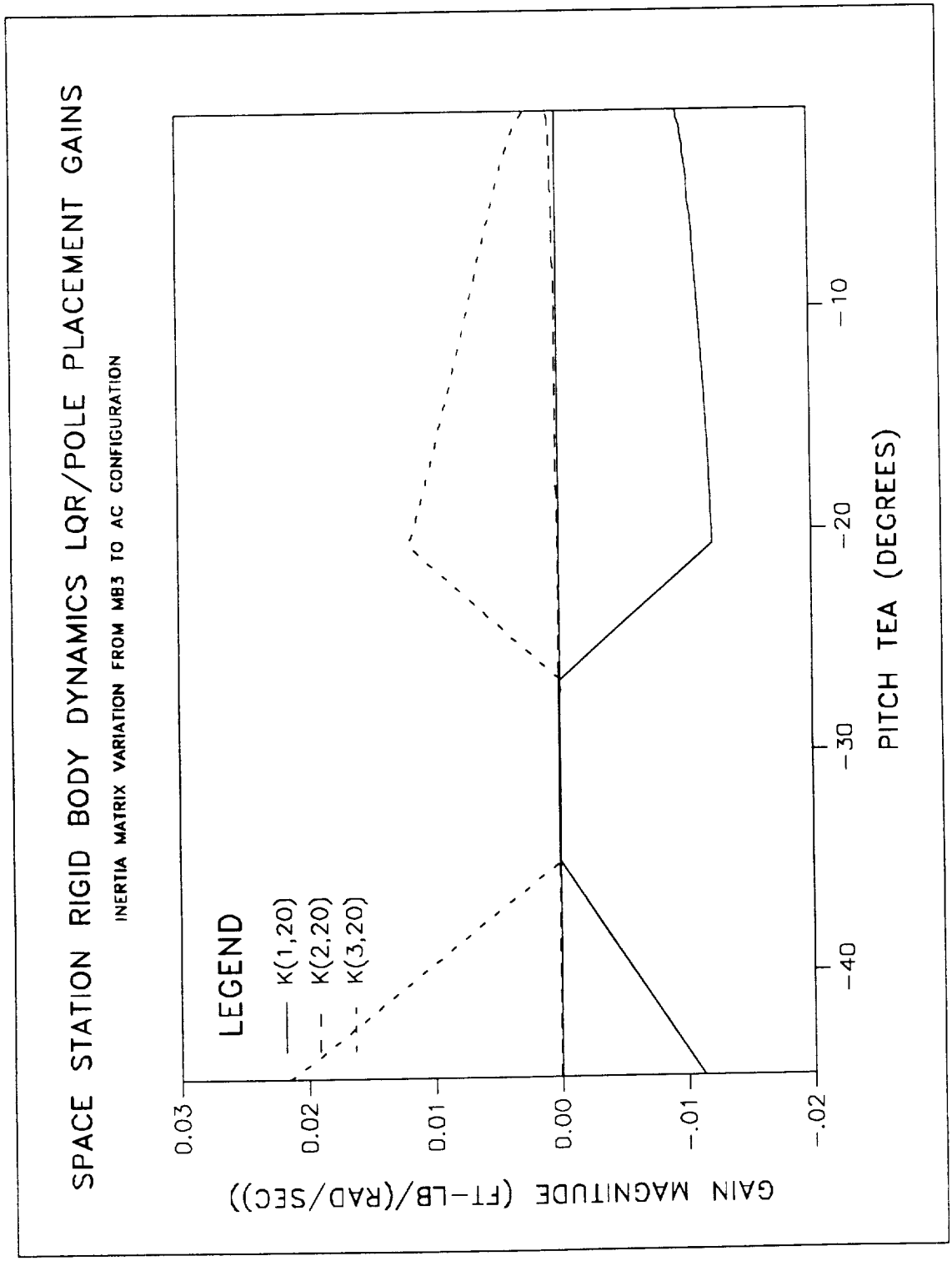

Figure 5.22: K(i,20) Gain Variation with the TEA.

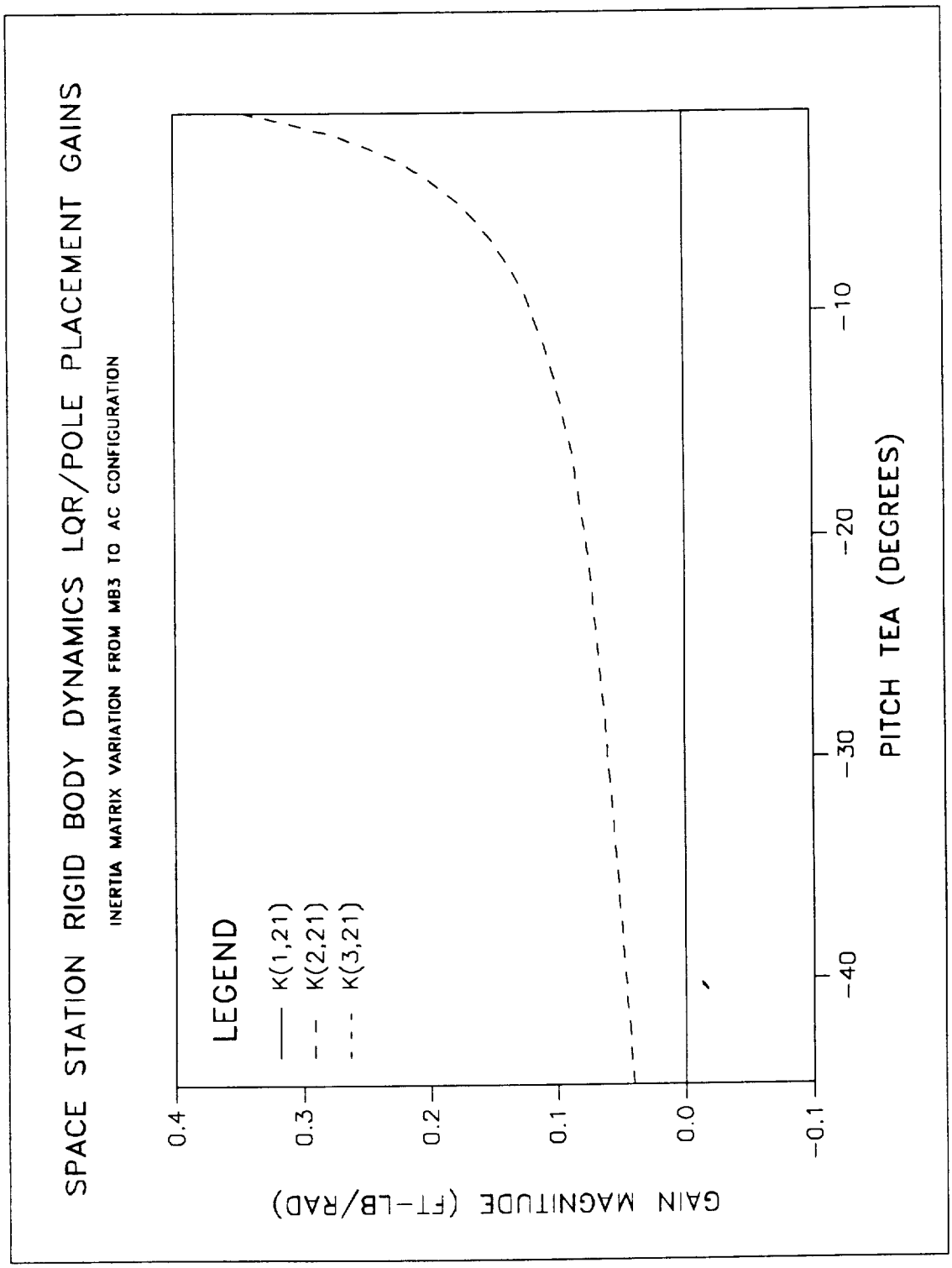

Figure 5.23: K(i,21) Gain Variation with the TEA.

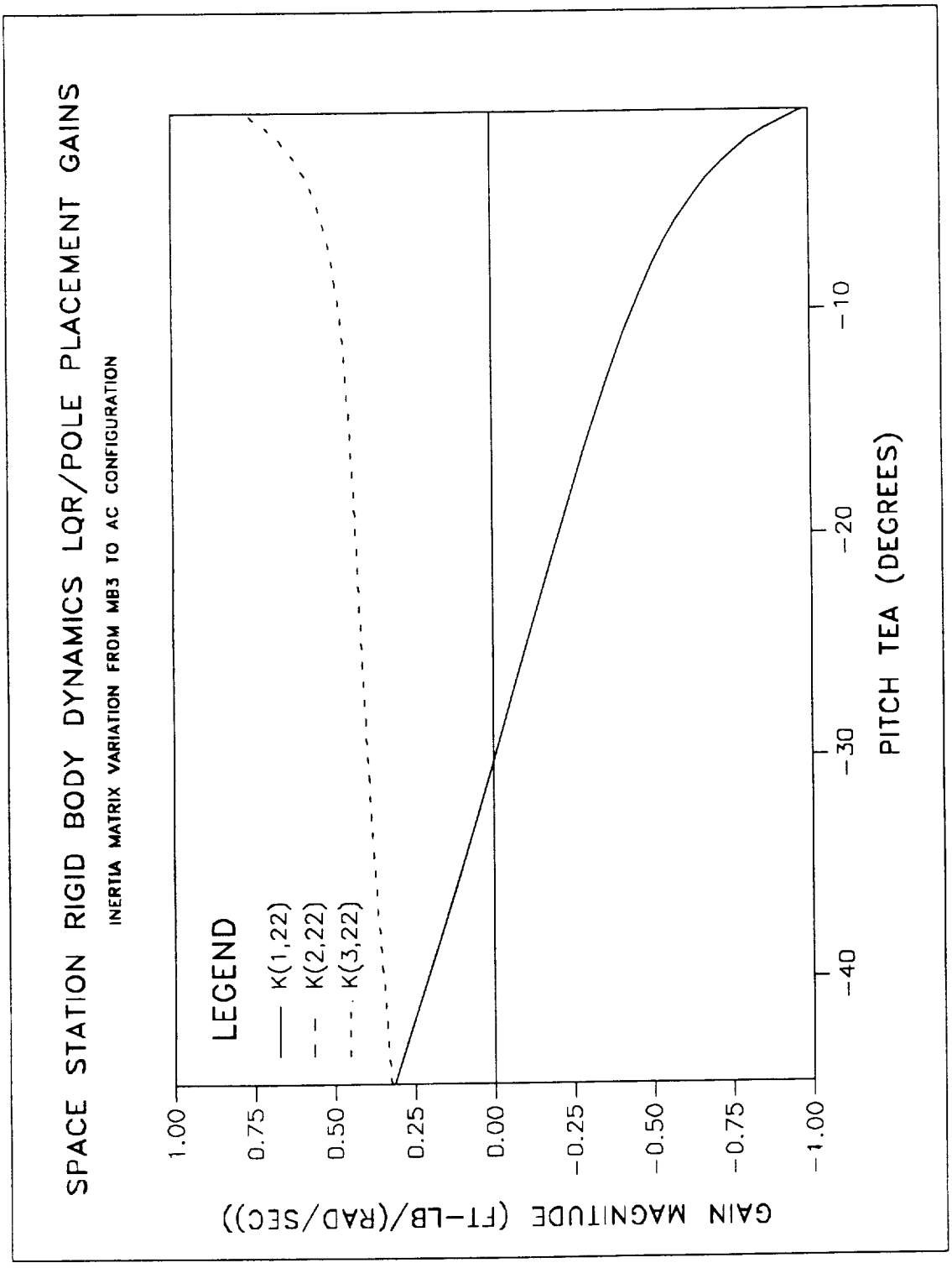

Figure 5.24: K(i,22) Gain Variation with the TEA.

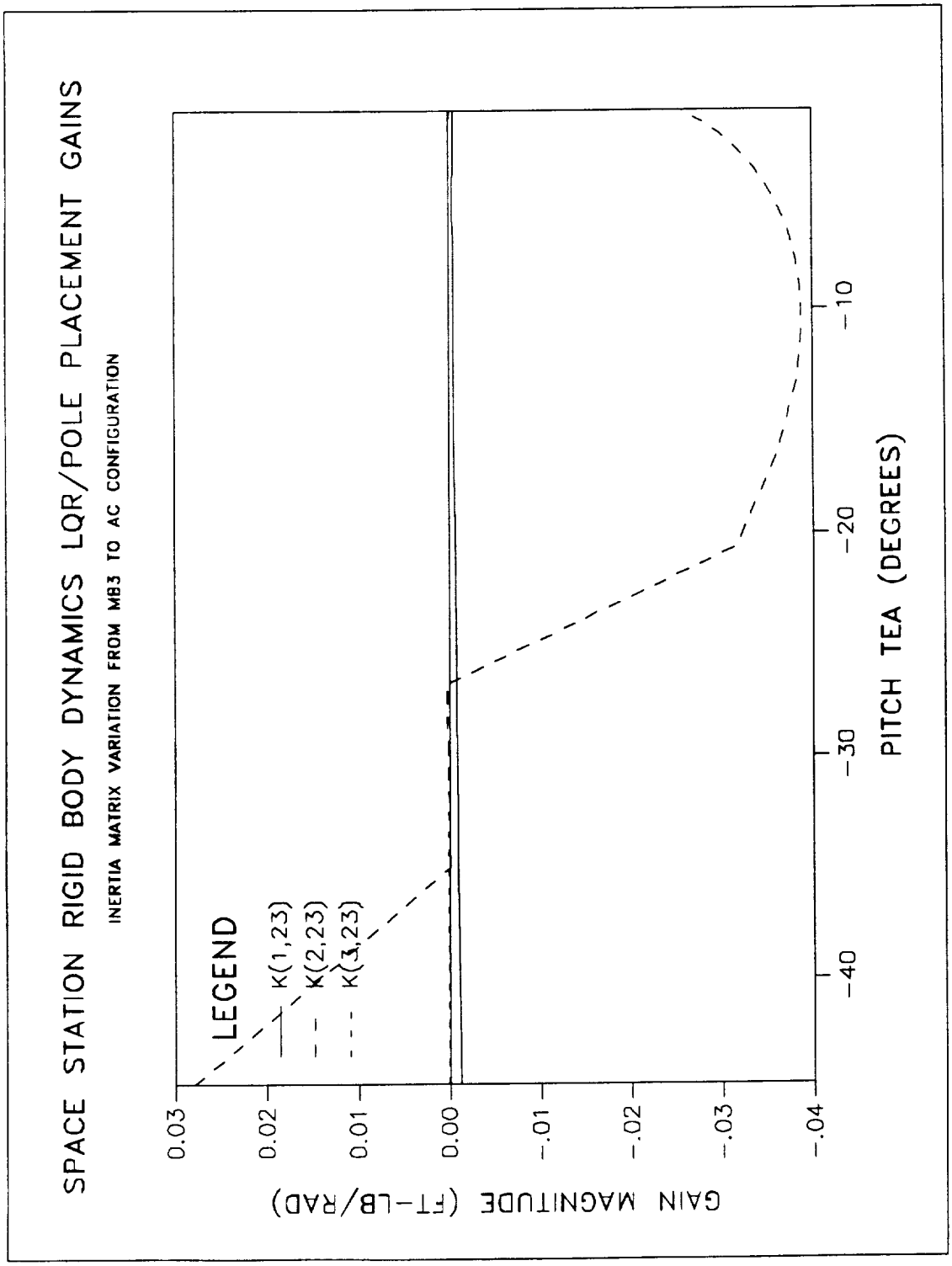

Figure 5.25: K(i,23) Gain Variation with the TEA.

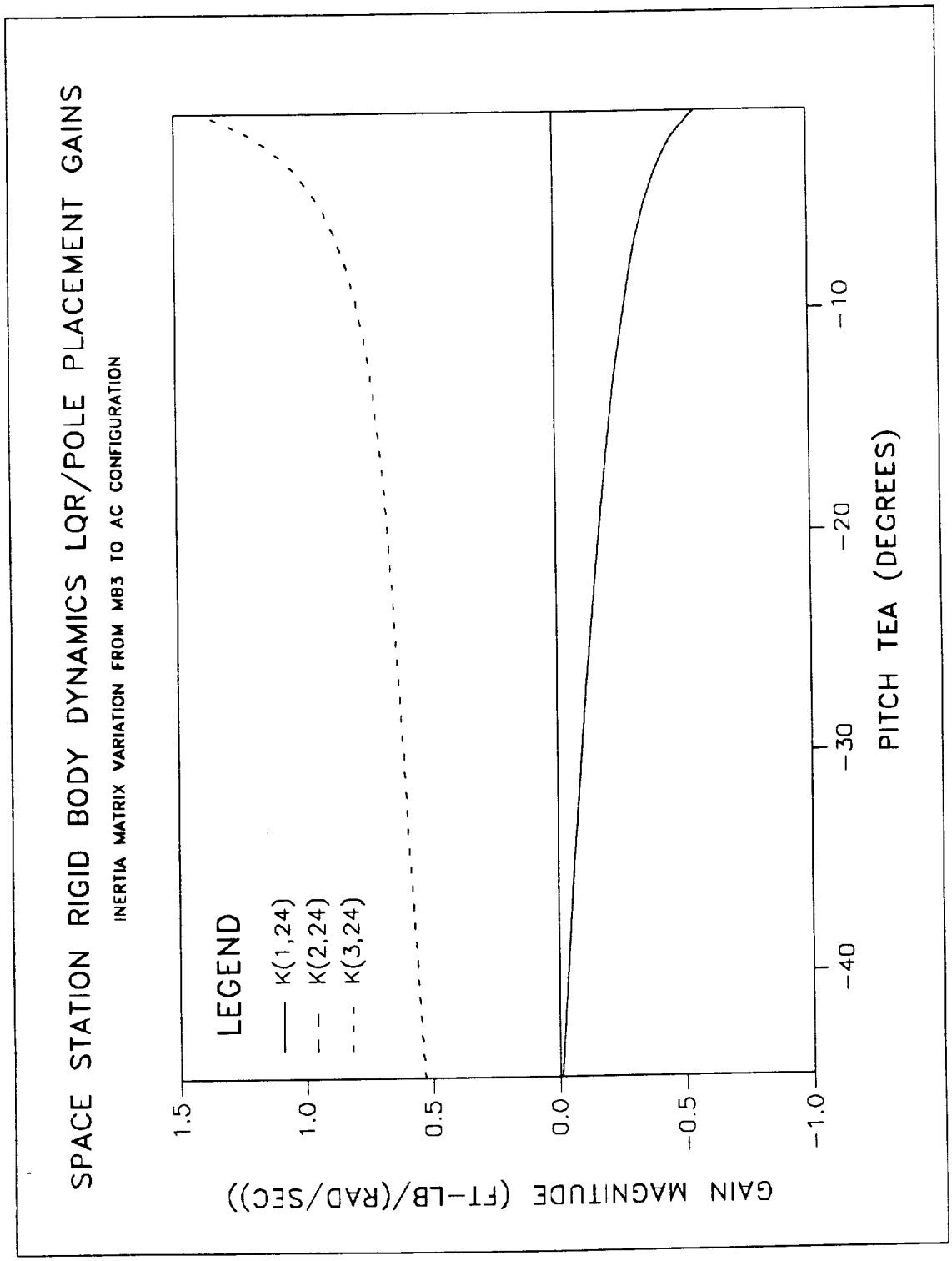

Figure 5.26: K(i,24) Gain Variation with the TEA.

Chapter 6

Simulation Results

The primary purpose of this section is to present some numerical simulations to substantiate the following two claims:

(1) Certain SSF configurations characterized by large cross-inertia terms, such as the earlier flights in the assembly sequence or during some of the MRMS operations [2], require special attention when designing linearized control systems.

(2) Because of the slowly time-varying nature of the SSF dynamics, a gain-scheduled control system provides "good" closed-loop performance, even for fairly large variations in the SSF inertia matrix. This results in less complex control laws as compared to alternate adaptive schemes requiring on-line identification, though, the system performance may suffer if the uncertainty in the inertia matrix is very high.

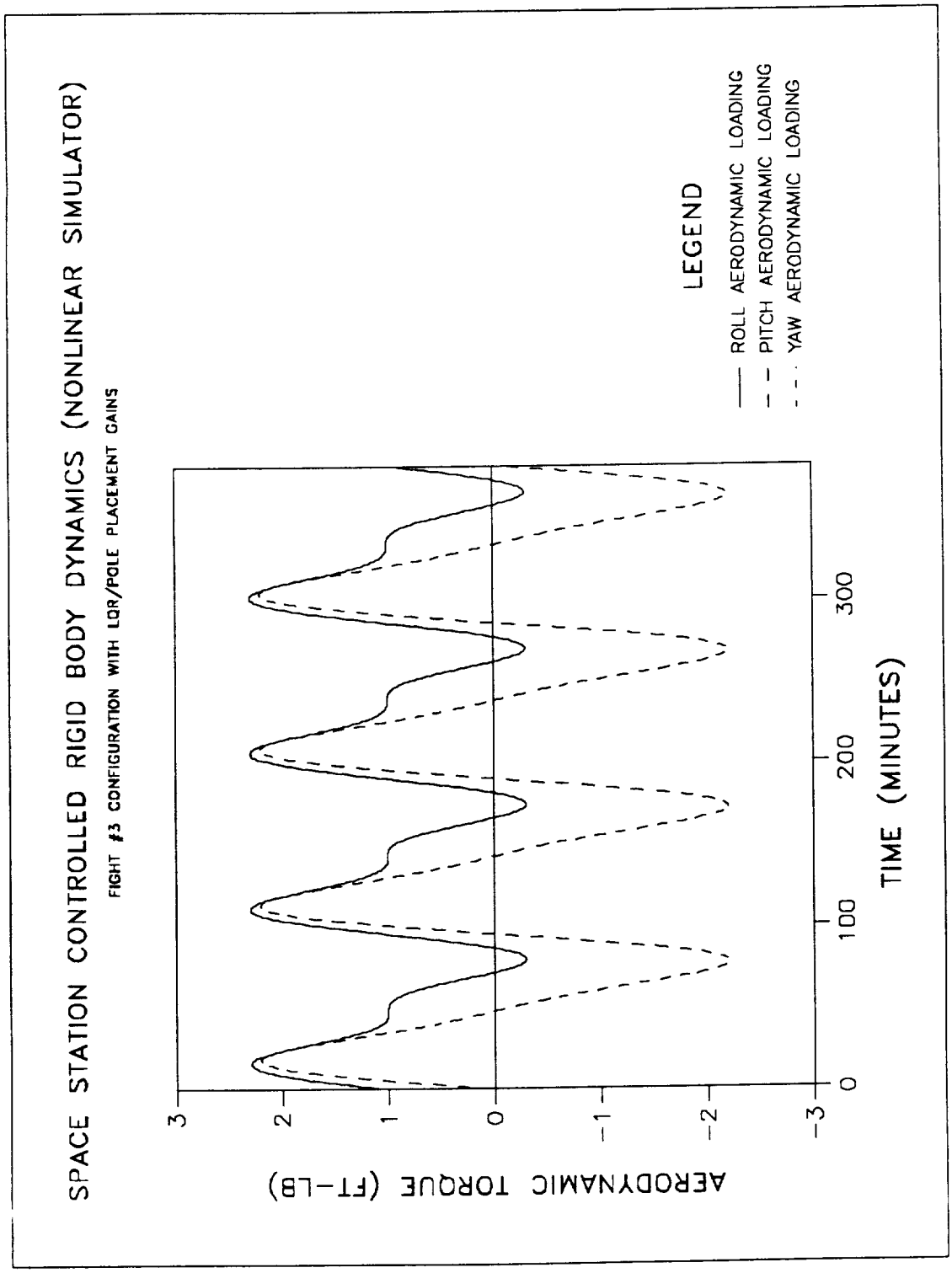

Figure 6.1: Aerodynamic Torque Profiles.

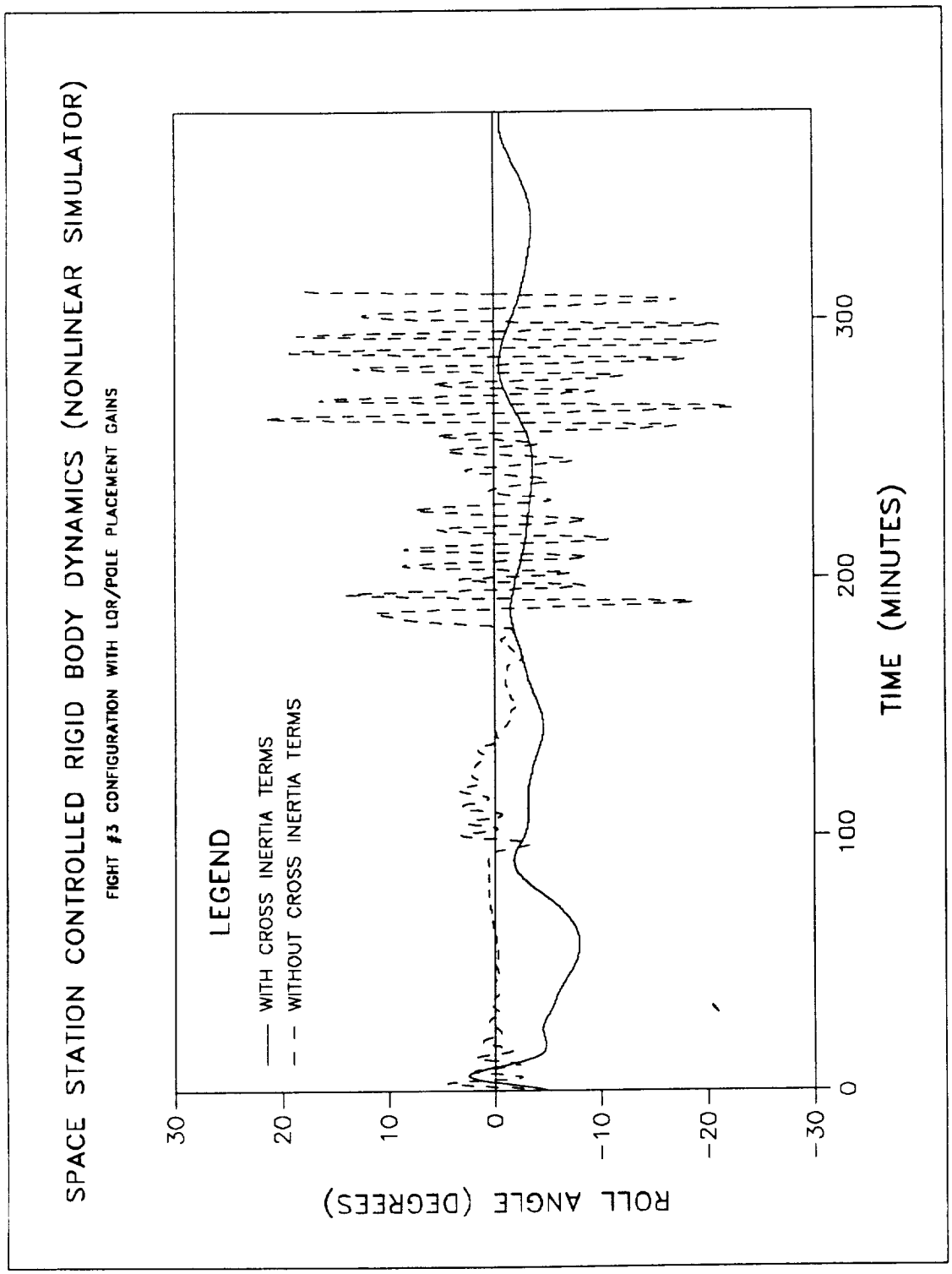

Figure 6.2: Roll Axis Angle Response for MB3 Configuration.

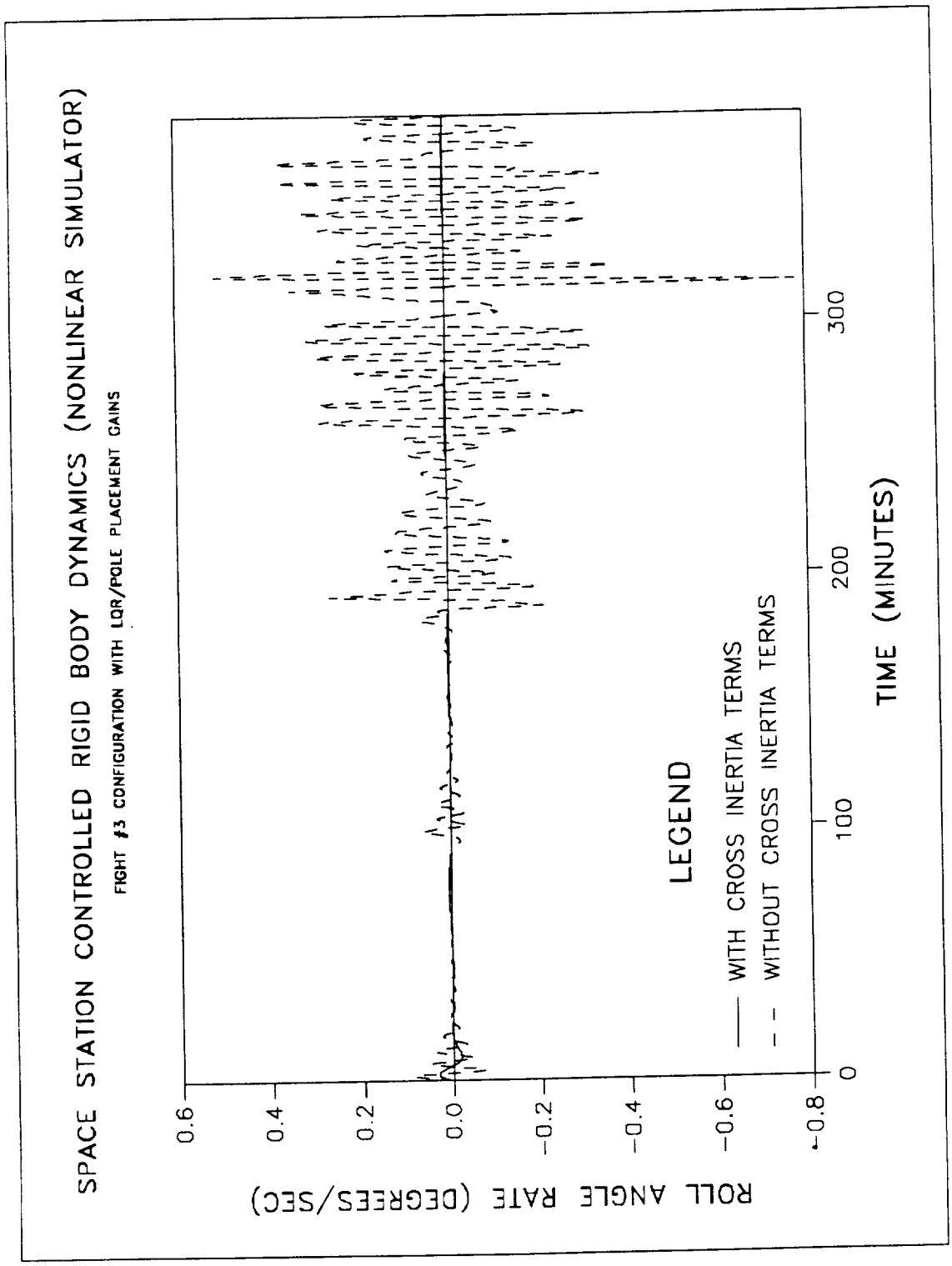

Figure 6.3: Roll Axis Angular Rate Response for MB3 Configuration.

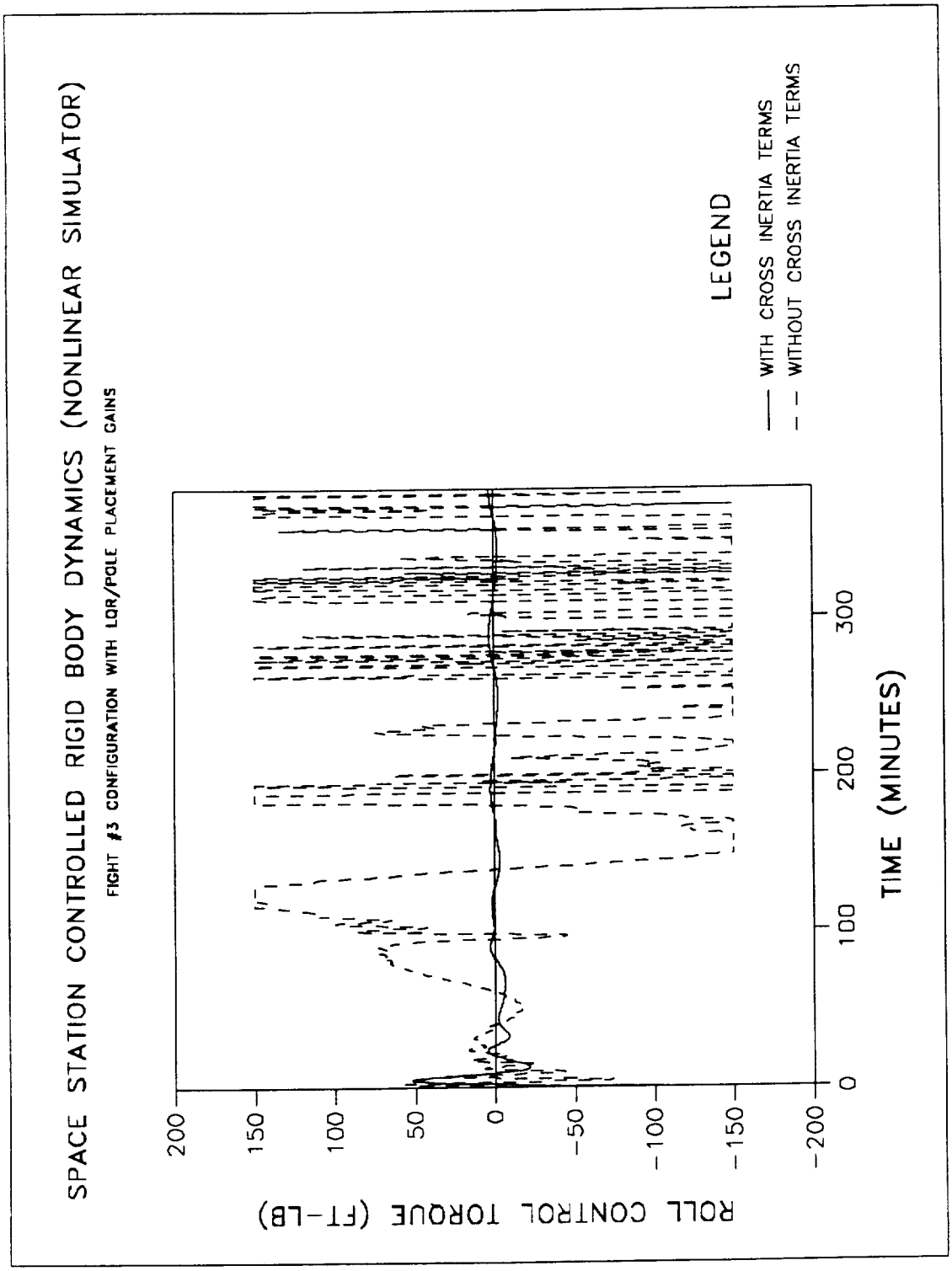

Figure 6.4: Roll Axis Control Torque Response for MB3 Configuration.

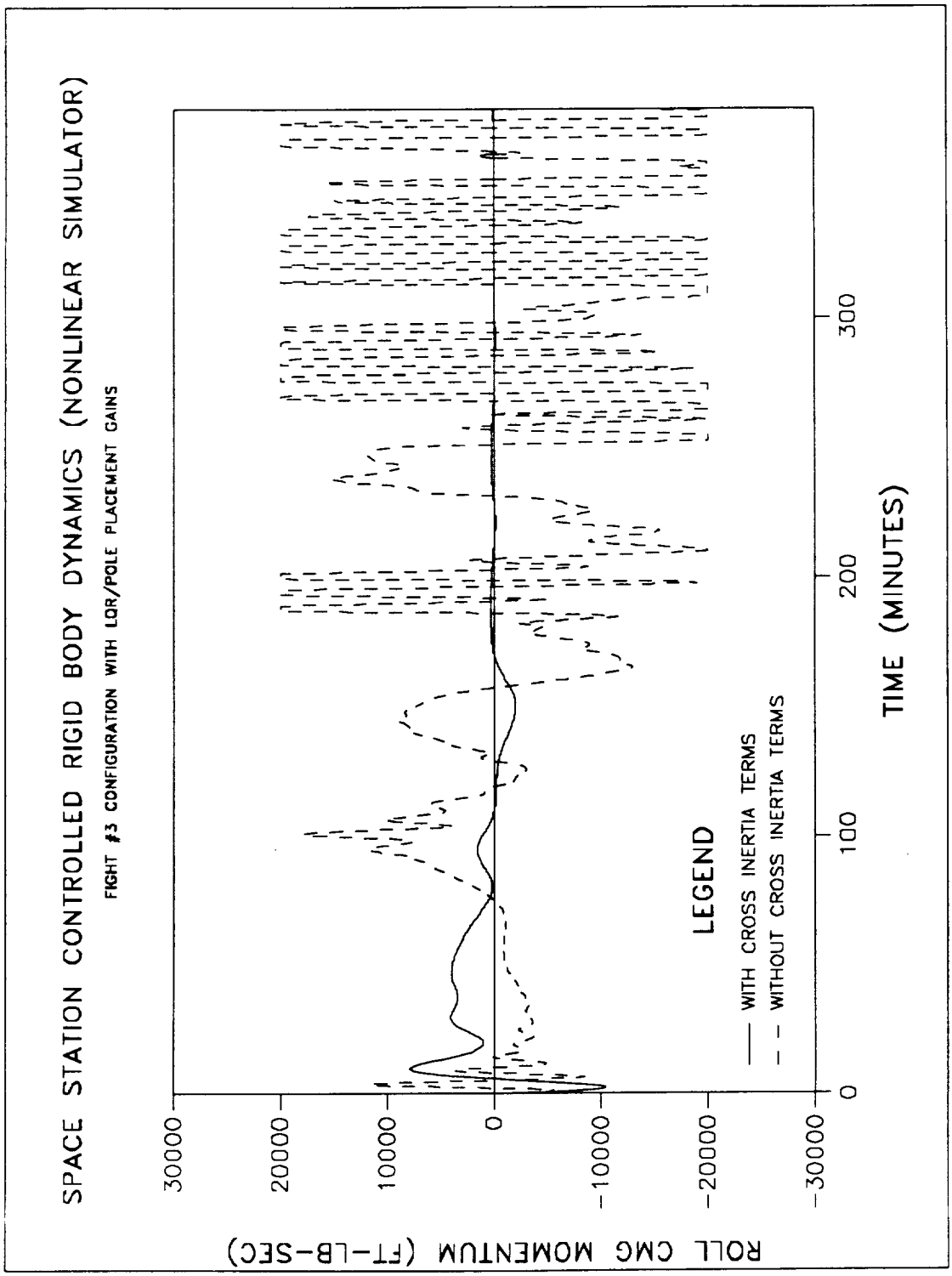

Figure 6.5: Roll Axis Angle Momentum Response for MB3 Configuration.

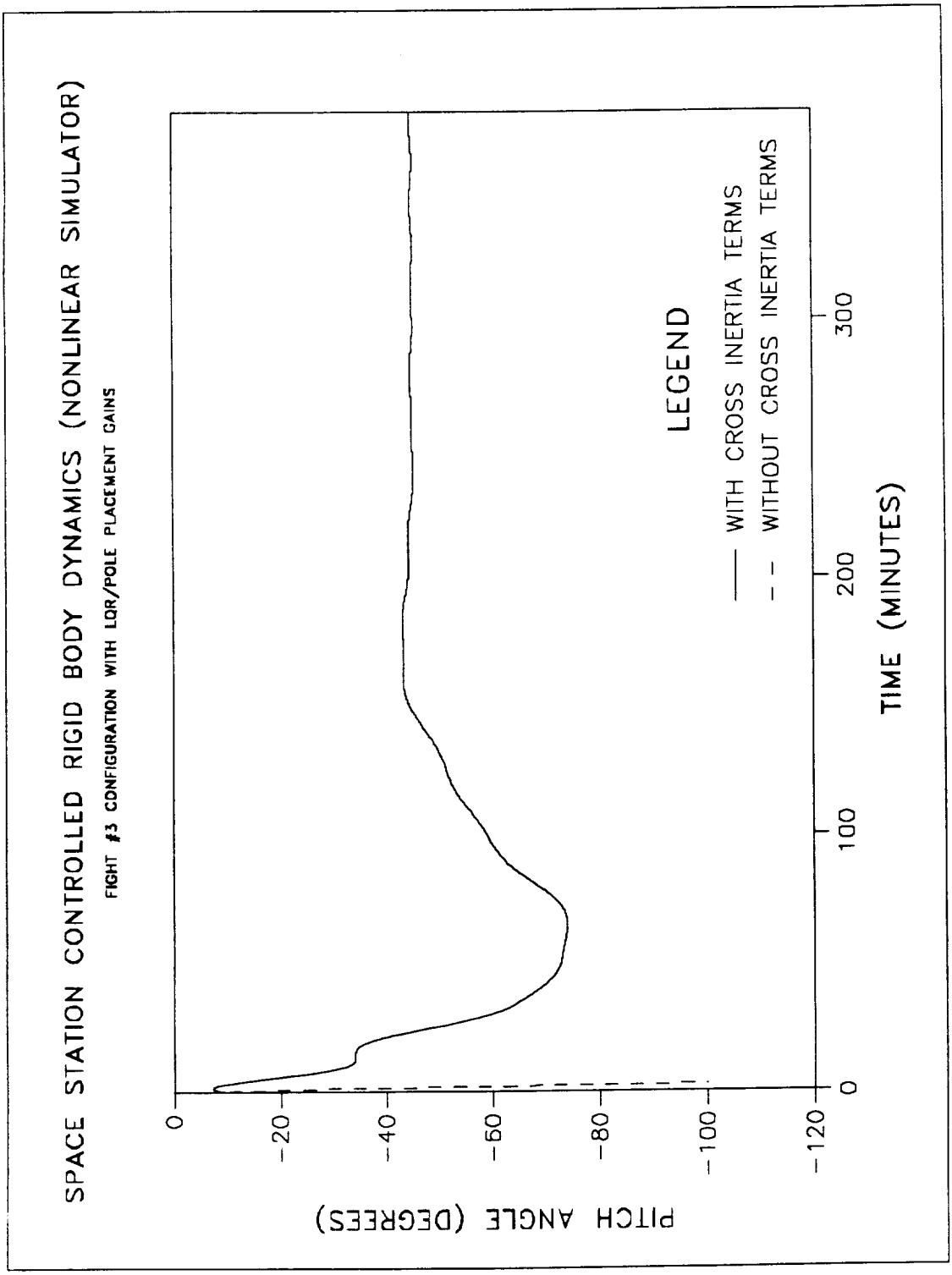

Figure 6.6: Pitch Axis Angle Response for MB3 Configuration.

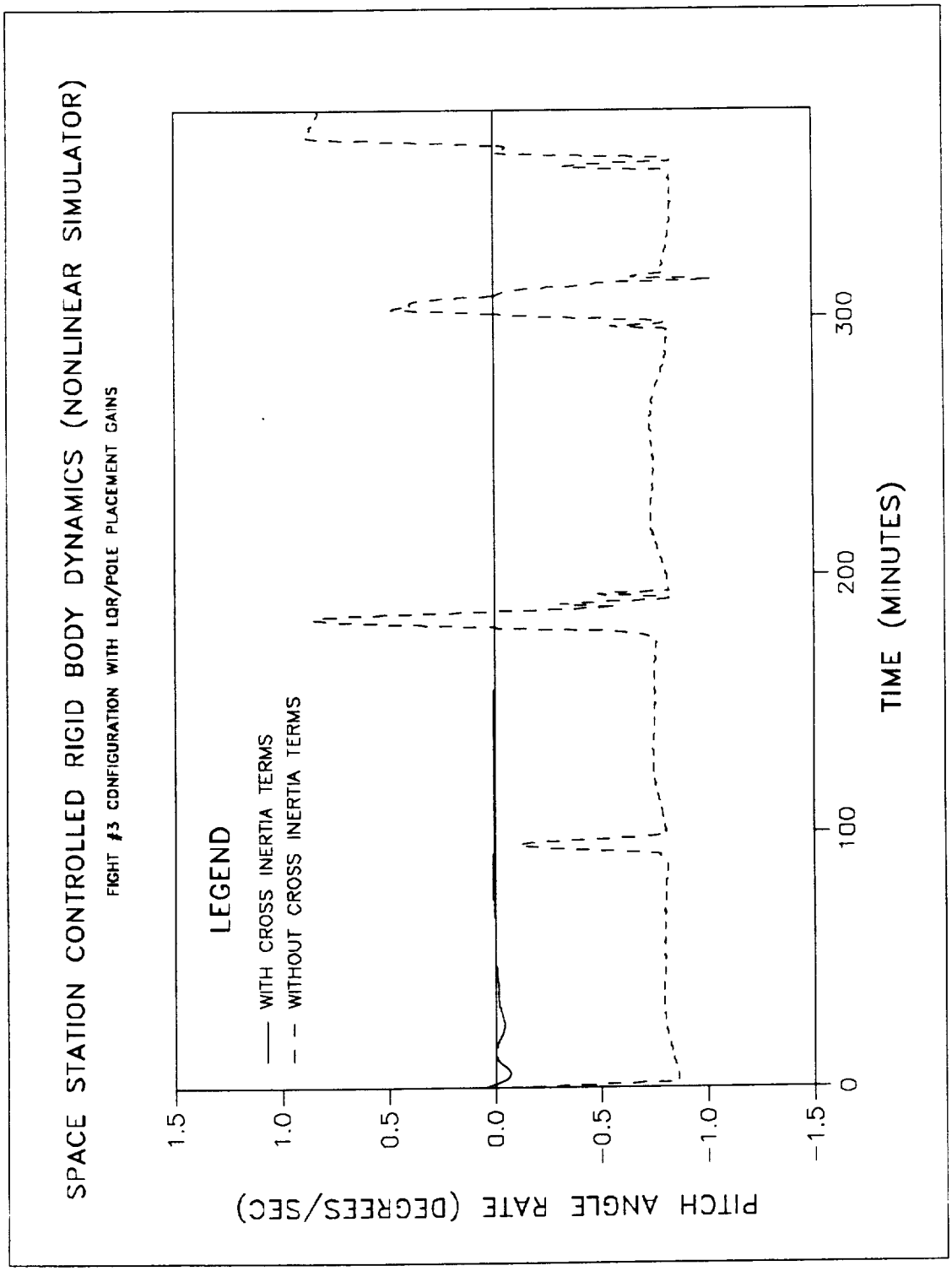

Figure 6.7: Pitch Axis Angular Rate Response for MB3 Configuration.

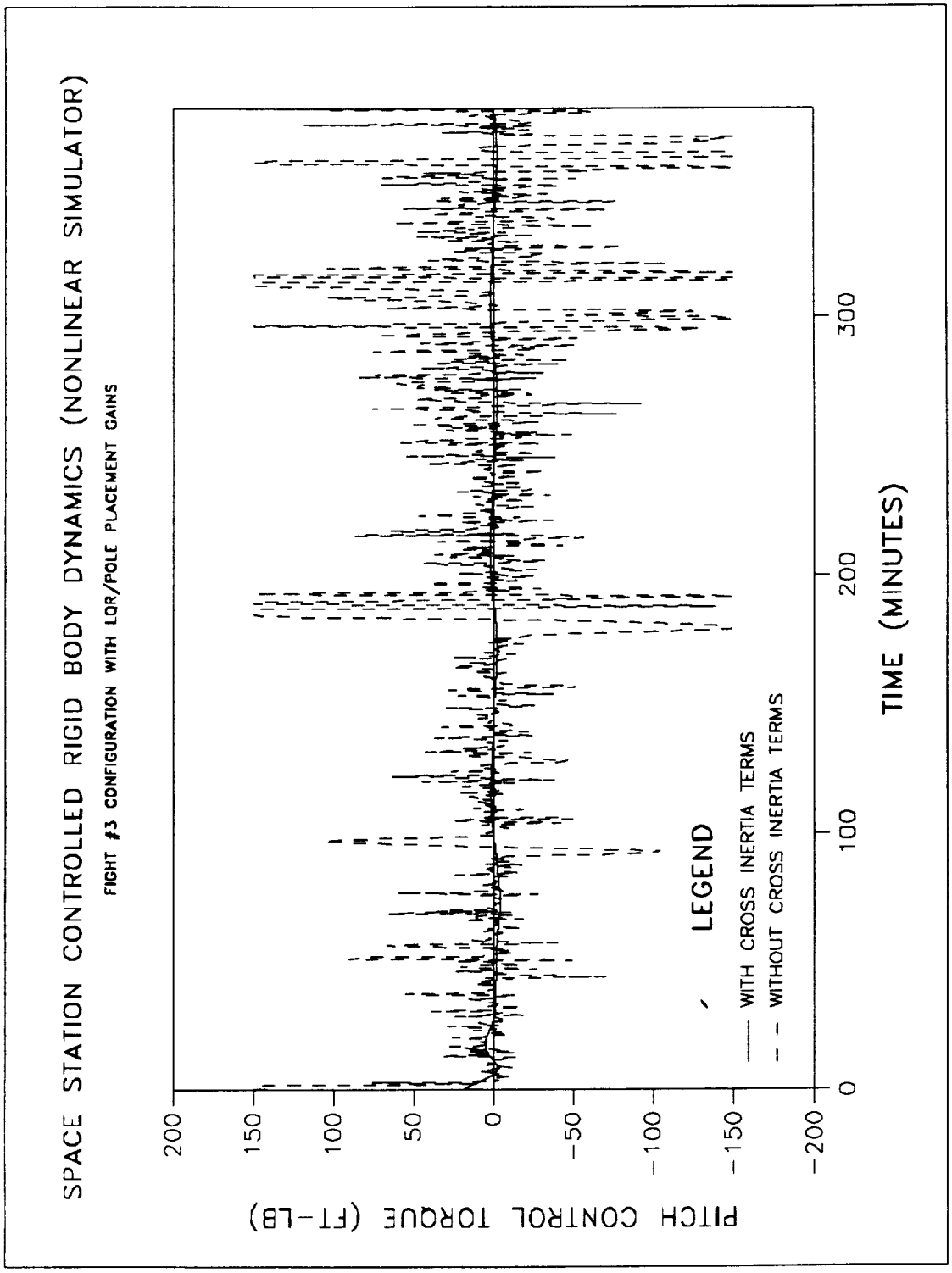

Figure 6.8: Pitch Axis Control Torque Response for MB3 Configuration.

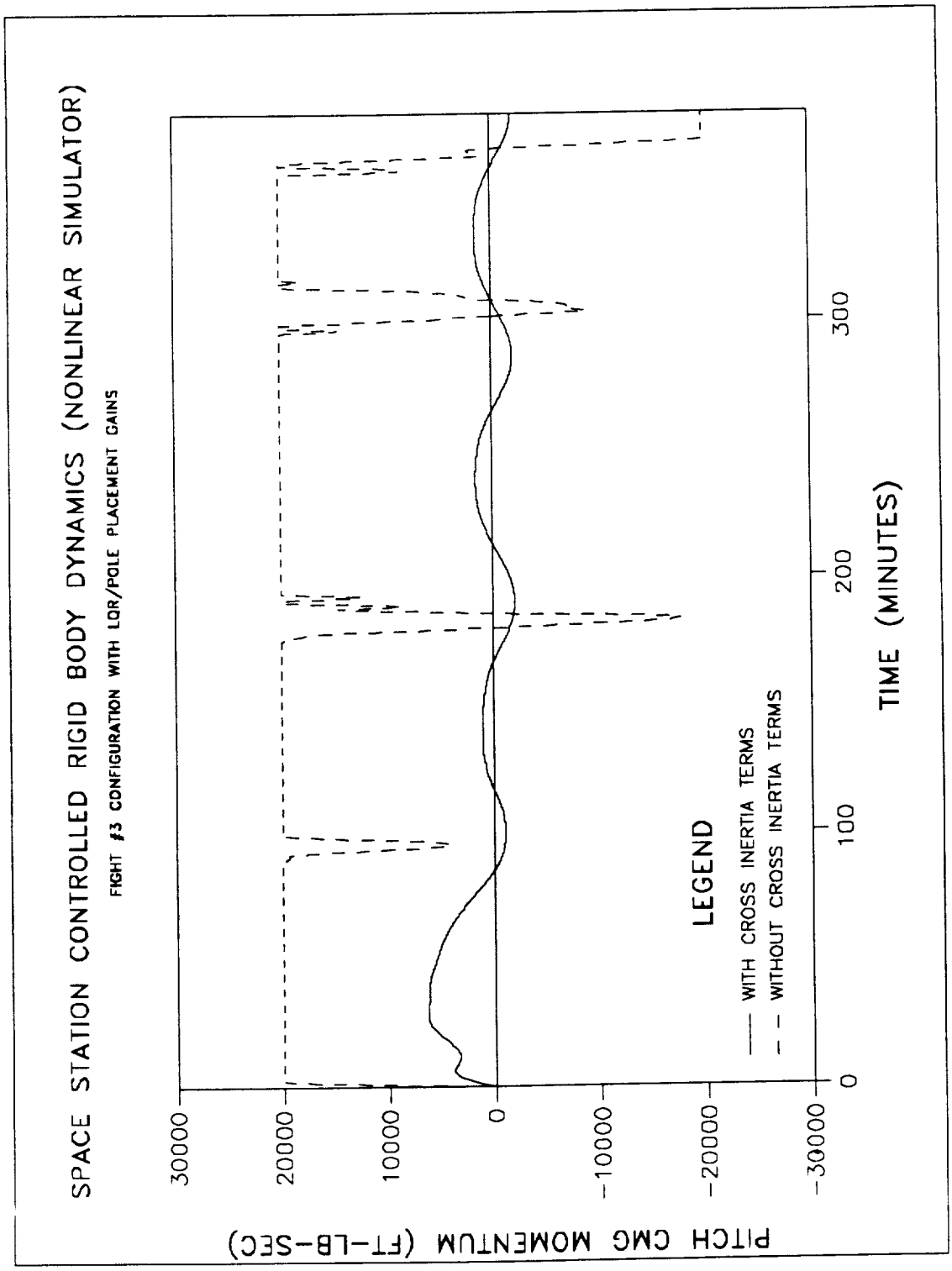

Figure 6.9: Pitch Axis Angle Momentum Response for MB3 Configuration.

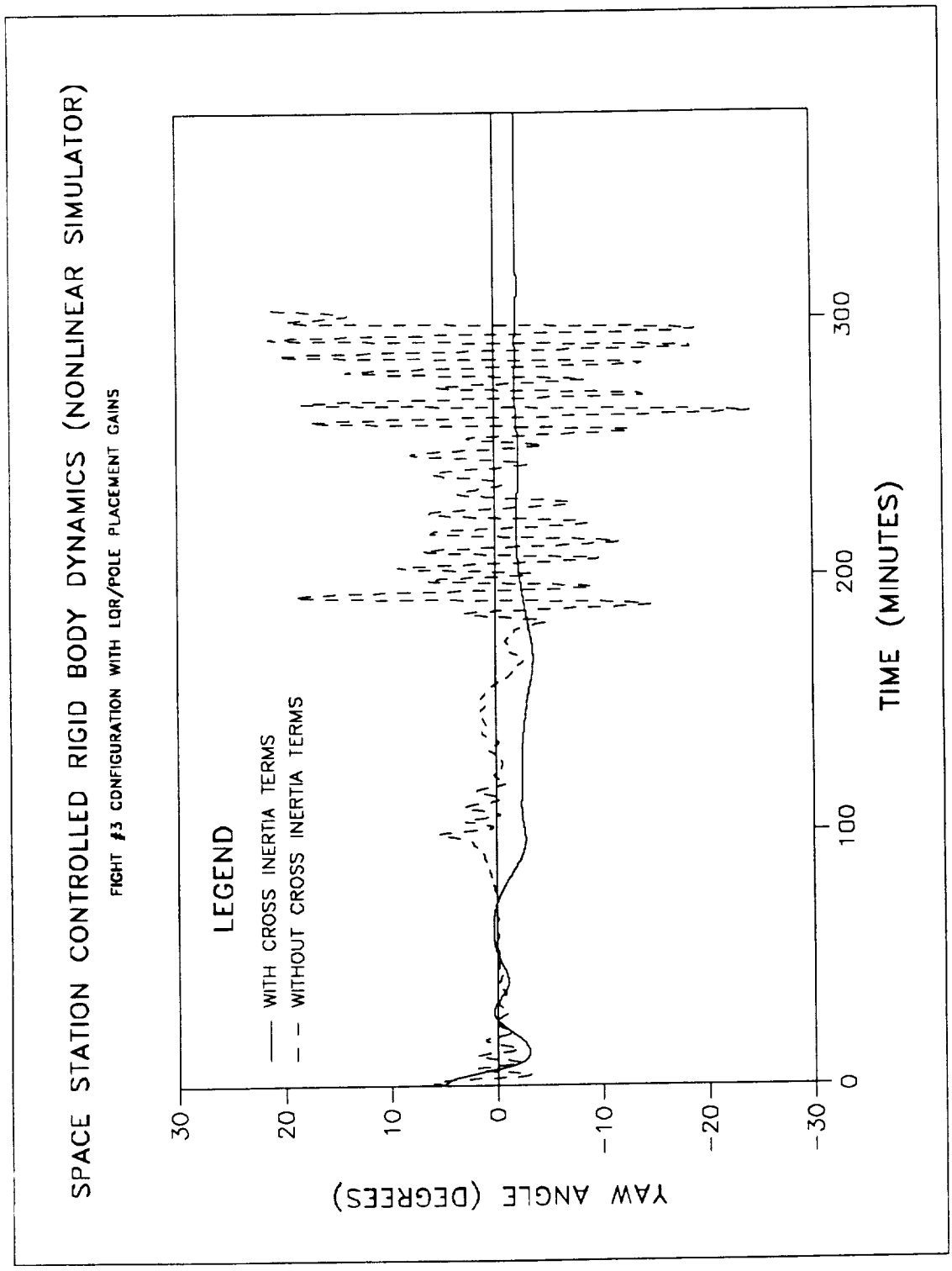

Figure 6.10: Yaw Axis Angle Response for MB3 Configuration.

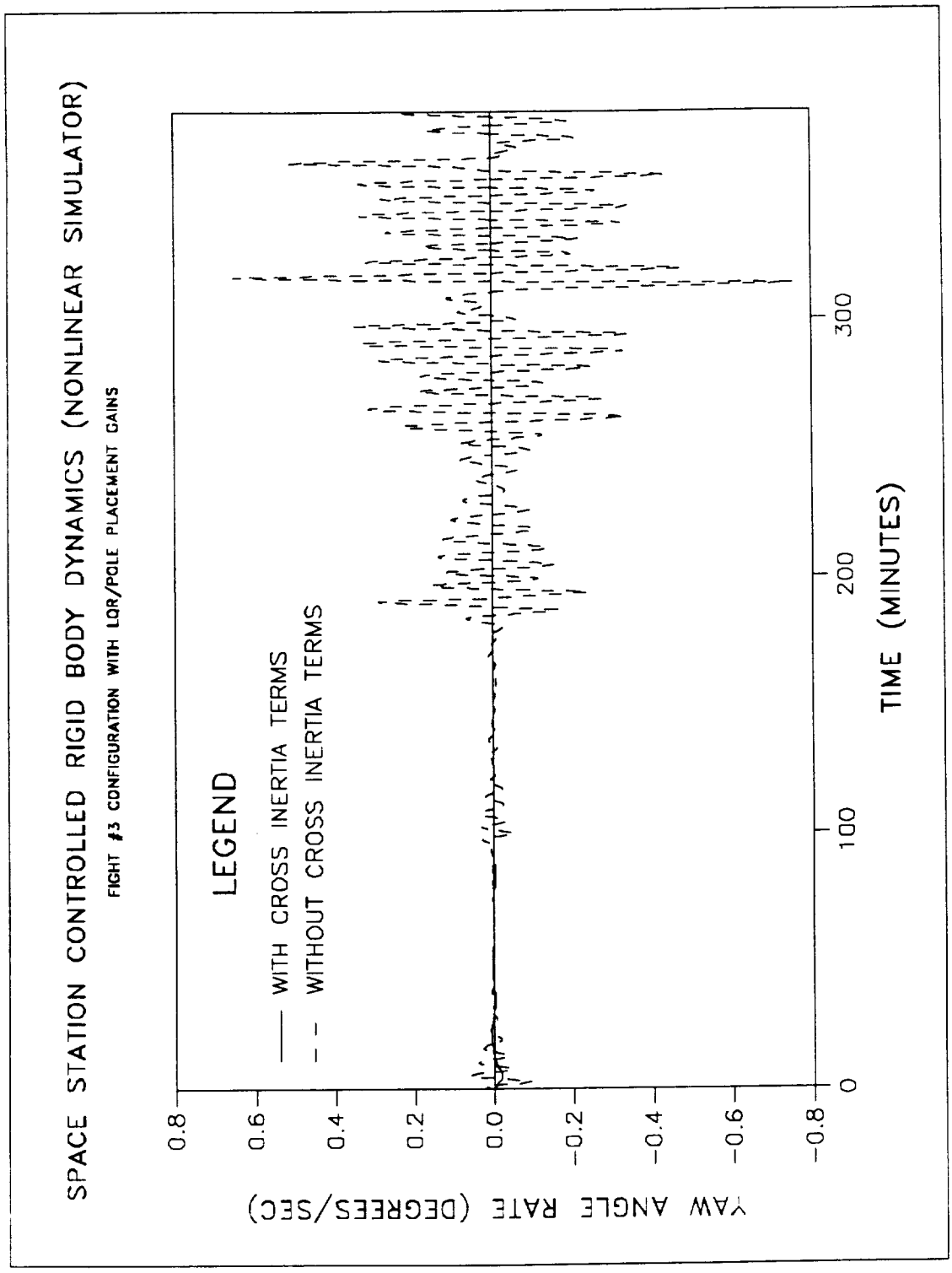

Figure 6.11: Yaw Axis Angular Rate Response for MB3 Configuration.

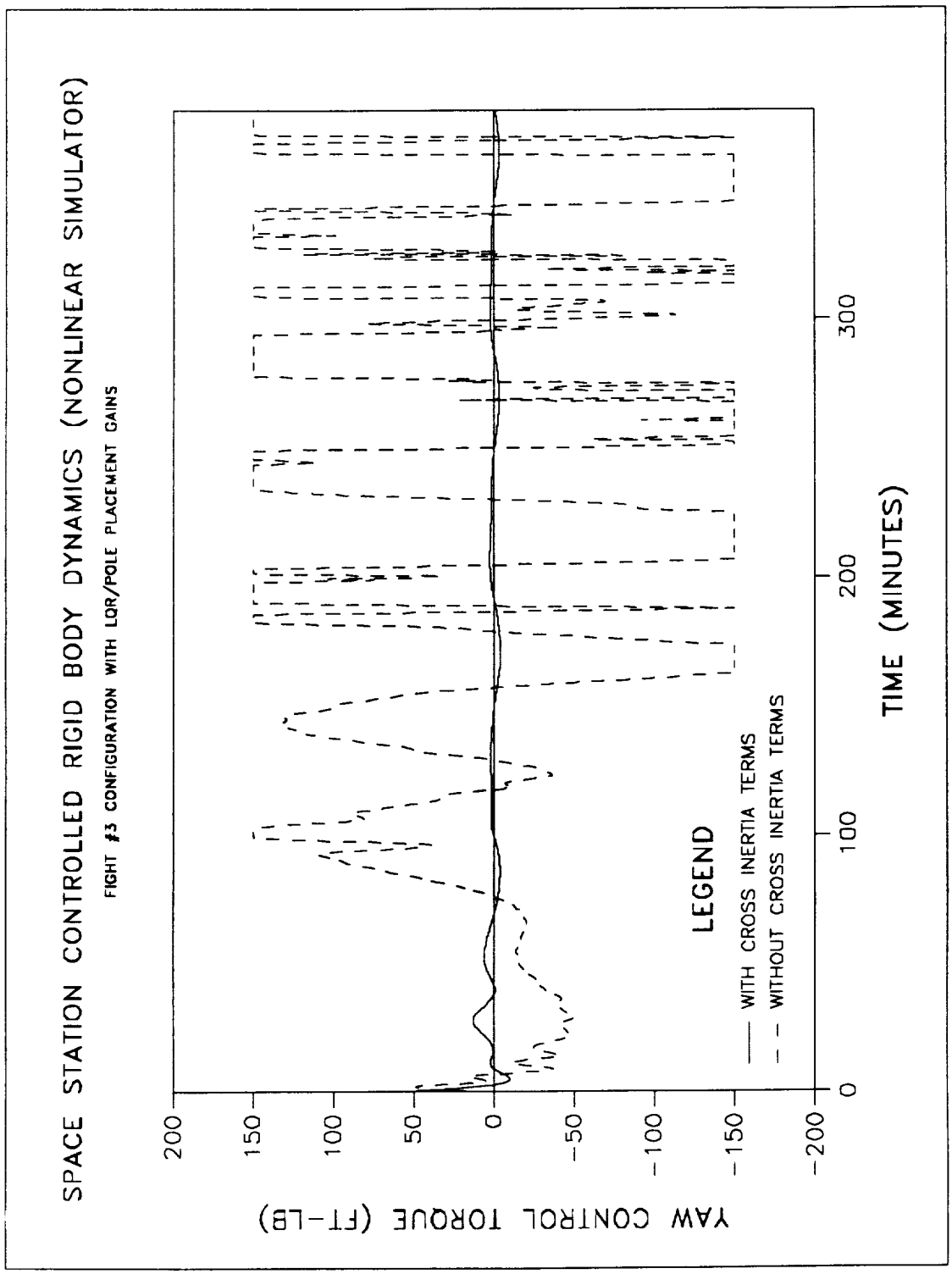

Figure 6.12: Yaw Axis Control Torque Response for MB3 Configuration.

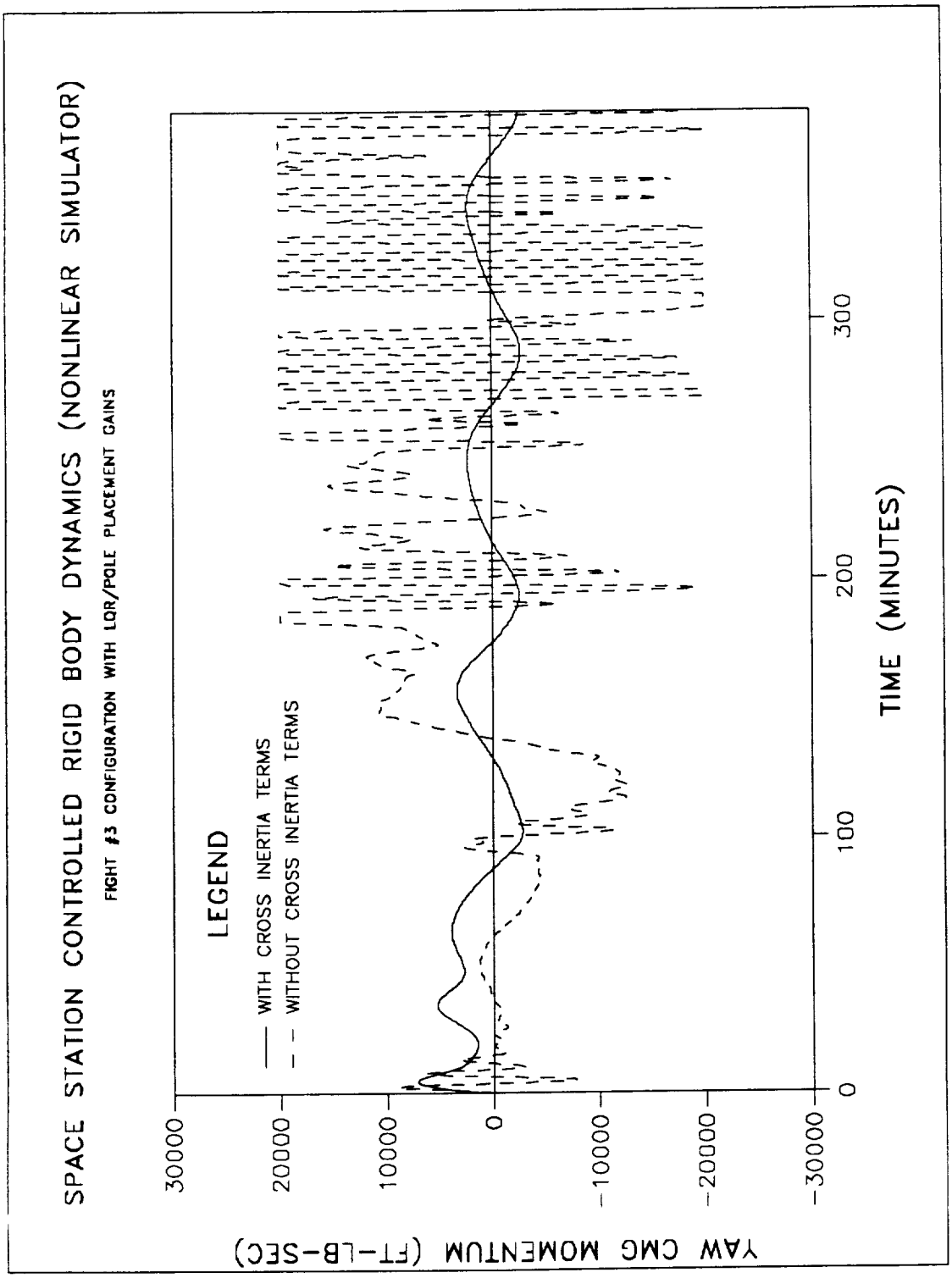

Figure 6.13: Yaw Axis Angle Momentum Response for MB3 Configuration.

All of the simulations subsequently presented in this section have been performed using the nonlinear simulation model for the SSF presented in section II of this paper. To demonstrate the first claim, two sets of simulations are performed using the MB3 configuration. In both cases the LQR synthesis algorithm with pole placement is used and the closed-loop poles are placed within the boundaries drawn by the two 45 deg lines and the $-0.5n$ vertical line, as shown in Figure 5.2. For the first set of simulations it was assumed that even though an accurate estimate of the TEA will be available, i.e. the TEA estimate will be obtained using the full inertia matrix, the controller design will be based on a model that ignores the cross-inertia terms. Therefore, these simulations utilized a linear control system designed using the model described by equation (4.46), with the cross-inertia terms set to zero. However, the actual values of the TEA, as given in Table 1, were used in the evaluation of the various non-zero matrix elements of the system dynamics, i.e. the LVLH approximation was not made. The second set of simulations were performed using a linear control system based on the fully coupled roll/pitch/yaw motion as described by equation (4.46), and with the same values of the TEA as before. In both sets of simulations, the same initial conditions and environmental disturbance terms were used.

The simulation results for these two cases are shown in Figures 6.1 through 6.13. These studies clearly demonstrate the error introduced in arbitrarily discarding the cross-inertia terms when the analyzed configurations correspond to large angle TEA. The transient response of the closed-loop system becomes unstable within less than one-tenth of an orbit, unless

the cross-inertia terms of the linearized system model used in the control synthesis are included. The controller response with the cross-inertia terms included, is not perhaps the best possible, as further fine tunning of the desired closed-loop pole locations could possible reveal transient responses with less excursions.

Demonstration of the second claim proved to be more time consuming and computationally more intensive. In order to arrive at a gain-scheduled controller, several linear designs were performed for various SSF configurations with TEA ranging form -45 deg to LVLH. These configurations correspond to inertia matrix variations of up to 1600%, for some of the cross-inertia elements. The gain-scheduled closed-loop dynamics were simulated for 130 orbits while the inertia matrix was allowed to change in a stair-case fashion from the MB3 configuration to the AC configuration, as shown in Figures 6.14 through 6.19. The results of these simulations are presented in Figures 6.20 through 6.30. With the exception of the bias terms the external disturbances were kept the same, as the inertia variations were made. These transient responses indicate that a gain-scheduled controller, whether it is in table look-up form or a continuous polynomial as presented in this study, is sufficient in handling large changes in the SSF inertia matrix, including configurations that are characterized by large angle TEA. This is primarily attributed to the slowly varying dynamics of the SSF, with characteristic time constants on the order of tens of minutes.

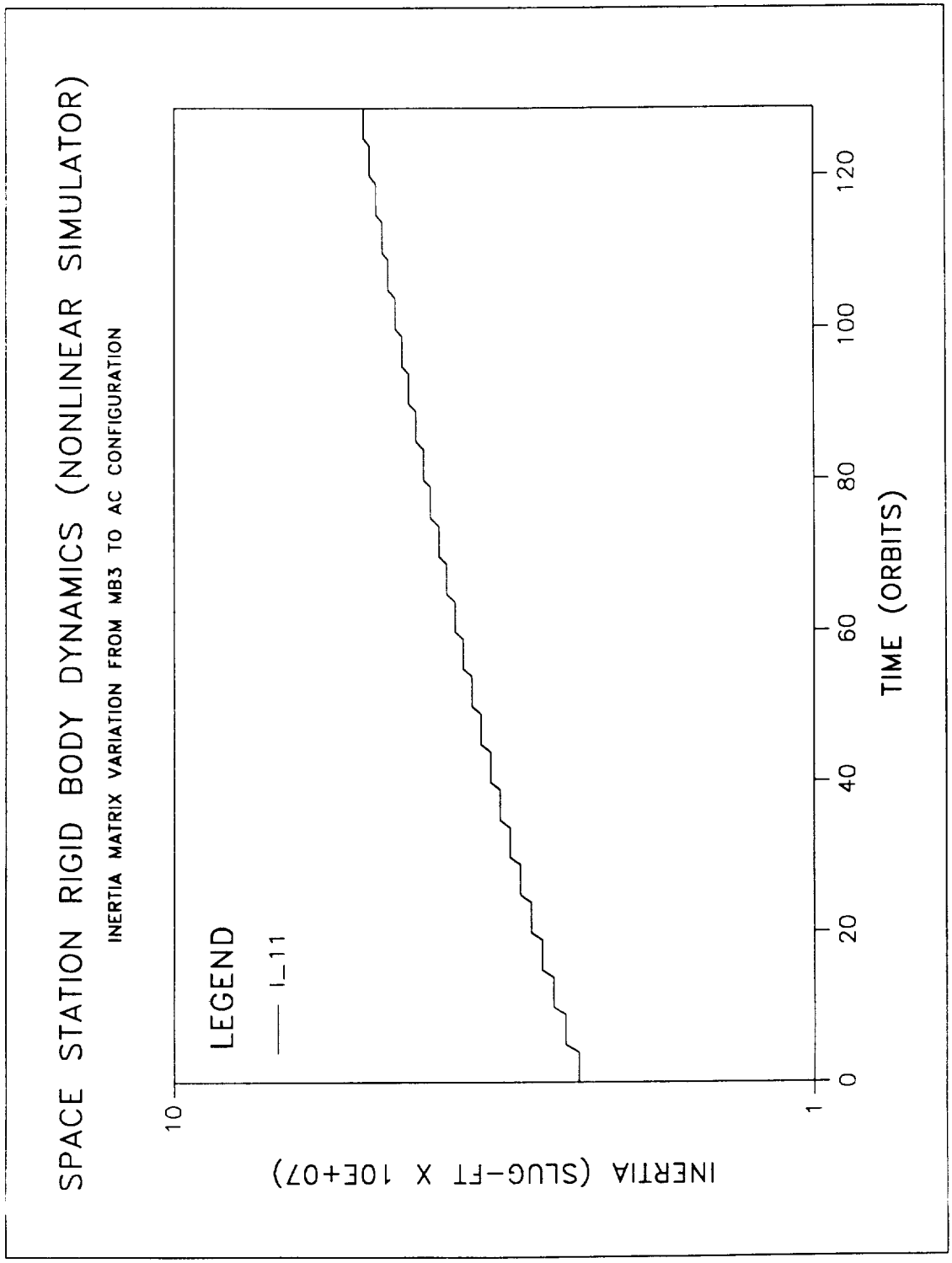

Figure 6.14: I(1,1) Inertia Variation from MB3 to AC Configuration.

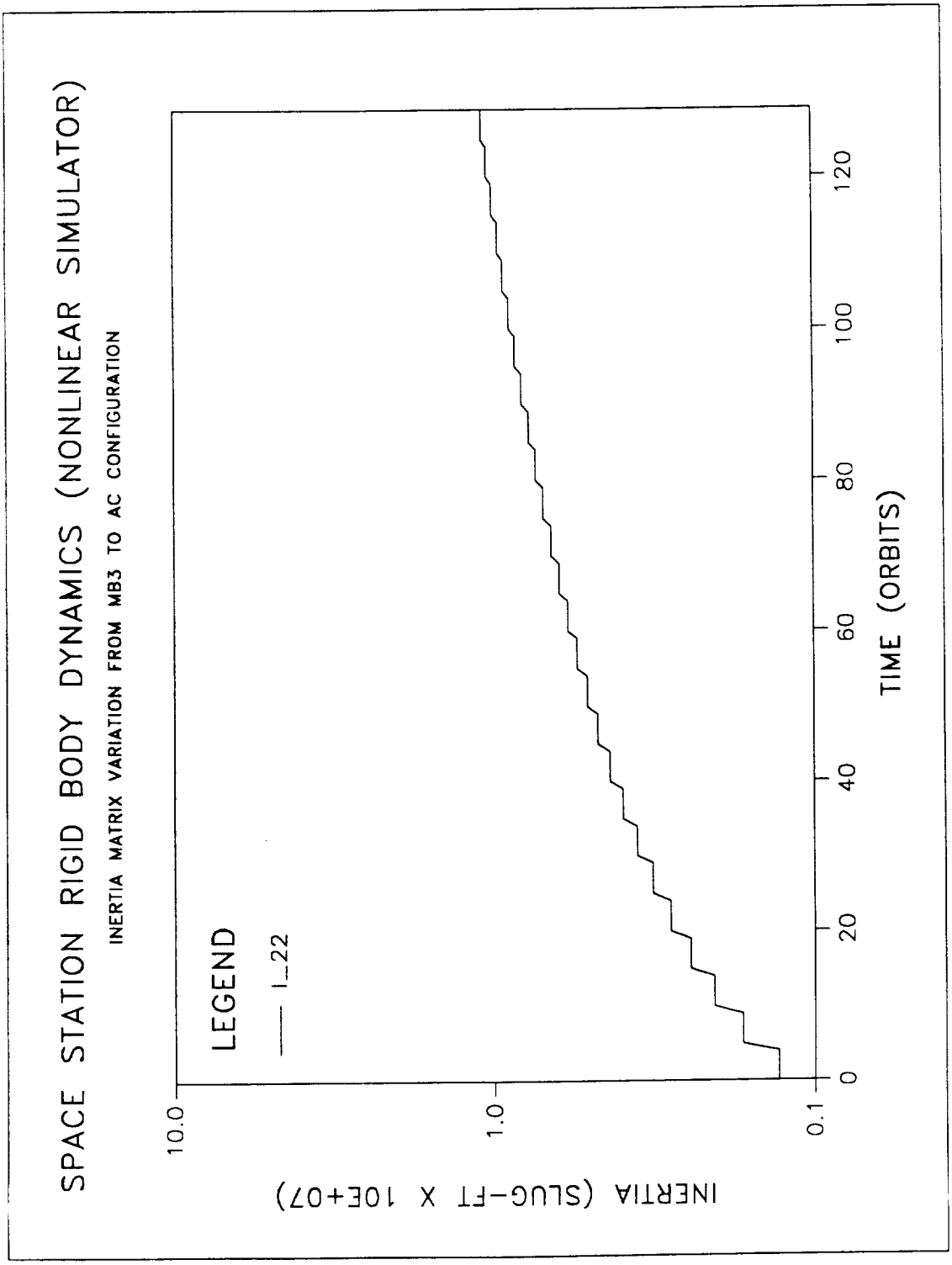

Figure 6.15: I(2,2) Inertia Variation from MB3 to AC Configuration.

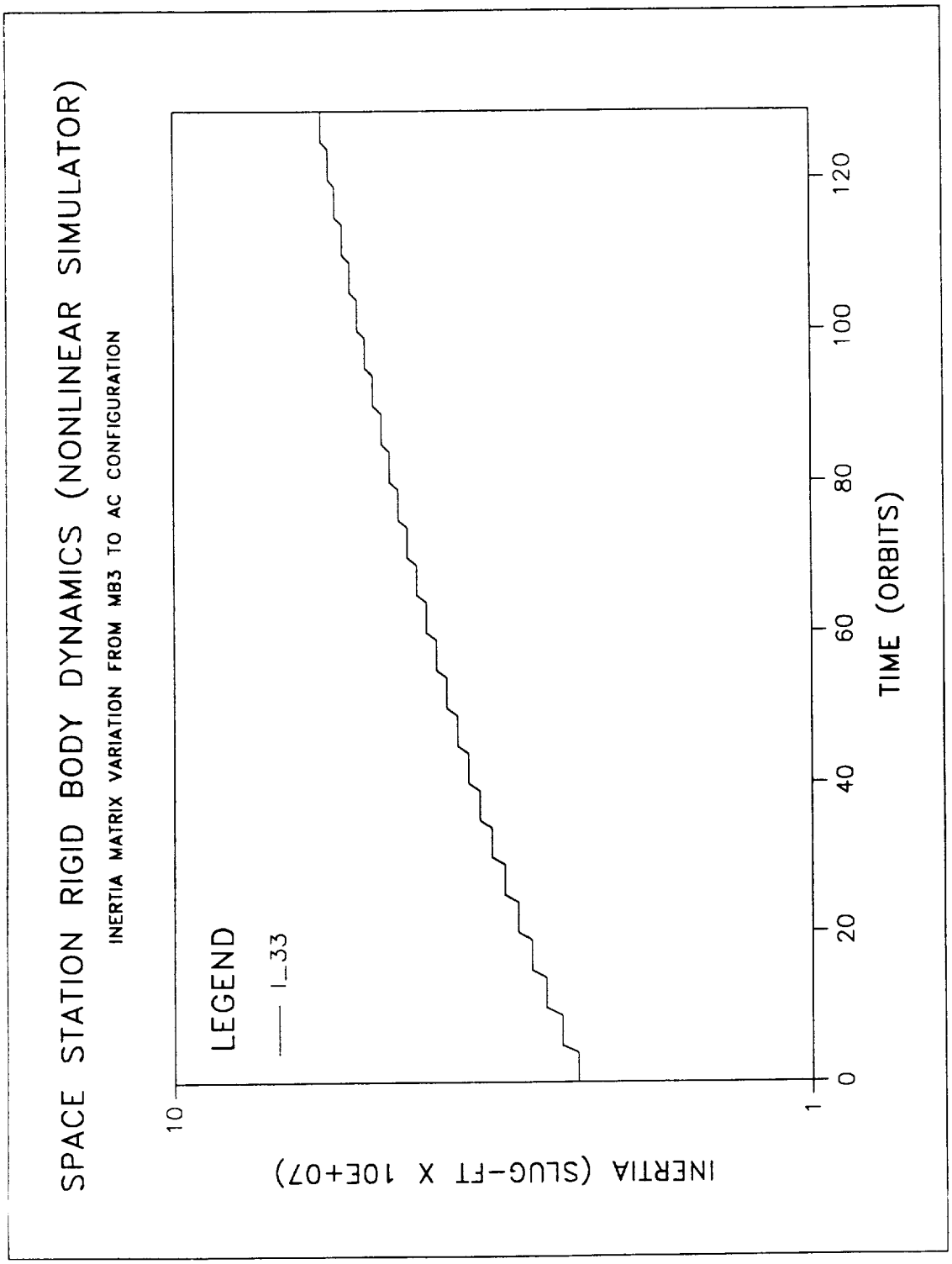

Figure 6.16: I(3,3) Inertia Variation from MB3 to AC Configuration.

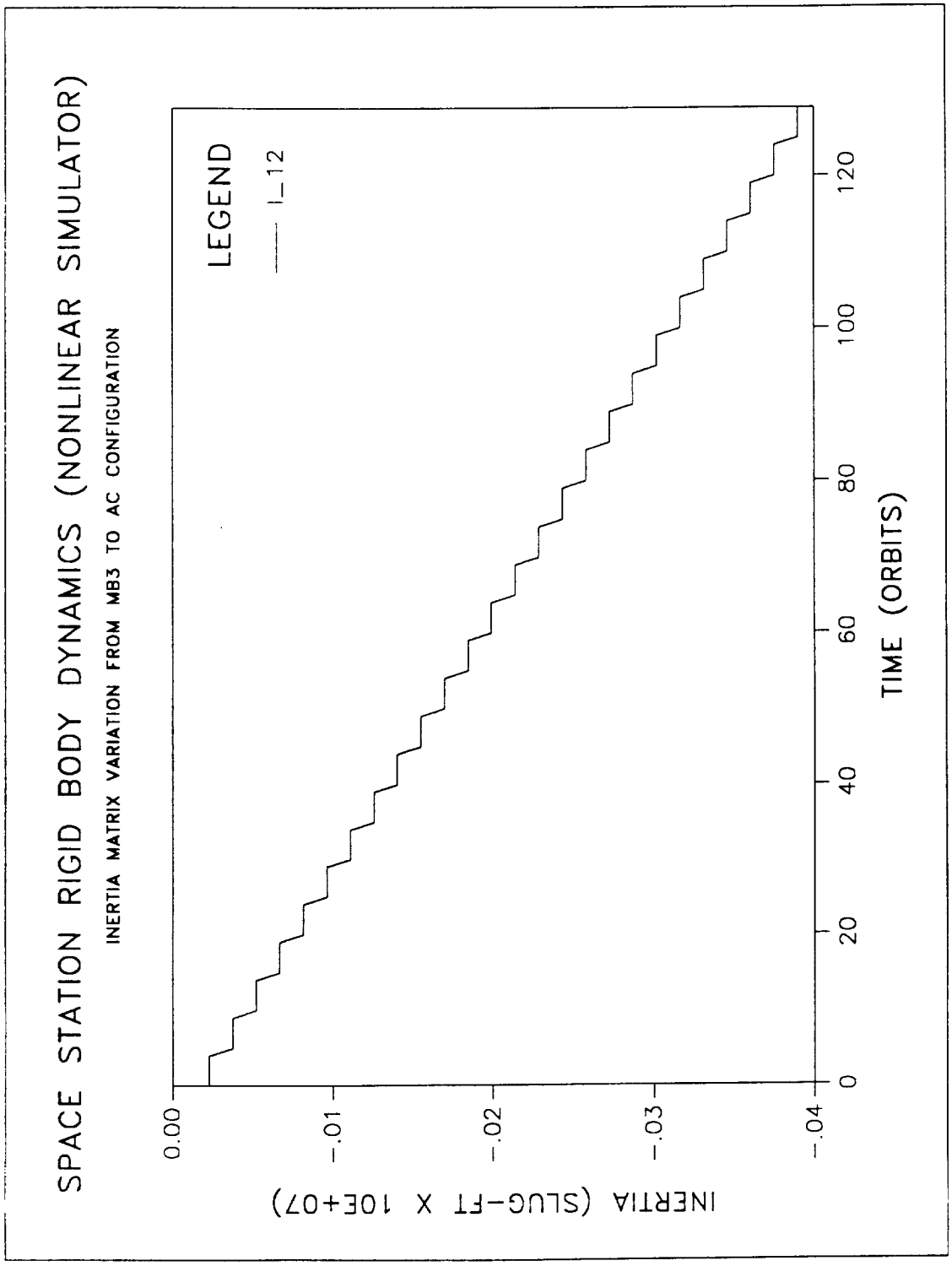

Figure 6.17: I(1,2) Inertia Variation from MB3 to AC Configuration.

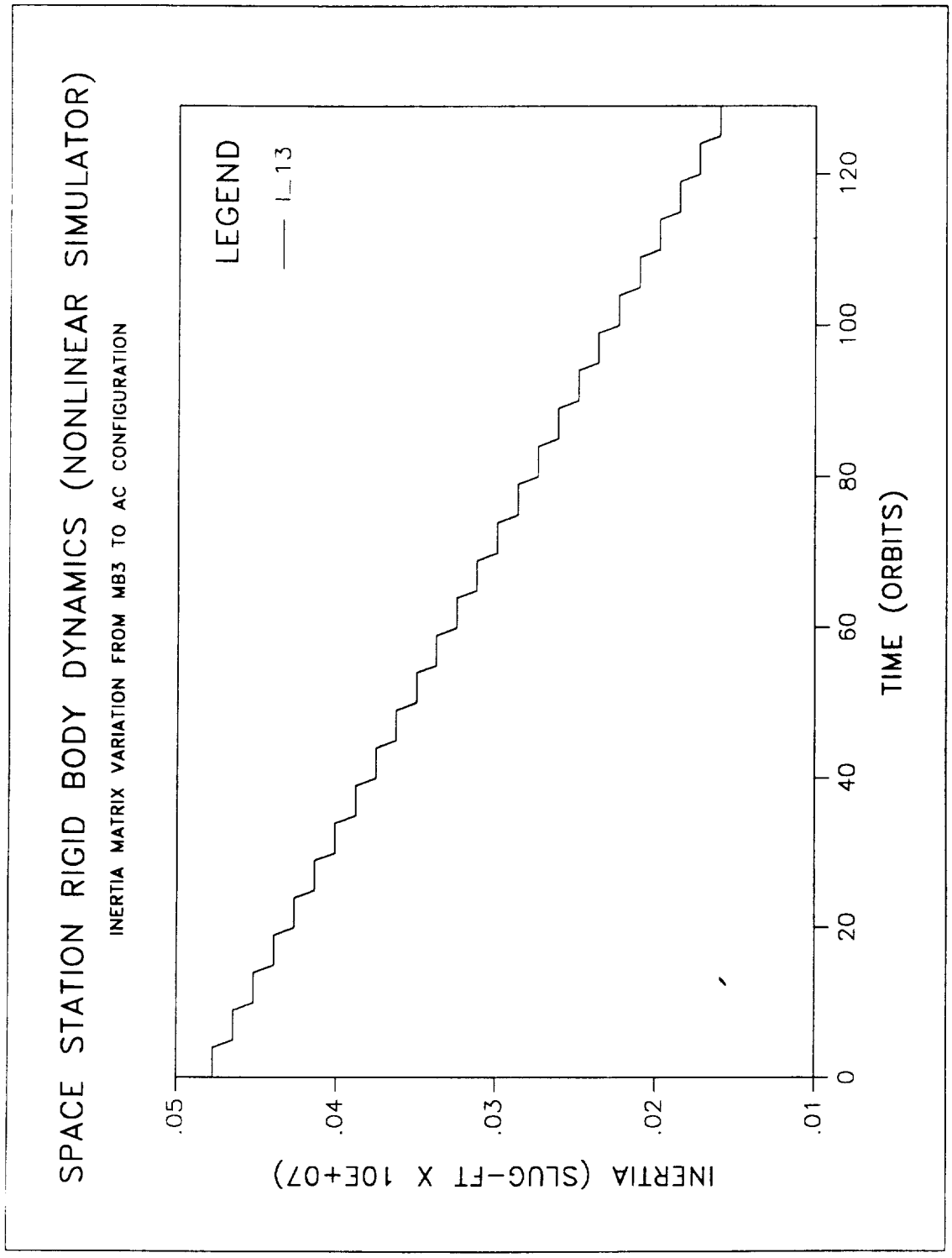

Figure 6.18: I(1,3) Inertia Variation from MB3 to AC Configuration.

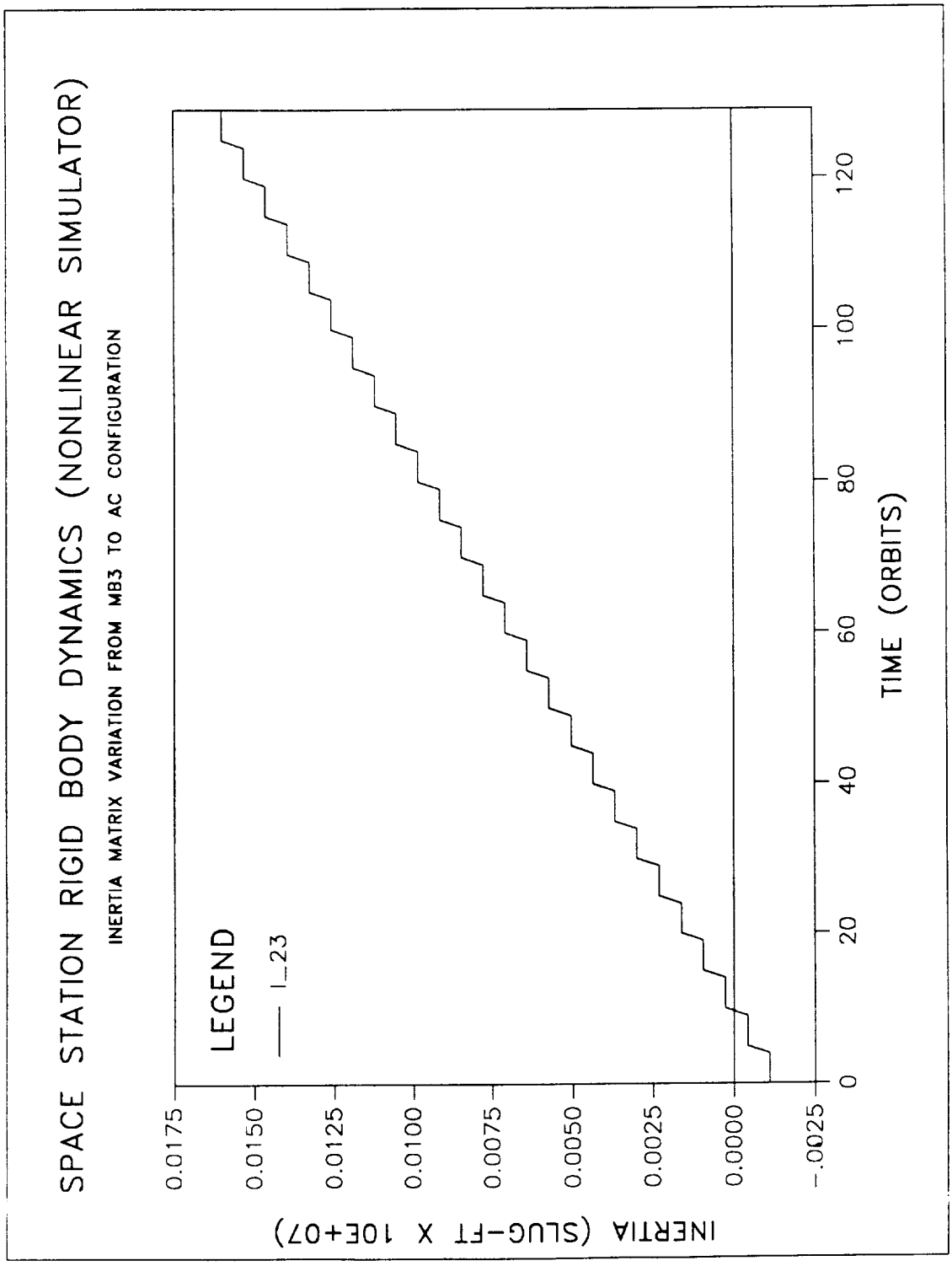

Figure 6.19: I(2,3) Inertia Variation from MB3 to AC Configuration.

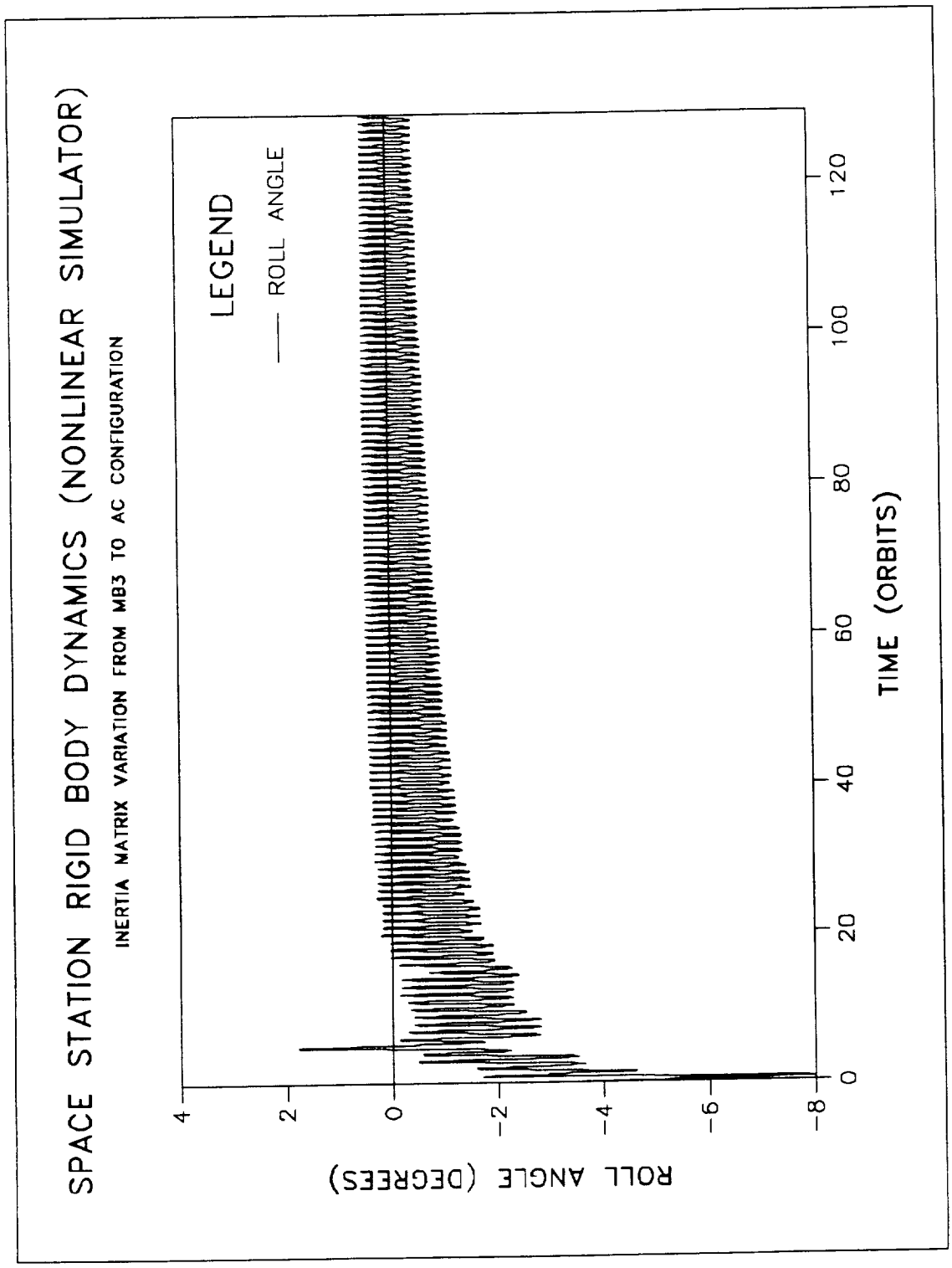

Figure 6.20: Roll Axis Angle Response for Inertia Variations from MB3 to AC Configuration.

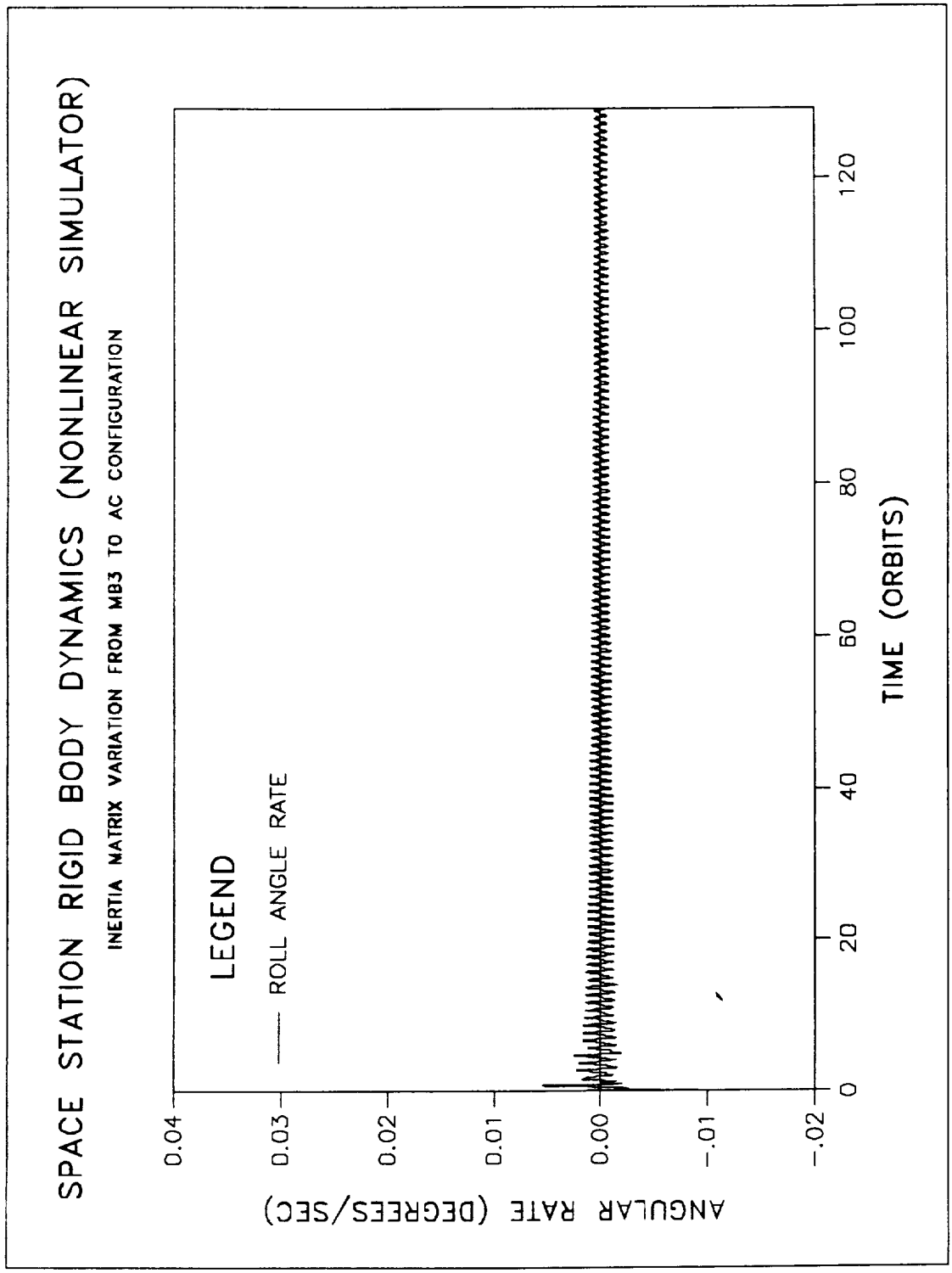

Figure 6.21: Roll Axis Angular Rate Response for Inertia Variations from MB3 to AC Configuration.

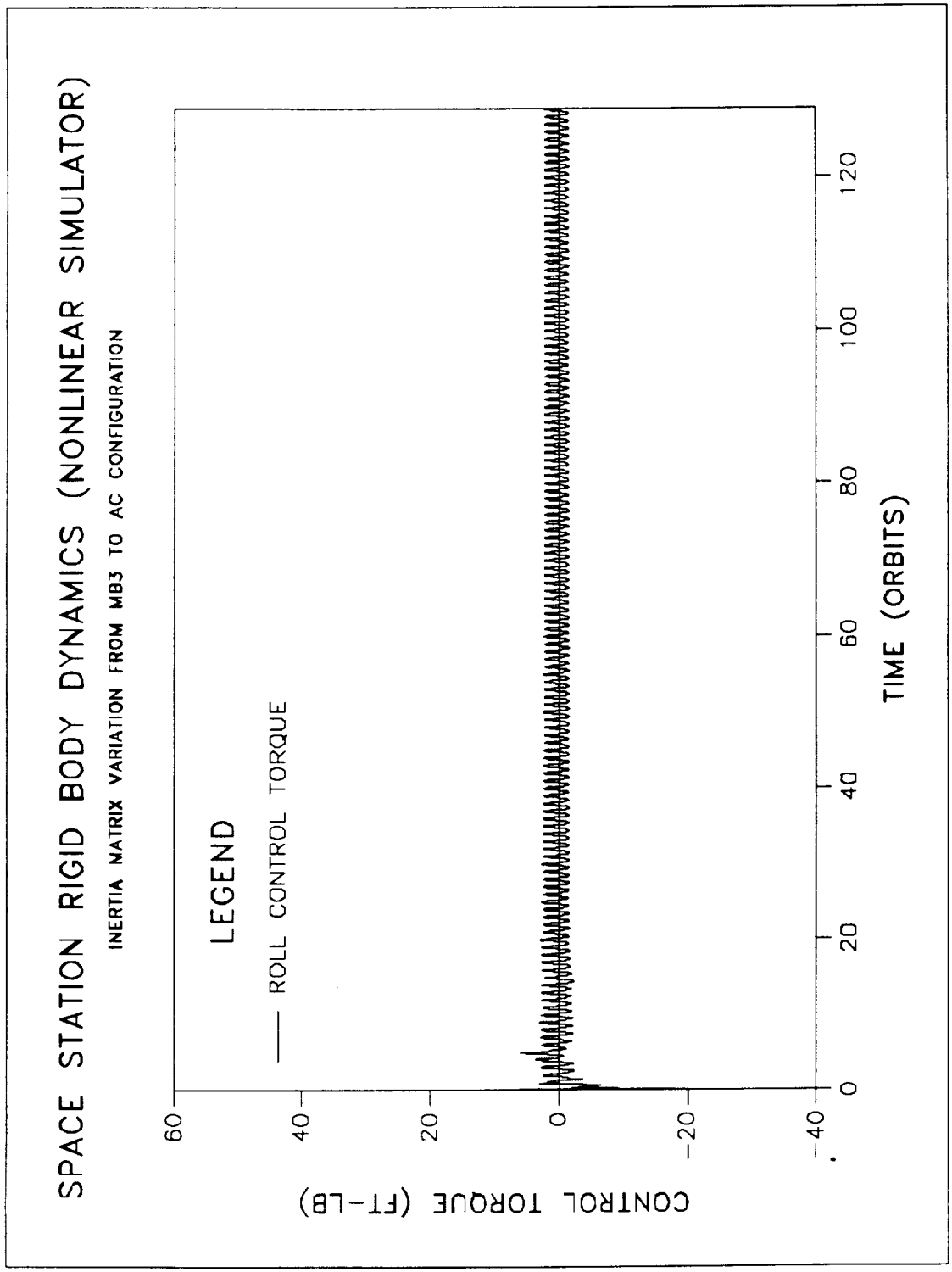

Figure 6.22: Roll Axis Control Torque Response for Inertia Variations from MB3 to AC Configuration.

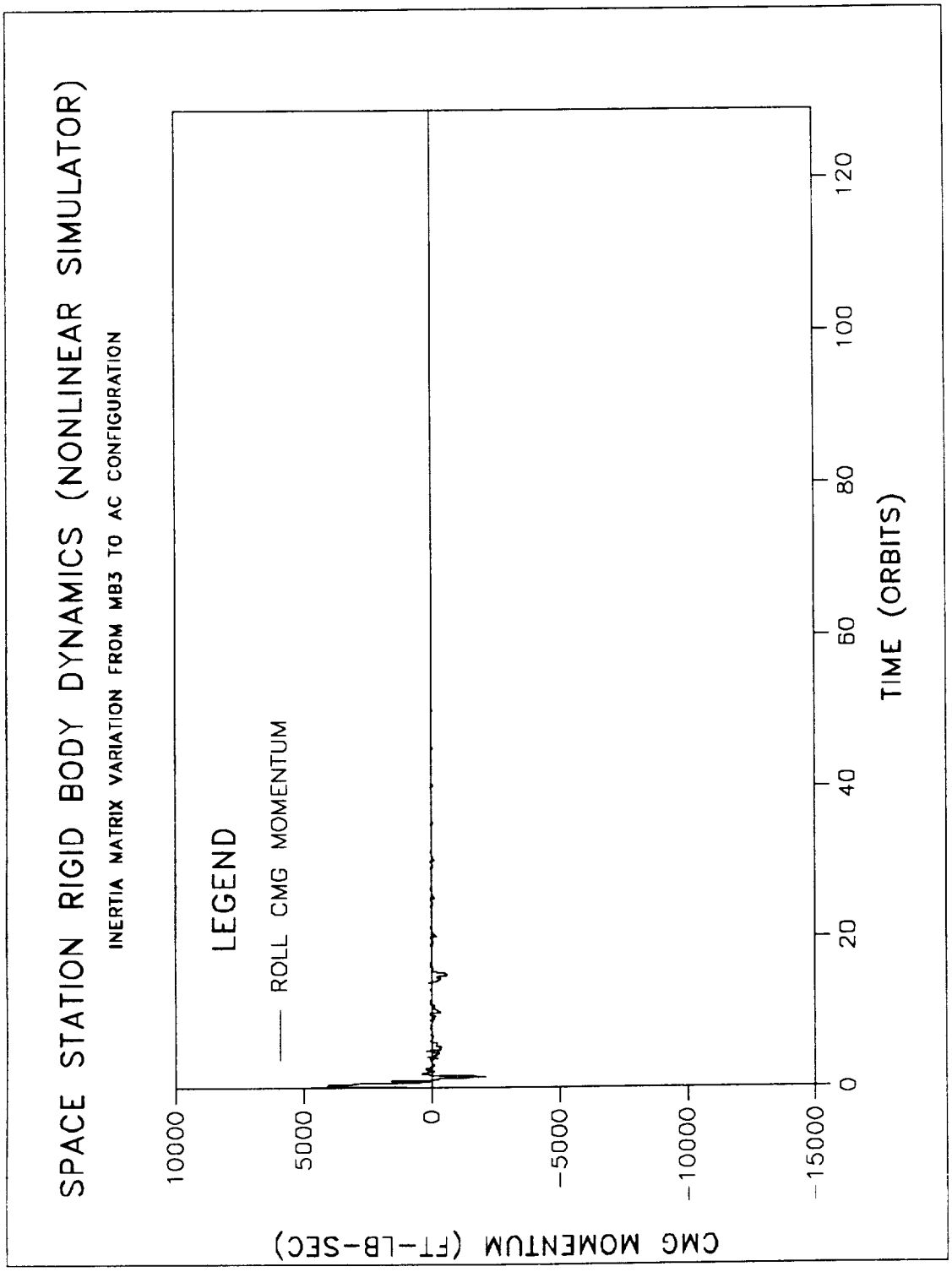

Figure 6.23: Roll Axis Momentum Response for Inertia Variations from MB3 to AC Configuration.

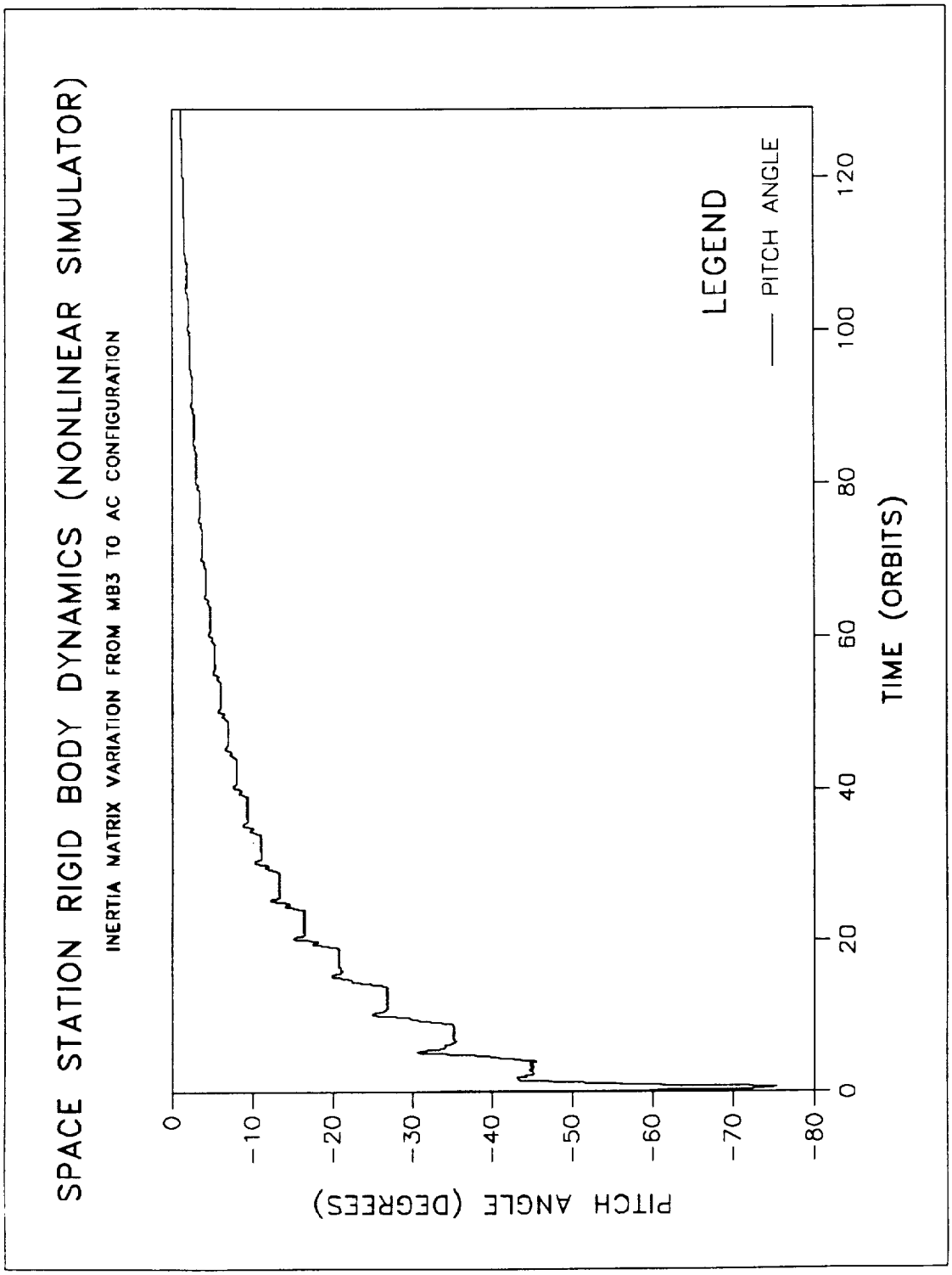

Figure 6.24: Pitch Axis Angle Response for Inertia Variations from MB3 to AC Configuration.

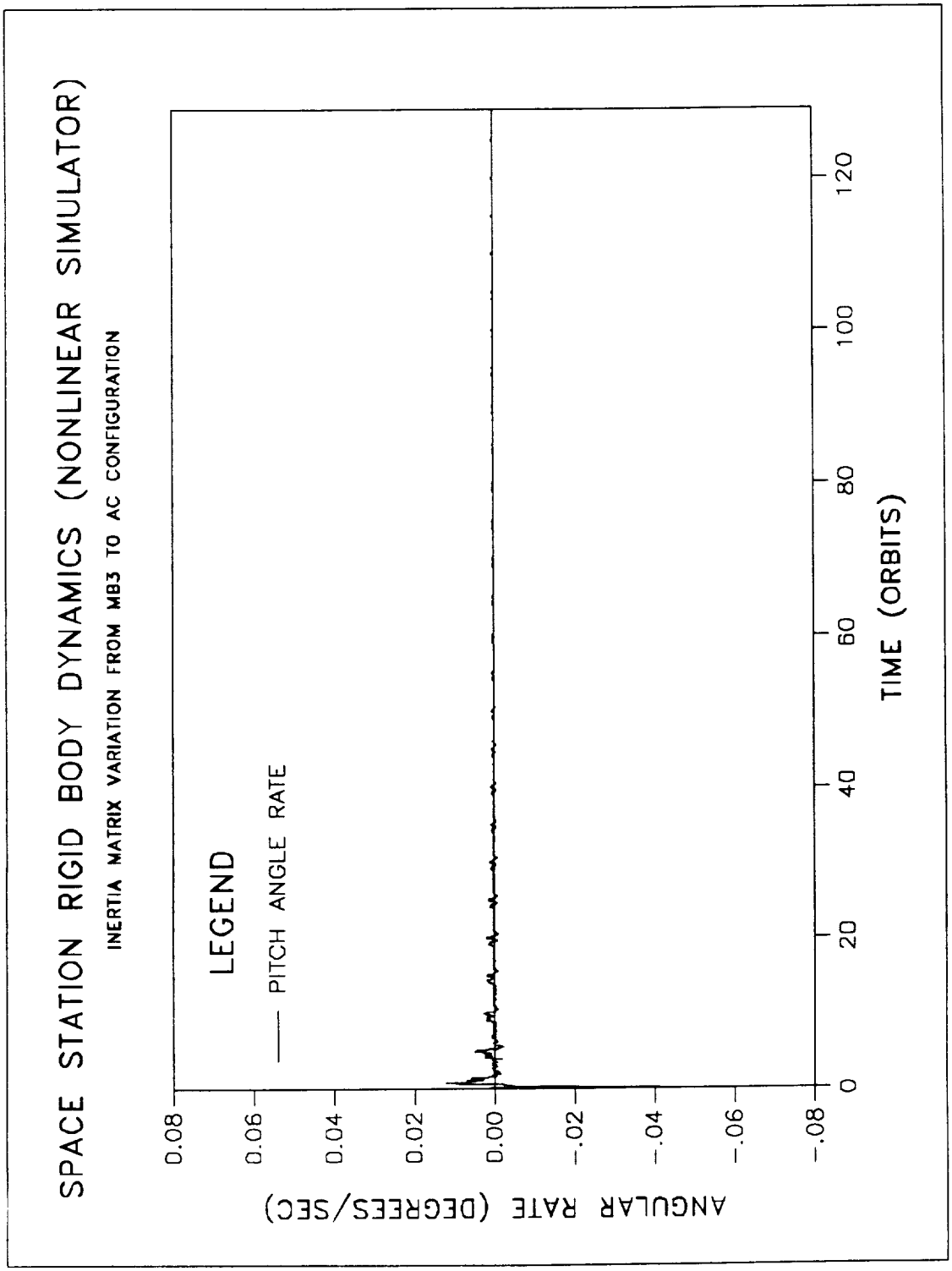

Figure 6.25: Pitch Axis Angular Rate Response for Inertia Variations from MB3 to AC Configuration.

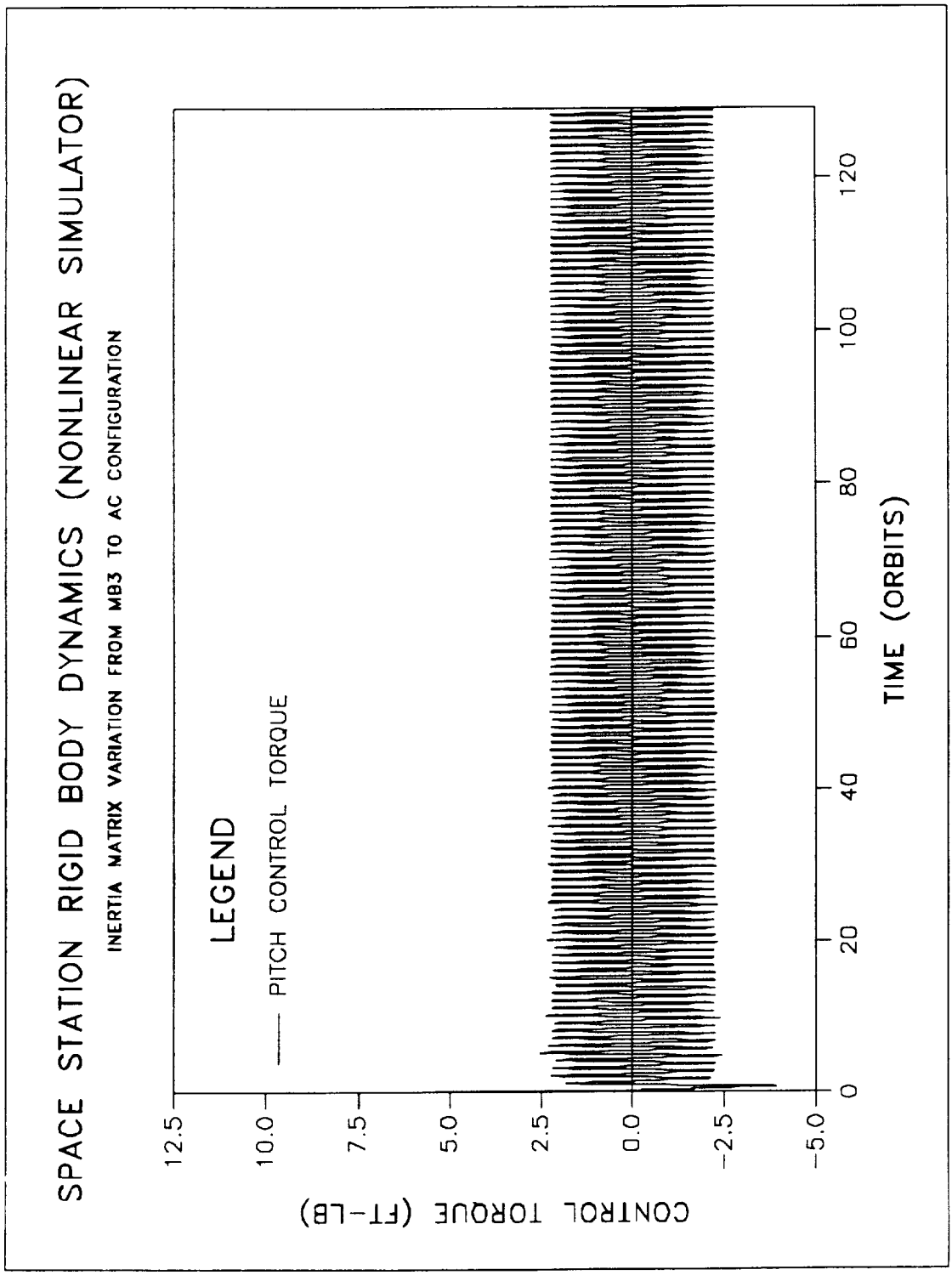

Figure 6.26: Pitch Axis Control Torque Response for Inertia Variations from MB3 to AC Configuration.

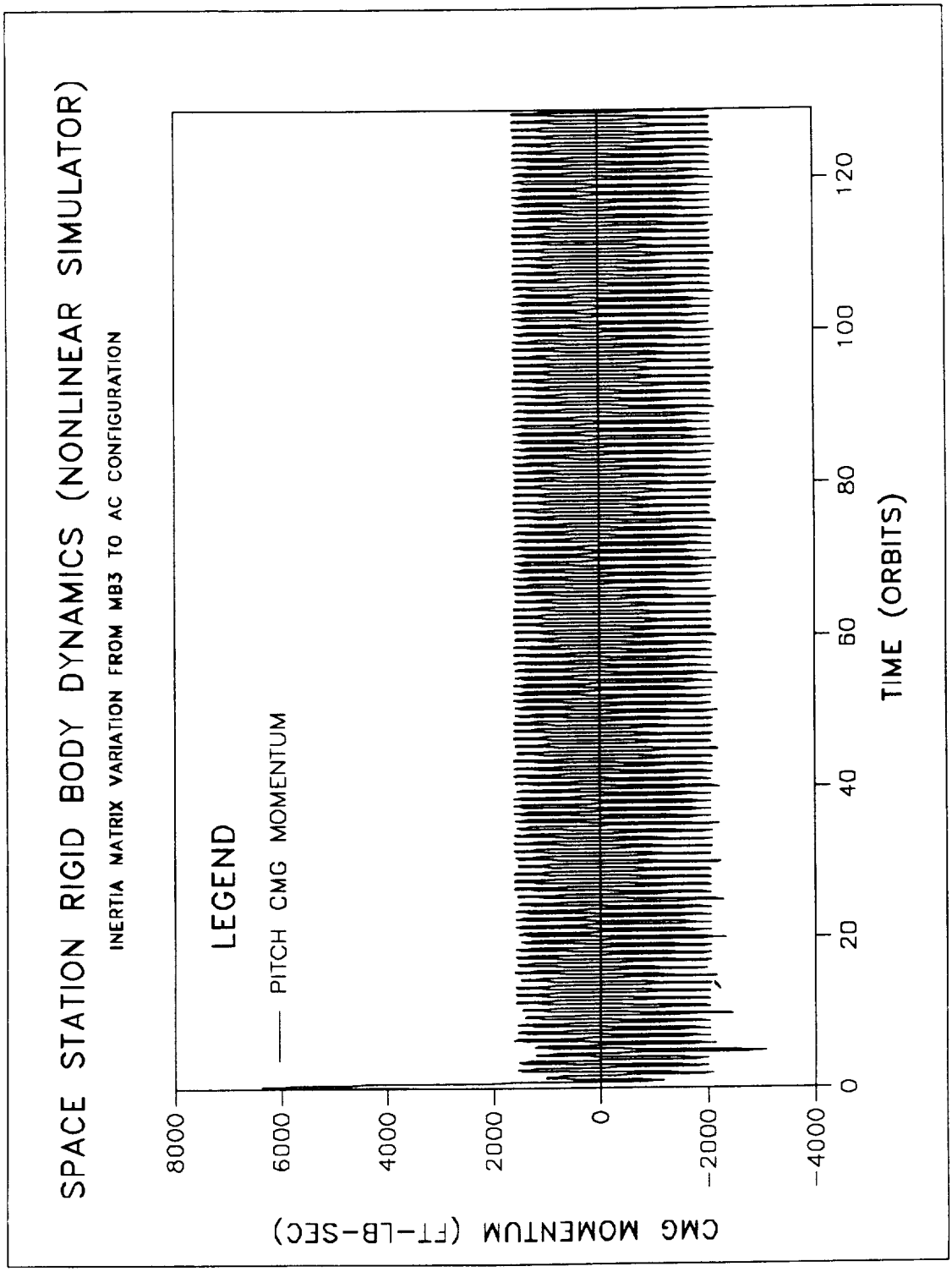

Figure 6.27: Pitch Axis Momentum Response for Inertia Variations from MB3 to AC Configuration.

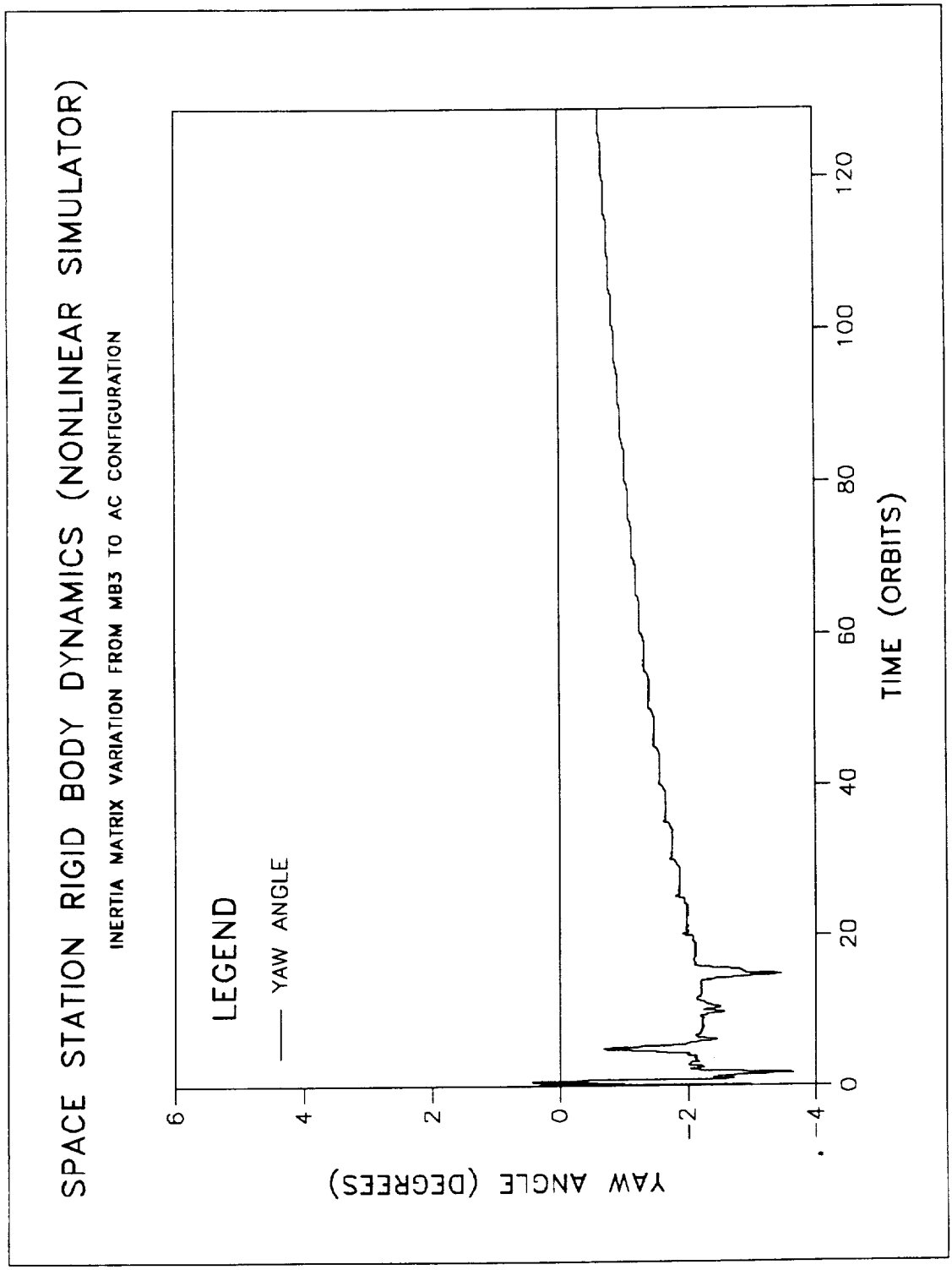

Figure 6.28: Yaw Axis Angle Response for Inertia Variations from MB3 to AC Configuration.

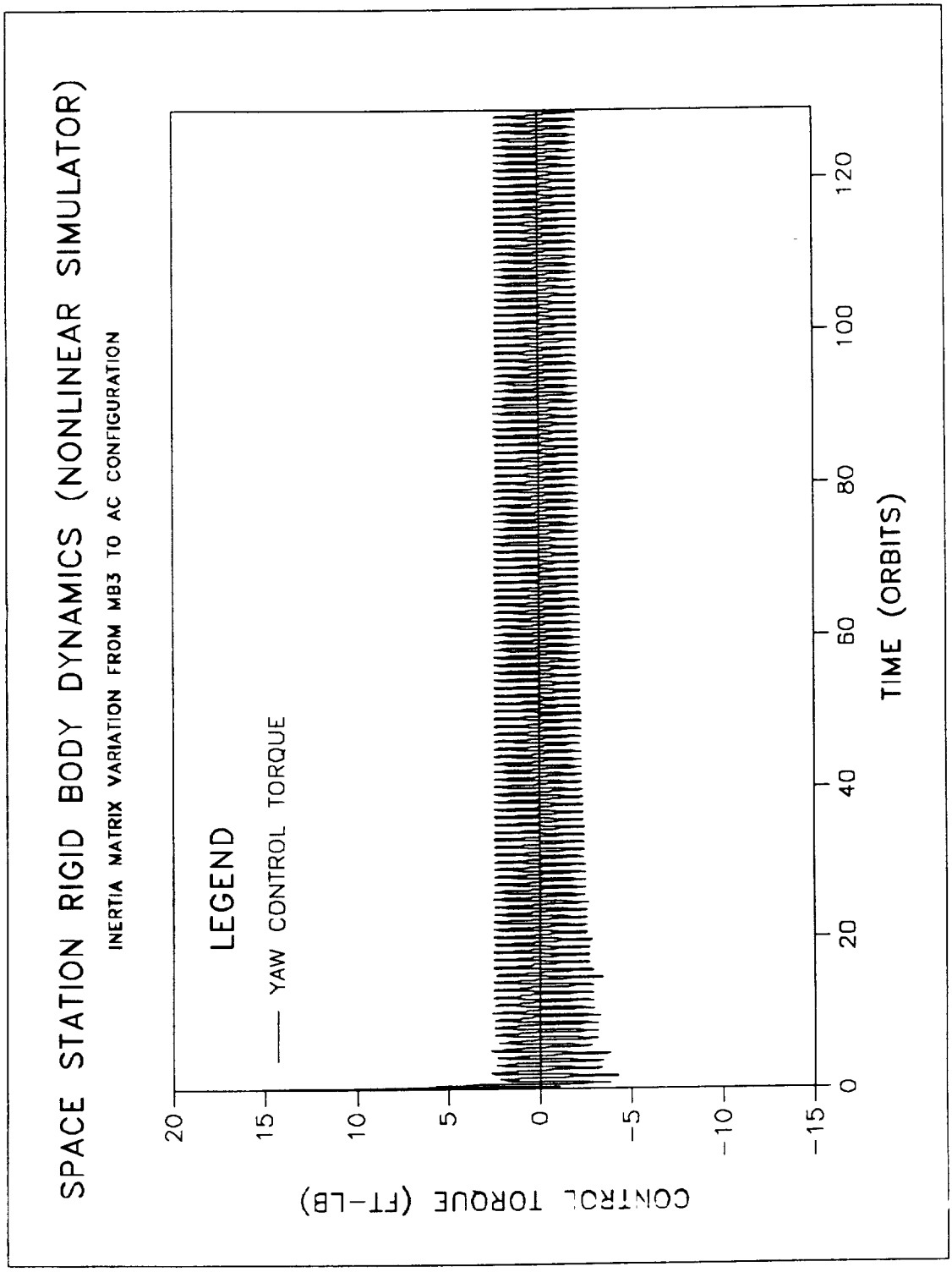

Figure 6.29: Yaw Axis Control Torque Response for Inertia Variations from MB3 to AC Configuration.

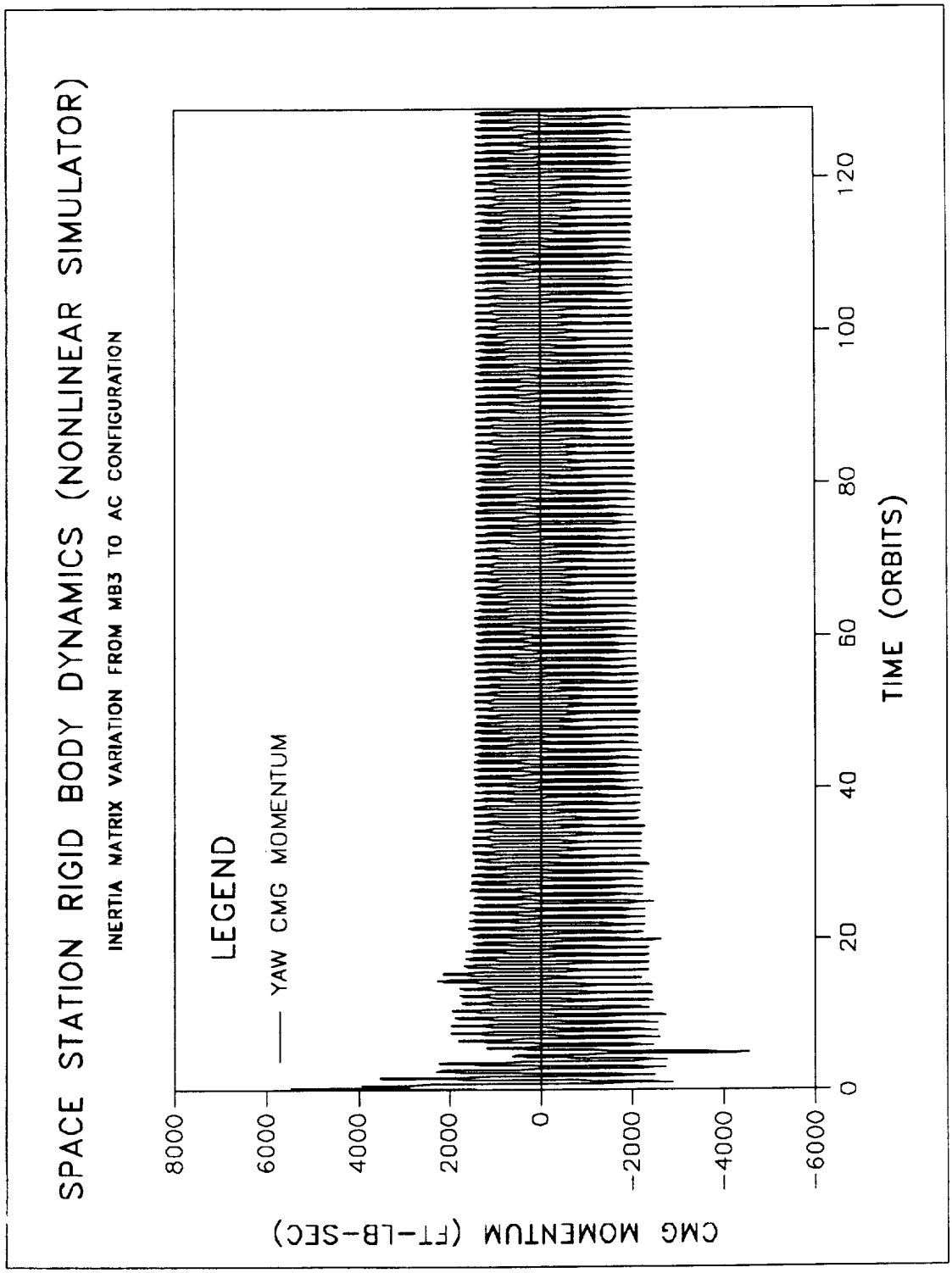

Figure 6.30: Yaw Axis Momentum Response for Inertia Variations from MB3 to AC Configuration.

Chapter 7

Summary and Conclusions

This study presents a systematic derivation of the SSF dynamics linearized around an arbitrary TEA. Linearized models which appeared in the literature can be obtained from the presented model by eliminating certain variables or by setting them to specific numerical values. The usefulness of the fully coupled model in control system design for large angle TEA configurations is demonstrated by designing linear control laws based on models with and without the contribution of the cross-inertia terms. The nonlinear simulations indicate that control laws for ACMM based on small angle linearized or pitch and roll/yaw motion decoupled models of the SSF may, under circumstances, result in unstable closed-loop systems, even though the linearized closed-loop systems appear stable and with good overall performance. Additionally, numerical robustness studies have revealed that the closed-loop system remains stable for up to $\pm$ 30% variations in the SSF inertia matrix, as previously reportes in the literature [1].

As the inertia properties of the SSF will be varying for a number of rea-

sons, such as the assembly sequence and MRMS operations during or after assembly complete configuration, it is desirable to allow smooth ACMM throughout such scenarios. From this study it is evident that a single set of gains will not allow the controller to stabilize the system. It has been therefore proposed to use a gain-scheduled controller with the TEA being the scheduling variable. The approach suffers, as estimates of the TEA must be available in order to update the gains, however, it compares favorably to alternate adaptive control techniques requiring on-line identification. Some additional computer storage will be required to retain the second order polynomial coefficients in memory. Alternate implementations, such as a tabular form of the gains, could be used to further reduce the storage requirements. Transient response simulations indicate that for inertia matrix element changes of up to 1600%, the gain-scheduled controller provides "good" ACMM. It is not the intention of this study to fine-tune the gain-scheduling for best performance and/or robustness. Additionally, no attempt has been made to determine the maximum variation in the inertia matrix that the gain-scheduled controller can tolerate. These and other practical implementation issues, such as controller complexity and storage requirements, remain to be explored.

References

[1] Wie, B., Byun, K.W., Warren, V.W., Geller, D., Long, D., and Sunkel, J., "New Approach to Attitude/Momentum Control for the Space Station," *Journal of Guidance, Control and Dynamics*, Vol.12, No.5, 1989.

[2] Dynacs Engineering Co. Inc., "Impact of Mobile Remote Manipulator System Operations on Attitude Control / Momentum Management System Performance and Design for Phase I Complete Space Station," Report prepared for NASA Johnson Space Center, November 1988.

[3] Space Station Engineering Integration Contractor, "The Limitations of Linearization Techniques on Nonlinear Space Station Equations of Motion," Space Stations Freedom Program, Program Support Contract, SE&I Report PSH-341-RP89-002, Reston, VA 22090.

[4] Warren, W., and Wie, B., "Periodic-Disturbance Accommodating Control of the Space Station for Asymptotic Momentum Management," AIAA Paper No. 89-3476-CP, August 1989.

[5] Hughes, P. C., *Spacecraft Attitude Dynamics*, Wiley, New York, 1986.

[6] Sunkel, J.W. and Shieh, L.S., "An Optimal Momentum Management Controller for the Space Station," AIAA Paper No. 89-3473-CP, August 1989.

[7] Astrom, K.J. and Wittenmark, B., *Adaptive Control*, Addison Wesley, Reading, MA, 1989.

Part III

Controller Synthesis for Input-Output Tracking in Uncertain Nonlinear Systems

Chapter 8

Introduction

One of the fundamental design requirements for feedback control systems is servo-tracking or the ability to regulate controlled outputs without any steady-state errors in the presence of disturbances and plant parameter variations. This problem has been extensively studied in the literature, especially in the context of linear-time-invariant (LTI) systems. It is worth emphasizing here that in the classic asymptotic servo-tracking problem, the one that has been treated extensively in the literature [e.g., Francis and Wonham (1975)], no particular attention is given to the initial tracking error, though it is clear that the initial errors will be bounded as a consequence of closed-loop stability. In the design of such systems the internal model principle proposed by Francis and Wonham (1975) plays an important role. The internal model principle states that the controlled output tracks a class of reference inputs with zero asymptotic error, if the reference is included in the stable closed-loop dynamics. For example, recall that no steady-state error occurs for step reference commands in a type 1,

stable, closed-loop system which has an integrator in the loop. Note that the integrator is the generator for step inputs. This type of a servo system, although is robust to plant parameter variations, is quite sensitive to variations in the reference input. For example, in the case of a step input, if a small sinusoidal variation is added, the steady state error will no longer be zero. The reason is that the integrator is not the generator of the reference command anymore. Consequently, at steady-state the closed-loop system will exhibit a sinusoidal oscillation. In real-world problems, however, one has to deal with such situations, and the internal model principle alone can not resolve these issues.

In order to deal with potential inaccuracies in reference command inputs, a novel notion of tracking, called tracking in the sense of spheres was recently introduced by Jayasuriya et al (1984). The emphasis there is that servotracking should be viewed as the ability to follow a desired output within a specified error bound over its entire duration; that is, to obtain a closed-loop system that tracks reference commands and rejects a class of external disturbances, to the extent required by the error bound, in the presence of plant uncertainties.

In asymptotic tracking, usually a desired output vector $\mathbf{y}_o(t) \in R^l$ is specified and the actual output vector $\mathbf{y}(t) \in R^l$ is required to follow the desired output asymptotically. The idea of tracking in the sense of spheres, unlike the asymptotic tracking case, requires that $\|\mathbf{y} - \mathbf{y}_o\|$ be smaller than a prespecified real number. Here $\|.\|$ denotes any L_p^l - norm though the specific norm we consider in the present study is the L_∞^l - norm.

Remark 1: (i) Let $\mathbf{y}, \mathbf{y}_o \in L_p^l$, then

$$\|\mathbf{y} - \mathbf{y}_o\|_{L_p^l} \equiv \max_i \left(\int_0^\infty |y_i(t) - y_{oi}(t)|^p dt\right)^{1/p}, \quad i = 1, 2, \ldots l$$

where p is a finite positive integer.

(ii) If $\mathbf{y}, \mathbf{y}_o \in L_\infty^l$, then

$$\|\mathbf{y} - \mathbf{y}_o\|_{L_\infty^l} \equiv \max_i [ess \sup_{t \in R} |y_i(t) - y_{oi}(t)|], \quad i = 1, 2, \ldots l.$$

The notion of tracking in the sense of spheres is primarily based on the fact that a system with uncertainties cannot be forced to track a given output precisely although it may be possible to do so with a small tracking error. When the tracking specifications are posed in a quantitative manner, as is done in this study, it becomes necessary to deal directly with the uncertainties of the system. Unlike in the classic servotracking problem, the necessity of having to deal directly with the uncertainties in this "precise" tracking problem makes it difficult to obtain criteria and design algorithms that are both sufficient and relatively simple.

In the literature the tracking problem in the sense of input-output spheres has been formulated by Jayasuriya et al (1984), Jayasuriya and Kee (1988), (1990) in terms of topological neighborhoods in normed function spaces L_∞ and L_2. The main design criterion central to the methodology of Jayasuriya et al (1984) can be stated as a quantitative pole placement (QPP) procedure for adjusting the size of a certain linear operator norm. In particular, the sphere specifications are satisfied provided a proper placement of eigenvalues can be found so that a certain closed-loop operator characterized by these eigenvalues belongs to a set of linear operators

whose L_∞ or L_2 induced norms are upper bounded by a real number determined by the radii of input-output spheres and the uncertainties in the system. However, it has been difficult to obtain such eigenvalue locations in a systematic way.

In Jayasuriya et al (1984) a trial and error procedure was suggested for the L_∞ - problem. In a recent paper, Jayasuriya and Kee (1990) studied the problem further and gave additional insight to the QPP. In particular, they proposed a certain perturbation of the classic Butterworth pole patterns as a solution to the L_∞ , QPP problem. Jayasuriya and Kee (1988) also studied the QPP problem when the tracking specifications are in terms of L_2 - measures and the plant is of the Lúre type. They gave a circle criterion for solving the latter QPP problem which was facilitated by the Hilbert space structure of the function space L_2.

A formal procedure for selecting the eigenvalues for the QPP problem, especially when L_∞ - tracking measures are employed, is currently lacking. The present study is aimed at partially filling this gap. We say partially because the class of nonlinear systems considered is limited to be of the Lúre type. A Lúre type system lends itself to an L_2 - formulation which can subsequently be adopted to an L_∞ - framework. Embedding the problem first in L_2 allows us to draw upon some classical results from nonlinear systems theory on one hand and to utilize H_∞ - minimization [Francis(1987)] for solving the QPP on the other hand. L_∞ - performance specifications are extracted from the L_2 - formulation by resorting to an exponential weighting of L_2 - functions, yielding L_∞ - functions.

Part III of this report is organized as follows. First, some preliminaries

are given in chapter 9. The input-output tracking problem related to Lurе type nonlinear systems is formulated in chapter 10. In chapter 11, an algorithm for minimizing the H_∞-norm is given, followed by a step by step design procedure for the nonlinear tracking problem in chapter 12. A simple second order system is used in chapter 13 to demonstrate the design methodology, followed by a two-degree-of-freedom (2 DOF) robotic manipulator in chapter 14. Summary and conclusions from part III of the report are presented in chapter 15.

Chapter 9

Some Preliminaries

Some basic concepts from elementary functional analysis and notation are collected below.

$L_p^k[0,\infty)$ **space:** is defined as the space of measurable functions with the norm defined as

$$\|\mathbf{f}\|_p = \max_i \left(\int_0^\infty |f_i(t)|^p dt\right)^{1/p} < \infty, \quad i = 1, 2, \ldots k$$

where $\mathbf{f}(t) \in R^k$. $\|.\|_p$ denotes the L_p - norm of the function (.) in the L_p^k - space. When it is understood that $\mathbf{f}(t) \in R^k$ we will simply use the notation $\mathbf{f} \in L_p[0,\infty)$ instead of $\mathbf{f} \in L_p^k[0,\infty)$ throughout this paper.

When $p = 2$ we have the Hilbert space L_2 specified by $\mathbf{f} \in L_2[0,\infty)$ where

$$\|\mathbf{f}\|_2 = \max_i \left(\int_0^\infty |f_i(t)|^2 dt\right)^{1/2} < \infty, \quad i = 1, 2, \ldots k$$

When $p = \infty$ we have the Banach space L_∞ defined by $\mathbf{f} \in L_\infty[0,\infty)$, where

$$\|\mathbf{f}\|_\infty = \max_i [ess \sup_{t \in [0,\infty)} |f_i(t)|] < \infty, \quad i = 1, 2, \ldots k$$

$L_{2e}[0,\infty)$ denotes the extended $L_2[0,\infty)$ space defined as

$$\Omega = \{f : \Im \longmapsto \mathbf{v} |\ \forall \tilde{T} \in \Im,\ \ \|(f)_{\tilde{T}}\|_2 \equiv (\int_0^{\tilde{T}} |f(t)|^2\, dt)^{1/2} < \infty\}$$

$$\text{with} \qquad f_{\tilde{T}} = \begin{cases} f & 0 \le t \le \tilde{T} \\ 0 & t \ge \tilde{T} \end{cases}$$

where $\tilde{T}$ denotes a truncation (Desoer, 1975).

Central to the present study is the novel concept of tracking based on topological notions first introduced by Jayasuriya et al (1984). This notion of tracking is referred to as tracking in the sense of spheres. Also used in the study are ideas drawn from the H_∞ - optimal control literature and the multivariable circle criterion cited below.

9.1 Tracking in the Sense of Spheres

Conventionally, tracking is considered to be the following of a specified trajectory $\mathbf{y}(t)$ in an asymptotic sense. That is, the actual trajectory $\mathbf{y}(t)$ should approach the reference trajectory $\mathbf{y}_o(t)$ as $t \to \infty$. As opposed to this classic definition of asymptotic tracking, the present work is based on a more stringent tracking requirement where the actual trajectory $\mathbf{y}(t)$ is forced to follow the reference $\mathbf{y}_o(t)$ as closely as possible for all times $t \in [0,\infty)$. This is the notion of tracking in the sense of spheres which is illustrated in Figure 9.1 and expressed in a mathematically precise fashion below.

Definition 1 : A given output (input), $\mathbf{y} : T \to R^p$ ($\mathbf{r} : T \to R^m$) is said to belong to an output (input) sphere $\Omega(\mathbf{y}, \mathbf{y}_o, \beta_o)$ ($\Omega(\mathbf{r}, \mathbf{r}_o, \beta_{ri})$) of

radius $\beta_o > 0$ ($\beta_{ri} > 0$) centered at $\mathbf{y}_o : T \rightarrow R^p$ ($\mathbf{r}_o : T \rightarrow R^m$) if $\|\mathbf{y} - \mathbf{y}_o\| \leq \beta_o$ ($\|\mathbf{r} - \mathbf{r}_o\| \leq \beta_{ri}$), where $\|.\|$ is any norm associated with the output (input) function space $\Gamma = \{\mathbf{y}|\mathbf{y} : T \rightarrow Y\}$ ($\Lambda = \{\mathbf{r}|\mathbf{r} : T \rightarrow R\}$) and T is the time set. $\mathbf{y}_o$ ($\mathbf{r}_o$) is referred to as the nominal output (input).

Definition 2: If for any input $\mathbf{r}$ in the input sphere $\Omega(\mathbf{r}, \mathbf{r}_o, \beta_{ri})$, the system output $\mathbf{y}$ stays in the output sphere $\Omega(\mathbf{y}, \mathbf{y}_o, \beta_o)$, then, we say that the system tracks the reference $\mathbf{y}_o$ in the sense of input-output-spheres of radii β_{ri} and β_o, respectively.

9.2 The Multivariable Circle Criterion

The multivariable circle criterion (Cook, 1972) can be summarized as follows:

Let a nonlinear, time-invariant system have the equations

$$\begin{aligned} \dot{\mathbf{x}}(t) &= \mathbf{A}\mathbf{x}(t) + \mathbf{B}\mathbf{u}(t) \\ \mathbf{y}(t) &= \mathbf{C}\mathbf{x}(t) \end{aligned} \tag{9.1}$$

where the nonlinear control $\mathbf{u}(t) = -\mathbf{F}\mathbf{y}(t)$, $\mathbf{F} = diag[f_i(t, y)]$ and $\alpha_i y^2(t) \leq f_i(t, y(t))y(t) \leq \beta_i y^2(t)$, $\alpha_i < \beta_i$, $i = 1, 2, ..., m$. Also, $\mathbf{x}(t), \mathbf{u}(t)$ and $\mathbf{y}(t)$ are real vectors, of dimension n, m and m respectively.

Let $\boldsymbol{\alpha} = diag(\alpha_i)$ and $\boldsymbol{\beta} = diag(\beta_i)$ such that $\boldsymbol{\alpha} \leq \mathbf{F} \leq \boldsymbol{\beta}$, and the $m \times m$ transfer function matrix $\mathbf{H}(s)$ be defined as

$$\mathbf{H}(s) = \mathbf{C}(s\mathbf{I} - \mathbf{A})^{-1}\mathbf{B} = [h_{ij}(s)], \quad i = 1, 2, ...m, \quad j = 1, 2, ...m$$

The resulting closed-loop system is described by the nonlinear, time varying

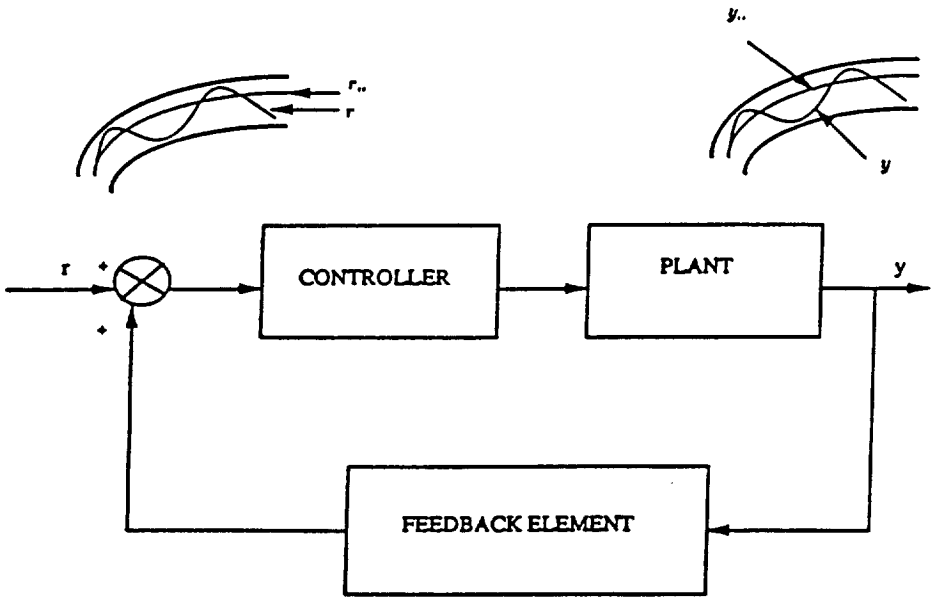

Figure 9.1: Illustration for Precision Tracking.

equation

$$\dot{\mathbf{x}}(t) = \{\mathbf{A} - \mathbf{B}(diag[f_i(t, y(t))])\mathbf{C}\}\mathbf{x}(t) \; . \tag{9.2}$$

Now define

$$d_i(s) = \Sigma_{j=1,\ j\neq i}^{m} |h_{ij}(s)|, \quad i = 1, 2, ...m$$

and

$$d_i^{'}(s) = \Sigma_{j=1,\ j\neq i}^{m} |h_{ji}(s)|, \quad i = 1, 2, ...m$$

and let D be a contour consisting of the imaginary axis from $s = -jR$ to $s = jR$, together with a semi-circle of radius R in the right half of the complex s-plane. Defined below are the ith Gershgorin mean band and the critical disc.

Definition 3: The band swept out by the discs with center $h_{ii}(s)$ and radius $[d_i(s) + d_i^{'}(s)]/2$ as the complex variable s traverses D by the disc with center $h_{ii}(s)$ and radius $[d_i(s) + d_i^{'}(s)]/2$ is named the ith Gershgorin mean band. The disc with the two points $(-1/\alpha_i, 0)$ and $(-1/\beta_i, 0)$ as diameter is called the ith critical disc, $D(\alpha_i, \beta_i)$. The ith Gershgorin band and the critical disc are illustrated in Figure 9.2.

With the above definition, the multivariable circle criterion (Cook, 1972) can be stated as lemma 1.

Lemma 1 (The Multivariable Circle Criterion): Let $(\mathbf{A}, \mathbf{B}, \mathbf{C})$ be a minimum-order realization of $\mathbf{H}(s)$ and let the ith Gershgorin mean band have no point in common with the ith critical disc, and let the ith Gershgorin mean band encircle the ith critical disc N_{ci} times clockwise as s goes once clockwise around D, these conditions remaining satisfied for all

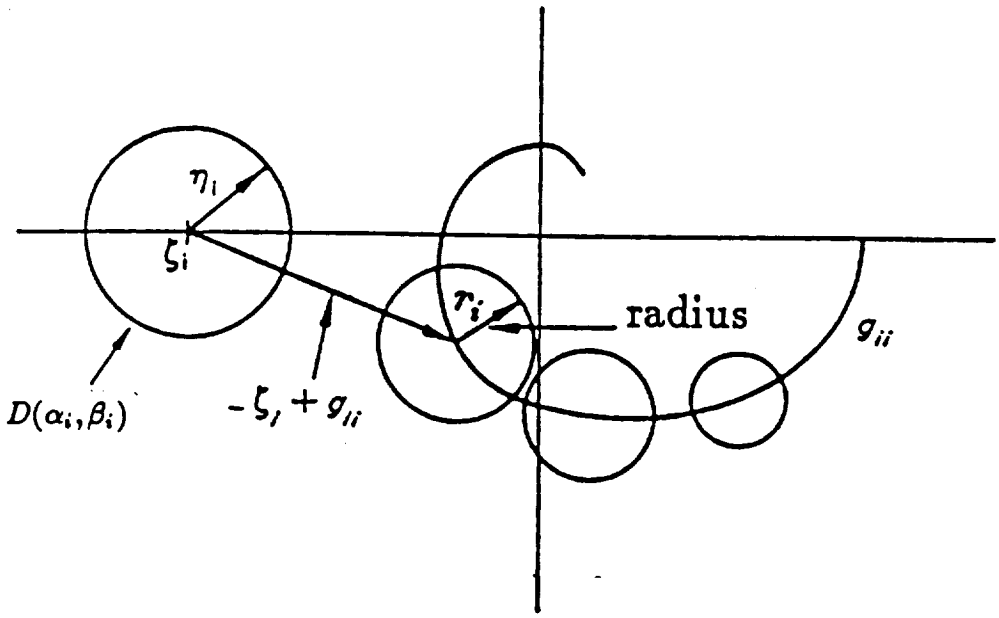

Figure 9.2: Illustration for ith Gershgorin Band and the Critical Disc.

such contours D' with radius $R' \geq R$, and suppose

$$\Sigma_{i=1}^{m} N_{ci} = -P_o \tag{9.3}$$

where P_o is the number of poles of the system transfer matrix $\mathbf{H}(s)$ lying in the closed right half s-plane. Then the system (9.2) is stable in the sense of Liapunov.

Proof: See Cook (1972)

Lemma 1 can be viewed as an extension of the Nyquist stability criterion to Lúre type systems with the actual disc playing the role of the -1 point and the Gershgorin mean band playing the role of the Nyquist plot.

The relationship between Liapunov stability and the L_2 stability is described in Desoer and Vidyasagar (1975) and can be stated as: If the nonlinear control $\mathbf{u}(t)$ in Eqn. (9.1) is of the form $-\mathbf{F}\mathbf{y}(t) + \mathbf{r}(t)$, where $\mathbf{r}(t)$ is a reference input, then, the closed loop system is L_2 stable (i.e., $\mathbf{y}(t) \in L_2$ whenever $\mathbf{r}(t) \in L_2$) provided the conditions of lemma 1 are satisfied.

Chapter 10

Problem Formulation

In this section, the L_∞ - tracking problem for Lurе type systems is formulated. The formulation consists of first showing the L_{2e} - stability of a certain exponentially weighted form of the actual system equations, to assure L_∞ - bounded-input, bounded-output stability of the actual system, followed by an estimation of the tracking errors in terms of the L_∞ - measures. The main design criterion is shown to be a "minimization" of the H_∞ - norm of a certain linear closed-loop operator. The approach to the problem is based on fixed-point techniques and some results drawn from nonlinear systems theory, especially the multivariable circle criterion.

10.1 Plant and Control Structure

Consider the nonlinear, uncertain system in the state-space form

$$\begin{aligned} \dot{\mathbf{x}}(t) &= \mathbf{A}\mathbf{x}(t) + \mathbf{B}\mathbf{u}(t) + \mathbf{G}\mathbf{d}(t) - \mathbf{f}(\mathbf{y}(t), \gamma, t) \\ \mathbf{y} &= \mathbf{C}\mathbf{x}(t) \end{aligned} \tag{10.1}$$

where $\mathbf{x}(t) \in R^n$ is the state, $\mathbf{y}(t) \in R^p$ is the output, $\mathbf{u}(t) \in R^m$ is the control, $\mathbf{d}(t) \in R^r$ is the disturbance vector, $t \in T = [0, \infty)$ and $\mathbf{f}(\mathbf{y}(t), \gamma, t) : R^p \times R^a \times T \rightarrow R^n$ is a nonlinear function. **A, B, G, C** are constant matrices of appropriate dimensions.

The control objective is to guarantee L_∞ - robust tracking in the sense of spheres. That is we require the output $\mathbf{y}(t)$ to be inside a sphere of radius β_o with the nominal output $\mathbf{y}_o(t)$ as center for every reference input $\mathbf{r}(t)$ lying inside a sphere of radius β_{ri} with the nominal reference input $\mathbf{r}_o(t)$ as center. In Jayasuriya and Kee (1988) a similar problem was studied but the input and output spheres were defined in terms of the L_2 - norm.

The controller structure shown in Figure 10.1, is adopted for effecting tracking in the sense of spheres where S_c denotes a servo-compensator, S_o a nonlinear observer and S_s a stabilizing compensator. State-space descriptions of each of the blocks S_c, S_o and S_s are given below.

10.1.1 Servo-Compensator S_c:

$$\dot{\mathbf{x}}_c(t) = \mathbf{A}_c\mathbf{x}_c(t) + \mathbf{B}_c(\mathbf{r}(t) - \mathbf{y}(t)) \tag{10.2}$$

The plant dynamics and the servo-compensator dynamics lead to the augmented state equations

$$\begin{aligned}\dot{\mathbf{x}}_a(t) &= \begin{bmatrix} \mathbf{A} & \mathbf{0} \\ -\mathbf{B}_c\mathbf{C} & \mathbf{A}_c \end{bmatrix} \begin{bmatrix} \mathbf{x}(t) \\ \mathbf{x}_c(t) \end{bmatrix} + \begin{bmatrix} \mathbf{B} \\ \mathbf{0} \end{bmatrix} \mathbf{u}(t) \\ &\quad + \begin{bmatrix} \mathbf{0} & \mathbf{G} \\ \mathbf{B}_c & \mathbf{0} \end{bmatrix} \begin{bmatrix} \mathbf{r}(t) \\ \mathbf{d}(t) \end{bmatrix} - \begin{bmatrix} \mathbf{f}(\mathbf{y}(t), \gamma, t) \\ \mathbf{0} \end{bmatrix}\end{aligned}$$

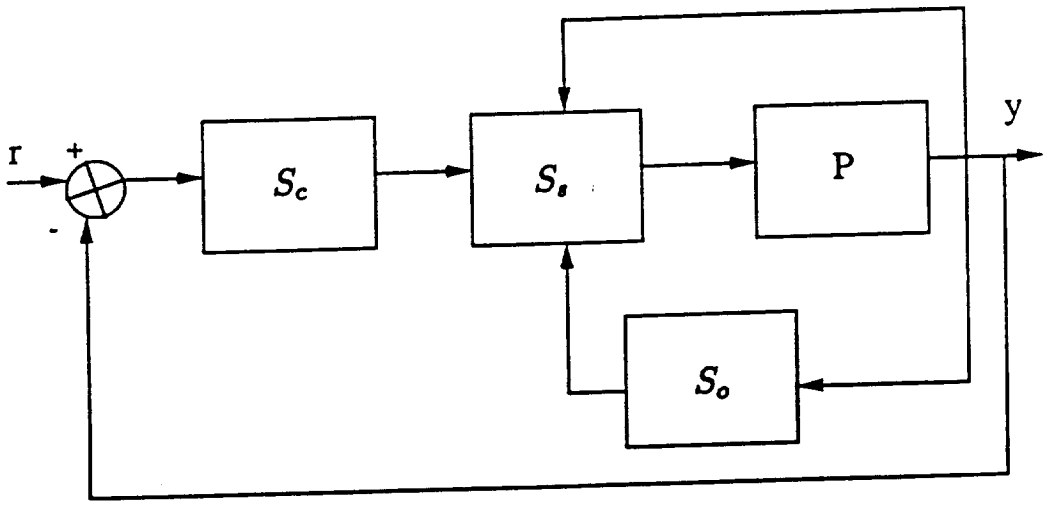

Figure 10.1: Controller Structure.

$$\equiv \mathbf{A}_a\mathbf{x}_a(t) + \mathbf{B}_a\mathbf{u}(t) + \mathbf{G}_a\mathbf{w}(t) - \mathbf{f}_a(\mathbf{y}(t), \boldsymbol{\gamma}, t) \quad (10.3)$$

$$\mathbf{y}(t) = [\mathbf{C}\ \ \mathbf{0}]\begin{bmatrix} \mathbf{x}(t) \\ \mathbf{x}_c(t) \end{bmatrix} \equiv \mathbf{C}_a\mathbf{x}_a(t) \quad (10.4)$$

where $\mathbf{r}(t) \in R^p$ is the reference input and $(\mathbf{A}_c, \mathbf{B}_c)$ is a controllable pair with $|\lambda\mathbf{I} - \mathbf{A}_c| = \lambda^a + \alpha_{a-1}\lambda^{a-1} + ... + \alpha_1\lambda + \alpha_o$. In addition $\mathbf{A}_c \in R^{pq \times pq}$, $\mathbf{B}_c \in R^{pq \times p}$ and $\mathbf{x}_c \in R^{pq}$. The purpose of including a servo-compensator in the control loop is to assure zero error at steady state when there is no input uncertainty.

10.1.2 Nonlinear Observer S_o:

In order to estimate the plant states, we use the nonlinear observer $\mathbf{S}_o$ having the following state equation:

$$\dot{\hat{\mathbf{x}}}(t) = \mathbf{A}\hat{\mathbf{x}}(t) + \mathbf{B}\mathbf{u}(t) - \mathbf{f}_o(\mathbf{y}(t), t) + \mathbf{H}(\mathbf{y}(t) - \hat{\mathbf{y}}(t)) \quad (10.5)$$

$$\hat{\mathbf{y}}(t) = \mathbf{C}\hat{\mathbf{x}}(t)$$

where $\hat{\mathbf{x}}(t) \in R^n$ is the estimated state and $\mathbf{H}$ is a constant observer gain matrix of order $n \times p$. $\mathbf{f}_o(\mathbf{y}(t), t)$ is a nonlinear design function obtained by replacing the uncertain parameters $\boldsymbol{\gamma}$ in $\mathbf{f}(\mathbf{y}(t), \boldsymbol{\gamma}, t)$ by their nominal values. Note that although the augmented state is $\left[\mathbf{x}^T(t)\ \mathbf{x}_c^T(t)\right]^T$, there is no need for an observer to estimate both $\mathbf{x}^T(t)$ and $\mathbf{x}_c^T(t)$, since $\mathbf{x}_c^T(t)$ is already available by the construction, given in Eqn. (10.2).

10.1.3 Stabilizing Control Law S_s:

The stabilizing control law $\mathbf{S}_s$ consists of state feedback from $\hat{\mathbf{x}}(t)$ and $\mathbf{x}_c(t)$ and a nonlinear control $\mathbf{f}_{10}(\mathbf{y}(t), t)$ given by

$$\mathbf{u}(t) = [\mathbf{K}_1 \;\; \mathbf{K}_c]\, \hat{\mathbf{x}}_a(t) + \mathbf{f}_{10}(\mathbf{y}(t), t) \tag{10.6}$$

where $\mathbf{K}_1$ and $\mathbf{K}_c$ are constant state feedback gain matrices. The nonlinear controller $\mathbf{f}_{10}(\mathbf{y}(t), t)$ is obtained by replacing the uncertain parameters γ in $\mathbf{f}_1(\mathbf{y}(t), \gamma, t)$ by their nominal values.

We make the following assumptions regarding the state-space representation of Eqn. (10.1):

(i) The triple $(\mathbf{A}, \mathbf{B}, \mathbf{C})$ is controllable and observable.

(ii) $\mathbf{f}(\mathbf{y}(t), \gamma, t)$ satisfies the matching condition :

$$\mathbf{f}(\mathbf{y}(t), \gamma, t) = \mathbf{B}\mathbf{f}_1(\mathbf{y}(t), \gamma, t)$$

$$\mathbf{f}_o(\mathbf{y}(t), t) = \mathbf{B}\mathbf{f}_{1o}(\mathbf{y}, t).$$

(iii) There exists a constant matrix $\mathbf{N}$ such that $\mathbf{B} = \mathbf{GN}$.

Now, by collecting equations (10.1 - 10.6), we arrive at the following closed-loop equations

$$\begin{aligned} \dot{\mathbf{z}}(t) &= \mathbf{A}_z\mathbf{z}(t) + \mathbf{B}_z\mathbf{w}(t) - \boldsymbol{\phi}_1(\mathbf{y}(t), \gamma, t) \\ &= \mathbf{A}_z\mathbf{z}(t) + \mathbf{B}_z\mathbf{w}(t) - \mathbf{B}_z\boldsymbol{\phi}(\mathbf{y}(t), \gamma, t) \\ \mathbf{y}(t) &= \mathbf{C}_z\mathbf{z}(t), \end{aligned} \tag{10.7}$$

where

$$\mathbf{A}_z \equiv \begin{bmatrix} \mathbf{A} & \mathbf{BK}_c & \mathbf{BK}_1 \\ -\mathbf{B}_c\mathbf{C} & \mathbf{A}_c & \mathbf{0} \\ \mathbf{HC} & \mathbf{BK}_c & \mathbf{A}+\mathbf{BK}_1-\mathbf{HC} \end{bmatrix}, \quad \mathbf{B}_z \equiv \begin{bmatrix} \mathbf{0} & \mathbf{G} \\ \mathbf{B}_c & \mathbf{0} \\ \mathbf{0} & \mathbf{0} \end{bmatrix}$$

$$\mathbf{C}_z \equiv [\mathbf{C} \quad \mathbf{0}], \quad \phi_1(\mathbf{y}(t),\gamma,t) = \mathbf{B}\begin{bmatrix} \mathbf{f}_1(\mathbf{y}(t),\gamma,t) - \mathbf{f}_{10}(\mathbf{y}(t),t) \\ \mathbf{0} \\ \mathbf{0} \end{bmatrix}$$

$$\phi(\mathbf{y}(t),\gamma,t) = \begin{bmatrix} \mathbf{0} \\ \mathbf{N} \end{bmatrix}(\mathbf{f}_1(\mathbf{y}(t),\gamma,t) - \mathbf{f}_{10}(\mathbf{y}(t),t)), \quad \text{and } \mathbf{z}(t) \equiv \begin{bmatrix} \mathbf{x}(t) \\ \mathbf{x}_c(t) \\ \hat{\mathbf{x}}(t) \end{bmatrix}.$$

In the above closed-loop arrangement the design parameters are the matrices $\mathbf{K}_1, \mathbf{K}_c, \mathbf{H}$ and the nonlinear function $\mathbf{f}_{10}$.

Since the control objective is L_∞ - tracking in the sense of spheres, we now proceed to establish BIBO stability of the exponentially weighted closed-loop system with an appropriate bound on L_∞ tracking error. In order to establish the results, we first prove L_2 - stability of the closed-loop system by exploiting the fact that Eqn. (10.7) is of the classic Lúre form. The circle criterion gives conditions for L_2 - stability. Once L_2 - stability is guaranteed, we conclude L_∞ stability of the closed-loop system by the exponential weighting technique. After proving L_∞ - stability, we provide estimates for the tracking errors in terms of the L_∞ - norm. One primary motivation for embedding the problem first in L_2 is to utilize H_∞ - optimal control theory for obtaining the design matrices $\mathbf{K} = [\mathbf{K}_1, \mathbf{K}_c]$, and $\mathbf{H}$.

10.2 L_2 - Stability

Consider the closed-loop system shown in Figure 10.2, described by Eqn. (10.7).

By defining $\mathbf{H}(s) = \mathbf{C}_z(s\mathbf{I} - \mathbf{A}_z)^{-1}\mathbf{B}_z$ with $\mathbf{h}(t)$, the impulse response corresponding to $\mathbf{H}(s)$, Eqn. (10.7) can be written in the following integral form.

$$\begin{aligned} \mathbf{y}(t) &= \int_0^t \mathbf{h}(t-\tau)\mathbf{w}(\tau)d\tau - \int_0^t \mathbf{h}(t-\tau)\boldsymbol{\phi}(\mathbf{y}(\tau),\boldsymbol{\gamma},\tau)d\tau \\ &= \mathbf{v}(t) - \int_0^t \mathbf{h}(t-\tau)\boldsymbol{\phi}(\mathbf{y}(\tau),\boldsymbol{\gamma},\tau)d\tau, \qquad (10.8) \\ \text{where} \quad \mathbf{v}(t) &= \int_0^t \mathbf{h}(t-\tau)\mathbf{w}(\tau)d\tau. \end{aligned}$$

On multiplying both sides of Eqn. (10.8) by $e^{at}, a \in R^1$, we obtain

$$e^{at}\mathbf{y}(t) = e^{at}\mathbf{v}(t) - \int_0^t e^{a(t-\tau)}\mathbf{h}(t-\tau)e^{a\tau}\boldsymbol{\phi}(\mathbf{y}(\tau),\boldsymbol{\gamma},\tau)d\tau \qquad (10.9)$$

which can be written as

$$\mathbf{y}_a(t) = \mathbf{v}_a(t) - \int_0^t \mathbf{h}_a(t-\tau)e^{a\tau}\boldsymbol{\phi}(e^{-a\tau}\mathbf{y}_a(\tau),\boldsymbol{\gamma},\tau)d\tau\ , \qquad (10.10)$$

on substituting $\mathbf{y}_a = e^{at}\mathbf{y}(t), \mathbf{h}_a = e^{at}\mathbf{h}(t)$, and $\mathbf{v}_a = e^{at}\mathbf{v}(t) = \int_0^t \mathbf{h}_a(t-\tau)\mathbf{w}_n(\tau)d\tau$ with $\mathbf{w}_n(t) = e^{at}\mathbf{w}(t)$.

We assume that the nonlinearity $\boldsymbol{\phi}(\mathbf{y}(t),\boldsymbol{\gamma},t)$ lies in the sector $[\boldsymbol{\alpha},\boldsymbol{\beta}]$, $\boldsymbol{\beta} > \mathbf{0}$ (Desoer, 1975). With $\boldsymbol{\alpha} = diag(\alpha_i)$, $\boldsymbol{\beta} = diag(\beta_i)$ and $\boldsymbol{\phi} = diag(\phi_i)$, $i = 1, m$, where m is the dimension of $\boldsymbol{\phi}$, the sector condition becomes $\alpha_i y_i^2 \leq y_i\phi_i \leq \beta_i y_i^2$ for $i = 1, m$. We further assume that $\mathbf{h}_a = e^{at}\mathbf{h}(t) \in L_1 \cap L_2$, for some $a > 0$. The L_2 - stability of the exponentially weighted system (10.10) can be obtained by the multivariable circle criterion and is summarized in the following lemma :

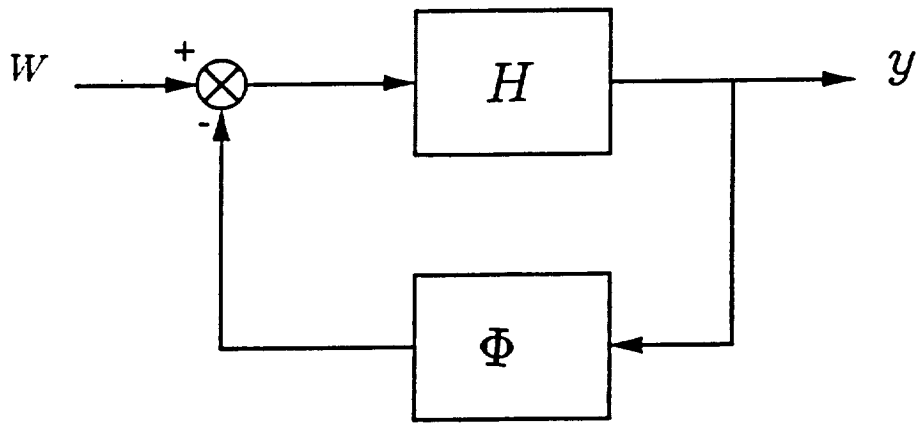

Figure 10.2: Block Diagram of the Closed-Loop System.

Lemma 2: If the Nyquist diagram $\omega \mapsto \mathbf{H}_a(j\omega) = \mathbf{H}(-a + j\omega)$ satisfies conditions of the multivariable circle criterion, then, the system of Eqn. (10.10) is L_{2e} stable (i.e., $\mathbf{w}_n \in L_{2e} \Rightarrow \mathbf{y}_a \in L_{2e}$).

Proof: From Eqn. (10.10), we have

$$\mathbf{y}_a(t) = \mathbf{v}_a(t) - \int_0^t \mathbf{h}_a(t-\tau)e^{a\tau}\phi(e^{-a\tau}\mathbf{y}_a(\tau), \gamma, \tau)d\tau \tag{10.11}$$

which is equivalent to Eqn. (10.9)

$$\begin{aligned} e^{at}\mathbf{y}(t) &= e^{at}\mathbf{v}(t) - \int_0^t e^{a(t-\tau)}\mathbf{h}(t-\tau)e^{a\tau}\phi(\mathbf{y}(\tau), \gamma, \tau)d\tau \\ &= e^{at}\int_0^t \mathbf{h}(t-\tau)\mathbf{w}(\tau)d\tau - \int_0^t e^{a(t-\tau)}\mathbf{h}(t-\tau)e^{a\tau} \\ &\quad \phi(\mathbf{y}(\tau), \gamma, \tau)d\tau \end{aligned} \tag{10.12}$$

The block diagram corresponding to equation (10.12) is shown in Figure 10.3.

Since the output $\mathbf{y}_a = e^{at}\mathbf{y}(t)$ and $\phi(\mathbf{y}(t), \gamma, t) \in [\alpha, \beta]$ with respect to $\mathbf{y}(t)$, it can be easily concluded that $e^{at}\phi(\mathbf{y}(t), \gamma, t) = e^{at}\phi(e^{-at}\mathbf{y}_a(t), \gamma, t)$ belongs to the same sector $[\alpha, \beta]$ with respect to $\mathbf{y}_a(t)$ because the latter simply involves a scaling by e^{at} (see Figure 10.4).

Since $\phi_a = e^{at}\phi \in [\alpha, \beta]$, we can directly apply the circle criterion to determine the stability of system (10.10). Consequently when $\mathbf{w}_n(t) \in L_{2e}$ and $\mathbf{H}_a(j\omega)$ satisfy the conditions of the circle criterion or lemma 1, it follows that $\mathbf{y}_a \in L_{2e}$.

Note that since $\mathbf{H}_a(j\omega) = \mathbf{H}(-a + j\omega)$, the L_{2e} stability of the system given by Eqn. (10.10) is verified by replacing the standard polar plot $\mathbf{H}(j\omega)$ by $\mathbf{H}(-a + j\omega)$ in the circle criterion.

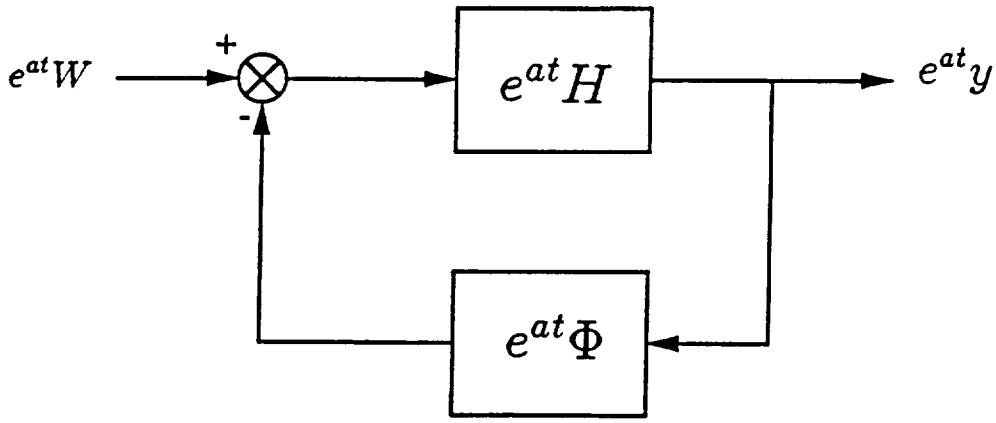

Figure 10.3: Block Diagram of the Exponentially Weighted Closed-Loop System.

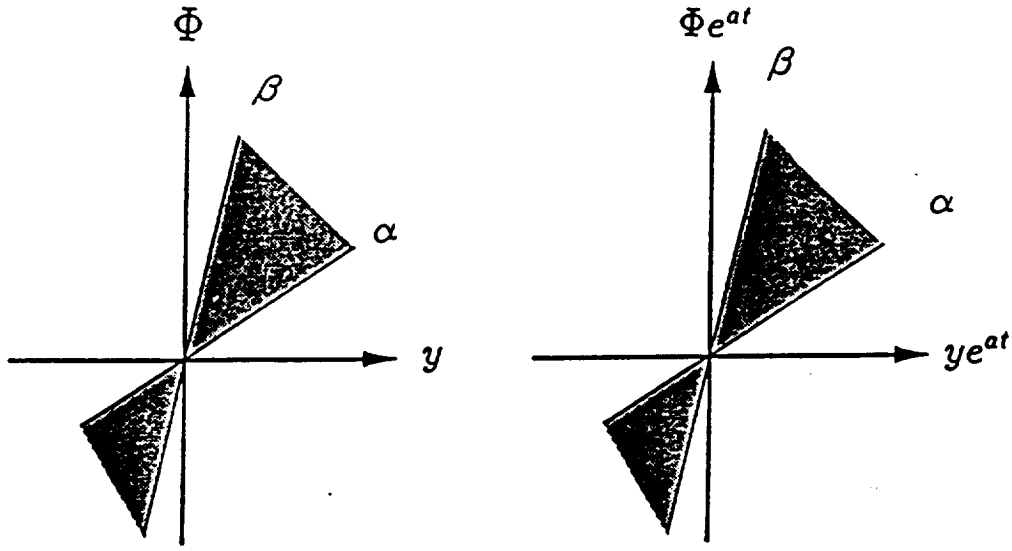

Figure 10.4: The Sector Bound Condition Comparison.

10.3 L_∞ - Stability

In what follows, we use the L_{2e} - stability conditions of the exponentially weighted system (10.10) to establish the L_∞ stability of the actual closed-loop system represented in the integral form in Eqn. (10.8).

Lemma 3: If the exponentially weighted system is L_{2e} stable then the original system is L_∞ stable.

Proof: Recall that system (10.10) is

$$\mathbf{y}_a(t) = \mathbf{v}_a(t) - \int_0^t \mathbf{h}_a(t-\tau)e^{a\tau}\phi(e^{-a\tau}\mathbf{y}_a(\tau),\gamma,\tau)d\tau \tag{10.13}$$

where the nonlinear element $\phi \in [\alpha, \beta]$. Since system (10.10) is L_{2e} stable, there exists some finite constant ρ such that

$$\|[\mathbf{y}_a(.)]_T\|_2 \leq \rho\|[\mathbf{v}_a(.)]_T\|_2 \tag{10.14}$$

where $\|[\mathbf{y}_a(.)]_T\|_2$ denotes the L_2 norm of the truncated function $[\mathbf{y}_a(.)]_T$. Using the fact that $\mathbf{h}_a \in L_1$ and

$$\mathbf{v}_a(t) = \int_0^t \mathbf{h}_a(t-\tau)\mathbf{w}_n(\tau)d\tau \tag{10.15}$$

and the Parseval Theorem [Desoer and Vidyasagar (1975)], we obtain

$$\|[\mathbf{v}_a(.)]_T\|_2 \leq \sup_\omega \|\mathbf{H}_a(j\omega)\|\|[\mathbf{w}_n(.)]_T\|_2. \tag{10.16}$$

Substitution of Eqn. (10.16) into Eqn. (10.14) yields

$$\|[\mathbf{y}_a(.)]_T\|_2 \leq \rho \sup_\omega \|\mathbf{H}_a(j\omega)\|\|[\mathbf{w}_n(.)]_T\|_2 \tag{10.17}$$

and from the proof of the circle criterion [Desoer and Vidyasagar (1975)], we obtain

$$\|[\mathbf{y}_a(.)]_T\|_2 \leq \frac{1}{1-l\gamma_0}\,\gamma_0\|[\mathbf{w}_n(.)]_T\|_2 \tag{10.18}$$

where

$$\begin{aligned} l &= \frac{1}{2}\|\boldsymbol{\beta}-\boldsymbol{\alpha}\|, \quad m=\frac{1}{2}\|\boldsymbol{\beta}+\boldsymbol{\alpha}\| \ , \\ \mathbf{H}_t(s) &\equiv (\mathbf{I}+\mathbf{m}\mathbf{H}_a(s))^{-1}\mathbf{H}_a(s) \\ \gamma_0 &\equiv \sup_{\omega}\|\mathbf{H}_t(j\omega)\|. \end{aligned}$$

By comparing Eqns. (10.17) and (10.18), it now follows that

$$\rho = (\sup_{\omega}\|\mathbf{H}_a(j\omega)\|)^{-1}\frac{\gamma_0}{1-l\gamma_0} \tag{10.19}$$

substitution of which in Eqn. (10.14) yields

$$\|[\mathbf{y}_a(.)]_T\|_2 \leq (\sup_{\omega}\|H_a(j\omega)\|)^{-1}\frac{\gamma_0}{1-l\gamma_0}\|[\mathbf{v}_a(.)]_T\|_2. \tag{10.20}$$

It can be easily seen that when $\mathbf{w}(t)\in L_\infty$, then $\mathbf{v}(t)\in L_\infty$, since $\mathbf{h}(t)\in L_1$. Moreover,

$$\begin{aligned} \|[\mathbf{v}_a(.)]_T\|_2 &\equiv \|[e^{at}\mathbf{v}(.)]_T\|_2 = (\int_0^T \|e^{at}\mathbf{v}(t)\|^2dt)^{1/2} \\ &\leq \sup_t\|\mathbf{v}(t)\|(\int_0^T e^{2at}dt)^{1/2} = \|\mathbf{v}(.)\|_\infty\left[\frac{(e^{2aT}-1)^{1/2}}{(2a)^{1/2}}\right] \\ &\leq (2a)^{-1/2}\sqrt{e^{2aT}-1}\|\mathbf{h}(.)\|_1\|\mathbf{w}\|_\infty \ . \end{aligned} \tag{10.21}$$

Since the nonlinear element $e^{at}\boldsymbol{\phi}(e^{-at}\mathbf{y}_a(t),\boldsymbol{\gamma},t)$ belongs to the sector $[\boldsymbol{\alpha},\boldsymbol{\beta}]$ with respect to $\mathbf{y}_a(t)$, we obtain

$$\|[e^{at}\boldsymbol{\phi}(e^{-at}\mathbf{y}_a(t),\boldsymbol{\gamma},t)]_T\|_2 \leq \boldsymbol{\beta}\|[\mathbf{y}_a]_T\|_2 \tag{10.22}$$

which becomes

$$\begin{aligned} \|[e^{at}\boldsymbol{\phi}(e^{-at}\mathbf{y}_a(t),\boldsymbol{\gamma},t)]_T\|_2 &\leq \boldsymbol{\beta}(\sup_{\omega}\|\mathbf{H}_a(j\omega)\|)^{-1}\frac{\gamma_0}{1-l\gamma_0} \\ &\quad ((2a)^{-1/2}\sqrt{e^{2aT}-1})\|\mathbf{h}(.)\|_1\|\mathbf{w}\|_\infty \end{aligned} \tag{10.23}$$

upon substitution of Eqns. (10.20) and (10.21). Taking the amplitude on both sides of Eqn. (10.8), we obtain

$$\begin{aligned}
|\mathbf{y}(t)| &\leq |\mathbf{v}(t)| + \int_0^t |\mathbf{h}(t-\tau)||\boldsymbol{\phi}(\mathbf{y}(\tau),\boldsymbol{\gamma},\tau)|d\tau \\
&\leq \|\mathbf{h}\|_1\|\mathbf{w}\|_\infty + e^{-at}\int_0^t e^{a(t-\tau)}|\mathbf{h}(t-\tau)|e^{a\tau}|\boldsymbol{\phi}(e^{-a\tau}\mathbf{y}_a(\tau),\boldsymbol{\gamma},\tau)|d\tau \\
&\leq \|\mathbf{h}\|_1\|\mathbf{w}\|_\infty + e^{-at}\|\mathbf{h}(\tau)e^{a\tau}\|_2\|[e^{at}\boldsymbol{\phi}(e^{-at}\mathbf{y}_a(t),\boldsymbol{\gamma},t)]_T\|_2 \\
&\qquad \text{(from Schwartz Inequality)} \\
&\leq \|\mathbf{h}\|_1\|\mathbf{w}\|_\infty + \|\mathbf{h}(\tau)e^{a\tau}\|_2\|[e^{at}\boldsymbol{\phi}(e^{-at}\mathbf{y}_a(t),\boldsymbol{\gamma},t)]_T\|_2 \qquad (10.24) \\
&\qquad \text{(since } t \geq 0, \quad a > 0).
\end{aligned}$$

Now using Eqn. (10.23) in (10.24), the following is obtained:

$$\begin{aligned}
\|\mathbf{y}(t)\|_\infty &\leq [\|\mathbf{h}\|_1 + \|\mathbf{h}(\tau)e^{a\tau}\|_2\boldsymbol{\beta}(\sup_\omega|\mathbf{H}_a(j\omega)|)^{-1} \\
&\qquad \frac{\gamma_0}{1-l\gamma_0}\{(2a)^{-1/2}\sqrt{e^{2aT}-1}\}\|\mathbf{h}(.)\|_1]\|\mathbf{w}\|_\infty \\
&\equiv K_k\|\mathbf{w}\|_\infty, \text{ where } \mathrm{K_k} \text{ is a finite constant.} \qquad (10.25)
\end{aligned}$$

From Eqn. (10.25) it is now clear that if $\mathbf{w}(t) \in L_\infty$ (i.e., $\|\mathbf{w}(t)\|_\infty < \infty$) then $\|\mathbf{y}(t)\|_\infty < \infty$ implying that the original system is BIBO stable. This completes the proof of Lemma 3.

Lemmas 2 and 3 are now combined in theorem 1 below to give conditions for guaranteeing L_∞ - stability of the closed-loop system (10.8).

Theorem 1 : Given the nonlinear equation (10.8), with $\mathbf{h}(.) \in L_1$, $e^{at}\mathbf{h}(.) \in L_1 \cap L_2$ for some $a > 0$, and with the nonlinear element $\boldsymbol{\phi}(\mathbf{y}(.),\boldsymbol{\gamma},.)$ belonging to the sector $[\boldsymbol{\alpha},\boldsymbol{\beta}]$, $\boldsymbol{\beta} > \mathbf{0}$, the closed-loop system (10.8) is L_∞ stable, provided that the Nyquist diagram $\omega \mapsto \mathbf{H}_a(j\omega) = \mathbf{H}(-a+j\omega)$ satisfies the conditions of the multivariable circle criterion given in lemma 1.

Proof: The proof of theorem 1 is immediate from lemmas 2 and 3.

10.4 L_∞ - Tracking

From theorem 1 we note that the closed-loop stability in the L_∞ - sense is established by considering the modified Nyquist locus $\mathbf{H}(-a+j\omega)$ resulting from Eqn. (10.12). The transfer matrix $\mathbf{H}(-a+s)$ can be thought of as representing a system equivalent to the modified state equations

$$\begin{aligned} \dot{\mathbf{z}}_a(t) &= (a\mathbf{I}+\mathbf{A}_z)\mathbf{z}_a(t)+\mathbf{B}_z\mathbf{w}_n(t)-\mathbf{B}_z\boldsymbol{\phi}_a(t) \\ \mathbf{y}_a(t) &= \mathbf{C}_z\mathbf{z}_a(t) \end{aligned} \tag{10.26}$$

having the integral form

$$\begin{aligned} \mathbf{y}_a(t) = {} & \mathbf{C}_z\int_0^t e^{\mathbf{A}_n(t-\tau)}\mathbf{B}_z\mathbf{w}_n(\tau)d\tau - \\ & \mathbf{C}_z\int_0^t e^{\mathbf{A}_n(t-\tau)}\mathbf{B}_z\boldsymbol{\phi}_a(\mathbf{y}_a(\tau),\gamma,\tau)d\tau + \mathbf{C}_z e^{\mathbf{A}_n t}\mathbf{z}_a(0) \end{aligned}$$

where

$$\mathbf{A}_n = a\mathbf{I}+\mathbf{A}_z \tag{10.27}$$

or the operator form

$$\mathbf{y}_a(t) = \mathbf{C}_z\boldsymbol{\Gamma}\mathbf{B}_z\mathbf{w}_n(t) - \mathbf{C}_z\boldsymbol{\Gamma}\mathbf{B}_z\boldsymbol{\phi}_a(t)\mathbf{y}_a(t)+\mathbf{y}_a(0) \tag{10.28}$$

where $\mathbf{y}_a(0) = \mathbf{C}_z e^{\mathbf{A}_n t}\mathbf{z}_a(0)$ denotes the system initial conditions, and

$$\begin{aligned} (\boldsymbol{\Gamma}\mathbf{x})(t) &= \int_0^t e^{\mathbf{A}_n(t-\tau)}\mathbf{x}(\tau)d\tau, \\ \boldsymbol{\phi}_a(t)\mathbf{y}_a(t) &= \boldsymbol{\phi}_a(\mathbf{y}_a(t),\gamma,t)\in[\boldsymbol{\alpha},\boldsymbol{\beta}]. \end{aligned}$$

Remark 2: Since $(\mathbf{A},\mathbf{B},\mathbf{C})$ is controllable and observable, the control gains $\mathbf{K}=[\mathbf{K}_1,\mathbf{K}_c]$ and $\mathbf{H}$ can be found so that $\mathbf{A}_n(=(a\mathbf{I}+\mathbf{A}_z))$, $a>0$, is Hurwitz. Moreover, under the assumption that $\boldsymbol{\phi}(\mathbf{y}(t),\gamma,t)$ in Eqn. (10.8)

is sector bounded in $[\alpha, \beta]$, and the circle criterion in lemma 1 is satisfied, we know that the system (10.28) is L_{2e} stable because $\phi_a(t)$ also belongs to the same sector. Thus, when w_n belongs to L_{2e}, the linear and the nonlinear operators Γ and $\phi_a(t)$, map L_{2e} back into itself.

We now recall that our control objective is to effect L_∞ - tracking in the sense of spheres for the uncertain nonlinear system (10.8). So far we have established L_∞ stability of (10.8) and L_{2e} - stability of the exponentially weighted system (10.10). Because one of our goals is to specify the design matrices $\mathbf{K}_1, \mathbf{K}_c, \mathbf{H}$ by an H_∞ - formulation, we first solve the tracking problem in L_{2e} to obtain H_∞ - conditions on the linear closed loop operator $(\mathbf{C}_z \Gamma \mathbf{B}_z)$ and subsequently enforce the required L_∞ - tracking specifications required of the original system.

Consequently, we start by considering a nominal system output specified by $(\mathbf{w}_{ao}(t), \mathbf{z}_{ao}(t), \mathbf{y}_{ao}(t))$ satisfying the following equations for the exponentially weighted system.

$$\begin{aligned} \dot{\mathbf{z}}_{ao}(t) &= \mathbf{A}_n \mathbf{z}_{ao}(t) + \mathbf{B}_z \mathbf{w}_{no}(t) - \mathbf{B}_z \phi_{ao}(\mathbf{y}_{ao}(t), t) \qquad (10.29) \\ \mathbf{y}_{ao}(t) &= \mathbf{C}_z \mathbf{z}_{ao}(t) \end{aligned}$$

which is a completely known hypothetical plant corresponding to (10.26). $\phi_{ao}(\mathbf{y}_{ao}(t), t)$ is a nonlinear design function, which is obtained by replacing the uncertainty in $\phi_a(\mathbf{y}_a(t), \gamma, t)$ with the nominal values. Equation (10.29) has the equivalent operator form

$$\mathbf{y}_{ao}(t) = \mathbf{C}_z \Gamma \mathbf{B}_z \mathbf{w}_{no}(t) - \mathbf{C}_z \Gamma \mathbf{B}_z \phi_{ao}(t) \mathbf{y}_{ao}(t) + \mathbf{y}_{ao}(0) \qquad (10.30)$$

where $\phi_{ao}(t)\mathbf{y}_{ao}(t) = \phi_{ao}(\mathbf{y}_{ao}(t), t)$ and $\mathbf{y}_{ao}(0)$ is the initial condition of the nominal system. It is easy to show that the system given by Eqn. (10.30)

is L_{2e} stable (see **Remark 2**).

Then, a comparison of the actual system and the nominal system (10.30) leads to the error operator equation

$$\mathbf{y}_a(t)-\mathbf{y}_{ao}(t) = \mathbf{C}_z\boldsymbol{\Gamma}\mathbf{B}_z(\mathbf{w}_n(t)-\mathbf{w}_{no}(t))-\mathbf{C}_z\boldsymbol{\Gamma}\mathbf{B}_z(\boldsymbol{\phi}_a(t)\mathbf{y}_a(t)-\boldsymbol{\phi}_{ao}(t)\mathbf{y}_{ao}(t)) \tag{10.31}$$

on assuming $\mathbf{y}_a(0) = \mathbf{y}_{ao}(0)$, from which we obtain

$$\begin{aligned} \mathbf{y}_a(t) &= \mathbf{C}_z\boldsymbol{\Gamma}\mathbf{B}_z(\mathbf{w}_n(t) - \mathbf{w}_{no}(t)) \\ &\quad -\mathbf{C}_z\boldsymbol{\Gamma}\mathbf{B}_z(\boldsymbol{\phi}_a(t)y_a(t) - \boldsymbol{\phi}_{wo}(t)\mathbf{y}_{ao}(t)) + \mathbf{y}_{ao}(t) \\ &= \boldsymbol{\Psi}\mathbf{y}_a(t). \end{aligned} \tag{10.32}$$

Thus, from (10.30) and remark 1, it immediately follows that $\boldsymbol{\Psi}$ is an operator mapping L_{2e} into itself. If $\mathbf{w}_n(t)$ belongs to L_2, it is easy to see that the satisfaction of the circle criterion of lemma 2 guarantees L_2 stability, because $\mathbf{A}_n$ is Hurwitz and $\boldsymbol{\phi}_a(t)$ belongs to the sector $[\boldsymbol{\alpha}, \boldsymbol{\beta}]$. Hence, the operator $\boldsymbol{\Psi}$ also maps L_2 back into itself. If $\mathbf{w}_n(t)$ belongs to L_{2e}, instead of L_2, it is worth noting that the truncated function $[\mathbf{w}_n(t)]_T$ is still in L_2, where T is the truncation time. Thus, up to the truncation time T, the input $\mathbf{w}_n(t)$ is in L_2, and so is the output $\mathbf{y}_a(t)$.

Note that Eqn. (10.32) is a fixed point equation with the mapping $\boldsymbol{\Psi}$: $L_2 \longrightarrow L_2$. Hence, we can utilize fixed point theory to obtain a criterion for the tracking performance. To this end, we summarize the local contraction mapping theorem in the following lemma:

Lemma 4: Let $\mathbf{y}_{ao} \in (\mathbf{Y}, \|.\|)$, $\mathbf{Y}$ is a Banach Space, and let B_{yw} be defined as a closed sphere in $\mathbf{Y}$ with center at $\mathbf{y}_{ao}$ given by

$$B_{yw} = \{\mathbf{y}_a | \|\mathbf{y}_a - \mathbf{y}_{ao}\| \leq \alpha_n\}, \quad \text{where } \alpha_n > 0 \tag{10.33}$$

Let $\mathbf{\Psi} : \mathbf{Y} \rightarrow \mathbf{Y}$ be a linear map. If there exists a constant k, $0 < k < 1$, such that

$$(i) \quad \|\mathbf{\Psi y}_a - \mathbf{\Psi y}_a^{'}\| \leq k\|\mathbf{y}_a - \mathbf{y}_a^{'}\|, \quad \forall\, \mathbf{y}_a,\ \mathbf{y}_a^{'} \in \mathbf{B}_{yw}$$

$$(ii) \quad \|\mathbf{\Psi y}_{ao} - \mathbf{y}_{ao}\| \leq \alpha_n(1-k).$$

Then, it follows that

(i) $\mathbf{\Psi}$ maps B_{yw} into itself

(ii) $\mathbf{\Psi}$ has a unique fixed point $\mathbf{y}_a^* \in B_{yw}$ such that $\mathbf{\Psi y}_a^* = \mathbf{y}_a^*$.

Proof: See Martin (1976).

Lemma 4, together with the fixed point equation (10.32), and the sphere specification on input-output tracking, lead to the following main result for guaranteeing L_∞ - tracking in the sense of spheres for the closed-loop system (10.8):

Theorem 2 : Let $\mathbf{w}(t) \in R^r$ and $\mathbf{y}(t) \in R^p$ denote the exogenous input and the plant output vector of the closed-loop system and let the design matrices $\mathbf{K}_1, \mathbf{K}_c, \mathbf{H}$ and the nonlinear design function $\mathbf{f}_{1o}(t)$ be such that the closed-loop system satisfies the conditions stipulated in theorem 1. Let $\mathbf{w}_o(t)$ $(\equiv [\mathbf{r}_o^T(t) \;\; \mathbf{d}_o^T(t)]^T$, $\mathbf{d}_o(t) = \mathbf{0})$, $\mathbf{z}_o(t)$ and $\mathbf{y}_o(t)$ be the known nominal input-output combination satisfying the nominal tracking model of Eqn. (10.30), and $\mathbf{w}(t)(= [\mathbf{r}^T(t) \;\; \mathbf{d}^T(t)]^T)$, $\mathbf{z}(t), \mathbf{y}(t)$ be any combination satisfying the actual closed-loop equations (10.28). Then, for any reference input $\mathbf{r}(t)$ in the prespecified input sphere

$$\Omega(\mathbf{r}, \mathbf{r}_o, \beta_{ri}) = \{\mathbf{r}(t) \in L_\infty^p |\ ||\mathbf{r}(t) - \mathbf{r}_o(t)||_{L_\infty} \leq \beta_{ri}\} \tag{10.34}$$

and a bounded disturbance with norm $\|\mathbf{d}(t)\|_\infty$, there exists a unique plant

output $\mathbf{y}(t)$ in the prespecified output sphere

$$\Omega(\mathbf{y}, \mathbf{y}_o, \beta_o) = \{\mathbf{y}(t) \in L_\infty^p | \ ||\mathbf{y}(t) - \mathbf{y}_o(t)||_{L_\infty} \leq \beta_o\} \tag{10.35}$$

provided that

$$\beta_1 \leq \frac{\beta_o}{\beta_{ri} + \|\mathbf{d}(t)\|_\infty + \beta_o\beta_3 + \beta_4} \tag{10.36}$$

where

$$\begin{aligned}
\beta_1 &\equiv \|\mathbf{C}_z(s\mathbf{I} - \mathbf{A}_n)^{-1}\mathbf{B}_z\|_{H_\infty}, \quad \mathbf{A}_n \equiv a\mathbf{I} + \mathbf{A}_z, \ a > 0 \\
\beta_3 &= \sup_{\boldsymbol{\gamma} \in \Im} \|[\nabla_{\mathbf{y}} \boldsymbol{\phi}(\mathbf{y}(t), \boldsymbol{\gamma}, t)]_T\|_2 \\
\beta_4 &= \sup_{\boldsymbol{\gamma} \in \Im} \|(\boldsymbol{\phi}(\mathbf{y}_o(t), \boldsymbol{\gamma}, t) - \boldsymbol{\phi}_o(\mathbf{y}_o(t), t))_T\|_2
\end{aligned}$$

with $\boldsymbol{\phi}_o(t)$ serving as the nominal value of $\boldsymbol{\phi}(t)$ at $\mathbf{y}_o(t)$.

Proof: First we consider the fixed point form (10.32) of the exponentially weighted system and obtain conditions for assuring that the mapping $\boldsymbol{\Psi}$ is a local contraction over the exponentially weighted output sphere $\|\mathbf{y}_a(t) - \mathbf{y}_{ao}(t)\|_2 \leq \alpha_n$.

Consider

$$\begin{aligned}
\|(\boldsymbol{\Psi}\mathbf{y}_a(t) - \boldsymbol{\Psi}\mathbf{y}_a'(t))_T\|_2 &= \| - \mathbf{C}_z\boldsymbol{\Gamma}\mathbf{B}_z(\boldsymbol{\phi}_a(t)\mathbf{y}_a(t) - \boldsymbol{\phi}_a(t)\mathbf{y}_a'(t))_T\|_2 \\
&\leq \|\mathbf{C}_z\boldsymbol{\Gamma}\mathbf{B}_z\|_{i2}\|(\boldsymbol{\phi}_a(t)\mathbf{y}_a(t) - \boldsymbol{\phi}_a(t)\mathbf{y}_a'(t))_T\|_2 \\
&\leq k\|(\mathbf{y}_a(t) - \mathbf{y}_a'(t))_T\|_2
\end{aligned} \tag{10.37}$$

where

$$k = \|\mathbf{C}_z\boldsymbol{\Gamma}\mathbf{B}_z\|_{i2} \sup_{\mathbf{y}_a \neq \mathbf{y}_a', \ \mathbf{y}_a, \mathbf{y}_a' \in B_{yw}, \boldsymbol{\gamma} \in \Im \subset R^r} \frac{\|(\boldsymbol{\phi}_a(t)\mathbf{y}_a(t) - \boldsymbol{\phi}_a(t)\mathbf{y}_a'(t))_T\|_2}{\|(\mathbf{y}_a(t) - \mathbf{y}_a'(t))_T\|_2}$$

$$= \|\mathbf{C}_z \boldsymbol{\Gamma} \mathbf{B}_z\|_{i2} \sup_{*} \frac{\|(\boldsymbol{\phi}_a(t)\mathbf{y}_a(t) - \boldsymbol{\phi}_a(t)\mathbf{y}_a'(t))_T\|_2}{\|(\mathbf{y}_a(t) - \mathbf{y}_a'(t))_T\|_2}. \tag{10.38}$$

From lemma 4, for $\boldsymbol{\Psi}$ to be a local contraction, we require

$$\begin{aligned}
&\|(\boldsymbol{\Psi}\mathbf{y}_{ao}(t) - \boldsymbol{\Psi}\mathbf{y}_{ao}(t))_T\|_2 \\
= \;& \|\mathbf{C}_z \boldsymbol{\Gamma} \mathbf{B}_z(\mathbf{w}_n(t) - \mathbf{w}_{no}(t))_T - \mathbf{C}_z \boldsymbol{\Gamma} \mathbf{B}_z(\boldsymbol{\phi}_a(t)\mathbf{y}_{ao}(t) - \boldsymbol{\phi}_{ao}(t)\mathbf{y}_{ao}(t))_T\|_2 \\
\leq \;& \|\mathbf{C}_z \boldsymbol{\Gamma} \mathbf{B}_z\|_{i2}\{\|(\mathbf{w}_n(t) - \mathbf{w}_{no}(t))_T\|_2 + \sup_{\boldsymbol{\gamma} \in \Im} \|(\boldsymbol{\phi}_a(t)\mathbf{y}_{ao}(t) - \boldsymbol{\phi}_{ao}(t)\mathbf{y}_{ao}(t))_T\|_2\} \\
\leq \;& \alpha_n(1-k).
\end{aligned} \tag{10.39}$$

Now, let $\|(\mathbf{w}_n(t) - \mathbf{w}_{no}(t))_T\|_2 \leq \beta_{ni}$ be a prespecified input sphere radius in L_2 and define

$$\begin{aligned}
\beta_1 &= \|\mathbf{C}_z \boldsymbol{\Gamma} \mathbf{B}_z\|_{i2} \equiv \|\mathbf{C}_z(s\mathbf{I} - \mathbf{A}_n)^{-1}\mathbf{B}_z\|_{H_\infty} \\
\beta_2 &= \sup_{\boldsymbol{\gamma} \in \Im} \|(\boldsymbol{\phi}_a(t)\mathbf{y}_{ao}(t) - \boldsymbol{\phi}_{ao}(t)\mathbf{y}_{ao}(t))_T\|_2 \\
\beta_3 &= \sup_{*} \frac{\|(\boldsymbol{\phi}_a(t)\mathbf{y}_a(t) - \boldsymbol{\phi}_a(t)\mathbf{y}_a'(t))_T\|_2}{\|(\mathbf{y}_a(t) - \mathbf{y}_a'(t))_T\|_2}
\end{aligned} \tag{10.40}$$

yielding

$$k = \beta_1 \beta_3 < 1. \tag{10.41}$$

Expression (10.39) leads to

$$\beta_1(\beta_{ni} + \beta_2) \leq \alpha_n(1-k) \tag{10.42}$$

which on combining with (10.41) yields

$$\beta_1 \leq \frac{\alpha_n}{\beta_{ni} + \alpha_n\beta_3 + \beta_2}. \tag{10.43}$$

Hence from lemma 4, it now follows that inequality (10.43) is a sufficient condition for guaranteeing that $\|(\mathbf{y}_a(t) - \mathbf{y}_{ao}(t))_T\|_2 \leq \alpha_n$ whenever $\|(\mathbf{w}_n(t) - \mathbf{w}_{no}(t))_T\|_2 \leq \beta_{ni}$.

Note that inequality (10.43) assures L_2 tracking in the sense of spheres with respect to the input sphere radius β_{ni} and the output sphere radius α_n. Since the design parameters are chosen to satisfy conditions of theorem 1, we know that the original system is L_∞ - stable. Hence, we now use the L_2 - stability condition (10.43) to bound the L_∞ tracking error.
Consider

$$\begin{aligned} \|(\mathbf{w}_n(t) - \mathbf{w}_{no}(t))_T\|_2 &= (\int_0^T |\mathbf{w}_n(t) - \mathbf{w}_{no}(t)|^2 dt)^{1/2} \\ &= (\int_0^T e^{2at} |\mathbf{w}(t) - \mathbf{w}_o(t)|^2 dt)^{1/2} \\ &\leq \|\mathbf{w}(t) - \mathbf{w}_o(t)\|_\infty [\frac{1}{2a}(e^{2aT} - 1)]^{1/2} \\ &\equiv E\|\mathbf{w}(t) - \mathbf{w}_o(t)\|_\infty \leq \beta_{ni} \end{aligned} \tag{10.44}$$

where $E \equiv [\frac{1}{2a}(e^{2aT} - 1)]^{1/2}$. Similarly, the relation between the variation of the output $\mathbf{y}_a(t) \in L_{2e}$ in (10.10) and $y \in L_\infty$ in (10.8) is

$$\|(\mathbf{y}_a(t) - \mathbf{y}_{ao}(t))_T\|_2 \leq E\|\mathbf{y}(t) - \mathbf{y}_o(t)\|_\infty \leq \alpha_n \ . \tag{10.45}$$

Since we want the output of system (10.8) (measured by the L_∞ norm) to lie in the output sphere $\|\mathbf{y}(t) - \mathbf{y}_o(t)\|_\infty \leq \beta_o$ whenever the input $\mathbf{w}(t)$ is in the input sphere $\|\mathbf{w}(t) - \mathbf{w}_o(t)\|_\infty \leq \beta_i$, from (10.44) and (10.45), we obtain

$$\beta_{ni} = E\beta_i \quad \text{and} \tag{10.46}$$

$$\alpha_n = E\beta_o \ . \tag{10.47}$$

Substituting (10.46) and (10.47) in (10.43), we obtain

$$\beta_1 \leq \frac{E\beta_o}{E\beta_i + E\beta_o\beta_3 + \beta_2} \tag{10.48}$$

which is a sufficient condition for guaranteeing that

$$\|\mathbf{w}(t) - \mathbf{w}_o(t)\|_\infty \leq \beta_i \Rightarrow \|\mathbf{y}(t) - \mathbf{y}_o(t)\|_\infty \leq \beta_o \ . \tag{10.49}$$

Because $\mathbf{w}(t)$ in (10.49) consists of both the reference $\mathbf{r}(t)$ and the disturbance $\mathbf{d}(t)$, by letting $\mathbf{r}_o(t)$ and the null vector denote the nominal reference input and the nominal disturbance respectively, we compute

$$\begin{aligned} \|\mathbf{w}(t) - \mathbf{w}_o(t)\|_\infty &\equiv \| \begin{bmatrix} \mathbf{r}(t) - \mathbf{r}_o(t) \\ \mathbf{d}(t) - \mathbf{0} \end{bmatrix} \|_\infty \\ &\leq \|\mathbf{r}(t) - \mathbf{r}_o(t)\|_\infty + \|\mathbf{d}(t)\|_\infty \leq \beta_i \end{aligned} \tag{10.50}$$

since the reference input $\mathbf{r}(t)$ is prespecified to be in the sphere $\|\mathbf{r}(t) - \mathbf{r}_o(t)\|_\infty \leq \beta_{ri}$, we let $\beta_i = \beta_{ri} + \|\mathbf{d}(t)\|_\infty$. Inequality (10.48) can then be rewritten as

$$\beta_1 \leq \frac{E\beta_o}{E(\beta_{ri} + \|\mathbf{d}(t)\|_\infty) + E\beta_o\beta_3 + \beta_2} \tag{10.51}$$

which is a sufficient condition for guaranteeing that

$$\|\mathbf{r}(t) - \mathbf{r}_o(t)\|_\infty \leq \beta_{ri} \Rightarrow \|\mathbf{y}(t) - \mathbf{y}_o(t)\|_\infty \leq \beta_o \tag{10.52}$$

Remark 3:

(i) In computing the upper bound on β_1 specified by (10.51), a value for E is needed. E depends on the truncation time T. The system settling time, for instance, can be used for T.

(ii) β_1 is the H_∞ norm of the linear operator $\mathbf{C}_z\boldsymbol{\Gamma}\mathbf{B}_z$. β_1 depends on the gains $\mathbf{K}_1, \mathbf{K}_c, \mathbf{H}$ and the chosen positive number a.

(iii) β_2, β_3 and β_4 can be computed as follows.

$$\begin{aligned}
\beta_2 &= \sup_{\gamma\in\Im} \|(\phi_a(t)\mathbf{y}_{ao}(t) - \phi_{ao}(t)\mathbf{y}_{ao})(t)_T\|_2 \\
&\leq \|(e^{at})_T\|_2 \sup_{\gamma\in\Im} \|(\phi(\mathbf{y}_o(t),\gamma,t) - \phi_o(\mathbf{y}_o(t),t))_T\|_2 \\
&= E \sup_{\gamma\in\Im} \|(\phi(\mathbf{y}_o(t),\gamma,t) - \phi_o(\mathbf{y}_o(t),t))_T\|_2 \\
&\equiv E\beta_4
\end{aligned} \tag{10.53}$$

$$\begin{aligned}
\beta_3 &= \sup_{*} \frac{\|(\phi_a(t)\mathbf{y}_a(t) - \phi_a(t)\mathbf{y}_a'(t))_T\|_2}{\|(\mathbf{y}_a(t) - \mathbf{y}_a'(t))_T\|_2} \\
&= \sup_{*} \frac{\|(e^{at}[\phi(\mathbf{y}(t),\gamma,t) - \phi(\mathbf{y}'(t),\gamma,t)])_T\|_2}{\|[e^{at}(\mathbf{y}(t) - \mathbf{y}'(t))]_T\|_2} \\
&= \sup_{*} \|[\nabla_{\mathbf{y}}\phi]_T\|_2.
\end{aligned} \tag{10.54}$$

Since $\phi \in [\alpha, \beta]$, $\forall\ \gamma \in \Im$ and the bounds α, β are known apriori, we can simplify the computation of the inequality (10.51) by letting $\phi_o(\mathbf{y}_o(t), t) = \frac{1}{2}\|\alpha + \beta\|\mathbf{y}_o$ yielding

$$\beta_4 = (\frac{\|\beta - \alpha\|}{2})\|(\mathbf{y}_o(t))_T\|_2\ . \tag{10.55}$$

Thus, the sufficient condition guaranteeing

$$\|\mathbf{r}(t) - \mathbf{r}_o(t)\|_\infty \leq \beta_{ri} \Rightarrow \|\mathbf{y}(t) - \mathbf{y}_o(t)\|_\infty \leq \beta_o \tag{10.56}$$

can be expressed as

$$\beta_1 \leq \frac{\beta_o}{\beta_{ri} + \|\mathbf{d}(t)\|_\infty + \beta_o\beta_3 + \beta_4}. \tag{10.57}$$

Remark 4: Although the parameters a and T do not explicitly appear in the inequality (10.57), the selection of these two parameters does affect it implicitly, since β_1 depends on $a > 0$ and β_3, β_5 depends on T. To obtain

less conservative results, a and T can be chosen as small as possible. The smaller the values of a and T are, the smaller are the value of β_1 and that of β_3, β_4 in the inequality (10.57).

10.5 Computation of the Gains K and H

The sufficiency criterion (60) of theorem 2, essentially separates the uncertain effects from the nominal linear portion $\mathbf{L} = \mathbf{C}_z \boldsymbol{\Gamma} \mathbf{B}_z$ ($\beta_1 = \|\mathbf{L}\|_{H_\infty}$). Thus, the design problem now reduces to obtaining the state feedback gain matrices $\mathbf{K} = [\mathbf{K}_1, \mathbf{K}_c]$ and the observer gain matrix $\mathbf{H}$ such that β_1 is close to its threshold value. To select $\mathbf{K}$ and $\mathbf{H}$, we consider the following hypothetical linear system representing the transfer function matrix $\mathbf{C}_z(s\mathbf{I} - \mathbf{A}_n)^{-1}\mathbf{B}_z$. That is:

$$\begin{aligned} \dot{\mathbf{z}}_l(t) &= \mathbf{A}_n \mathbf{z}_l(t) + \mathbf{B}_z \mathbf{w}(t) \\ \mathbf{y}(t) &= \mathbf{C}_z \mathbf{z}_l(t) \end{aligned} \tag{10.58}$$

where

$$\mathbf{A}_n \equiv \begin{bmatrix} a\mathbf{I} + \mathbf{A} & \mathbf{B}\mathbf{K}_c & \mathbf{B}\mathbf{K}_1 \\ -\mathbf{B}_c\mathbf{C} & a\mathbf{I} + \mathbf{A}_c & \mathbf{0} \\ \mathbf{H}\mathbf{C} & \mathbf{B}\mathbf{K}_c & a\mathbf{I} + \mathbf{A} + \mathbf{B}\mathbf{K}_1 - \mathbf{H}\mathbf{C} \end{bmatrix}, \quad \mathbf{B}_z \equiv \begin{bmatrix} \mathbf{0} & \mathbf{G} \\ \mathbf{B}_c & \mathbf{0} \\ \mathbf{0} & \mathbf{0} \end{bmatrix}$$

$$\mathbf{C}_z \equiv [\mathbf{C} \quad 0 \quad 0].$$

By letting

$$\mathbf{z}_l(t) = \begin{bmatrix} \mathbf{x}_l(t) \\ \mathbf{x}_{cl}(t) \\ \hat{\mathbf{x}}_l(t) \end{bmatrix},$$

Eqn. (10.58) can be expressed as the combination of state dynamics :

$$\begin{bmatrix} \dot{\mathbf{x}}_l(t) \\ \dot{\mathbf{x}}_{cl}(t) \end{bmatrix} = \begin{bmatrix} a\mathbf{I}+\mathbf{A} & \mathbf{0} \\ -\mathbf{B}_c\mathbf{C} & a\mathbf{I}+\mathbf{A}_c \end{bmatrix} \begin{bmatrix} \mathbf{x}_l(t) \\ \mathbf{x}_{cl}(t) \end{bmatrix} + \begin{bmatrix} \mathbf{B} \\ \mathbf{0} \end{bmatrix} \mathbf{u}_l(t) + \begin{bmatrix} \mathbf{0} & \mathbf{G} \\ \mathbf{B}_c & \mathbf{0} \end{bmatrix} \mathbf{w}(t) \tag{10.59}$$

$$\mathbf{y}(t) = [\mathbf{C} \;\; \mathbf{0}] \begin{bmatrix} \mathbf{x}_l(t) \\ \mathbf{x}_{cl}(t) \end{bmatrix} \tag{10.60}$$

and of the full order observer for estimating the state $\mathbf{x}_l(t)$:

$$\dot{\hat{\mathbf{x}}}_l(t) = (a\mathbf{I}+\mathbf{A})\hat{\mathbf{x}}_l(t) + \mathbf{B}\mathbf{u}_l(t) + \mathbf{H}(\mathbf{y}(t) - \hat{\mathbf{y}}(t)) \tag{10.61}$$

$$\hat{\mathbf{y}}(t) = \mathbf{C}\hat{\mathbf{x}}_l(t)\,, \quad \mathbf{u}_l(t) = [\mathbf{K}_1 \;\; \mathbf{K}_c] \begin{bmatrix} \hat{\mathbf{x}}_l(t) \\ \mathbf{x}_{cl}(t) \end{bmatrix}.$$

In order to adjust the H_∞-norm of the hypothetical, linear system $\mathbf{C_z}(s\mathbf{I}-\mathbf{A_n})^{-1}\mathbf{B_z}$ by proper choice of $\mathbf{K_1}$, $\mathbf{K_c}$, and $\mathbf{H}$ we can use any H_∞-minimization algorithm available in the literature [Doyle et al (1989), Grimble (1988), Postlethwaite and Young (1988)] . The specific algorithm used in the present work was developed by the authors of the present paper, details of which can be found in Hwang et al (1990).

Chapter 11

An Algorithm for H_∞ Optimality

The objective of the algorithm given below is the determination of the controller and the observer gain matrices so that the closed loop system remains stable and $\|\mathbf{T_{wy}}\|_{H_\infty} \leq \nu$, where ν is the threshold value of the H_∞-norm of the transfer function matrix $\mathbf{T_{wy}}$ from the hypothetical exogenous input $\mathbf{w}(t)$ to the hypothetical output $\mathbf{y}(t)$ of Eqn. (61). For a specific weighting ρ on the hypothetical control inputs $\mathbf{u}_l(t)$, the H_∞-optimal control gains are determined by invoking theorem 3 and the existence conditions given below.

Theorem 3: The H_∞-optimal control law for the weighted hypothetical controlled output vector $\begin{bmatrix} \mathbf{y}(t) \\ \rho\mathbf{u}_l(t) \end{bmatrix}$ of system (61) is given by

$$[\mathbf{K}_1 \;\; \mathbf{K}_c] = -\left(\frac{1}{\rho^2}\right)\begin{bmatrix} \mathbf{B} \\ \mathbf{0} \end{bmatrix}^T \mathbf{k}_1 \qquad .$$

$$\text{and} \quad \mathbf{H} = -(\mathbf{I} - \mathbf{h}_\infty \mathbf{k}_1)^{-1} \mathbf{h}_\infty [\mathbf{C}\ \mathbf{0}]^T$$

where $\mathbf{k}_1$ is the positive definite solution of the algebraic Riccati equation

$$\begin{aligned} &\begin{bmatrix} a\mathbf{I}+\mathbf{A} & \mathbf{0} \\ -\mathbf{B_c C} & a\mathbf{I}+\mathbf{A_c} \end{bmatrix}^T \mathbf{k}_1 + \mathbf{k}_1 \begin{bmatrix} a\mathbf{I}+\mathbf{A} & \mathbf{0} \\ -\mathbf{B_c C} & a\mathbf{I}+\mathbf{A_c} \end{bmatrix} \\ &+ \mathbf{k}_1 \left(\begin{bmatrix} \mathbf{0} & \mathbf{G} \\ \mathbf{B_c} & \mathbf{0} \end{bmatrix} \begin{bmatrix} \mathbf{0} & \mathbf{G} \\ \mathbf{B_c} & \mathbf{0} \end{bmatrix}^T - \left(\frac{1}{\rho^2}\right) \begin{bmatrix} \mathbf{B} \\ \mathbf{0} \end{bmatrix} \begin{bmatrix} \mathbf{B} \\ \mathbf{0} \end{bmatrix}^T \right) \mathbf{k}_1 \\ &+ \begin{bmatrix} \mathbf{C} & \mathbf{0} \end{bmatrix}^T \begin{bmatrix} \mathbf{C} & \mathbf{0} \end{bmatrix} = \mathbf{0} \end{aligned} \tag{11.1}$$

and $\mathbf{h}_\infty$ is the positive definite solution of the following Lyapunov equation

$$[a\mathbf{I} + \mathbf{A}]\mathbf{h}_\infty + \mathbf{h}_\infty [a\mathbf{I} + \mathbf{A}]^T + \mathbf{G}\mathbf{G}^\mathbf{T} = \mathbf{0}\,. \tag{11.2}$$

Proof: The proof is omitted since it appears in Hwang et al (1990).

The necessary and sufficient conditions for the existence of the H_∞-optimal control law given in theorem 3, such that $\|\mathbf{T_{wy}}\|_{H_\infty} < \nu$, are:

(i)

$$\begin{bmatrix} \begin{bmatrix} a\mathbf{I}+\mathbf{A} & \mathbf{0} \\ -\mathbf{B_c C} & a\mathbf{I}+\mathbf{A_c} \end{bmatrix} & \left(\begin{bmatrix} \mathbf{0} & \mathbf{G} \\ \mathbf{B_c} & \mathbf{0} \end{bmatrix} \begin{bmatrix} \mathbf{0} & \mathbf{G} \\ \mathbf{B_c} & \mathbf{0} \end{bmatrix}^T - \begin{bmatrix} \mathbf{B} \\ \mathbf{0} \end{bmatrix} \begin{bmatrix} \mathbf{B} \\ \mathbf{0} \end{bmatrix}^T \right) \\ -\begin{bmatrix} \mathbf{C} & \mathbf{0} \end{bmatrix}^T \begin{bmatrix} \mathbf{C} & \mathbf{0} \end{bmatrix} & -\begin{bmatrix} a\mathbf{I}+\mathbf{A} & \mathbf{0} \\ -\mathbf{B_c C} & a\mathbf{I}+\mathbf{A_c} \end{bmatrix}^T \end{bmatrix},$$

$$\begin{bmatrix} (\mathbf{A}+a\mathbf{I})^T & \mathbf{0} \\ -\mathbf{G}\mathbf{G}^T & -(\mathbf{A}+a\mathbf{I}) \end{bmatrix} \in dom(Ric)$$

and

(ii)

$$\mathbf{k_1} > \mathbf{0} \text{ and } \mathbf{h}_\infty > \mathbf{0}$$

(iii)

$$\lambda_{max}(\mathbf{k_1 h}_\infty) < \nu^2$$

where $\lambda_{max}(\cdot)$ is the maximum eigenvalue of the matrix $(\cdot)$.

A complete treatment of the above existence conditions can be found in Doyle et al (1988).

The algorithm based on the existence conditions and theorem 3 can now be stated as follows for determining the relevant gain matrices. Henceforth, it is assumed that the design objective is $\|\frac{1}{\nu}\mathbf{T_{wy}}\|_{H_\infty} \leq 1$ or equivalently $\|\hat{\mathbf{T}}_{wy}\|_{H_\infty} \leq 1$, for insuring the existence of the H_∞-optimal control law. This transformation can be accomplished by scaling $\mathbf{w}(t)$ and/or $\mathbf{y}(t)$ such that the H_∞-norm of $\mathbf{T_{wy}}$ is always less than or equal to 1. This scaling of the disturbance and controlled output terms requires the following transformation of the matrices involved in the hypothetical system dynamics:

$$\begin{bmatrix} \mathbf{0} & \mathbf{G} \\ \mathbf{B_c} & \mathbf{0} \end{bmatrix} \rightarrow \nu^{-1/2} \begin{bmatrix} \mathbf{0} & \mathbf{G} \\ \mathbf{B_c} & \mathbf{0} \end{bmatrix}, \begin{bmatrix} \mathbf{B} \\ \mathbf{0} \end{bmatrix} \rightarrow \nu^{1/2} \begin{bmatrix} \mathbf{B} \\ \mathbf{0} \end{bmatrix}, \mathbf{C} \rightarrow \nu^{-1/2}\mathbf{C}. \tag{11.3}$$

We also define:

$$\|\mathbf{T_{wy}}\|_{H_\infty} \equiv \delta \ , \tag{11.4}$$

to facilitate the description of the algorithm below:

Step 1: Select the (control) weight ρ and an initial value for ν. The initial value of ν is set at $\|\mathbf{T_{wy}}\|_{H_\infty}$, though alternate choices are acceptable [see Hwang et al (1990)].

Step 2: Apply the aforementioned scaling and solve the Riccati equation (65) and the Lyapunov equation (66) for the scaled system.

Step 3: Evaluate the gains $\mathbf{k}_1$ and $\mathbf{h}_\infty$ corresponding to the unscaled system and calculate $\|\mathbf{T_{wy}}\|_{H_\infty}$, i.e. the value of δ.

Step 4: If $\mathbf{k}_1 \geq \mathbf{0}$ and $\mathbf{h}_\infty \geq \mathbf{0}$, then go to Step 5, or else,

if $\delta \geq \nu$, then decrease ρ and repeat Steps 2 through 4,
or else,
set $\nu = \delta$ and repeat Steps 2 through 4.

Step 5: If $\lambda_{max}(\mathbf{k}_1\mathbf{h}_\infty) < 1$, then go to Step 6, or else,

if $\delta \geq \nu$, then decrease ρ and repeat Steps 2 through 4,
or else,
set $\nu = \delta$ and repeat Steps 2 through 4.

Step 6: If $\delta < \nu$, then set $\nu = \delta$ and proceed to Step 7, or else,

if $\rho \leq \epsilon$, ϵ a small number, then set $\nu = \delta$ and go to Step 8,
or else,
decrease ρ and repeat Steps 2 through 6.

Step 7: If ν is less than the minimum value of ν evaluated so far then repeat Steps 2 through 7 with a smaller value of ν, or else proceed to Step 8.

Step 8: Form the H_∞-optimal controller gains $\mathbf{K_1}$, $\mathbf{K_c}$and the observer gain $\mathbf{H}$. Moreover, $\|\mathbf{T_{wy}}\|_{H_\infty} \approx \nu$.

Remark 5: The above algorithm is organized in such a way that it is versatile enough to accommodate other design specifications in addition to minimizing the H_∞-norm of $\mathbf{T_{wy}}$.

Chapter 12

Nonlinear Synthesis Procedure

Based on the H_∞-optimal control law given in the previous section, the controller gain matrices $\mathbf{K}_1, \mathbf{K}_c$ and the observer gain matrix $\mathbf{H}$, needed for synthesis can be obtained for Lurе type nonlinear systems through a step by step design procedure proposed below. This leads to a systematic placement of eigenvalues for the QPP problem for guaranteeing L_∞ tracking in the sense of spheres for Lurе type systems.

12.1 Design Procedure

First compute the threshold

$$m = \frac{\beta_o}{\beta_{ri} + \|\mathbf{d}(t)\|_\infty + \beta_o\beta_3 + \beta_4} \tag{12.1}$$

from the given specifications $\beta_o, \beta_{ri}, \|\mathbf{d}(t)\|_\infty$, the nonlinear function $\phi(t)$ and assumed initial guesses for a and T. m gives an initial upper bound on $\|\mathbf{L}\|_{H_\infty} = \|\mathbf{C}_z(s\mathbf{I} - \mathbf{A}_n)^{-1}\mathbf{B}_z\|_{H_\infty}$.

Then use the H_∞ - algorithm given previously in section IV to select a set of gain matrices $\mathbf{K} = [\mathbf{K_1} \;\; \mathbf{K_c}]$ and $\mathbf{H}$ so that $\|\mathbf{L}\|_{H_\infty} \leq m$. A new value of T can also be found by adopting the settling time of the closed-loop system. With these values of $\mathbf{K} = [\mathbf{K_1} \;\; \mathbf{K_c}]$ and $\mathbf{H}$, we can determine $a > 0$ to satisfy the conditions of the circle criterion. With this newly found value of a and T, we can recompute the updated value m_1 of m. If the updated value $m_1 \approx \beta_1$, then the design is complete. If not the procedure is repeated with the newly found values of a and T. We have found the following step by step procedure to be effective for executing the design methodology developed in chapter 10.

Step 1: Select values for a and T, and compute the threshold m.

Step 2: Select ρ and use the H_∞ search algorithm
until $\beta_1 = \|\mathbf{L}\|_{H_\infty} \leq m$ and determine $\mathbf{K}$ $(= [\mathbf{K}_1, \; \mathbf{K}_c])$ and $\mathbf{H}$.

Step 3: Form the closed-loop system. Adapt T to the system settling time and repeat step 1 to update m until T is close to the system settling time.
If $\beta_1 > m$, decrease ρ and repeat step 2.

Step 4: If $\omega \longmapsto \mathbf{H}_a(j\omega)$ satisfies the circle criterion, go to step 5.
otherwise adjust a and go to step 1.

Step 5: Repeat steps 2 - 4
until β_1 is close to but lower than the threshold m. Then form the gain matrices $\mathbf{K}$ and $\mathbf{H}$.

Two examples that utilize the above step by step procedure for executing the design method are given in the next chapters.

Chapter 13

A Simple Example

Consider the uncertain, nonlinear system:

$$\begin{aligned} \dot{\mathbf{x}}(t) &= \mathbf{A}\mathbf{x}(t) + \mathbf{B}u(t) + \mathbf{G}d(t) + \mathbf{f}(y(t), \Delta m, t) \\ y(t) &= \mathbf{C}\mathbf{x}(t) \end{aligned} \tag{13.1}$$

with

$$\mathbf{A} = \begin{bmatrix} 0 & 1 \\ 0 & -1 \end{bmatrix}, \quad \mathbf{B} = \begin{bmatrix} 0 \\ 1 \end{bmatrix}, \quad \mathbf{C} = [1 \quad 0], \quad G = \begin{bmatrix} 0 \\ 0.1 \end{bmatrix}$$

$$\mathbf{f}(y(t), \Delta m, t) = \begin{bmatrix} 0 \\ 1 \end{bmatrix} \{2y(t) + (1.5 \pm \Delta m)y(t)sint\} ,$$

where $\Delta m \in [-0.05, 0.05]$ is the uncertainty, $\mathbf{x}(t) \in R^2$ are the states, y(t) is the output and d(t) is the external disturbance.

13.1 Design Objective and Performance Requirements

The output of the above system is required to track a nominal sinusoidal input $r_o(t) = sin\ 5t$ within a sphere of radius 0.2 for any reference input $r(t)$ in a sphere of radius 0.1 centered at the nominal input, i.e.,

$$\|r(t) - r_o(t)\|_\infty \leq 0.1 \Rightarrow \|y(t) - y_o(t)\|_\infty \leq 0.2 \qquad (13.2)$$

in the presence of the disturbance $d(t)$ and the plant uncertainty $\mathbf{f}(y(t), \Delta m, t)$.

13.2 Design Execution

To assure good steady state tracking, a servo compensator $\mathbf{S}_c$, denoted by $(\mathbf{A}_c, \mathbf{B}_c, \mathbf{C}_c)$, can be chosen as :

$$\begin{aligned} \dot{\mathbf{x}}_c(t) &= \mathbf{A}_c\mathbf{x}_c(t) + \mathbf{B}_c e(t) \\ y_c(t) &= \mathbf{C}_c\mathbf{x}_c(t) \end{aligned}$$

with the tracking error $e(t) \equiv (r(t) - y(t))$, and $|s\mathbf{I} - \mathbf{A_c}| = s^2 + 25 = 0$, which is the internal model of the signal $sin\ 5t$, yielding

$$\mathbf{A}_c = \begin{bmatrix} 0 & 1 \\ -25 & 0 \end{bmatrix}, \quad \mathbf{B}_c = \begin{bmatrix} 0 \\ 1 \end{bmatrix}, \quad \mathbf{C}_c = [1 \quad 0] \ . \qquad (13.3)$$

With S_c chosen as above, the following augmented nonlinear plant is obtained by combining $\mathbf{S_c}$ and the plant model (13.1).

$$\begin{aligned}
\dot{\mathbf{x}}_a(t) &= \begin{bmatrix} 0 & 1 & 0 & 0 \\ 0 & -1 & 0 & 0 \\ 0 & 0 & 0 & 1 \\ -1 & 0 & -25 & 0 \end{bmatrix} \mathbf{x}_a(t) + \begin{bmatrix} 0 \\ 1 \\ 0 \\ 0 \end{bmatrix} u(t) + \\
&\quad \begin{bmatrix} 0 & 0 \\ 0 & 0.1 \\ 0 & 0 \\ 1 & 0 \end{bmatrix} \mathbf{w}(t) + \mathbf{f}_1(y(t), \Delta m, t) \\
&= \mathbf{A}_a \mathbf{x}_a(t) + \mathbf{B}_a u(t) + \mathbf{G}_a \mathbf{w}(t) + \mathbf{f}_1(y(t), \Delta m, t) \ , \\
y(t) &\equiv [1 \ 0 \ 0 \ 0] \mathbf{x}_a(t) \ ,
\end{aligned}$$

where

$$\mathbf{x}_a(t) \equiv \begin{bmatrix} \mathbf{x}(t) \\ \mathbf{x}_c(t) \end{bmatrix}, \quad \mathbf{f}_1(y, \Delta m, t) = \begin{bmatrix} \mathbf{f}(y(t), \Delta m, t) \\ \mathbf{0} \end{bmatrix} \quad \mathbf{w}(t) = \begin{bmatrix} r(t) \\ d(t) \end{bmatrix} . \tag{13.4}$$

13.3 Computation of Gains K and H

Invoking the H_∞-minimization algorithm described in Part I with $\rho = 0.0001$, $a = 10^{-8}$, and

$$\mathbf{z}(t) = \begin{bmatrix} \rho u_l(t) \\ \mathbf{w}_s e(t) \end{bmatrix}, \quad \mathbf{w}_s = \mathbf{S}_c, \quad u_l(t) = \mathbf{K}\mathbf{x}_\mathbf{a}(t) \tag{13.5}$$

the controller gain matrices $\mathbf{K}_1, \mathbf{K}_c$ of the nonlinear controller, specified by Eqn. (9) of Part I and the observer gain matrix $\mathbf{H}$ of the nonlinear observer

specified by Eqn. (8) of Part I, are found to be

$$\begin{aligned} \mathbf{K_1} &= [-299.9 \ -23.5] \\ \mathbf{K_c} &= [2506.2 \ 1937.1] \\ \mathbf{H} &= \begin{bmatrix} -0.0955 \\ -0.0046 \end{bmatrix} \end{aligned}$$

With the above observer gain matrix $\mathbf{H}$ and the controller gain matrix $\mathbf{K}$, the closed-loop system becomes

$$\begin{aligned} \dot{\mathbf{z}}(t) &= \mathbf{A}_z\mathbf{z}(t) + \mathbf{B}_z\mathbf{w}(t) + \mathbf{B}_z\phi(y(t), \Delta m, t) \\ y(t) &= \mathbf{C}_z\mathbf{z}(t) \ , \end{aligned} \tag{13.6}$$

where

$$\mathbf{A}_z = \begin{bmatrix} 0. & 1. & 0. & 0. & 0. & 0. \\ 0. & -1. & 2506.2 & 1937.1 & -299.9 & -23.5 \\ 0. & 0. & 0. & 1. & 0. & 0. \\ -1. & 0. & -25. & 0. & 0. & 0. \\ 0.1 & 0. & 0. & 0. & -0.1 & 1. \\ 0. & 0. & 2506.2 & 1937.1 & -299.9 & -24.5 \end{bmatrix},$$

$$\mathbf{B}_z = \begin{bmatrix} 0. & 0. \\ 0. & 0.1 \\ 0. & 0. \\ 1. & 0. \\ -0.0955 & 0. \\ -0.0046 & 0. \end{bmatrix}, \quad \mathbf{z}(t) \equiv \begin{bmatrix} \mathbf{x}(t) \\ \mathbf{x}_c(t) \\ \hat{\mathbf{x}}(t) \end{bmatrix},$$

$$\mathbf{C}_z = [1. \ 0. \ 0. \ 0. \ 0. \ 0.], \quad \text{and}$$

$$\phi(y(t), \Delta m, t) = \begin{bmatrix} 0. \\ 10. \end{bmatrix} (\Delta m \; y(t) \; sint) \; .$$

It can be easily verified that the nonlinear element $\phi(y(t), \Delta m, t)$ belongs to the sector [-0.5 0.5].

By selecting T=0.5sec (the settling time), the Nyquist diagram $\omega \mapsto \mathbf{H}_a(j\omega)$ satisfies the circle criterion, as shown in Figure 13.1, confirming that the closed-loop is L_∞ stable.

With the above choice of gains $\mathbf{K} = [\mathbf{K}_1, \mathbf{K}_c]$ and $\mathbf{H}$, the right hand side of the inequality (39) of Part I becomes

$$\begin{aligned} m &= \frac{\beta_o}{\beta_{ri} + \|d(t)\|_\infty + \beta_o\beta_3 + \frac{\beta-\alpha}{2}\|(y_o)_T\|_2} \\ &= \frac{0.2}{0.1 + 0.2 * 0.02727 + 0.05 * 0.363} = 1.61807 \end{aligned}$$

and the computed value of β_1 is 1.61454, which is clearly less than the threshold m. The resulting nonlinear control law is $u(t) = \mathbf{K}_1\hat{\mathbf{x}}(t) + \mathbf{K}_c\mathbf{x}_c(t) - f_{2o}(y(t), t)$, $f_{20}(y(t), t) = 2 \; y(t) + 1.5 \; y(t) \; sin \; t$. The above control law is optimal in the sense that the value of β_1 is very close to its upper bound. To confirm the validity of the theorem, the closed-loop system of Eqn. (13.6) is simulated with the following results.

13.4 Computer Simulation Results:

The actual reference $r(t)$ is assumed to vary from the nominal reference input $r_o(t)$ with an amplitude of $r_o(t) - 0.1$ for a period of 2 seconds (from 0. seconds to 2.0 seconds). The histories of $r_o(t)$ and $r(t)$ are shown in

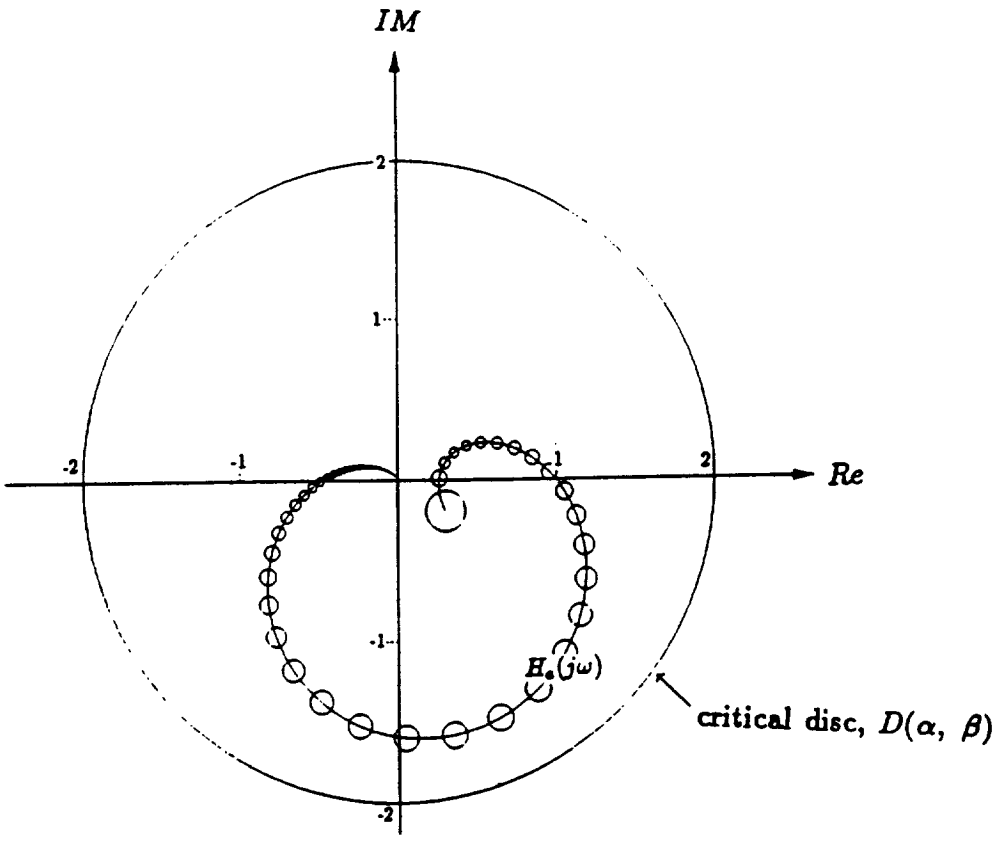

Figure 13.1: The Nyquist Diagram of $H_a(j\omega)$ and the Critical Disc $D(\alpha, \beta)$.

Figure 13.2. Thus, $\|r(t) - r_o(t)\|_\infty = 0.1$. Let $\Delta m = 0.05$, and $d(t) = 0$. The nominal reference $r_o(t)$, and the actual output y(t) are shown in Figure 13.3. As expected with the proposed nonlinear control law, as expected, the closed-loop system has low sensitivity to both the external disturbance and uncertainties. This is confirmed by Figure 13.4, showing that the actual output y(t) is close to the nominal one $y_o(t)$. Figure 13.5 shows that $\|y - y_o\|_\infty$ is less than 0.094. Clearly, good tracking can be achieved by using the proposed control law, u(t), whose control histories are shown in Figure 13.6.

To check the validity of the design criterion another reference, $r(t) = r_o(t) + 0.1\ sin10t$, was simulated. The histories of $r_o(t)$ and $r(t)$ are shown in Figure 13.7 with $\Delta m = 0.05$, and $d(t) = 0$. The nominal reference $r_o(t)$, and the actual output $y(t)$ are shown in Figure 13.8. Figure 13.9 shows that the tracking error $\|y(t) - y_o(t)\|_\infty$ is less than 0.16, which is in the desired output sphere of $\|y(t) - y_o(t)\|_\infty \leq 0.2$. The resulting control history is shown in Figure 13.10.

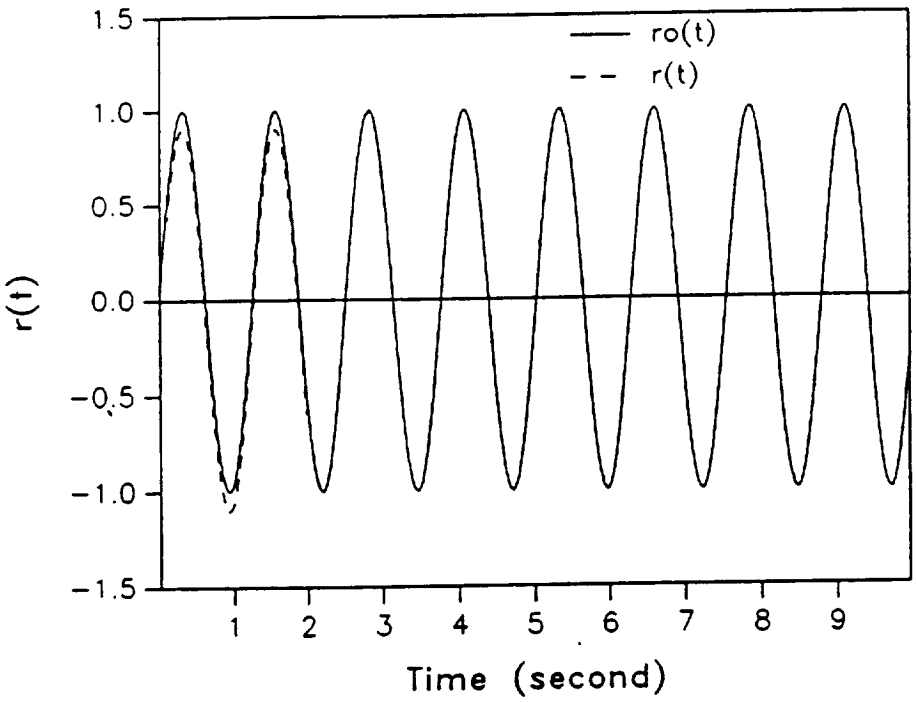

Figure 13.2: Reference r(t) and Nominal Reference $r_o(t)$.

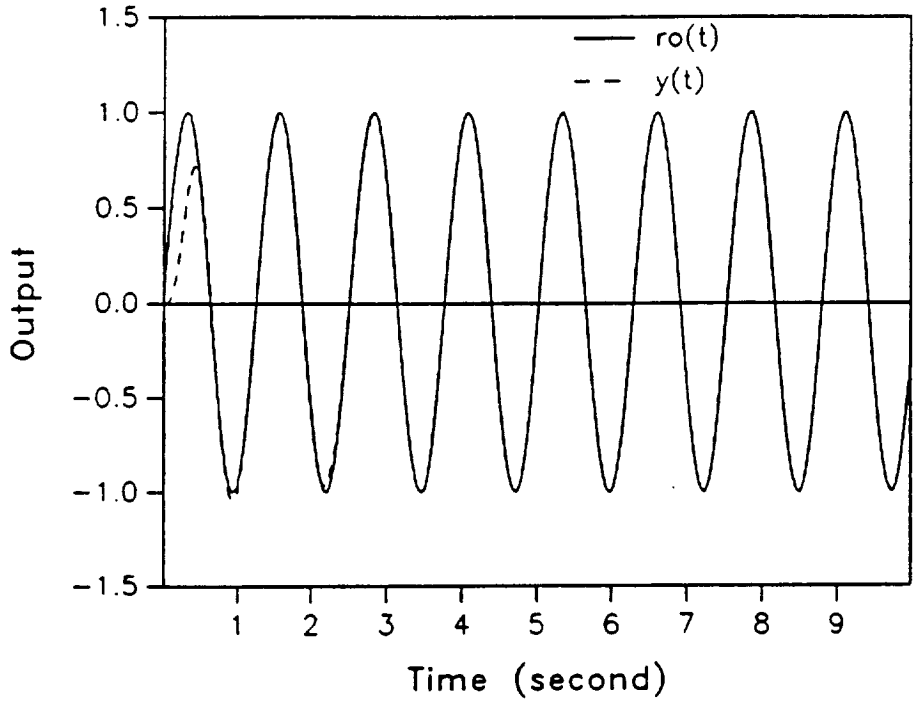

Figure 13.3: Output y(t) and References $r_o(t)$ vs Time t.

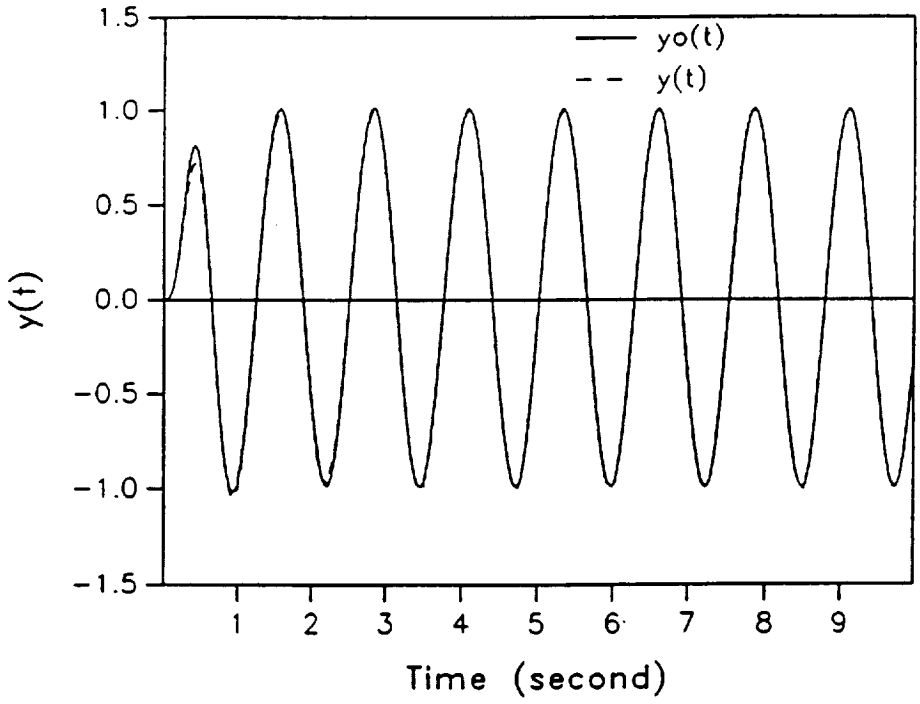

Figure 13.4: Output y(t) and Nominal Output y_o vs Time t.

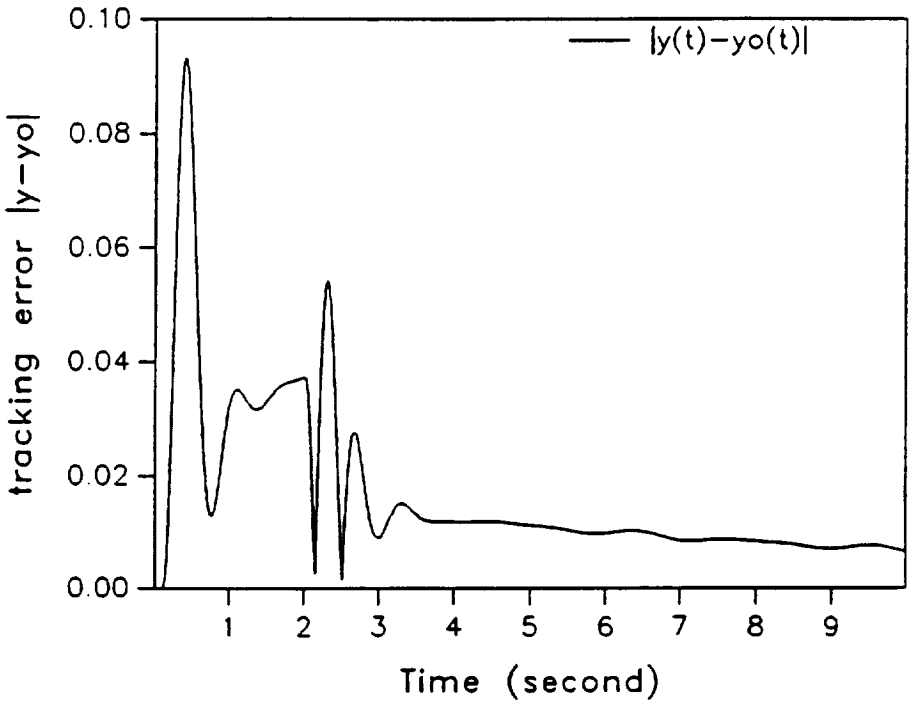

Figure 13.5: Tracking Errors vs Time t.

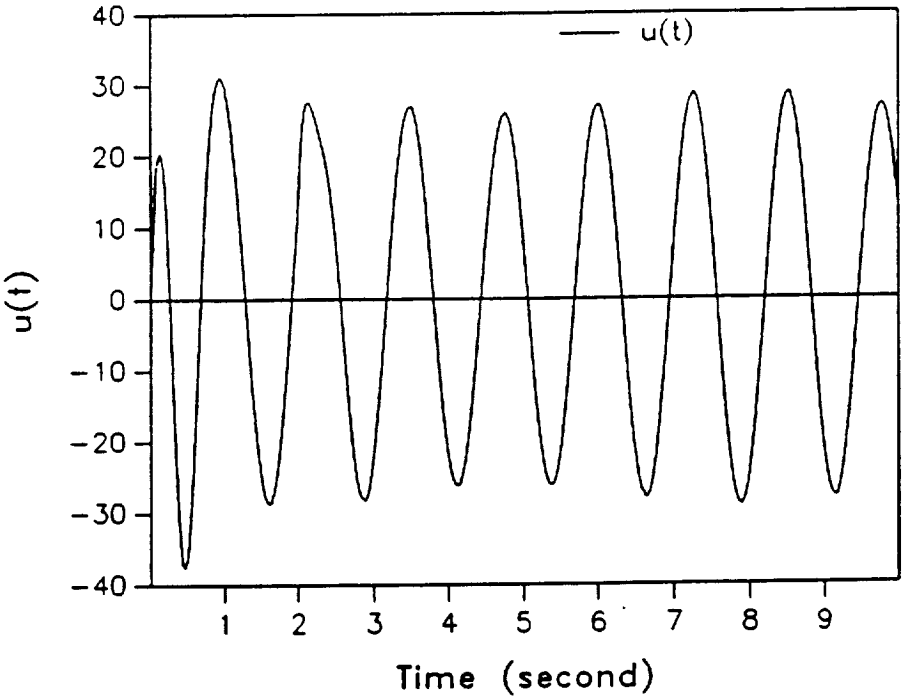

Figure 13.6: History of Control Input u(t).

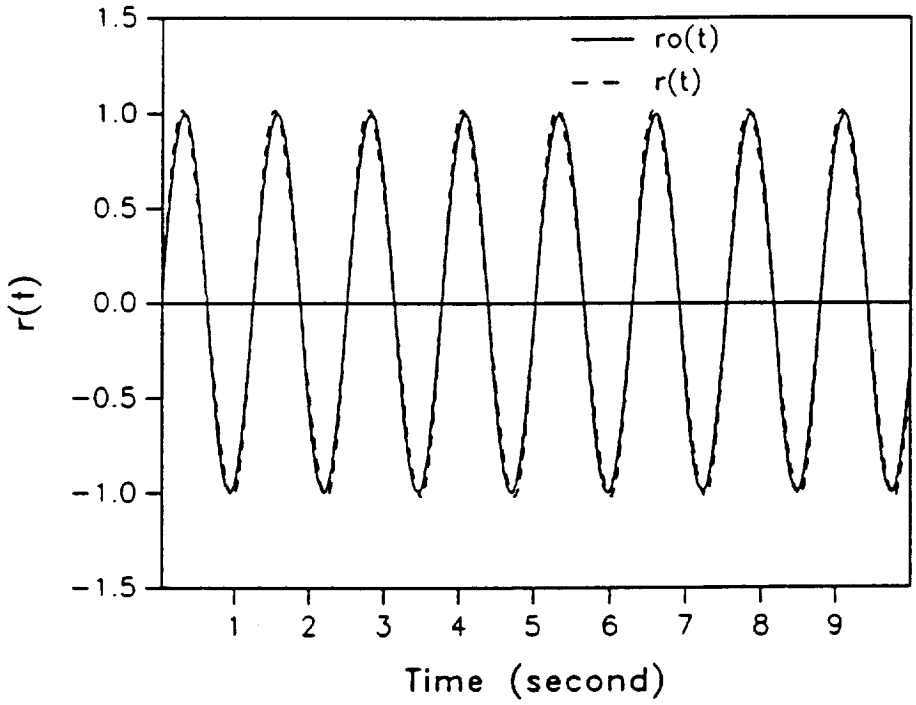

Figure 13.7: Reference r(t) and Nominal Reference $r_o(t)$.

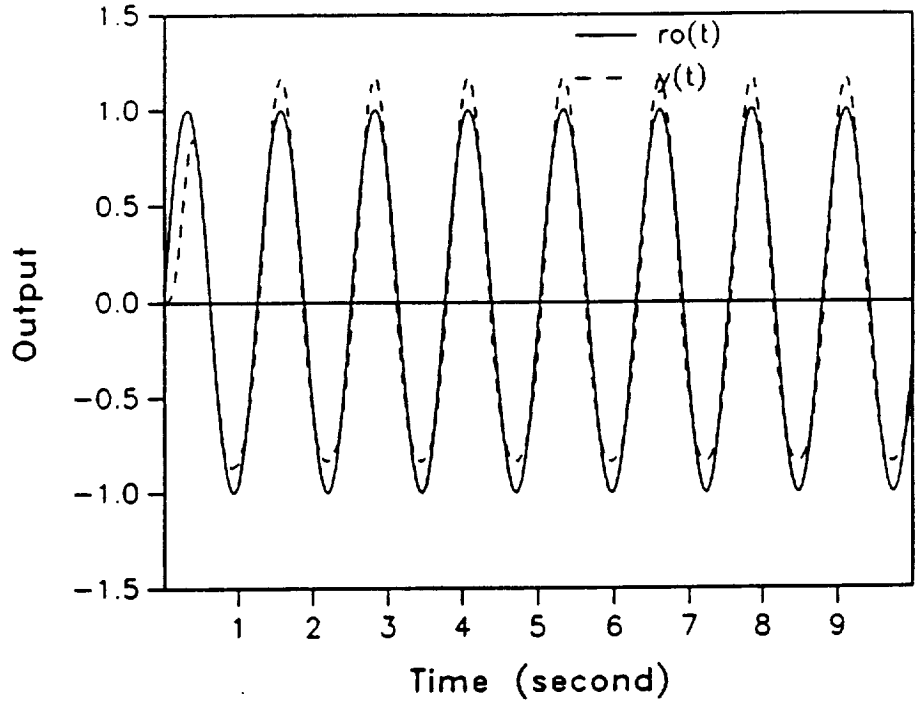

Figure 13.8: Output y(t) and References $r_o(t)$ vs Time t.

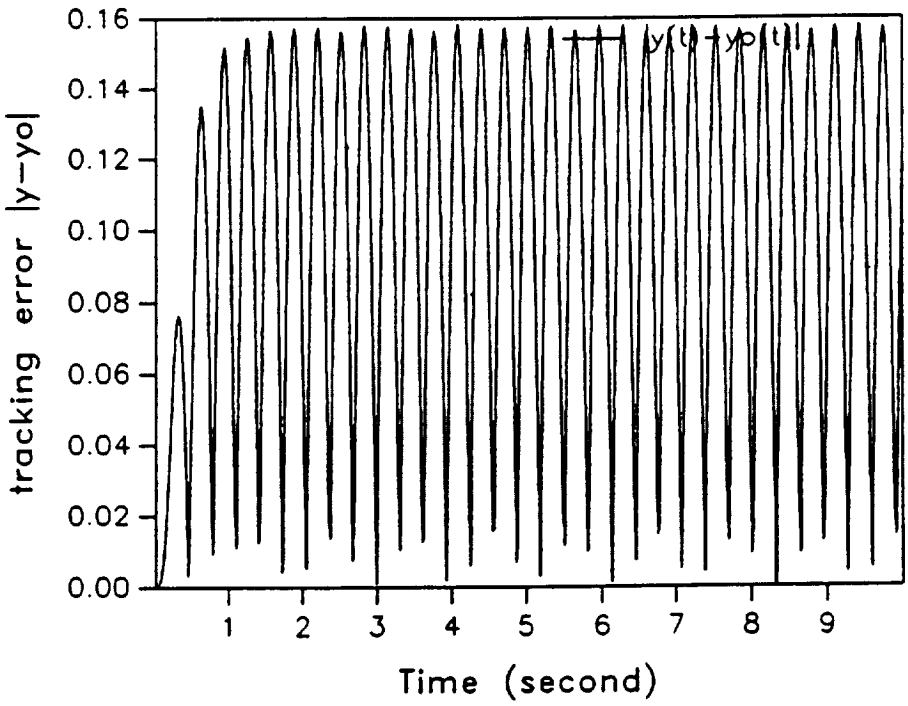

Figure 13.9: Tracking Errors vs Time t.

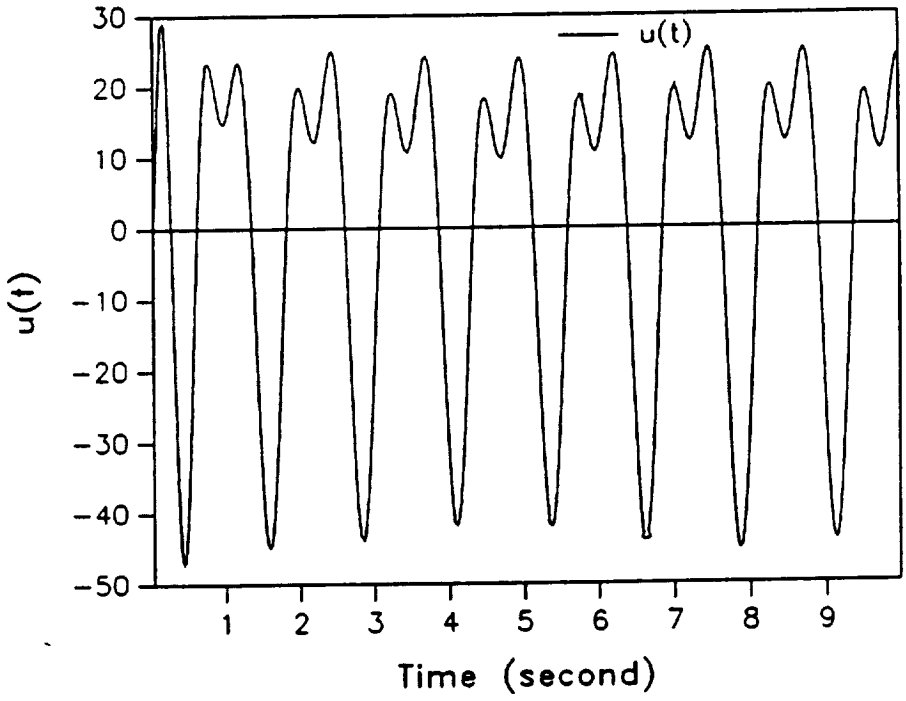

Figure 13.10: History of Control Input u(t).

Chapter 14

Two-Degrees-of-Freedom Robotic Manipulator

Now, we consider the realistic problem of a two-degrees-of-freedom manipulator studied in Corless et al (1984). This arm can extend or retract and rotate about an axis as shown in Figure 14.1, where s is the distance between the point load M and the pivot point O. $(x_1(t), x_2(t))$ denotes the position of the mass center C of the arm in polar coordinates. $V_1(t), V_2(t)$ are the force and the torque required to ensure that the point load M tracks a prescribed desired motion. $(Y_{A1}(t), Y_{A2}(t))$ denotes the actual position of the load M in cartesian coordinates. μ and M are the arm and load mass respectively. J_1 is the mass moment of inertia of the mechanism about the axis through O; J_2 is the mass moment of inertia of the arm about the axis through C. a is the distance from C to the load M. The dynamic equations governing the motion of the manipulator can be written as

$$(\mu + M)\ddot{x}_1(t) - R(x_1(t), M)\dot{x}_2^2(t) = V_1(t) \tag{14.1}$$

$$I(x_1(t), M)\ddot{x}_2(t) + 2R(x_1(t), M)\dot{x}_1(t)\dot{x}_2(t) = V_2(t)$$

where

$$\begin{aligned} R(x_1(t), M) &= \mu x_1(t) + M(x_1(t) + a) \\ I(x_1(t), M) &= J_1 + J_2 + \mu x_1^2(t) + M(x_1(t) + a)^2 \ . \end{aligned}$$

Assume that all the parameters are known exactly except the payload mass M, which is subjected to known bounds, $0 \leq \underline{M} \leq M \leq \overline{M}$, denoted as $M \in [\underline{M}, \overline{M}]$. Let M^o be the nominal payload mass $(= \frac{1}{2}(\underline{M} + \overline{M}))$. By defining

$$\begin{aligned} u_1(t) &= (\mu + M)^{-1} V_1(t) \\ u_2(t) &= (I(x_1(t), M))^{-1} V_2(t) \end{aligned}$$

as the new input variables, and

$$\begin{aligned} f_{n1}(t) &= (\mu + M)^{-1} R(x_1(t), M) x_4^2(t) \\ f_{n2}(t) &= -(I(x_1(t), M))^{-1} 2R(x_1(t), M) x_3(t) x_4(t) \end{aligned}$$

as the modified nonlinear functions with

$$\mathbf{u}(t) = \begin{bmatrix} u_1(t) \\ u_2(t) \end{bmatrix}, \quad \mathbf{x}(t) = \begin{bmatrix} x_1(t) \\ x_2(t) \\ x_3(t) \\ x_4(t) \end{bmatrix}, \quad \text{and} \quad \mathbf{f}(\mathbf{x}(t), M, t) = \begin{bmatrix} 0 \\ 0 \\ f_{n1}(t) \\ f_{n2}(t) \end{bmatrix},$$

the system (14.1) can be rewritten in the following state equation form:

$$\begin{aligned} \dot{\mathbf{x}}(t) &= \mathbf{A}\mathbf{x}(t) + \mathbf{B}\mathbf{u}(t) + \mathbf{G}\mathbf{d}(t) + \mathbf{f}(\mathbf{x}(t), M, t) \qquad (14.2) \\ \mathbf{y}(t) &= \mathbf{C}\mathbf{x}(t) \end{aligned}$$

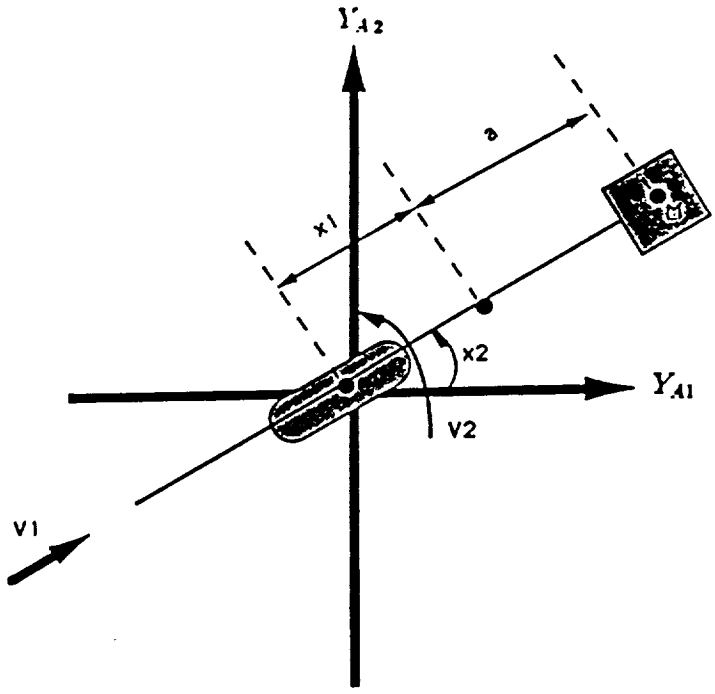

Figure 14.1: Robot Manipulator of Two-degree-of Freedom.

with

$$\mathbf{A} = \begin{bmatrix} 0 & 0 & 1 & 0 \\ 0 & 0 & 0 & 1 \\ 0 & 0 & 0 & 0 \\ 0 & 0 & 0 & 0 \end{bmatrix}, \quad \mathbf{B} = \begin{bmatrix} 0 & 0 \\ 0 & 0 \\ 1 & 0 \\ 0 & 1 \end{bmatrix},$$

$$\mathbf{C} = \begin{bmatrix} 1 & 0 & 0 & 0 \\ 0 & 1 & 0 & 0 \end{bmatrix}, \quad \mathbf{G} = \begin{bmatrix} 0 & 0 \\ 0 & 0 \\ 0.1 & 0 \\ 0 & 0.1 \end{bmatrix}$$

where $\mathbf{u}(t)$, $\mathbf{x}(t)$, $\mathbf{y}(t)$, $\mathbf{d}(t)$ and $\mathbf{f}(.)$ are respectively the control, the state, the output, the disturbance and the nonlinear uncertain element of the system of Eqn. (14.2).

Parameter values used for computations are $\underline{M} = 45$ kg, $\overline{M} = 55$ kg, $J_1 = J_2 = 100$ kg.m^2 and a = 1 m, with uncertain mass $M \in [45kg,\ 55kg]$.

14.1 Design Objective and Performance Requirements

Suppose the payload M is required to track the semi-circle described by

$$\begin{aligned} [Y_{A1}(t), Y_{A2}(t)] &= [0\ m, 1.5\ m]\,, \quad t \leq 0 \\ [Y_{A1}(t), Y_{A2}(t)] &= [(x_1(t) + a)cos\ x_2(t)\ m, (x_1(t) + a)sin\ x_2(t)\ m] \\ &\qquad 0 < t \leq 3.1416\ sec. \\ [Y_{A1}(t), Y_{A2}(t)] &= [0\ m, -1.5\ m]\,, \quad t \geq 3.1416\ sec. \end{aligned}$$

In terms of polar coordinates the above desired motion, becomes

$$\begin{aligned}
[y_{r1}(t), y_{r2}(t)] &= [0.5\ m, 0\ rad], t \leq 0\ sec. \\
[y_{r1}(t), y_{r2}(t)] &= [0.5\ m, t\ rad], 0 < t \leq 3.1416\ sec. \\
[y_{r1}(t), y_{r2}(t)] &= [0.5\ m, 3.1416\ rad], t \geq 3.1416\ sec.
\end{aligned}$$

where $y_{r1}(t), y_{r2}(t)$ represent the desired motion of the system output $\mathbf{y}(t)(\equiv [y_1(t), y_2(t)]^T)$ in Eqn. (14.2).

The performance requirement is that

$$\|\mathbf{r}(t) - \mathbf{r}_o(t)\|_\infty = 0 \Rightarrow \|y_i(t) - y_{oi}(t)\|_\infty \leq 0.14, \quad i = 1, 2\ , \tag{14.3}$$

where the nominal reference input $\mathbf{r}_o(t) = [y_{r1}(t), y_{r2}(t)]^T$.

14.2 Design Execution

For steady-state tracking of the desired motion, a servo-compensator S_c denoted by $(\mathbf{A}_c, \mathbf{B}_c, \mathbf{C}_c)$ is chosen as :

$$\begin{aligned}
\dot{\mathbf{x}}_c(t) &= \mathbf{A}_c\mathbf{x}_c(t) + \mathbf{B}_c\mathbf{e}(t) \\
\mathbf{y}_c(t) &= \mathbf{C}_c\mathbf{x}_c(t)\ ,
\end{aligned}$$

where the tracking error $\mathbf{e}(t) \equiv (\mathbf{r}(t) - \mathbf{y}(t))$,

$$\mathbf{A}_c = \begin{bmatrix} 0 & 0 & 0 \\ 0 & 0 & 1 \\ 0 & 0 & 0 \end{bmatrix}, \quad \mathbf{B}_c = \begin{bmatrix} 1 & 0 \\ 0 & 0 \\ 0 & 1 \end{bmatrix}, \quad \mathbf{C}_c = \begin{bmatrix} 1 & 0 & 0 \\ 0 & 1 & 0 \end{bmatrix}\ . \tag{14.4}$$

The above servo-compensator $\mathbf{S}_c$ is chosen to realize the internal model, which is specified by the desired motion, so that the desired trajectories can be followed. With $\mathbf{S}_c$ chosen as above, the augmented nonlinear system becomes

$$\begin{aligned}\dot{\mathbf{x}}_a(t) &= \begin{bmatrix} \mathbf{A} & \mathbf{0} \\ -\mathbf{B}_c\mathbf{C} & \mathbf{A}_c \end{bmatrix} \mathbf{x}_a(t) + \begin{bmatrix} \mathbf{B} \\ \mathbf{0} \end{bmatrix} \mathbf{u}(t) + \begin{bmatrix} \mathbf{0} & \mathbf{G} \\ \mathbf{B}_c & \mathbf{0} \end{bmatrix} \mathbf{w}(t) + \mathbf{f}_1(\mathbf{x}(t), M, t) \\ &= \mathbf{A}_a\mathbf{x}_a(t) + \mathbf{B}_a\mathbf{u}(t) + \mathbf{G}_a\mathbf{w}(t) + \mathbf{f}_1(\mathbf{y}(t), M, t) \ , \end{aligned} \tag{14.5}$$

and

$$\begin{aligned}\mathbf{y}(t) &= [C \quad 0]\,\mathbf{x}_a(t) = \mathbf{C}_a\mathbf{x}_a(t), \text{ where } \mathbf{w}(t) \equiv \begin{bmatrix} \mathbf{r}(t) \\ \mathbf{d}(t) \end{bmatrix}, \\ \mathbf{f}_1(\mathbf{x}(t), M, t) &= \begin{bmatrix} \mathbf{f}(\mathbf{x}(t), M, t) \\ \mathbf{0} \end{bmatrix} .\end{aligned}$$

Now we invoke the design procedure outlined previously in Part I.

14.3 Computation of the gains K and H

Choosing

$$\mathbf{z}(t) \equiv \begin{bmatrix} \rho\mathbf{u}_l(t) \\ \mathbf{W}_s\mathbf{e}(t) \end{bmatrix} \quad \mathbf{W}_s \equiv \mathbf{S}_c, \quad \mathbf{e}(t) = \mathbf{r}(t) - \mathbf{y}(t) \tag{14.6}$$

where $\mathbf{u}_l(t) = \mathbf{K}\mathbf{x}_a(t)$, with $\rho = 0.001$ and $a = 10^{-9}$, the state feedback gain matrix $\mathbf{K} = [\mathbf{K}_1 \quad \mathbf{K}_c]$ and the observer gain matrix $\grave{\mathbf{H}}$ are computed, yielding :

$$\mathbf{K} = \begin{bmatrix} -202.9 & 0. & -20.2 & 0. & 1020.4 & 0. & 0. & \\ 0. & & -108.4 & 0. & -14.7 & 0. & 1005.9 & 466.9 \end{bmatrix}$$

$$\mathbf{H} = \begin{bmatrix} -0.4571 & 0.0000 \\ 0.0000 & -0.4501 \\ -0.1022 & 0.0000 \\ 0.0000 & -0.1007 \end{bmatrix}$$

14.4 Formulation of the Closed-loop System

The closed-loop system can now be expressed as

$$\begin{aligned} \dot{\mathbf{z}}(t) &= \mathbf{A}_z\mathbf{z}(t) + \mathbf{B}_z\mathbf{w}(t) + \mathbf{B}_z\phi(\mathbf{x}(t), M, t) \\ \mathbf{y}(t) &= \mathbf{C}_z\mathbf{z}(t)\ , \end{aligned} \tag{14.7}$$

where $\mathbf{A}_z, \mathbf{B}_z$, and $\mathbf{C}_z$ are shown in Table 14.1, and

$$\phi(\mathbf{x}(t), M, t) = \begin{bmatrix} 0 & 0 \\ 0 & 0 \\ 10 & 0 \\ 0 & 10 \end{bmatrix} (\mathbf{f}_1(\mathbf{x}, M, t) - \mathbf{f}_{1o}(\mathbf{x}, t))$$

$$\mathbf{f}_1(\mathbf{x}, M, t) \equiv \begin{bmatrix} f_{21}(t) \\ f_{22}(t) \end{bmatrix} = \begin{bmatrix} (\mu + M)^{-1} R(x_1(t), M) x_4^2(t) \\ -(I(x_1(t), M))^{-1} 2R(x_1(t), M) x_3(t) x_4(t) \end{bmatrix}$$

$$\mathbf{f}_{1o}(\mathbf{x}, t) \equiv \begin{bmatrix} f_{2o1}(t) \\ f_{2o2}(t) \end{bmatrix} = \begin{bmatrix} (\mu + M^o)^{-1} R(x_1(t), M^o) x_4^2(t) \\ -(I(x_1(t), M^o))^{-1} 2R(x_1(t), M^o) x_3(t) x_4(t) \end{bmatrix}$$

with the nominal mass $M^o = 50$ kg.

Remark: Note that $\mathbf{f}_{1o}(\mathbf{x}, t)$ is the well known computed torque.

With $a = 10^{-9}$ and $T = 3.1416$ sec, Figures 14.2 and 14.3 show that the Nyquist locus $\omega \mapsto \mathbf{H}_a(j\omega)$ satisfies the MIMO circle criterion, proving that the closed-loop system is L_∞ stable.

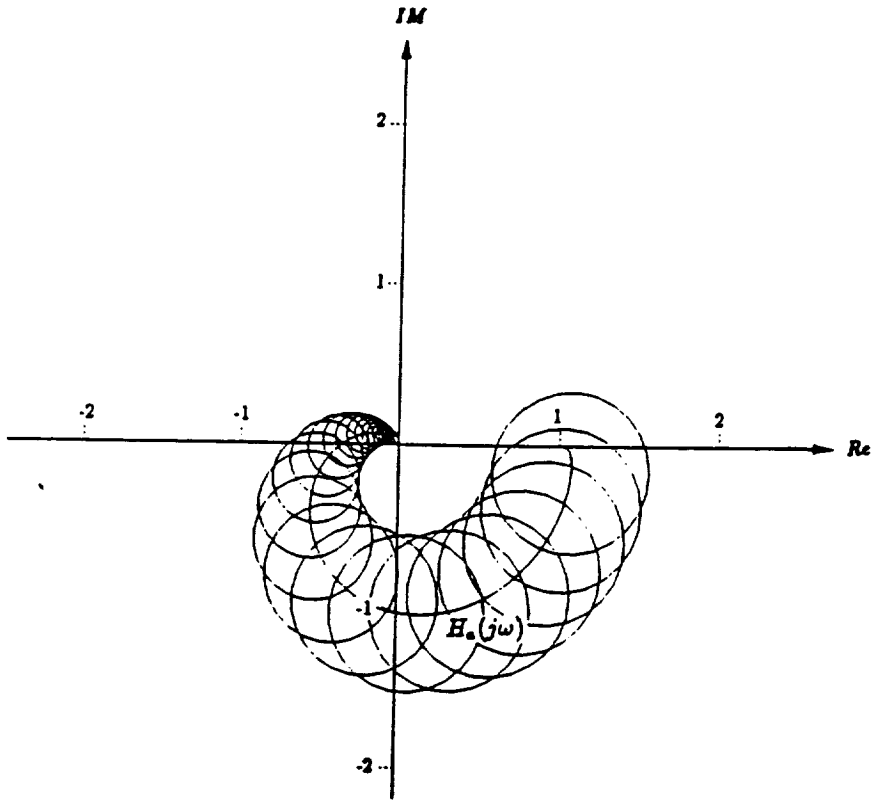

Figure 14.2: Satisfaction of the Circle Criterion (for Sector = $[\alpha_1,\ \beta_1]$).

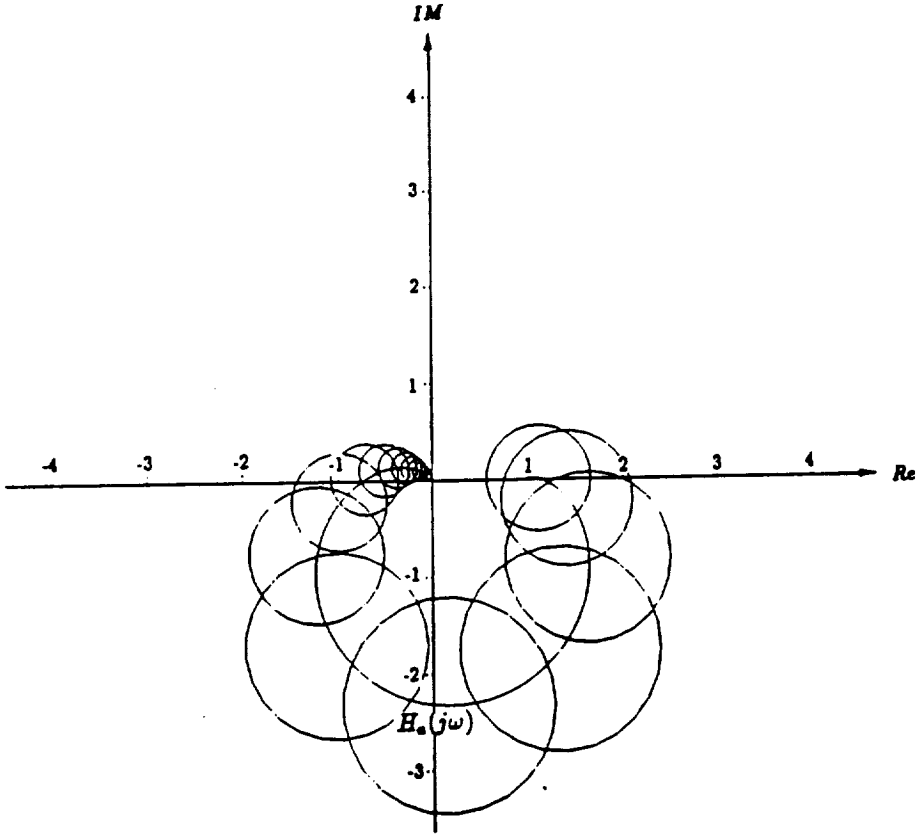

Figure 14.3: Satisfaction of the Circle Criterion (for Sector = $[\alpha_2,\ \beta_2]$).

The numerical values of the parameters in inequality (39) of Part I are computed as follows:

$$\begin{aligned}
\beta_3 &= \sup_{M \in \Im} \|[\nabla_{\mathbf{y}} \boldsymbol{\phi}(\mathbf{y}(t), M, t)]_T\|_2 \\
&= \|[\frac{\partial \phi_{11}}{\partial y_1} \quad \frac{\partial \phi_{21}}{\partial y_1}]_T\|_2 \\
&= 0.018 \\
\beta_4 &= \sup_{M \in \Im} \|(\boldsymbol{\phi}(\mathbf{y}_o(t), M, t) - (\boldsymbol{\phi}_o(\mathbf{y}_o(t), t))_T\|_2 = 0.056 \ .
\end{aligned} \tag{14.8}$$

TABLE 14.1 The Closed-Loop System Matrices of the Robot Manipulator

A_z (11 × 11 matrix) =

10^3 *

Columns 1 thru 8

0.0000	0.0000	0.0010	0.0000	0.0000	0.0000	0.0000	0.0000
0.0000	0.0000	0.0000	0.0010	0.0000	0.0000	0.0000	0.0000
0.0000	0.0000	0.0000	0.0000	1.0204	0.0000	0.0000	-0.2029
0.0000	0.0000	0.0000	0.0000	0.0000	1.0059	0.4669	0.0000
-0.0010	0.0000	0.0000	0.0000	0.0000	0.0000	0.0000	0.0000
0.0000	0.0000	0.0000	0.0000	0.0000	0.0000	0.0010	0.0000
0.0000	-0.0010	0.0000	0.0000	0.0000	0.0000	0.0000	0.0000
0.0005	0.0000	0.0000	0.0000	0.0000	0.0000	0.0000	-0.0005
0.0000	0.0005	0.0000	0.0000	0.0000	0.0000	0.0000	0.0000
0.0001	0.0000	0.0000	0.0000	1.0204	0.0000	0.0000	-0.2030
0.0000	0.0001	0.0000	0.0000	0.0000	1.0059	0.4669	0.0000

Columns 9 thru 11

0.0000	0.0000	0.0000
0.0000	0.0000	0.0000
0.0000	-0.0202	0.0000
-0.1084	0.0000	-0.0147
0.0000	0.0000	0.0000

TABLE 14.1 (cont.)

0.0000	0.0000	0.0000
0.0000	0.0000	0.0000
0.0000	0.0010	0.0000
-0.0005	0.0000	0.0010
0.0000	-0.0202	0.0000
-0.1085	0.0000	-0.0147

B_z (11 × 4 matrix) =

0.0000	0.0000	0.0000	0.0000
0.0000	0.0000	0.0000	0.0000
0.0000	0.0000	0.1000	0.0000
0.0000	0.0000	0.0000	0.1000
1.0000	0.0000	0.0000	0.0000
0.0000	0.0000	0.0000	0.0000
0.0000	1.0000	0.0000	0.0000
-0.4571	0.0000	0.0000	0.0000
0.0000	-0.4501	0.0000	0.0000
-0.1022	0.0000	0.0000	0.0000
0.0000	-0.1007	0.0000	0.0000

TABLE 14.1 (cont.)

C_z (2 × 11 matrix) =

Columns 1 thru 8

1.0000 0.0000 0.0000 0.0000 0.0000 0.0000 0.0000 0.0000

0.0000 1.0000 0.0000 0.0000 0.0000 0.0000 0.0000 0.0000

Columns 9 thru 11

0.0000 0.0000 0.0000

0.0000 0.0000 0.0000

Thus, the threshold m becomes

$$m = \frac{\beta_o}{\beta_{ri} + \|\mathbf{d}(t)\|_\infty + \beta_o\beta_3 + \beta_4} = \frac{0.14}{0. + 0.14 * 0.018 + 0.056} = 2.3923 ,$$

and the computed value of β_1 is 2.34285, which clearly satisfies the inequality (39) of Part I. The resulting nonlinear control law is $\mathbf{u}(t) = \mathbf{K}_1\hat{\mathbf{x}}(t) + \mathbf{K}_c\mathbf{x}_c(t) - \mathbf{f}_{1o}(t)$. The above control law is optimal in the sense that the value of β_1 is close to its upper bound. From theorem 2 of Part I, the closed-loop system is now guaranteed to have the required tracking performance. Effectiveness of the above controller is confirmed by the following transient response simulation results.

14.5 Computer Simulation Results:

Let $\mathbf{d}(t)$ be an impulse disturbance. With the lower bound mass $M = 45\ kg$, the plant outputs $\mathbf{y}(t)$ are shown in Figure 14.4, which shows that the plant outputs $y_1(t)$ and $y_2(t)$ closely track the reference inputs $r_1(t) = 0.5\ m$ and $r_2(t) = t$ radians respectively. The maximum tracking errors between the plant outputs and the nominal outputs are 0.006 m and 0.0015 *radians*. The errors are relatively small in comparison to the imposed output sphere radius $\beta_o = 0.14$. The superiority of the proposed control law for disturbance rejection and its low sensitivity to uncertainties can clearly be seen from the trajectories of the masses $M = 45\ kg$, $M = 50\ kg$, and $M = 55\ kg$ in the Cartesian coordinates, which are shown in Figure 14.5. The histories of the required control force $V_1(t)$ and the torque $V_2(t)$ for $M = 45\ kg$ are shown in Figure 14.6 along with those for the nominal mass $M = 50\ kg$. Due to the desired high-speed tracking, it is not surprising that the required control inputs are relatively high.

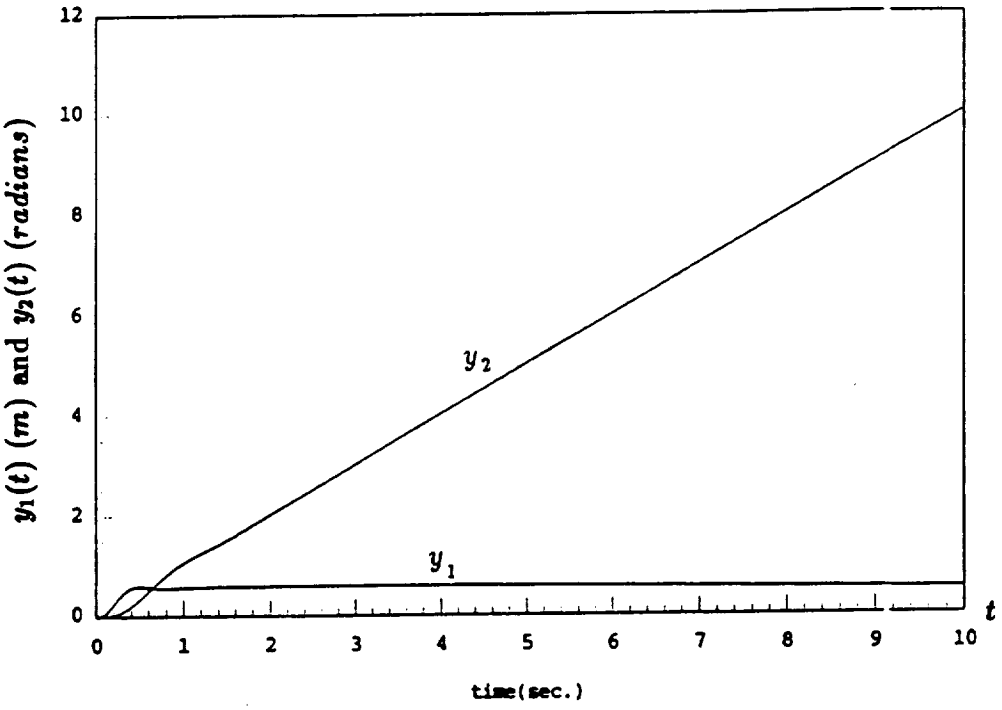

Figure 14.4: The Plant Output y(t) vs Time t.

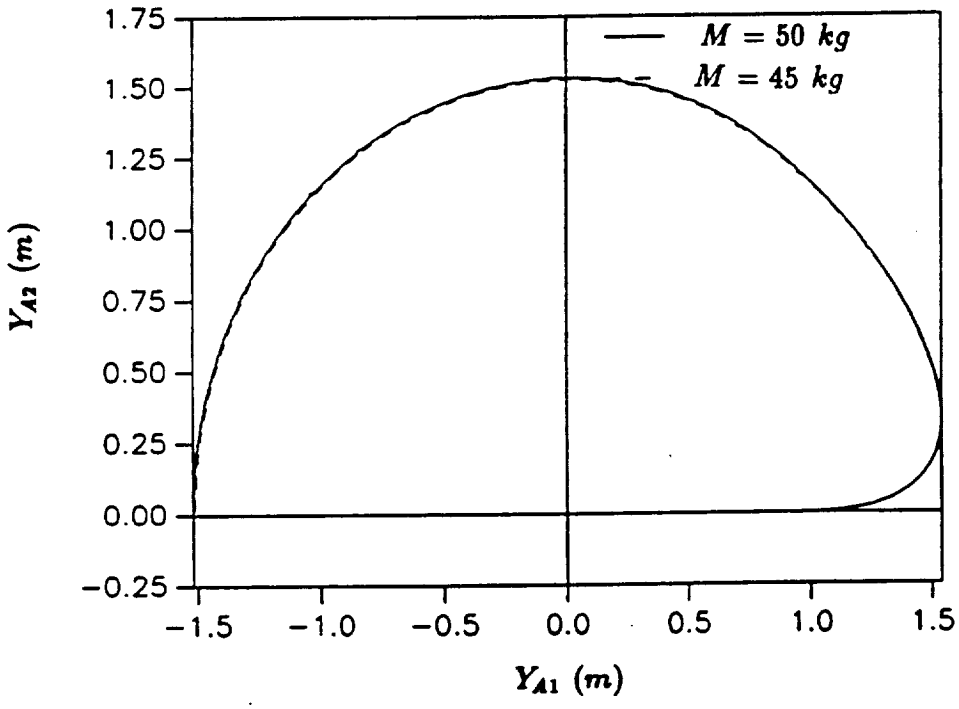

Figure 14.5: Output y(t) in Cartesian Coordinates (Y_{A1}, Y_{A2}).

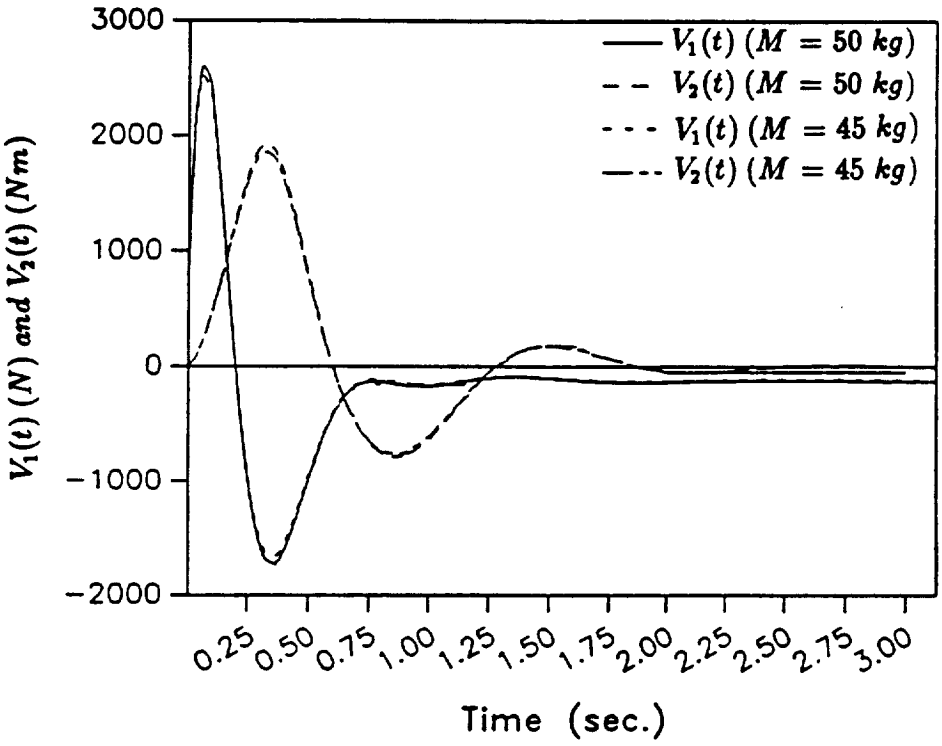

Figure 14.6: Histories of Control Force $V_1(t)$ and Torque $V_2(t)$.

Chapter 15

Summary and Conclusions

In this paper the problem of tracking in the sense of spheres, for a class of multivariable nonlinear uncertain systems of the Lurе type, is considered. Design criteria developed, extend the circle criterion developed in Jayasuriya & Kee (1988) for the L_2 - problem to L_∞ - tracking. Controller synthesis is reduced to a quantitative pole placement scheme which is subsequently solved using the H_∞-formalism. The H_∞-formalism provides a framework for incorporating bandwidth issues, so crucial in any physical implementation of any resulting control law. However, in light of the operator methods used in the problem formulation, resulting designs can be somewhat conservative. This, is expected since any L_∞-function within the given input sphere is admissible.

Future work will consider alternate approaches for reducing the conservativeness of the proposed design criterion. Also, it would be very useful to have a complete characterization of the worst input lying in a given input sphere for the synthesized closed-loop system. The worst input here is the

input which leads to the maximum error in the actual output as measured with respect to the nominal output. Criteria for synthesizing controllers for more general nonlinear system are also needed. For example, it would be appropriate to study polynomial systems, discontinuous systems and systems in which the control does not enter the state equation in a linear way.

Two examples for the synthesis methodology presented in Part I of this paper are given. The simulation results confirm the effectiveness of the proposed design methodology. The H_∞-framework used in the synthesis procedure can be adapted to incorporate bandwidth limitations. The latter can be accomplished by adjusting the weighting ρ and the filter matrix W_s needed in the H_∞-algorithm. It should be emphasized, however, that incorporating such bandwidth limits may result in having to relax the tracking error specifications. The relationship between the tracking error and the bandwidth is implicitly given in the design criterion (60) developed in Part I of the paper. Qualitatively, a large bandwidth would yield a small H_∞-norm and vice-versa. Moreover, for a given bandwidth limitation, a controller can be found, whenever the minimum H_∞-norm with an appropriate set of ρ and W_s, is smaller than the threshold value m (see Eqn. (60) of Part I). If this is not the case the same inequality can be used to ascertain a new output sphere size.

References

[1] Cook, P. A., "Modified Multivariable Circle Theorems, " in *Frequency Response Methods in Control Systems*, Edited by Alistair G.J. MacFarlane, IEEE Press, New York, 1979.

[1] Corless, M., Leitmann, G. and Ryan, E. P., "Tracking in the Presence of Bounded Uncertainties," Proceedings of the Fourth International Conference on Control Theory, Cambridge, England, September 1984.

[2] Desoer, C.A., and Vidyasagar, M., *Feedback Systems: Input-Output Properties*, Academic Press, Inc., New York, 1975.

[3] Doyle, J., Glover, K., Khargonekar, P., and Francis, B., "State- Space Solutions to Standard H_2 and H_∞ Control Problems," *IEEE Transactions on Automatic Control*, Vol. AC-34, pp. 831-847, 1989.

[4] Francis, B.A., and Wonham, W.M., "The Internal Model Principle for Linear Multivariable Regulators," *Applied Mathematics and Optimization*, Vol. 2, pp. 170 - 194, 1975.

[5] Francis, B.A., *A Course in H_∞ Control Theory*, Lecture Notes in Control and Information Sciences, Springer - Verlag, Vol. 88, 1987.

[6] Grimble, M.J., "State-Space Approach to H_∞ Optimal Control," *International Journal of Systems Science*, Vol. 19, pp. 1451-1468, 1988.

[7] Hwang, C.N., "Controller Synthesis for Input-Output Tracking in Lure Type Uncertain Nonlinear Systems," Ph.D. Dissertation, Department of Mechanical Engineering, Texas A&M University, College Station, TX , August 1990.

[8] Hwang, C.N., Jayasuriya, S., Parlos, A.G., and Sunkel, J.W., "On the H_2 and H_∞ Optimal State Feedback Control," *ASME Winter Annual Meeting*, Dallas, TX, November 1990.

[9] Jayasuriya, S., and Rabins, M.J., and Barnard, B.D., "Guaranteed Tracking Behavior in the Sense of Input-Output Spheres for Systems with Uncertain Parameters," *Journal of Dynamic System, Measurement and Control*, vol. 106, pp. 273-279, 1984.

[10] Jayasuriya, S., "Robust Tracking for a Class of Uncertain Linear Systems," *International Journal of Control*, Vol. 45, pp. 875-892, 1987.

[11] Jayasuriya, S., and Kee, C., "Circle-type Criterion for Synthesis of Robust Tracking Controllers," *International Journal of Control*, Vol. 48, pp. 865-886, 1988.

[12] Jayasuriya, S., and Kee, C., "Perturbed Butterworth Pole Patterns For Tracking in the Sense of Spheres," *Journal of Dynamic System, Measurement and Control*, 1990 (to appear).

[13] Martin, Jr., *Nonlinear Operator and Differential Equations in Banach Space* , John Wiley & Sons, Inc., New York, 1976.

[14] Postlethwaite, Gu, D.W., and O'Young S.D., "Some Computational Results on Size Reduction in H_∞ Design," *IEEE Transactions on Automatic Control*, Vol. 33, pp. 177-185, 1988.

NASA
National Aeronautics and Space Administration

REPORT DOCUMENTATION PAGE

1. Report No.	2. Government Accession No.	3. Recipient's Catalog No.
CR 185644		

4. Title and Subtitle	5. Report Date
Attitude Control/Momentum Management and Payload Pointing in Advanced Space Vehicles	August 1990
	6. Performing Organization Code
7. Author(s)	8. Performing Organization Report No.
Alexander G. Parlos	90-DISL-05
9. Performing Organization Name and Address	10. Work Unit No.
Decision and Information Systems Laboratory Department of Nuclear Engineering Texas A&M University College Station, Texas 77843	11. Contract or Grant No. NAG 9-275
12. Sponsoring Agency Name and Address	13. Type of Report and Period Covered
NASA Johnson Space Center Houston, Texas 77058	Contractor Report 6/88 - 5/90
	14. Sponsoring Agency Code

15. Supplementary Notes

16. Abstract

This report describes the research performed in the two year period between June 1988 and May 1990, under the NASA Johnson Space Center Grant NAG 9-275 to Texas A&M University. The two major parts of the report describe the research results and findings of the two major tasks of the project. Namely, the report details the design and evaluation of an Attitude Control/Momentum Management System for highly asymmetric spacecraft configuration, and the preliminary development and application of a nonlinear control system design methodology of tracking control of uncertain systems, such as spacecraft payload pointing systems. Control issues relevant to both linear and nonlinear rigid-body spacecraft dynamics are addressed, whereas any structural flexibilities are not taken into consideration.

17. Key Words (Suggested by Author(s))	18. Distribution Statement
Spacecraft Attitude Control Adaptive Control Payload Pointing	Unclassified - Unlimited Category 18

19. Security Classification (of this report)	20. Security Classification (of this page)	21. No. of pages	22. Price
Unclassified	Unclassified	190	

For sale by the National Technical Information Service, Springfield, VA 22161-2171